DOE/PC/88889-T15
(DE94005629)
Distribution Category UC-105

PROOF-OF-CONCEPT TESTING OF THE ADVANCED NOXSO FLUE GAS CLEANUP PROCESS

FINAL REPORT
April 1993

Prepared for

Ohio Department of Development
Ohio Coal Development Office
77 South High Street
Columbus, Ohio 43266-0101
Grant No. CDO/D-87-74

and

U.S. Department of Energy
Pittsburgh Energy Technology Center
P.O. Box 10940
Pittsburgh, Pennsylvania 15236-0940
Contract No. DE-AC22-89PC88889

Prepared by

NOXSO
Corporation
P.O. Box 469
Library, Pennsylvania 15129-0469

DISCLAIMER

TABLE OF CONTENTS

1.0 ABSTRACT 1-1

2.0 INTRODUCTION 2-1

3.0 PROCESS CHEMISTRY 3-1
3.1 Existing Reaction Models 3-1
3.1.1 Sorbent Adsorption 3-1
3.1.2 Sorbent Regeneration 3-1
3.2 New Findings and Proposed Reaction Model 3-2
3.2.1 Sorbent Adsorption 3-3
3.2.2 NO_x Desorption 3-10
3.2.3 Sorbent Reduction 3-10
3.3 Summary 3-10

4.0 THE NOXSO 5 MW PILOT PLANT 4-1
4.1 Pilot Plant Description 4-1
4.2 Analytical Equipment 4-3
4.3 Data Acquisition and Reduction 4-6
4.4 Pilot Plant Availability 4-7
4.5 Sorbent Sampling and Analysis 4-7
4.6 Plant Safety 4-11

5.0 MATERIALS OF CONSTRUCTION 5-1
5.1 Vessel Corrosion Coupons 5-1
5.2 Accelerated Corrosion Tests 5-7
5.3 Vessel Inspections 5-11

6.0 SORBENT PROPERTIES 6-1

7.0 SORBENT ATTRITION 7-1
7.1 Sorbent Makeup 7-1
7.2 Baghouse Collection Data 7-2
7.3 Dust Sampling 7-2
7.4 Sorbent Attrition Summary 7-6

8.0 FLUIDIZATION 8-1
8.1 Downcomer Design 8-1
8.2 Heat Transfer 8-8

9.0 SORBENT TRANSPORT 9-1
9.1 MAC Dense Phase Transport 9-1
9.2 J-Valves 9-1

10.0 PILOT PLANT OPERABILITY 10-1
10.1 Plant Shutdowns 10-1
10.2 Plant Trips 10-5
10.3 Suggested Plant Modifications 10-6

11.0 PARAMETRIC TEST RESULTS 11-1
11.1 Material Balances 11-4
11.2 Parametric Results 11-4
11.2.1 Effect of Gas/Sorbent Residence Time in Adsorber 11-4
11.2.2 Effect of Adsorber Bed Temperature 11-10
11.2.3 Effect of SO_2/NO_x Concentration 11-18
11.2.4 Effect of Gas-Sorbent Contacting 11-21
11.2.5 NO_x and SO_2 Adsorption Heat 11-25
11.2.6 NO_2 in Adsorber Outlet 11-27
11.2.7 Summary 11-31
11.3 Fluid Bed Adsorber Model 11-34
11.3.1 Model Derivation 11-35
11.3.2 Comparison of POC Adsorption Results with Model Prediction 11-41
11.4 Statistical Design and Analysis Results, Pilot Plant Facility 11-44
11.5 NO_x Regeneration 11-55
11.5.1 SO_2 Desorption 11-55
11.5.2 NO_x Desorption 11-58
11.6 Sulfur Regeneration 11-58
11.7 65 MW Model Plant 11-68

12.0 DURATION TEST RESULTS 12-1

13.0 SUMMARY AND CONCLUSION 13-1

14.0 REFERENCES 14-1

APPENDIX A A-1

APPENDIX B B-1

APPENDIX C C-1

APPENDIX D D-1

APPENDIX E E-1

APPENDIX F F-1

LIST OF FIGURES

Figure	Caption	Page
3-1.	Effect of Temperature on SO_2 Adsorption	3-4
3-2.	Effect of Temperature on NO_x Adsorption	3-5
3-3.	Effect of Water on SO_2 Adsorption	3-6
3-4.	Effect of Water on NO_x Adsorption	3-7
3-5.	Effect of the Amount of Adsorber SO_2 on the Amount of Adsorbed NO_x	3-8
3-6.	NO_2 Adsorption Profile by NOXSO Sorbent	3-9
3-7.	Evolving NO_x Profile While Heating the NO_x-Rich NOXSO Sorbent Prepared by NO_2 Adsorption	3-11
4-1.	NOXSO Process Tower	4-2
4-2.	Gas Monitoring System	4-4
4-3.	Pilot Plant Operating Hours by Month	4-8
4-4	Pilot Plant Availability by Month	4-9
5-1.	Corrosion Spool Test Rack	5-2
5-2.	High Temperature Corrosion Test Apparatus	5-8
6-1.	Pilot Plant Sorbent Surface Area Decay	6-2
6-2.	Sorbent Chloride Content	6-4
7-1.	Baghouse Collection Data	7-3
8-1.	Rectangular Weir	8-3
8-2.	The Experimental and Correlated h_c U_0 of the Pilot Plant Sorbent Cooler	8-5
8-3.	Sorbent Cooler Downcomer	8-9
8-4.	Comparison of Sorbent Cooler Gas and Solid Temperatures	8-14
8-5.	Gas and Sorbent Temperatures Inside the Sorbent Cooler at Different Sorbent Residence Times	8-15
8.6.	Comparison of Sorbent Cooler Gas and Solid Temperatures (Literature Correlation)	8-16
8-7.	Gas and Sorbent Temperatures Inside the Sorbent Cooler at Different Sorbent Residence Time (Literature Correlation)	8-17
9-1.	MAC System	9-2
9-2.	Schematic of a J-Valve	9-3
10-1.	Pilot Plant Availability (3/1/92 to 8/16/92)	10-2
10-2.	Pilot Plant Availability (8/23/92 to 1/17/93)	10-3
11-1.	NOXSO Process Flow Diagram	11-5
11-2.	SO_2 Removal Versus Gas/Sorbent Residence Time (All Data from Tests at Mini and Base Load)	11-6
11-3.	SO_2 Removal Versus Gas/Sorbent Residence Time (All Data from Tests at Mini and Base Load)	11-7
11-4.	SO_2 Removal Versus Gas/Sorbent Residence Time (Data Regression)	11-9
11-5.	SO_2 Removal as a Function of Gas/Sorbent Residence Time (Data Regression)	11-11

LIST OF FIGURES (continued)

Figure	Caption	Page
11-6.	NO_x Removal Versus Gas/Sorbent Residence Time (All Data from Tests at Mini and Base Load)	11-12
11-7.	NO_x Removal Versus Gas/Sorbent Residence Time (All Data from Tests at Mini and Base Load)	11-13
11-8.	Spike Flue Gas With SO_2/NO_x (10000 pph, 7000 scfm, 14" H_2O)	11-14
11-9.	Spike Flue Gas With SO_2/NO_x (10000 pph, 7000 scfm, 14" H_2O)	11-16
11-10.	NO_x Sorbent Loading at Varying Adsorber Bed Temperatures	11-17
11-11.	SO_2 Sorbent Loading as a Function of Adsorber Bed Temperature	11-19
11-12.	SO_2 Removal as a Function of Inlet SO_2 (All Tests at 7000 scfm)	11-20
11-13.	NO_x Removal as a Function of Inlet NO_x (10000 pph, 7000 scfm, 14"H_2O)	11-22
11-14.	SO_2 Removal Versus Flue Gas Flowrate Effect of Bubble-Buster	11-23
11-15.	NO_x Removal Versus Flue Gas Flowrate Effect of Bubble-Buster	11-24
11-16.	NO_x and SO_2 Adsorption Heat	11-28
11-17.	NO/NO_2 in Adsorber Offgas (11/13/92 to 1/16/93)	11-29
11-18.	NO/NO_2 in Adsorber Offgas (NO_x Spiking Tests)	11-30
11-19.	Sorbent Versus Gas Residence Time 90% Removal Versus Actual Model Plant	11-33
11-20.	SO_2/NO_x Sorption Rate Constant Obtained from PDU Tests	11-40
11-21.	Comparison of Predicted and Measured NO_x Removal Efficiency	11-42
11-22.	Comparison of Predicted and Measured SO_2 Removal Efficiency	11-43
11-23.	Comparison of Predicted and Measured NO_x Removal Efficiency (PDU, LCTU and POC Test Results)	11-45
11-24.	Comparison of Predicted and Measured SO_2 Removal Efficiency (PDU, LCTU and POC Test Results)	11-46
11-25.	Predicted Versus Measured NO_x Removal for Data Used to Fit Model	11-49
11-26.	Predicted Versus Measured SO_2 Removal for Data Used to Fit Model	11-50
11-27.	Predicted Vs Measured NO_x Removal Recent POC Runs Not Used in Model Fitting Bubble Buster Predictions Adjusted by Adding 3.8%	11-52
11-28.	Predicted Vs Measured NO_x Removal Recent POC Runs Not Used in Model Fitting	11-53
11-29.	Predicted NO_x and SO_2 Removals Bed Height = 3 ft, Bed Temp = 325°F, Regenerator Residence Time = 30 min, Inlet NO_x = 725 ppm, Inlet SO_2 = 2900 ppm	11-56
11-30.	Predicted NO_x and SO_2 Removals Bed Height = 3 ft, Bed Temp = 325°F, Regenerator Residence Time = 30 min, Inlet NO_x = 300 ppm, Inlet SO_2 = 1800 ppm	11-57
11-31.	Regenerator and Sorbent Sample Ports	11-59
11-32.	Heater and Regenerator Temperature	11-61

LIST OF FIGURES (continued)

Figure	Caption	Page
11-33.	Sorbent Sulfur Regeneration (10/05/92 to 12/10/92)	11-62
11-34.	Effect of Heater Bottom-Bed Temperature on Sulfur Regeneration	11-64
11-35.	Temperature Effect of the First Regeneration Rate Constant	11-65
11-36.	Regenerator Offgas H_2S/SO_2 Ratio	11-67
11-37.	Regeneration Reaction Heat (Heater Bottom-Bed Temperature = 1150°F)	11-69
11-38.	NO_x/SO_2 Removal Efficiencies of the 65 MW Model Plant with Different Sorbent Flowrates (100,000 - 250,000 lbs/hr)	11-71
11-39.	NO_x/SO_2 Removal Efficiencies of the 65 MW Model Plant Using Different Sorbent Na and SiO_2 Loading (100,000 lbs/hr Sorbent)	11-72
11-40.	Optimum Residual Sulfur Content of Regenerated Sorbent for Reaching 90% SO_2 Removal Efficiency in the 65 MW Model Plant	11-73
12-1.	POC Duration Test	12-2
12-2.	POC Duration Test	12-3
12-3.	POC Duration Test	12-7
12-4.	POC Duration Test	12-8
12-5.	POC Duration Test	12-10
12-6.	POC Duration Test	12-11

LIST OF TABLES

Table	Caption	Page
4-1	Gas Monitoring System Sample Points	4-3
4-2	Continuous Analyzers	4-5
4-3	Radical Ions Used for Mass Spectrometer Analysis	4-6
4-4	Sorbent Sampling Locations, Frequency and Analysis	4-10
4-5	Safety Equipment at the NOXSO POC	4-13
4-6	Original Trip Initiators	4-13to15
4-7	Trip Devices	4-16
4-8	Changes to Original Trip Initiators	4-17
5-1	Location of Vessel Corrosion Coupons	5-1
5-2	Types of Coupons on Corrosion Test Racks	5-3
5-3	Average Exposure Conditions for the Corrosion Test Racks	5-4
5-4	Corrosion Rates in Regenerator and Steam Treater	5-5
5-5	Corrosion Rates in Adsorber Inlet and Outlet	5-5&6
5-6	Corrosion Test Conditions	5-7
5-7	Accelerated Test Results	5-9&10
5-8	POC Vessel and Piping Inspection Locations	5-11
6-1	Sorbent Properties	6-1
6-2	Summary of ICP Data	6-5
6-3	Summary of PIXE Data	6-6
7-1	Sorbent Makeup Rate	7-1
7-2	Dust Sample Port Location and Dimension Data	7-4
7-3	Particulate Sampling Results	7-4&5
7-4	Summary of Attrition Data	7-6
10-1	Trip Summary	10-5
11-1	POC Tests Conducted at Mini Load	11-1&2
11-2	POC Tests Conducted at Base Load	11-2&3
11-3	POC Spiking Tests	11-3
11-4	Model Plant	11-31
11-5	Adsorber Design (65 MW)	11-34
11-6	NOXSO POC Experimental Design	11-47
11-7	Regression Coefficients and Statistics for NO_x and SO_2 Removal Models	11-48&51
11-8	Prediction Equations for NO_x and SO_2 Conversion	11-55
11-9	Key Process Variables and Measured and Predicted NO_x and SO_2 Removals	11-54
11-10	Steady Operating Data	11-60
11-11	Optimum Regenerated Sorbent Sulfur Content for 65 MW Coal-Fired Model Plant	11-74

LIST OF TABLES (continued)

Table	Caption	Page
11-12	Effect of Sorbent Flowrate and Sulfur Content on the Adsorber Fluid-Bed Pressure Drop for the 65 MW Model Plant	11-74
12-1.	POC Duration Test - Set Points	12-1
12-2.	POC Duration Test	12-4
12-3.	POC Duration Test	12-5
12-4.	POC Duration Test	12-6
12-5.	POC Duration Test - Utility Consumption	12-9

1.0 ACKNOWLEDGEMENTS

NOXSO wishes to express its thanks to the Ohio Coal Development Office of the Ohio Department of Development (Grant No. CDO/D87-74) for its generous financial and technical support of this project. NOXSO also wishes to thank the U.S. Department of Energy's Pittsburgh Energy Technology Center (Contract No. DE-AC22-89PC88889) for its financial and technical support. The support of these State and Federal agencies is critical to the development of technologies like the NOXSO Process which make possible the clean use of coal, America's most abundant energy resource.

NOXSO wishes to thank Ohio Edison for the use of the Toronto Power Plant as the host site for this Proof-of-Concept test. NOXSO also wishes to thank its partners in the development of the NOXSO technology: W.R. Grace & Co. and MK-Ferguson.

Finally, this project would not have been possible without the hard work, dedication, and technical expertise of the employees of NOXSO Corporation, W.R. Grace, and MK-Ferguson who were personally responsible for getting the job done.

1.1 ABSTRACT

The NOXSO Process uses a regenerable sorbent that removes SO_2 and NO_x simultaneously from flue gas. The sorbent is a stabilized γ-alumina bead impregnated with sodium carbonate. The process was successfully tested at three different scales, equivalent to 0.017, 0.06 and 0.75 MW of flue gas generated from a coal-fired power plant. The Proof-of-Concept (POC) Test is the last test prior to a full-scale demonstration. A slip stream of flue gas equivalent to a 5 MW coal-fired power plant was used for the POC test. This paper summarizes the NOXSO POC plant and its test results.

2.0 INTRODUCTION

The NOXSO Process is a dry, regenerable flue gas treatment system that simultaneously removes 90% of the SO_2 and 70-90% of the NO_x from flue gas generated from the combustion of coal. The process has been successfully tested at small scale (0.017 MW) on high sulfur coal (2.5%) at the TVA Shawnee Steam Plant. The test results are contained in two U.S. Department of Energy reports.[1,2]

Tests of a NOXSO Process Development Unit (PDU, 0.75 MW) were conducted at the Pittsburgh Energy Technology Center (PETC) under a cooperative research agreement between NOXSO and the Department of Energy (DOE). Testing in the adsorber was done by continuously feeding a batch of sorbent into a fluidized bed adsorber and collecting the spent sorbent from the adsorber overflow. Regeneration took place in a separate batch reactor. The test results were reported by Yeh *et al.* in 1987,[3] and by Haslbeck *et al.* in 1988.[4]

A Life-Cycle Test Unit (LCTU, 0.06 MW) was built at PETC in 1988 to test the NOXSO Process in an integrated, continuous-operation mode. The LCTU test program was designed to determine long-term effects of the process on the sorbent reactivity and attrition properties. The LCTU unit was operated for over 1200 hours on flue gas. The test results were published by Ma *et al.* in 1991,[5] and by Yeh *et al.* in 1992.[6]

The POC test is the last test prior to the full-scale demonstration. The POC test collected all of the information needed to design the full-scale NOXSO plant: e.g., data pertaining to materials of construction, process performance and cost, process safety, process control. sorbent activity, sorbent attrition, heat recovery, etc. The POC plant (5 MW) is located at Ohio Edison's Toronto power plant in Toronto, Ohio. Flue gas was first introduced to the plant on November 23, 1991. The current test results and process performance are presented in this report.

3.0 PROCESS CHEMISTRY

The NOXSO sorbent is prepared by spraying Na_2CO_3 solution on the surface of γ-alumina spheres. Both sodium ions and alumina contribute to the NOXSO sorbent's capacity to adsorb SO_2 and NO_x from the flue gas. In this chapter, the existing reaction models are reviewed and a new model is presented based upon the latest findings in the POC pilot plant and in NOXSO's Clairton Research Center (CRC).

3.1 Existing Reaction Models

In this section, the existing reaction models proposed in earlier reports are reviewed.

3.1.1 Sorbent Adsorption

The reaction of the alkali in the NOXSO Process is described in earlier reports as follows[1]:

$$Na_2CO_3 + Al_2O_3 \rightarrow 2\ NaAlO_2 + CO_2 \quad (3.1\text{-}1)$$

$$2\ NaAlO_2 + H_2O \rightleftarrows 2\ NaOH + Al_2O_3 \quad (3.1\text{-}2)$$

$$2\ NaOH + SO_2 + 1/2\ O_2 \rightarrow Na_2SO_4 + H_2O \quad (3.1\text{-}3)$$

$$2\ NaOH + 2\ NO + 3/2\ O_2 \rightleftarrows 2\ NaNO_3 + H_2O \quad (3.1\text{-}4)$$

$$2\ NaOH + 2\ NO_2 + 1/2\ O_2 \rightarrow 2\ NaNO_3 + H_2O \quad (3.1\text{-}5)$$

Equation (3.1-1) should only be carried out in the first several cycles of the sorbent circulation in the system until all the Na_2CO_3 sites have evolved CO_2. The model emphasized the role of water in the process, but failed to explain recent findings: the formation of NO_2 during the adsorption process, and the fact that the SO_2/NO adsorption can proceed without water.

3.1.2 Sorbent Regeneration

In the current process design, regeneration occurs in a two-stage regenerator at 620 °C. Upon heating to the regeneration temperature, the adsorbed NO_x is evolved in the sorbent heater. The heated sorbent is then charged into the first stage of the regenerator and contacted with natural gas. The adsorbed SO_2 on the sorbent surface reacts with the reducing gas (natural gas) at the regeneration temperature and produces SO_2, H_2S, COS, CS_2 and H_2O. A part of the sodium sulfate on the sorbent surface is also reduced to sodium sulfide. Therefore, the sorbent is subsequently treated with steam hydrolyzing the sulfide and producing H_2S. The offgases from both stages are sent to a Claus plant in order to produce saleable elemental sulfur.

The regeneration kinetics studies carried out to date[2] have shown that the kinetics of the regeneration process are first order. The reducing gases investigated include H_2S, CO, H_2, CO/H_2, natural gas (CH_4), etc. The following reactions were suggested in earlier reports for the regeneration:[1, 3-11]

Using Methane:

$$4\ Na_2SO_4 + CH_4 \rightarrow 4\ Na_2SO_3 + CO_2 + 2\ H_2O \quad (3.1\text{-}6)$$

$$4\ Na_2SO_3 + 3\ CH_4 \rightarrow 4\ Na_2S + 3\ CO_2 + 6\ H_2O \quad (3.1\text{-}7)$$

$$Al_2O_3 + Na_2SO_3 \rightleftarrows 2\ NaAlO_2 + SO_2 \quad (3.1\text{-}8)$$

$$Al_2O_3 + Na_2S + H_2O \rightleftarrows 2\ NaAlO_2 + H_2S \quad (3.1\text{-}9)$$

Using Hydrogen:

$$Na_2SO_4 + 4\ H_2 \rightarrow Na_2S + 4\ H_2O \quad (3.1\text{-}10)$$

$$Na_2SO_4 \cdot Al_2O_3 + H_2 \rightarrow 2\ NaAlO_2 + SO_2 + H_2O \quad (3.1\text{-}11)$$

$$Na_2SO_4 \cdot Al_2O_3 + 4\ H_2 \rightarrow 2\ NaAlO_2 + H_2S + 3\ H_2O \quad (3.1\text{-}12)$$

Using Carbon Monoxide:

$$Na_2SO_4 + 4\ CO \rightarrow Na_2S + 4\ CO_2 \quad (3.1\text{-}13)$$

$$Na_2SO_4 \cdot Al_2O_3 + CO \rightarrow 2\ NaAlO_2 + SO_2 + CO_2 \quad (3.1\text{-}14)$$

$$Na_2SO_4 \cdot Al_2O_3 + 4\ CO \rightarrow 2\ NaAlO_2 + COS + 3\ CO_2 \quad (3.1\text{-}15)$$

The sodium sulfide formed in the above reaction is hydrolyzed by steam in the steam treatment vessel to produce H_2S[4]:

$$Na_2S + Al_2O_3 + H_2O \text{ --> } 2\ NaAlO_2 + H_2S \quad (3.1\text{-}16)$$

The relative distribution of sulfur products formed on regeneration depends upon the type of reducing gas used[8]:

	Mole, %		
Reducing Gas	SO_2	H_2S	Sulfur
H_2	64	27	9
CO	30	62	8
H_2/CO	46	49	5
H_2S	21	35	44
CH_4	65	30	5

The SO_2 and H_2S produced from the above regeneration process are then converted to elemental sulfur in a Claus-type reactor.

3.2 New Findings and Proposed Reaction Model

In the past year, extensive efforts were devoted to a better understanding of the chemistry in the NOXSO Process. Although most of the laboratory work concentrated on the sorbent adsorption in the adsorber and the NO_x desorption in the heater, some studies were also conducted on the sorbent regeneration. In the following sections, the new experimental findings both from POC pilot plant and from the laboratory are illustrated and discussed. Based on these observations, two sets of reaction models were proposed, one for the SO_2/NO_x adsorption in the adsorber, and the other for NO_x desorption. A model for the sorbent regeneration is also provided based only on the POC results.

3.2.1 Sorbent Adsorption

From numerous laboratory experiments, the important findings in sorbent adsorption can be summarized as follows:

- Reaction of NO, SO_2 and O_2 on sorbent produces NO_2.
- NO_2 adsorption produces NO.
- NO removal efficiency improves with higher O_2 concentration.
- NO adsorption strongly enhances SO_2 adsorption.
- NO_2 adsorption proceeds in the absence of SO_2 and O_2.
- SO_2 adsorbed without O_2 in the flue gas evolves upon heating the sorbent.
- The presence of O_2 and SO_2 in the flue gas is vital to NO adsorption.

Temperature also exerts a strong effect on SO_2/NO_x adsorption. Figures 3-1 and 3-2 compare the SO_2 and NO_x adsorption curves, respectively, using a fixed-bed reactor. Clearly, lower temperature promotes NO_x adsorbing capability, but does not change SO_2 adsorption in the POC operating range, i.e., about 1.2 wt% of sulfur loading from the adsorber.

In Figures 3-3 and 3-4, the effect of water is given for SO_2 and NO_x adsorption, respectively. Apparently, the presence of water may also promote the adsorption of SO_2 and NO_x.

In an EPRI report[11], a mechanism of SO_2/NO_x adsorption using sodium carbonate (Na_2CO_3) was proposed. It was found that this mechanism fit the results obtained from POC and laboratory testing. The mechanism is:

$$Na_2O + SO_2 \rightleftarrows Na_2SO_3 \qquad (3.2\text{-}1)$$

$$Na_2SO_3 + 1/2\ O_2 \rightarrow Na_2SO_4 \qquad (3.2\text{-}2)$$

$$Na_2O + SO_2 + NO + O_2 \rightleftarrows Na_2SO_4 + NO_2 \qquad (3.2\text{-}3)$$

$$Na_2O + 3\ NO_2 \rightleftarrows 2\ NaNO_3 + NO \qquad (3.2\text{-}4)$$

Multiplying Equation (3.2-3) by 3 and then adding Equation (3.2-4) shows that

$$4\ Na_2O + 3\ SO_2 + 2\ NO + 3\ O_2 \rightleftarrows 3\ Na_2SO_4 + 2\ NaNO_3 \qquad (3.2\text{-}5)$$

The above equation indicates that when the reactions approach steady state operation, 1.5 moles of adsorbed SO_2 are needed for each mole of adsorbed NO. Meanwhile, Equations (3.2-1) and (3.2-2) suggest that there is another SO_2 adsorption reaction occurring in parallel. Therefore, for a steady state operation, 2.5 moles of SO_2 are necessary to be adsorbed on the sorbent surface for adsorbing each mole of NO. Figure 3-5 shows the experimental evidence for the above argument.

Figure 3-6 demonstrates the adsorption of NO_2 by NOXSO sorbent as suggested by Equations (3.2-4). From simple integration, the adsorbed amount of NO_2 is three times that of evolved NO, which is identical to the stoichiometric ratio used in Equation (3.2-4).

Figure 3-1
Effect of Temperature of SO2 Adsorption

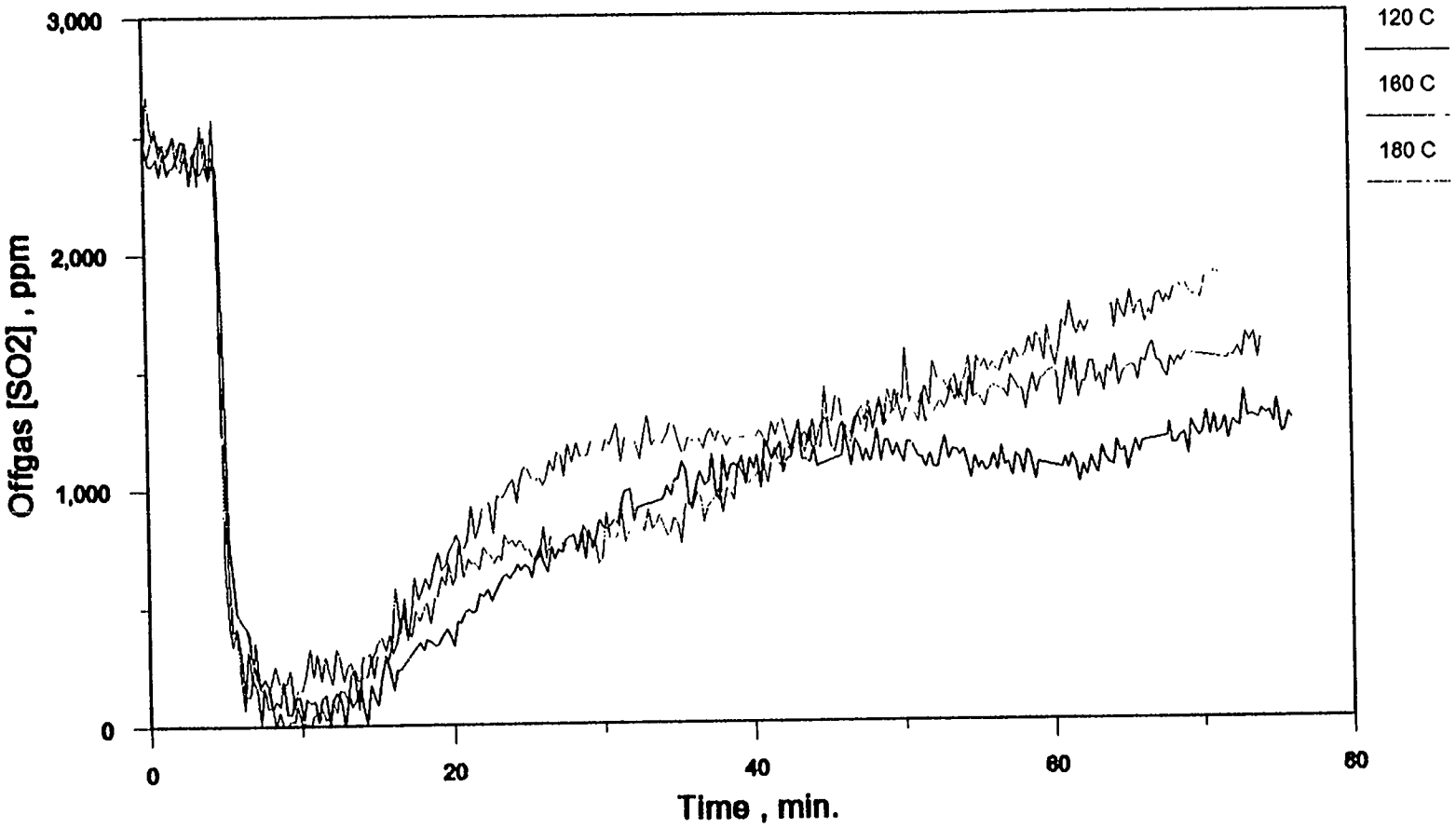

Gas Input: 2500 ppm SO2+1000 ppm NO + 2% O2 + 15% CO2 + 8% H2O + N2

Figure 3-2
Effect of Temperature on NOx Adsorption

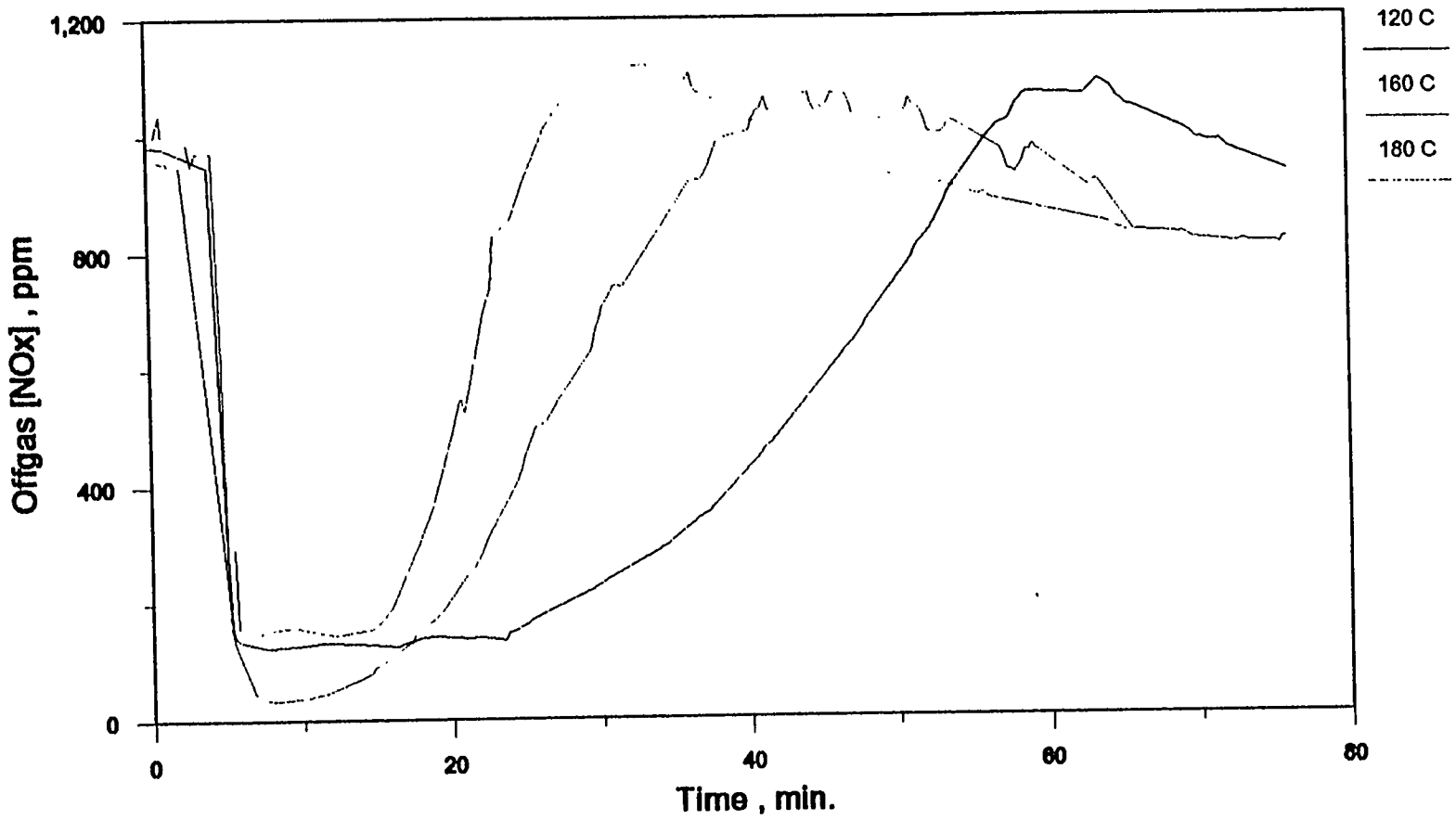

Gas input: 2500 ppm SO2 + 1000 ppm NO + 2% O2 + 15% CO2 + 8% H2O + N2

Figure 3-3
Effect of Water on SO2 Adsorption

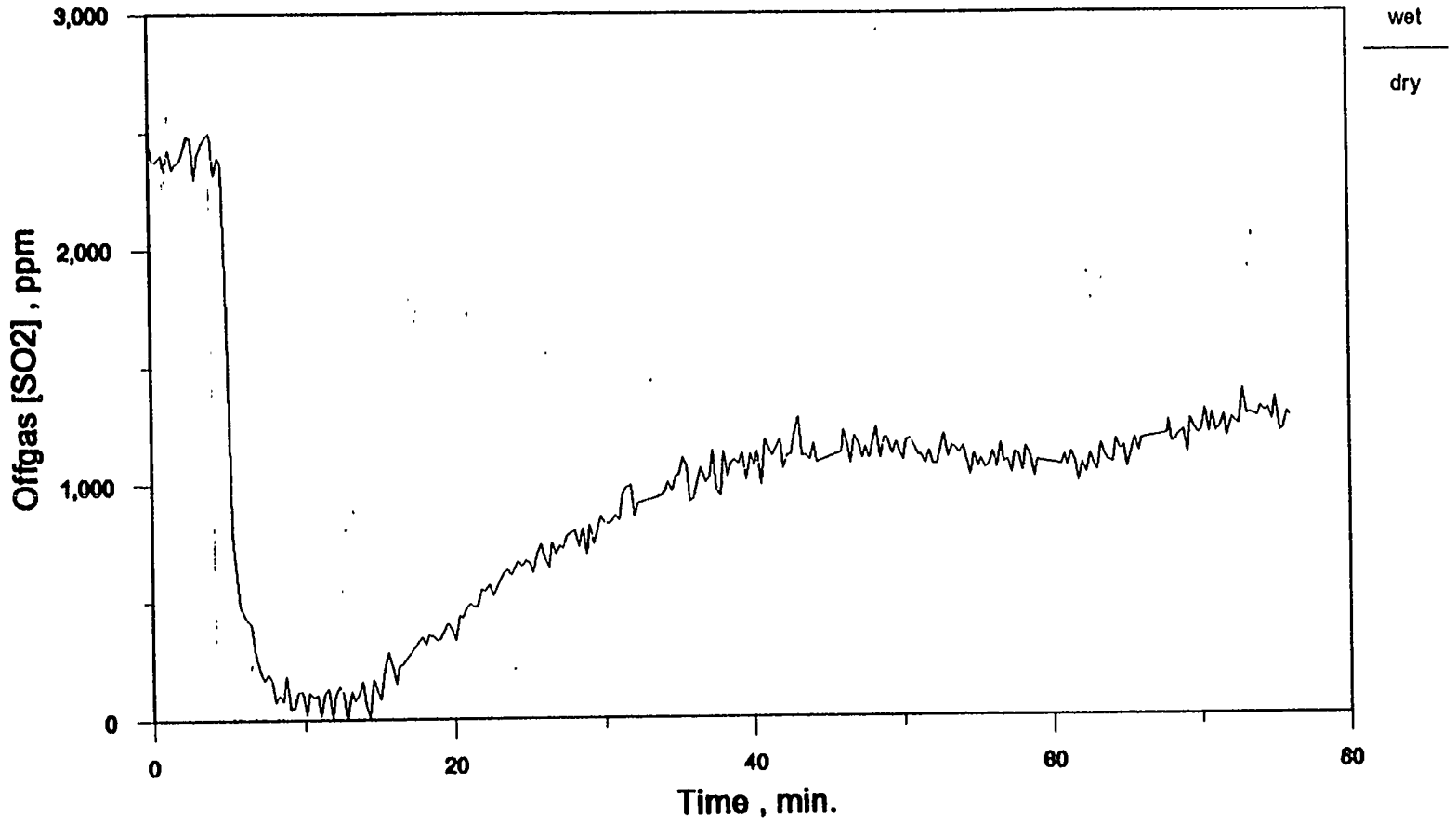

Gas input: 2500 ppm SO2 + 1000 ppm NO + 2% O2 + 15% CO2 + N2 (add 8% H2O when wet)

Figure 3-4
Effect of Water on NOx Adsorption

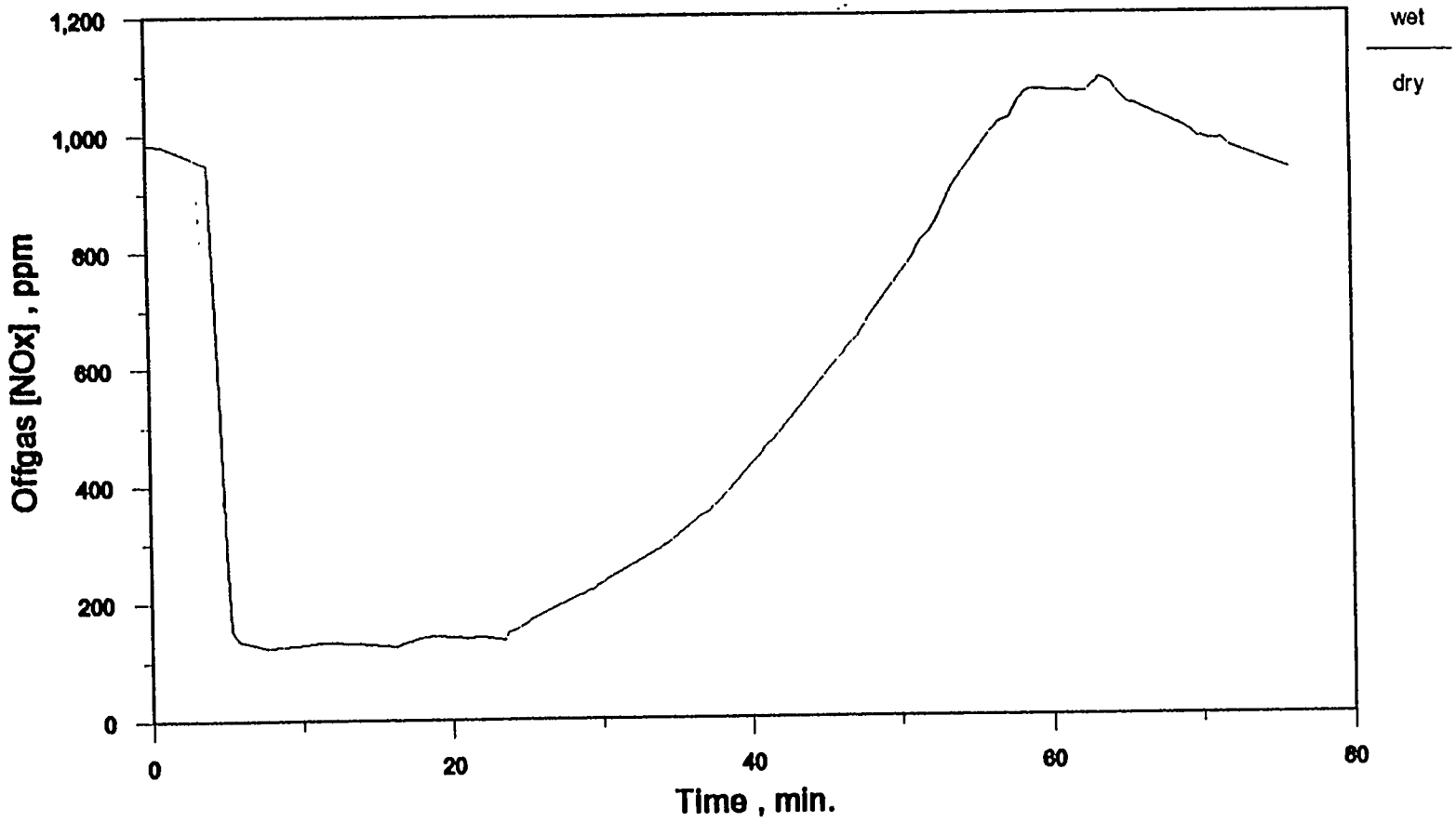

Gas Input: 2500 ppm SO2, 1000 ppm NO+ 2% O2+ 15% CO2 + N2 (add 8% H2O when wet)

Figure 3-5
Effect of the Amount of Adsorbed SO2
on the Amount of Adsorbed NOx

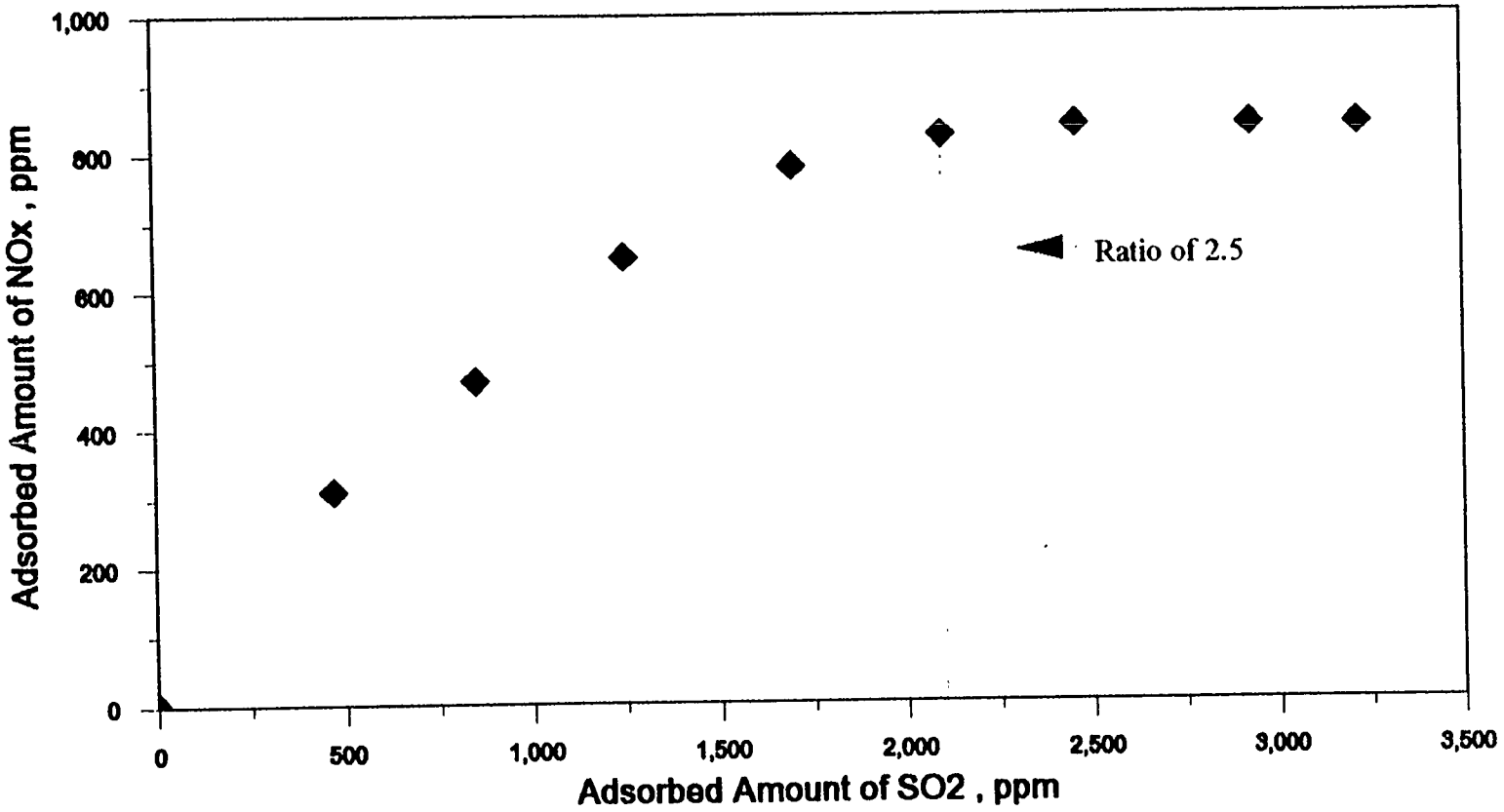

Gas input: 1000 ppm NO + 8% O2 + N2 + various concentrations of SO2

Figure 3-6
NO2 Adsorption Profile by NOXSO Sorbent

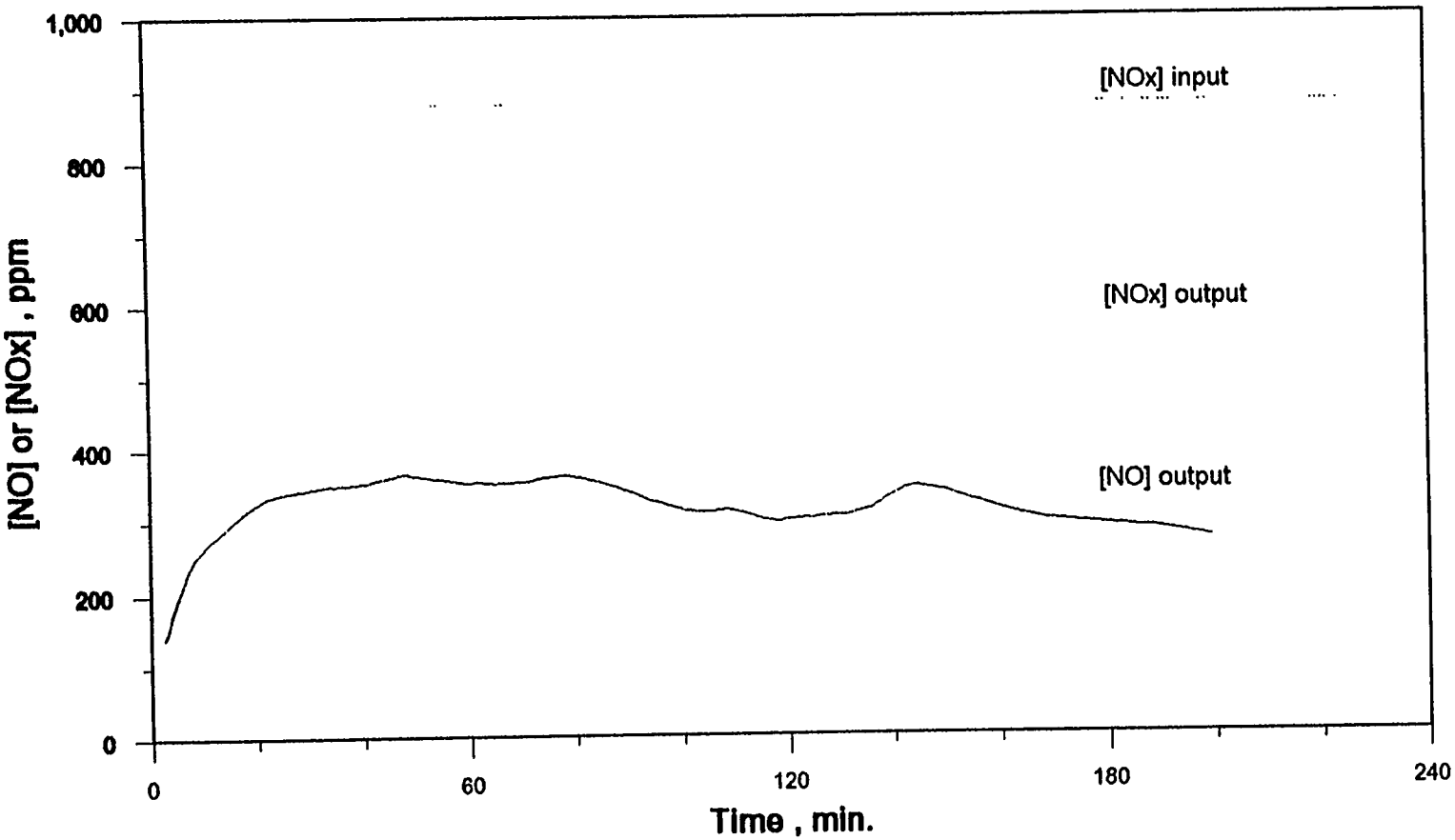

Gas Input: 791 ppm NO2 + 89 ppm NO + N2 at 160 C

3.2.2 *NO_x Desorption*

When the spent sorbent was heated in the sorbent heater, the adsorbed NO_x was evolved. This observation was made at the POC pilot plant as well as in the laboratory. The observations showed:

- NO_x desorption produces both NO and NO_2, where the latter is about 65-75% of the evolved NO_x.
- The type of gas (air, N_2, H_e) used to heat the sorbent does not affect the production of NO and NO_2 significantly.
- A small fraction of SO_2 may also be evolved while heating the sorbent.

Figure 3-7 shows the typical NO_x concentration curves produced on heating the sorbent used in the NO_2 adsorption test. The ratio of the evolved NO_2 to NO is between 2 to 4. depending upon the operating temperature. Based on the findings, the following reactions are proposed to explain the NO_x desorption.

$$2\ NaNO_3 \rightarrow Na_2O + 2\ NO_2 + 1/2\ O_2 \qquad (3.2\text{-}6)$$
$$2\ NaNO_3 \rightarrow Na_2O + NO_2 + NO + O_2 \qquad (3.2\text{-}7)$$

Part of the adsorbed SO_2 was also evolved while heating the sorbent to the regeneration temperature. This is believed to be the decomposition of the sodium sulfite which is less stable than sodium sulfate. The reaction is, therefore, the reverse reaction of Equation (3.2-1), or

$$Na_2SO_3 \rightleftarrows Na_2O + SO_2 \qquad (3.2\text{-}8)$$

3.2.3 *Sorbent Reduction*

After all the adsorbed NO_x evolves on heating, the sorbent carrying mainly sulfate enters the regenerator. Based on the POC results, the following regenerator mechanism is proposed:

$$1/4\ CH_4 + Na_2SO_4 \rightarrow 1/4\ CO_2 + SO_2 + 1/2\ H_2O + Na_2O \qquad (3.2\text{-}9)$$
$$SO_2 + Na_2O \rightarrow Na_2SO_3 \qquad (3.2\text{-}10)$$
$$3/4\ CH_4 + Na_2SO_3 \rightarrow 3/4\ CO_2 + H_2S + 1/2\ H_2O + Na_2O \qquad (3.2\text{-}11)$$
$$H_2S + Na_2O \rightleftarrows Na_2S + H_2O \qquad (3.2\text{-}12)$$
$$CO_2 + Na_2S \rightarrow COS + Na_2O \qquad (3.2\text{-}13)$$
$$1/2\ CO_2 + Na_2S \rightarrow 1/2\ CS_2 + Na_2O \qquad (3.2\text{-}14)$$

3.3 Summary

The proposed mechanisms of SO_2/NO_x adsorption, NO_x desorption, SO_2 desorption, and SO_2 reduction can explain the observations from both POC and CRC. Although more studies are needed to illuminate the role of alumina and water, the current models are suitable for the purpose of process design.

Figure 3-7
Evolving NOx Profile While Heating the NOx-rich
NOXSO Sorbent Prepared by NO2 Adsorption

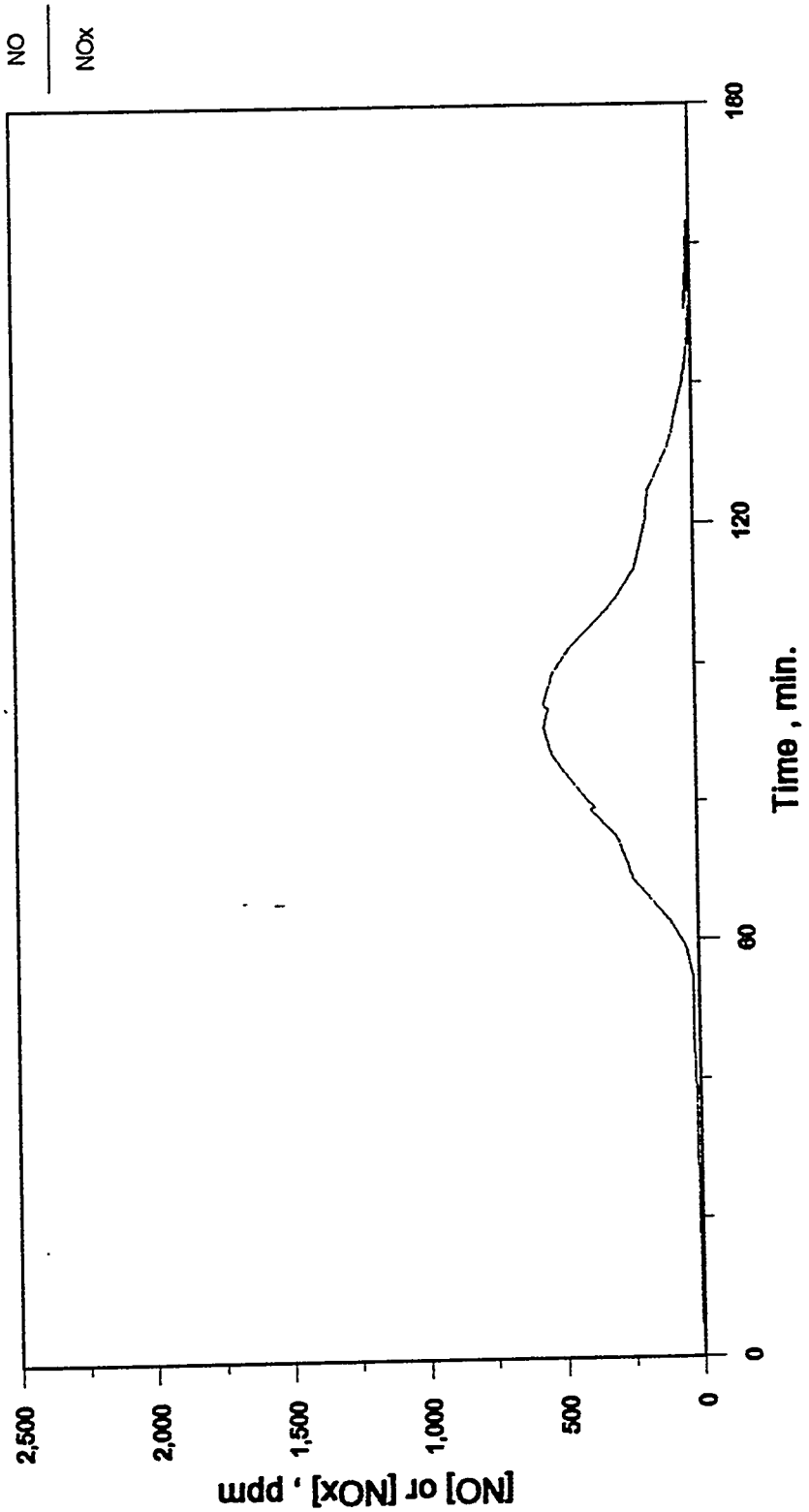

4.0 THE NOXSO 5 MW PILOT PLANT

4.1 Pilot Plant Description

The NOXSO POC at Toronto, Ohio is shown schematically in Figure 4-1. A slip stream of flue gas (equivalent to 5 MW coal-fired power) is extracted from either Boiler #10 or #11 of Ohio Edison's Toronto Power Plant. The flue gas first flows through a 250 HP, I.D. fan, then is cooled to 160°C (320°F) by spraying water into the flue gas ducts. The cooled flue gas then enters a 3.2-m (126") diameter single-stage, fluid-bed adsorber. The NOXSO sorbent, 1.23mm diameter γ-alumina beads impregnated with 5.2 wt% Na, removes the SO_2 and NO_x simultaneously from the flue gas as it passes through the fluid bed adsorber. The cleaned flue gas mixes with the hot offgas from the sorbent heater, then passes through the baghouse to remove all the attrited sorbent before the gas vents to the atmosphere through the power plant's stack. A cyclone is installed after the adsorber to recycle fines to the bed (50% efficient on 50 micron diameter particles).

The spent sorbent in the adsorber underflows into the dense-phase conveying system where 128.9 kPa (35 psig) air lifts the sorbent 24.4-m (80 ft) high to the top of the sorbent heater, which is a 2.34-m (92") diameter, three-stage, fluid bed vessel. A natural gas-fired air heater supplies the hot air to heat the sorbent in the sorbent heater to 621°C (1150°F). During the sorbent heating process, all the adsorbed NO_x and a small portion of adsorbed SO_2 desorb from the sorbent. The hot sorbent heater offgas can either be directly vented to the atmosphere through the power plant's stack or can be mixed with the cleaned flue gas to enter the baghouse. Mixing with the flue gas is needed to protect the baghouse from exceeding the high temperature limit of the bags. No cyclone is installed on the top of the sorbent heater. The hot sorbent in the bottom bed of the sorbent heater underflows into a J-valve (hereafter called top J-valve). Either nitrogen or steam can be used to carry the sorbent through the J-valve into a 1.22-m (48") diameter moving-bed regenerator. Natural gas is used as the regenerant to treat the hot sorbent. The sulfate on the sorbent is reduced to SO_2, H_2S, and sulfide. Steam is then used to hydrolyze any residual sulfide to H_2S. The offgas from the natural gas treater mixes with that from the steam treater before the combined stream enters the incinerator, in which all the sulfur species are converted to SO_2.

The regenerated sorbent flows into a second J-valve (hereafter called middle J-valve because of its relative elevation to other J-valves) from which it enters the 1.73-m (68") diameter, three-stage, fluid-bed cooler. A fan supplies ambient air to cool the sorbent. The heat of the regenerated sorbent is recovered by the cooling air which is then used as the combustion air in the air heater. The cool sorbent in the bottom bed of the cooler overflows into a 1.83-m (72") diameter surge tank. A third J-valve (hereafter called bottom J-valve) is used to transport the sorbent from the surge tank to the adsorber.

The top and middle J-valves isolate the reducing section (regenerator) of the NOXSO plant from its oxidation section (heater and cooler train). The steam (for normal operation) or nitrogen (for start-up) enters the middle and top J-valve to carry the sorbent upward. Since the steam is introduced at the lowest point of the J-valve, which is also the highest pressure point

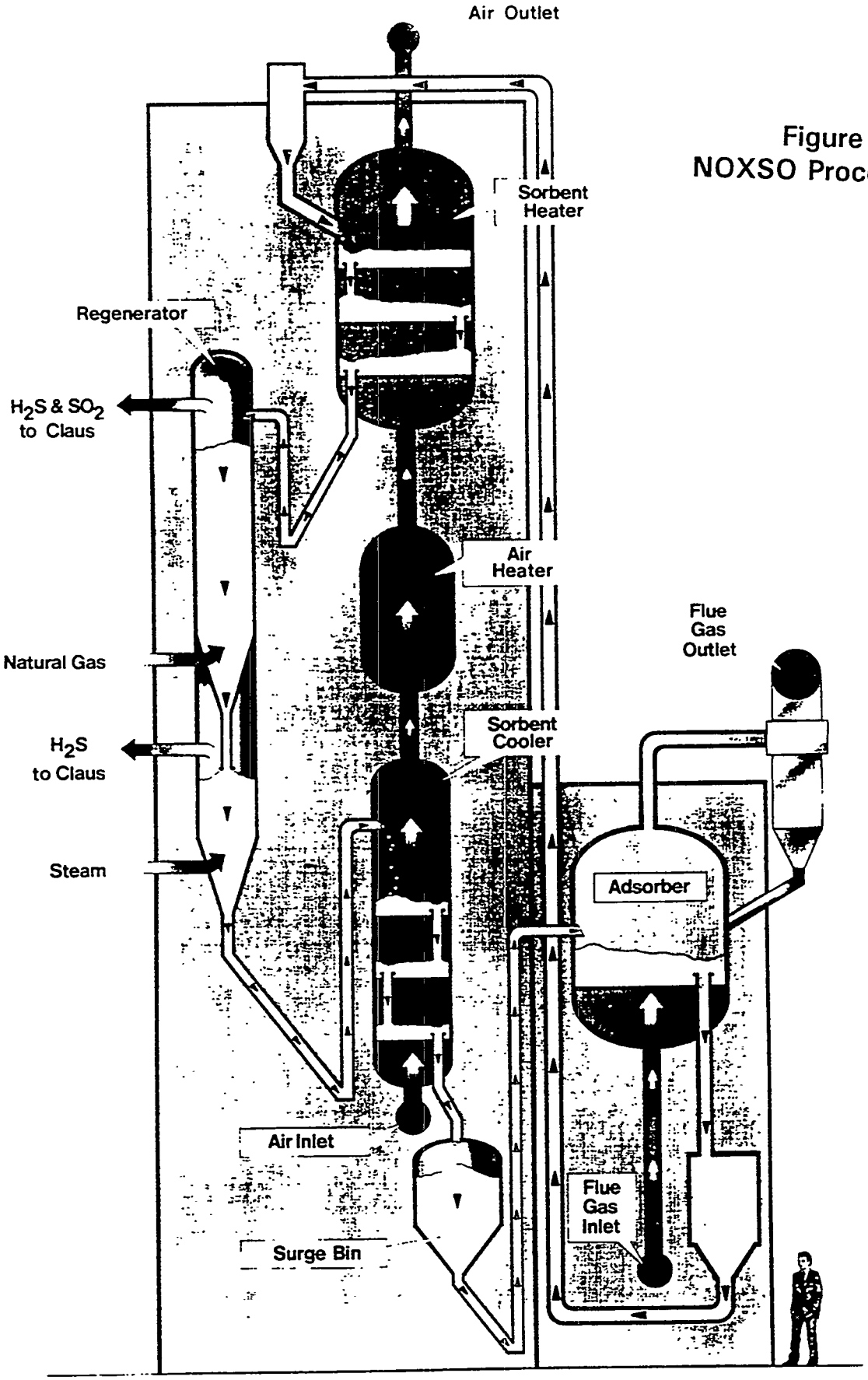

Figure 4-1
NOXSO Process Tower

between the two vessels, a steam barrier is, therefore, created to prevent the mixing of the reducing gas with the oxygen or vice versa. The bottom J-valve is operated with air to lift the sorbent from the surge tank to the adsorber.

Since the POC plant uses only a slip stream of flue gas from the power plant, the amount of NO_x evolved from the sorbent heater is too small to affect the NO_x thermal equilibrium inside the coal combustor. Therefore, NO_x is not recycled to the coal combustor during the POC testing. However, the ability of a coal combustor to reduce excess NO_x introduced into the combustion chamber was proven in a series of simulated NO_x recycle tests. The simulated NO_x recycle tests were carried out in PETC's tunnel furnace and 227 kg/hr (500 lb/hr) pulverized coal combustor.[3,4] In order to obtain the NO_x recycle data to design the NOXSO full-scale demonstration plant in Niles, Ohio, a simulated NO_x recycle test program was conducted in parallel to the POC test at the Babcock and Wilcox (B&W) modular cyclone coal combustor in Alliance, Ohio.[8]

4.2 Analytical Equipment

The gas monitoring system measures concentrations of gas components in the process streams. These measurements are used to assess system performance and characterize process streams. The measurements are used to determine gas and gas-solid mass balances for reaction vessels. Gas samples are continuously pulled from six points for analysis. They are analyzed using both a series of continuous analyzers and a process mass spectrometer. Sample locations. sample type, analyzer type, and components measured are listed in Table 4-1. The monitoring system is diagrammed in Figure 4-2.

Table 4-1. Gas Monitoring System Sample Points

Sample Location	Sample Type	Analyzer	Components Analyzed
Adsorber Inlet	Flue Gas	Continuous	SO_2, NO_x, CO, CO_2, O_2
Adsorber Outlet	Flue Gas	Continuous	SO_2, NO_x, CO, CO_2, O_2
Sorbent Heater Outlet	Flue Gas	Continuous	SO_2, NO_x, CO, CO_2, O_2
Incinerator Outlet	Flue Gas	Mass Spec	SO_2, O_2, N_2, CO_2
Regenerator Offgas	* Process Gas	Mass Spec	H_2O, H_2S, SO_2, CO_2, CH_4, CS_2, COS
Steam Treater Offgas	* Process Gas	Mass Spec	H_2O, H_2S, SO_2, CO_2, CH_4, CS_2, COS

* These gas samples are diluted 10:1 with 10% Ar/90%N_2 at the sample point.

Gas streams are sampled using two different extractive techniques. The flue gas type streams (adsorber inlet, adsorber outlet, sorbent heater outlet, and incinerator outlet) are sampled using filtered extractive probes. Two types of filter probes are used. For samples with very low dust loadings (adsorber inlet and incinerator outlet) a Balston type 30/25 sample filter is connected to a 3/4" diameter SS tube extending into the center of each duct. Mott model 7611

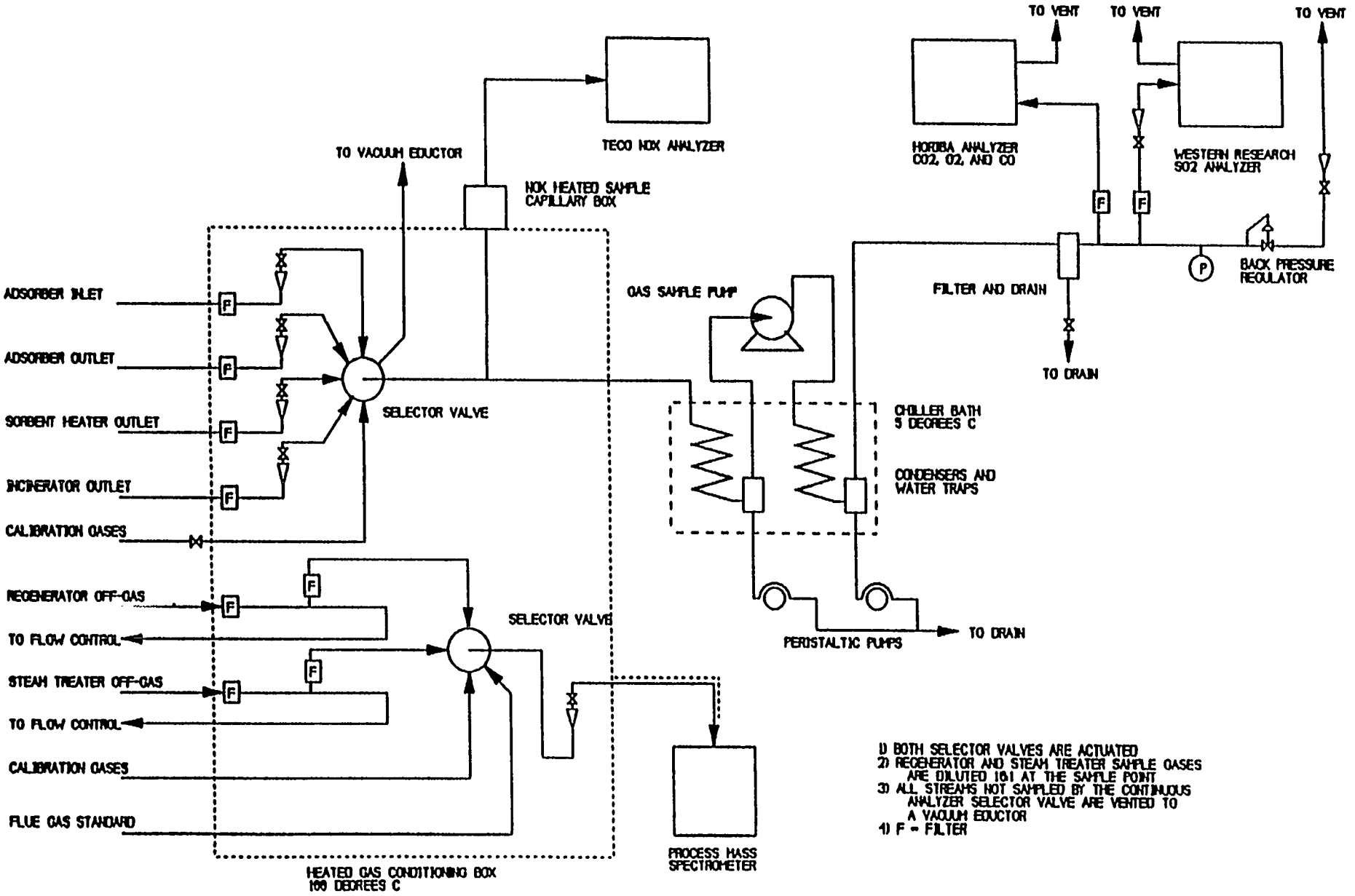

Figure 4-2
Gas Monitoring System

inertial gas sampling systems are used on the adsorber outlet and sorbent heater outlet. These probes allow particulate free samples to be collected without pulling samples through a filter cake of particulate. The second extractive technique is applied to the regeneration offgas and the steam treater offgas. These streams are diluted 10:1 with a mixture of 10% argon and 90% N_2 at the sample point. This dilution allows sample collection and analysis without condensation of water from the sample. The argon in the dilution gas allows accurate measurement of the dilution ratio. Gas samples are conveyed from the sample point to a heated sample conditioning box (100°C) through 3/8" Teflon tubes in heated tube bundles (130°C). The gas is filtered in the sample conditioning box. Two actuated sample valves in the conditioning box are used to select the gas sample analyzed by the continuous analyzers and the mass spectrometer. The mass spectrometer samples are analyzed hot and wet (with no condensing of the water in the sample). The continuous analyzer sample is analyzed (hot and wet) for NO_x using a heated sample capillary assembly. This allows for accurate measurement of NO_2 in the sample gases (if water was condensed from the sample, NO_2 would be scrubbed from the gas and produce 1/3 NO). Water is condensed from continuous analyzer samples prior to analysis for SO_2, O_2, CO, and CO_2.

A single bank of continuous analyzers are used to sequentially measure SO_2, NO_x, O_2, CO, and CO_2 in the adsorber inlet, adsorber outlet, and sorbent heater outlet. The continuous analyzers,which are calibrated daily, are listed in Table 4-2. Each stream is analyzed for 10 minutes, followed by a change to the next stream. After switching sample streams the system is allowed to purge for five minutes prior to collection of data. The total time for analysis of the three streams is 45 minutes. Data from the analyzers is transferred to the Bailey Network 90 process control system for operator display and data collection.

Table 4-2. Continuous Analyzers

Component	Analyzer Type	Analyzer Manufacture & Model
SO_2	UV	Western Research Model 721AT
NO_x	Chemiluminescence	Thermo Environmental Model 10S w/ Model 700 Heated Sample Capillary
O_2	Paramagnetic Pressure	Horiba Model CMA-3X1A
CO	Cross Modulation NDIR	Horiba Model CMA-3X1A
CO_2	Cross Modulation NDIR	Horiba Model CMA-3X1A

The process mass spectrometer is a Milton Roy Prospec 2000. The mass spectrometer is calibrated once a month. Sample gas is introduced to the analyzer through a heated sample capillary assembly and into an ionizer chamber. The sample is ionized and the resulting ions separate by mass/charge ratio in the quadrapole section of the mass spectrometer. Ions used for each component in the analysis are listed in Table 4-3.

Detection of the separated ions is by an electron multiplier. Sampling, analysis, and data storage is controlled by a dedicated Compaq 286 computer. Concentrations measured by the mass spectrometer are also output to the distributed control system using a 4-20 mA interface.

The mass spectrometer sequentially analyzes the regeneration offgas, steam treater offgas, and incinerator offgas. In addition to the sample analysis, a flue gas standard of SO_2, O_2, N_2, and CO_2 is analyzed as part of the sequence. Each stream is analyzed once every 20 minutes.

Table 4-3. Radical Ions Used for Mass Spectrometer Analysis

Component	Mass Peak for Analysis (M/Z)
H_2O	18
H_2S	34
SO_2	64
CO_2	44
CH_4	15
CS_2	76
COS	60
O_2	32
N_2	14

4.3 Data Acquisition and Reduction

Data from field devices are transmitted to the Bailey net 90 distributed control system in analog signals and are converted to digital data by the input slave converters. The digital data are then available to the PCU data bus for the control modules and for transfer by serial communications to the DC90 program operating on a dedicated personal computer. Following each shift of operation the DC90 software is used to convert the data files to Lotus spreadsheet format. The Bailey system also makes data values and trend lines available to the operator on the operator interface screens. Trend lines contain one week of data before being overwritten.

The first step of the data reduction process is the plotting of key process variables versus time from the 5 minute data samples. These plots are reviewed to determine if data must be rejected, either because the process was not at steady-state or because of excessive variations in gas concentrations. After rejecting unsuitable data, averages of all process variables are computed and transferred to an ASCII data file. The ASCII data file then serves as input to a FORTRAN program which calculates mass and energy balance closures and the performance of key unit operations. Data is rejected if the mass balances are not closed to within $\pm$ 15%.

4.4 Pilot Plant Availability

From November 1991 through December 1992, the NOXSO pilot plant processed flue gas for a total of 5213 hours. An additional 1615 hours was spent operating hot inert, i.e. sorbent was circulated throughout the system and heated, but air, instead of flue gas, was fed to the adsorber. Figure 4-3 shows the number of hours per month that flue gas was treated at the pilot plant.

Figure 4-4 shows the pilot plant availability factor per month. The plant availability factor is defined as the number of pilot plant operating hours on flue gas expressed as a percentage of the total number of hours in which flue gas was available for processing. The NOXSO pilot plant availability factor per month ranged from a low of 0% in January to a high of 94% in the month of June.

The first four months of operation were hampered by the usual startup/shakedown problems encountered in a first-of-a-kind installation. For example, the plant was shutdown the entire month of January (0% availability) to replace all seven grid plates in the fluid beds. The original 1/16" grid holes proved to be too small and plugged. However, the monthly average pilot plant availability over the period April - December 1992 was 76%. This is an excellent result for a pilot plant. The average availability for commercial FGD plants in 1989 was 82.9%.[12] Pilot plant availability is generally much worse than a commercial installation, since the pilot plant is a first-of-a-kind design and is subject to frequent changes in operating setpoints that stretch the limits of plant operability. Nevertheless, the NOXSO pilot plant availability factor was close to the industry standard for commercial plants over the last eight months of the POC test. This is proof that the process is simple, reliable and adjusts easily to changing operating conditions.

The pilot plant was run by two operators. A minimum of two was required for safety so that, in the event of an injury to one man, the other could assist the injured and call for help or emergency response. In actuality, our experience is that less than one full-time operator is needed to operate the pilot plant since process controls and process safety systems are fully automated through the Bailey distributed control system. Auxiliary personnel for maintenance. instrument calibration and repairs, etc., would be required on an as needed basis.

4.5 Sorbent Sampling and Analysis

Sorbent samples are collected on a routine basis to measure process performance and monitor changes in the NOXSO sorbent. Sorbent samples are taken from the operating process every six hours for measurement of sulfur content. The sample locations are listed below:

Cooler Top Bed
Adsorber Outlet
Middle Regenerator
Bottom Regenerator
Steam Treater

Figure 4-3
Pilot Plant Operating Hours by Month
Total Operating Hours = 5213

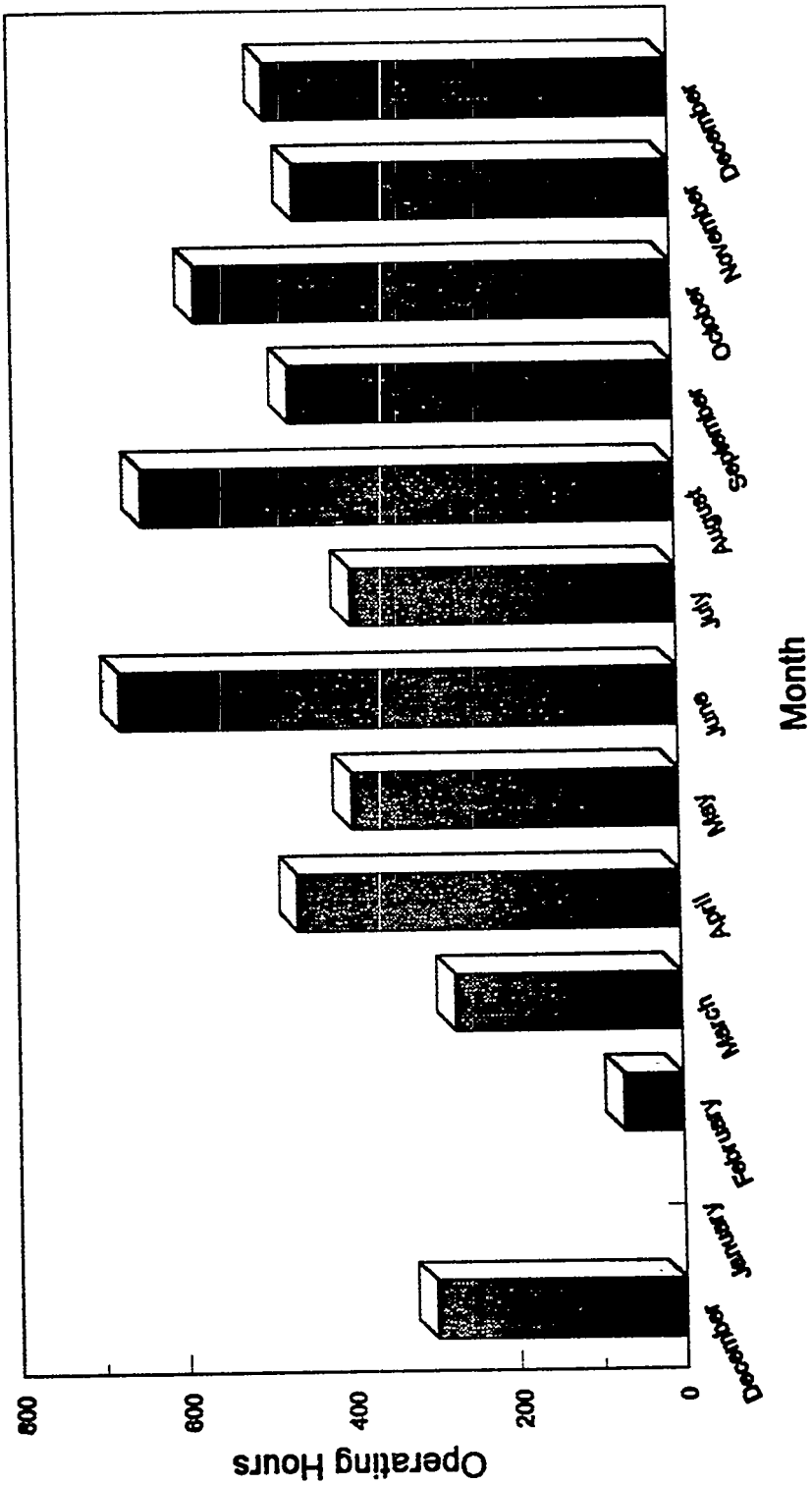

Figure 4-4

Pilot Plant Availability by Month

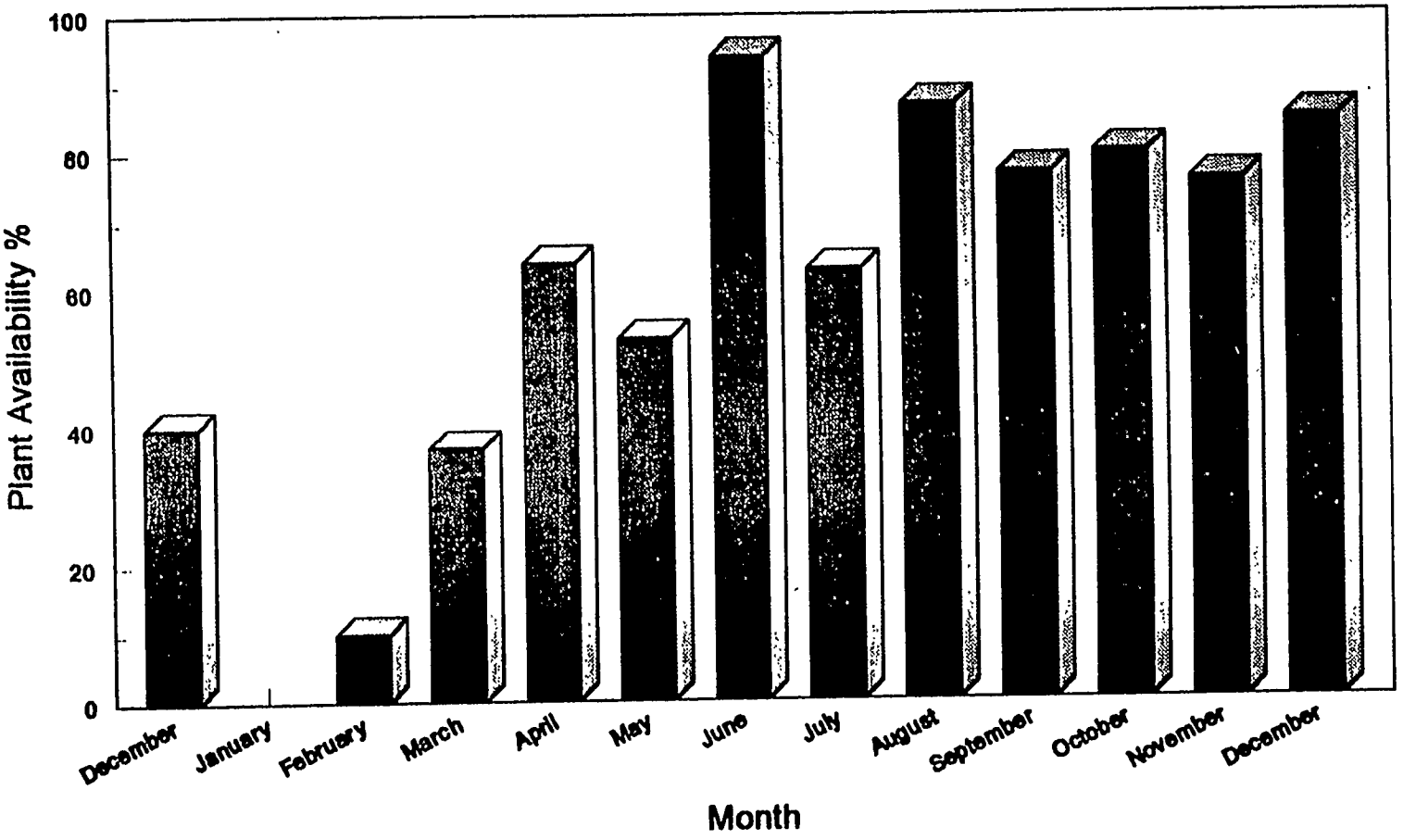

The samples are removed from the process through sampling lockhoppers. The lockhoppers for the cooler top bed and adsorber outlet are unpurged; while the regenerator and steam treater sample lockhoppers are purged with nitrogen to remove hazardous gases. Sorbent samples are analyzed for sulfur content using a LECO model 132 sulfur analyzer. This analyzer heats (furnace temperature = 2500°F) a weighed sample of sorbent in oxygen, driving off sulfur from the sample as SO_2. The gases from the combustion zone flow through an infrared cell for measurement of SO_2. Tungsten and iron powder accelerants are added to the samples to drive all of the sulfur from the sample. The analyzer is calibrated on a daily basis using NBS traceable coal standards. The results are used to perform mass balances around the adsorber and the regenerator.

In addition to the sulfur analysis samples, solid samples are taken from the process on a routine basis and analyzed in W.R. Grace laboratories. Table 4-4 lists the solids sampling locations, analysis frequency, and analysis performed. The cooler top bed was chosen as the primary sample location for sorbent samples since samples at this point are regenerated and have a sulfur content relatively independent of process conditions. Bottled samples are logged into W.R. Grace's Laboratory Information Management System (LIMS) system and sample labels printed and applied at the site. Analytical results are entered into the LIMS system and made available at the site via computer modem. Unanalyzed (retain) samples are taken and stored for possible future analysis should it be required.

Table 4-4. Sorbent Sampling Locations, Frequency and Analysis

Sample Location	Analysis	Frequency
Cooler top bed	S	4 times/day
Adsorber outlet	S	4 times/day
Middle regenerator	S	4 times/day
Bottom regenerator	S	4 times/day
Steam treater	S	4 times/day
Cooler top bed	ACS, SA, HGPV, TV, ICP, SiO_2	Daily
Cooler top bed	CBD, PSD, AJA	Twice weekly
Cooler top bed	Carbon	Weekly
Top J-valve	Carbon	Weekly
Middle J-valve	Carbon	Weekly
Baghouse	TV, ICP, PSD, SiO_2	Weekly
Adsorber cyclone dipleg	TV, ICP, PSD, SiO_2	Weekly
Adsorber outlet	S,N	Weekly
Makeup sorbent drums	ACS, CBD, SA, HGPV, TV	Each drum

ACS	-	Crush Strength
AJA	-	Air Jet Attrition
Carbon	-	Carbon Content
CBD	-	Compacted bulk Density
HGPV	-	Mercury Porosimetry
ICP	-	Elemental Analysis by Inductively Coupled Plasma
N	-	Nitrogen Content
PSD	-	Particle Size Distribution
S	-	Sulfur Analysis
SA	-	BET Surface Area
SiO_2	-	Silicon Measurement by ICP
TV	-	Total Volatiles (1750°C)

Analyses performed at the W.R. Grace laboratories measure both physical and chemical properties of the sorbent. Sorbent crush strength (ACS) is a measurement of the force required to break sorbent pellets. Loss of sorbent strength would indicate a loss of sorbent integrity and accompanying increases in sorbent attrition. The surface area analysis (SA) measures the total surface area of the sorbent on a mass basis. As with most adsorption processes, sorbent performance is strongly influenced by surface area. Mercury porosimetry (HGPV) measures the pore size distribution of the sorbent. Inductively Coupled Plasma (ICP) measures the metal contents of the sorbent. This is a check for any accumulating metals on the sorbent from process operation or flyash in the flue gas. Changes in sorbent particle size due to attrition of sorbent will appear in measurements of the compacted bulk density (CBD) and particle size distribution (PSD). The air jet attrition (AJA) test is a laboratory measurement of the sorbent's attrition resistance. The carbon analysis is for establishing a carbon balance of sorbent passing through the regenerator with the gas flows (natural gas, regenerator offgas, and steam treater offgas).

4.6 Plant Safety

The NOXSO POC pilot plant has been instrumented for intrinsically safe operation. The process and installation have been thoroughly reviewed to insure safe design and operation. There have been no lost-time accidents during the entire POC project. The process has operated safely for over 5213 hours on flue gas and 1615 hours hot inert operation during 18 months. This record is a direct result of proper design and operation of the NOXSO Process. Two system safety hazard analyses (what ifs) were performed by MK-Ferguson. One analysis was performed on the process as designed and a second after the process was constructed. W.R. Grace also performed two complete haz-op reviews of the process (one as designed, a second as installed). A safety inspection of the site and operation was performed by MK-Ferguson's director of corporate safety prior to system startup.

Nuclear level gauges are used at three locations in the pilot plant to measure the sorbent level. These gauges require five radioactive sources licensed by the U.S. Nuclear Regulatory Commission (NRC). The NRC performed a compliance inspection of the site in October 1992. Monthly inspections of these sources and procedures are performed by MK-Ferguson, with results sent to MK-Ferguson's director of radiation safety. All site workers use radiation film

badges to monitor the absence of exposure to the radiation sources. Monthly safety inspections are performed on safety equipment and the overall site by the NOXSO safety coordinator.

The process is controlled using a Bailey Network 90 Distributed Control System (DCS) with two operator interface stations. The DCS system has redundant control modules within the DCS, communication modules between the DCS and operator interfaces, and operator interfaces. If any of these items fail, the redundant module will automatically replace the failed module. Almost all of the process measurements and the control elements are tied into the DCS. The operator interface stations display measured values, control outputs, and sound alarms through over 20 graphic screens. The system was designed to shutdown safely in the event of a total power failure, with valve fail modes designed to shut off all natural gas to the tower and nitrogen purging of the regenerator.

Alarms on process values occur through the DCS and are displayed on the operator screens. The control system is designed to automatically take corrective action through process trips to insure process safety. A total of 34 process criteria interlock into 24 trip devices. Three independent trips exist to insure separation of the oxidizing environment in the heater/cooler system from the reducing environment in the regenerator. These are:

1. Sorbent heater bottom bed level: normal operation at 11" with trip at 3", measured by three separate pressure differential measurements and a nuclear level gauge.

2. Sorbent heater to regenerator differential pressure: normal operation at 10" H_2O. trip at 0" H_2O, measured by three separate pressure differential measurements.

3. Oxygen and methane measurements in the top and middle J-valves to detect gas transfer through the J-valve.

To ensure operator safety against hazardous gas leakage, the process tower is equipped with nitrogen purging of the regenerator and 16 remote gas sensors for H_2S (8 sensors), SO_2 (4 sensors), and CH_4 (4 sensors). These sensors are placed on the tower near areas of possible leaks. The sensor displays are in the control room and the sensor alarms are output to the DCS. A sounding alarm and flashing light at the base of the tower warns if concentrations of these gases exceed safe levels.

Operators are trained to operate the process safely, respond appropriately to process changes, and use proper safety equipment. A partial list of the available safety equipment is in Table 4-5. Hard hats, safety shoes, and safety glasses are required in the process area. Lockout procedures are used for all mechanical equipment and dangerous gases to ensure they will not be started during maintenance activities. Vessel entry forms are used for each process vessel to ensure safe confined space entry. Operator safety training includes an eight-hour, first-aid course certified by the Red Cross and eight hours of POC safety training. The POC safety training includes process review, hazard notification, respirator training, review of pertinent MSDS sheets, and use of safety equipment.

Table 4-6 shows the original trip initiators, their normal operating range, alarm points, and trip values for the process. When a trip occurs, the control system automatically takes action through 22 trip devices to protect personnel and equipment. Table 4-7 shows the 22 trip devices. Only some of which are activated for each trip initiator.

Table 4-5. Safety Equipment at the NOXSO POC
2 SCBA (self contained breathing apparatus) with 30 minute O_2 tanks
3 air line respirators, 2 emergency escape breathing apparatus
Dual cartridge respirators for organic and acid gases, dust masks
Earplugs, oxygen level meter, combustible gas meter, geiger counter, sound level meter
Drager tubes for H_2S, SO_2, CO, and NO_x concentration measurements
Dosimeter tubes for H_2S, SO_2, CO, and NO_x exposures
First aid kits, fire extinguishers (1 on each tower level and each trailer)
Emergency use oxygen (15 minute)
Available at power plant: backboard, blankets, resusci-kit

Table 4-6. Original Trip Initiators

Trip No.		Normal Operating Range	Alarm Point	Trip Point	Notes
1	High temperature at spray outlet (TAHH-107)	220-315°F	325°F	-----	
3	High gas temperature sorbent heater outlet (TAH-0533)	650-765°F	850°F	900°F	
4	Low ΔP bottom bed sorbent heater (PDALL-517)	5-9" H_2O	3.5" H_2O	2.0" H_2O	ΔP = 7.7" H_2O/ft sorbent bed height = 0.68-1.14 ft
5	High temperature bottom bed sorbent heater (TAHH-526)	1200-1250°F	1300°F	1325°F	Heater design temperature = 1400°
6	Low sorbent level bottom bed sorbent heater (LALL-501)	8-14"	5.5"	3"	Bed height = 0.68-1.14 ft
7	High skin temperature sorbent heater (TAHH-535)	1341-1381°F	1400°F	1425°F	Heater design temperature = 1400°F
8	Low aeration/lift flow heater/regenerator J-valve (FALL-557)	15"/scfm	10"/scfm	5"/scfm	
9	High aeration/lift flow heater/regenerator J-valve (FAHH-557)	15"/scfm	25"/scfm	30"/scfm	

Table 4-6. Original Trip Initiators					
Trip No.		**Normal Operating Range**	**Alarm Point**	**Trip Point**	**Notes**
10	Low sorbent level regenerator (LALL-302)	3-15 ft	2 ft	1 ft	
11	High skin temperature top of regenerator (TAHH-332 & TAHH-336)	1160-1250°F	1300°F	1350°F	Alarm set to indicate possible runaway reaction of CH_4 combustion
12	High ΔP between sorbent heater and regenerator (PDAHH-518)	8-12" H_2O	15" H_2O	20" H_2O	Pressure in regenerator is higher than pressure in sorbent heater
13	High skin temperature bottom of treater (TAHH-341)	1050-1200°F	1275°F	1325°F	
14	High oxygen in sorbent heater J-valve (AAHH-560A)	0%	0.5%	1.0%	
15	High methane in sorbent heater J-valve (AAHH-560B)	0%	0.5%	1.0%	
16	High oxygen in line between regenerator and incinerator (AAHH-324)	0%	0.5%	1.0%	
18	Low purge flow regenerator/cooler stripper (FALL-348)	6-12"/scfm	5"/scfm	3"/scfm	
19	High purge flow regenerator/cooler stripper (FAH-348)	6-12"/scfm	13"/scfm	-----	
20	High methane in sorbent cooler (AAHH-421)	0%	0.5%	1.0%	
22	High level bottom bed sorbent heater (LAHH-501)	8-14"	24"	-----	44'between grids
23	Low steam pressure in supply heater (PALL-703)	15 psi	12 psi	10 psi	
24	Low sorbent temperature in regenerator (TALL-352H)	1130-1250°F	1115°F	1100°F	
25	High temperature baghouse inlet (TAHH-120)	330-350°F	375°F	400°F	Bags designed for 400°F
26	Low pressure in air heater (PALL-803)	80-100 psi	70 psi	50 psi	
27	Incinerator trips out (UA-625) (vendor package)	-----	-----	-----	

Table 4-6. Original Trip Initiators					
Trip No.		Normal Operating Range	Alarm Point	Trip Point	Notes
28	Air heater trips out (UA-622) (vendor package)	-----	-----	-----	
29	Operator initiated trip	-----	-----	-----	
30	High ΔP bottom bed sorbent heater (PDAH-517)	5-9" H_2O	14" H_2O	-----	ΔP=7.7" H_2O/ft sorbent bed height=0.68-1.14 ft
31	High pressure sorbent cooler outlet (PAHH-402)	0.75-2.0 psig	2.8 psig	3.2 psig	Fan maximum discharge pressure=113" H_2O (4.1 psig)
32	High aeration/lift flow regenerator/cooler J-valve (FAH-322)	15"/scfm	25"/scfm	-----	
33	High O_2 regenerator/sorbent cooler line (AAHH-349)	0%	0.5%	1.0%	
34	Low ΔP between regenerator and incinerator (PDAHH-610)	10-70" H_2O	8" H_2O	4" H_2O	
37	Adsorber feed blower (K-101) not running (XI-116)	-----	-----	-----	
38	High purge flow to sorbent heater stripper (FAH-555)	6-12"/scfm	13"/scfm	-----	
39	Low purge flow to sorbent heater stripper (FALL-555)	6-12"/scfm	5"/scfm	3"/scfm	
40	Low aeration/lift flow to regenerator/cooler J-valve (FALL-322)	15"/scfm	10"/scfm	5"/scfm	
41	Low ΔP regenerator/cooler stripper (PDALL-309)	200-50" H_2O	30" H_2O	20" H_2O	
42	Low ΔP heater/regenerator stripper (PDALL-562)	200-50" H_2O	30" H_2O	20" H_2O	
43	Low sorbent level treater (LALL-303)	1'-9" - 10'	1'	0.5'	
44	Low ΔP between sorbent heater and regenerator (PDALL-518)	8-12" H_2O	5" H_2O	0" H_2O	
45	Operator initiated trip	-----	-----	-----	

Table 4-7. Trip Devices	
Stop natural gas to regenerator	Close CV-3021*
Shut down incinerator	UA-624
Shut down air heater	UA-623
Close isolation balves between regenerator and sorbent heater	CV-5023 & FV-566
Close isolation valves between regenerator and sorbent cooler	CV-4011 & FV-395
Stop steam to regenerator	Close CV-3019
Close isolation valve regenerator to incinerator	CV-3022
Stop adsorber feed blower	K-101
Stop cooling air blower	K-103
Stop dense phase conveying system,	Close CV-207A & D
Stop flow to heater/regenerator stripper	Close CV-5027
Stop flow to heater/regenerator J-valve	Close CV-5021
Stop flow to regenerator/cooler stripper	Close CV-3025
Stop sorbent flow through regenerator/cooler J-valve	Close CV-3027
Stop sorbent flow from surge bin	Close CV-4021
Start nitrogen purge to sorbent heater	Open CV-7030
Start purge to top of regenerator	Open CV-3820
Start purge to treater	Open CV-3026
Start purge of regenerator	Open CV-3017 & CV3018
Close spray water control valve	TV-107
Stop steam to natural gas preheat exchanger	Close CV-7024 &TV-804
Stop natural gas to regenerator and air heater	Close CV-8027

*Tag numbers from P&ID

During NOXSO POC operation some changes were made to the original trip matrix. These are summarized in Table 4-8. The J-valve gas flow Trips 8, 9, 18, 39, and 40 were found to be unnecessary, prone to frequent unnecessary trips, and redundant to other trips. They were deleted as trips. Because the regeneration of sorbent occurred at lower temperatures than originally anticipated, the trip for low sorbent temperature in the regenerator (Trip 24) was lowered from 1100°F to 1000°F. This was also incorporated as an interlock to prevent natural gas entry into the regenerator at average temperatures below 1000°F (Trip 46). The J-valve stripper differential pressure (Trips 41 and 42) were lowered to prevent unnecessary trips. The upper pressure taps for the differential pressure measurements were moved to the vessel itself (rather than having both pressure taps in the stripper section of the J-valve).

Table 4-8. Changes to Original Trip Matrix		
Trip No.	**Description**	**Change**
8	Low aeration/lift flow heater/regenerator J-valve (FALL-567)	Deleted Trip
9	High aeration/lift flow heater/regenerator J-valve (FAHH-567)	Deleted Trip
18	Low purge flow regenerator/cooler stripper (FALL-348)	Deleted Trip
39	Low purge flow to sorbent heater stripper (FALL-555)	Deleted Trip
40	Low aeration/lift flow to regenerator/cooler J-valve (FALL-322)	Deleted Trip
24	Low sorbent temperature in regenerator (TALL-352H)	Alarm at 1025°C Trip at 1000°C
25	High temperature baghouse inlet (TAHH-120)	Alarm at 450°F Trip at 475°F
41	Low ΔP regenerator/cooler stripper (PDALL-309)	Alarm at 3" H_2O Trip at 1" H_2O
42	Low ΔP heater/regenerator stripper (PDALL-562)	Alarm at 5" H_2O Trip at 3" H_2O
14	High oxygen in sorbent heater J-valves (AAHH-560A)	Alarm at 5% O_2 Trip at 10% O_2
15	High methane in sorbent heater J-valves (AAHH-506B)	Alarm at 2.5% CH_4 Trip at 5%CH_4
16	High oxygen in line between regenerator and incinerator (AAHH-324)	Alarm at 5% O_2 Trip at 10% O_2
20	High methane in sorbent cooler (AAHH-421)	Moved to Incinerator Outlet, Alarm at 1% CH_4
33	High O_2 regenerator/sorbent cooler line (AAHH-349)	Alarm at 5% O_2 Trip at 10% O_2
46	Upper regenerator/average temperature (TI351 AVG)	Interlock Trip at 1000°F
47	Incinerator low temperature (TSL-608)	Alarm at 950°F Trip at 900°F

Process gas measurements of oxygen and methane were found to trip principally due to analyzer malfunction. The measurement cells for oxygen were changed and the trip points increased to more appropriate levels (Trips 14, 15, 16, and 33). The methane alarm and trip on the sorbent cooler were found to be unnecessary. The cooler air flow is typically 2800 scfm while the natural gas flow to the regenerator is 15 scfm. This gives a maximum concentration of 0.5 volume percent if all the natural gas going into the regenerator came out through the cooler. This analyzer sample point was moved to the incinerator outlet for natural gas measurement. An additional Trip 47 was added to the process to cut the incinerator should its combustion chamber temperature fall below 700°F.

There is some redundancy with respect to trips on the pilot unit which should be removed on commercial units. The sorbent heater bottom bed level is measured by three differential pressure transmitters and a nuclear level gauge. Both these level indicators have alarm levels and trips. For commercial units, this should be reduced to one differential pressure measurement and a nuclear gauge or two differential pressure measurements. This would leave two measurements of the heater bottom bed level for independent trips on the level, while removing some redundancy. (The two differential pressure measurements would be less expensive than a differential pressure measurement and nuclear level gauge.)

There are three differential pressure transmitters monitoring the pressure difference between the bottom bed of the heater and the regenerator. These could be reduced to two transmitters in a commercial unit. The stripper gas inlets on the J-valves should be reduced from four inlets to a single steam inlet. The stripper gas is used on the sorbent heater to regenerator J-valve (FI-5059, using a single steam inlet) while the J-valve stripper gas between the regenerator and sorbent cooler is unused.

The pressure measurement between the slide gate valves on the sorbent heater to regenerator (PT-563) and regenerator to sorbent cooler J-valves (PT-433) are unused and should be deleted from future installations. They were originally installed to measure the pressure between the two slide gates when the slide gates were both shut. The pressure transmitter lines are frequently plugged with sorbent and the slide gates bypass sufficient gas that the pressure never builds in the manner originally anticipated.

It is not necessary to purge the regenerator with high volumes of nitrogen whenever a trip occurs. The purge nitrogen flows from pressure transmitters and sorbent sampling stations are sufficient to maintain regenerator pressure in the event of trips.

These process control changes can be made without any compromise to operating safety.

5.0 MATERIALS OF CONSTRUCTION

Material tests collected performance data on construction materials used at the NOXSO POC and possible materials which could be used in future NOXSO installations. Corrosion data on materials has been measured via corrosion coupons mounted in vessels during process operation, periodic vessel inspections, and accelerated corrosion tests in the laboratory.

5.1 Vessel Corrosion Coupons

Corrosion coupons were used for corrosion measurements at seven locations in vessels at the POC. Corrosion test racks containing metal test samples were installed prior to startup of the facility and removed for examination and analysis at the end of 5500 hours of process operation. Figure 5-1 shows a test rack with installed sample coupons. The samples were exposed to approximately 18 months of total operation (including shakedown and startup). Coupon weights, dimensions, and physical conditions were measured before and after exposure. These results were used to calculate corrosion rates of the materials.

Seven corrosion racks were installed at different locations to provide corrosion data for specific components of the process. Table 5-1 summarizes the rack locations and components corresponding to the locations. Racks 1 and 2 measured corrosion rates before and after flue gas contact with the sorbent. Rack 3 measured corrosion rates between the air heater and sorbent heater. This area contains hot air with combustion products from the air heater. Racks 4 through 7 measured corrosion rates in the regenerator, with Rack 5 contacting sorbent in the regenerator. Test materials were chosen to include materials with both high and low corrosion rates for comparison purposes. The coupons on each rack are summarized in Table 5-2.

Table 5-1. Location of Vessel Corrosion Coupons

Rack Number and Location	Components
1. Adsorber inlet	Ductwork between spray cooler and adsorber, base of adsorber, and adsorber gas distributor.
2. Adsorber outlet (top of adsorber)	Adsorber (above distributor), adsorber cyclone, and ductwork between adsorber and stack.
3. Air heater outlet	Air heater, duct between air heater and sorbent heater, bottom gas distributor in sorbent heater, and sorbent heater.
4. Regenerator (top of methane regenerator)	Methane regenerator, piping between regenerator and incinerator, and control valves on piping.
5. Regenerator (sorbent bed)	Methane regenerator, sorbent transfer line from sorbent heater to regenerator, and any vessel surface in contact with sorbent beads.
6. Steam treater (top of steam treater)	Steam treater, piping between steam regenerator and incinerator, and control valves on piping.
7. Steam treater (middle of steam treater)	Steam treater and vessel surface in contact with sorbent.

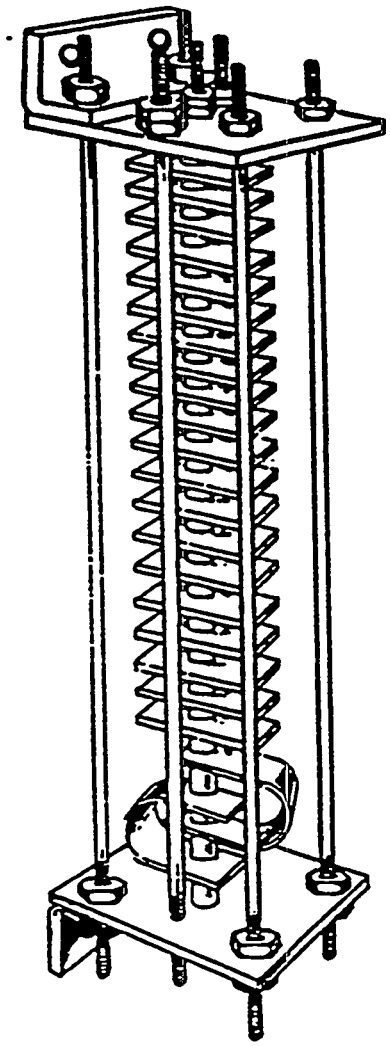

Figure 5-1
Corrosion Spool Test Rack

Table 5-2. Types of Coupons on Corrosion Test Racks							
	Corrosion Coupon Racks						
Materials	**1**	**2**	**3**	**4**	**5**	**6**	**7**
Stainless Steels							
304 SS	2	2	2	1	1	1	1
304H SS			1	1	1	1	1
316 SS	2	2	2	2	2	2	2
446 SS	2	2	2	2	2	2	2
Carbon Steels							
C1010	2	2	2	1	1	1	1
Hastelloy C -276	2	2					
Hastelloy C -22	2	2					
Hastelloy C -4	2	2					
Haynes 556	2	2	2	1	1	1	1
Haynes HR-160	2	2	2	1	1	1	1
Carpenter 20Cb3	2	2					
Jessop C276	2	2					
INCO C-276	2	2					
INCO 625	2	2					
Teflon	2	2					
Alonized							
Alonized 304 SS			2	2	2	2	2
Alonized 304H SS			1	1	1	1	1
Alonized 316 SS			1	1	1	1	1
Alonized C1010			2	2	2	2	2
Weld Overlay							
304 SS w/ 556 Weld			2	2	2	2	2
304H SS w/ HR-160 Weld			1	1	1	1	1
304 SS w/ 446 Weld			2	2	2	2	2
304H SS w/ 446 Weld			1	1	1	1	1
Spray Coated After Welds							
Alonized 304H SS				1	1	1	1
Alonized 304				1	1	1	1
304 SS				1	1	1	1
304H SS				1	1	1	1
Backing Ring Coupon				1	1	1	1
Numbers in table indicate number of coupons of each type on rack .							

Rack 4 was removed from the regenerator after 1110 hours of exposure. The corrosion of coupons on this spool was substantial, and this was the area of the most severe corrosion in the process. The coupons were photographed, weighed, replaced on the rack, and placed into the regenerator for further exposure. Some of the coupons showed substantial corrosion while others were unchanged. The HR160, alonized 304, alonized 304H, and alonized 316 were visually unchanged and had corrosion rates of less than 0.3 mils/yr. The 556 and 446 coupons showed minor corrosion while the unalonized 304, 304H, and 316 stainless showed substantial corrosion. The C1010 coupon had massive corrosion with expansion of the coupon. The alonized C1010 coupon showed some corrosion on the edge of the coupon.

All the corrosion racks (except the air heater outlet) were removed from the process after 5500 hours of operation. The coupons were photographed, cleaned of scale (scale was retained), dimensioned and weighed. Selected coupons were cross sectioned for measurement of weld corrosion and corrosion of the alonized finish on coupons.

Average exposure conditions for each of the corrosion coupon racks are summarized in Table 5-3. Coupon corrosion rates are summarized in Table 5-4 and 5-5. The HR160 and alonized coupons showed minimal weight loss in both the regenerator and steam treater. The 446 coupons had corrosion rates of 2.4 to 4.1 mils/yr in the regenerator and minimal corrosion in the steam treater. The stainless steels (304H, 304, 316) had substantial corrosion in the regenerator (24 to 51 mils/yr) but much lower corrosion rates in the steam treater (3 to 10 mils/yr). The 304 and 304H stainless steel coupons performed better than the 316 stainless in both the regenerator and steam treater. The alonized C1010 carbon steel showed corrosion through the alon layer, with much more corrosion in the regenerator than the steam treater.

Table 5-3. Average Exposure Conditions for the Corrosion Test Racks

	Adsorber Inlet	Adsorber Outlet	Regenerator	Steam Treater	Air Heater Outlet
Temperature, °F	320	329	1123	1100	1350
Gas Composition					
H_2O	8.5%	8.5%	59.2%	74.2%	4.0%
CO_2	12.0%	12.0%	10.7%	1.0%	1.7%
SO_2	1800 ppm	180 ppm	13.5%	0.6%	7 ppm
NO_x	300 ppm	45 ppm			5 ppm
O_2	9.0%	9.0%			18.5%
N_2	70.3%	70.5%	4.5%	12.8%	75.8%
CH_4			7.6%	3.6%	
H_2S			3.5%	7.8%	
COS			0.2%	0.0%	
CS_2			0.8%	0.0%	

Table 5-4. Corrosion Rates in Regenerator and Steam Treater				
Coupon	Corrosion Rates, mils/yr			
	Top Regenerator	Middle Regenerator	Steam Treater	Steam Treater
HR160	-0.04	0.18	0.04	0.04
304, Alonized	0.15	0.14	0.32	0.33
304, Alonized	0.15	0.20	0.27	0.28
304H, Alonized	0.10	0.02	0.09	0.12
316, Alonized	0.01	0.07	0.06	0.12
556	2.71	4.96	0.52	-0.42
446	2.40	4.02	-0.04	0.03
446	3.12	4.06	-0.46	0.25
304H	25.12	40.24	4.26	3.04
304SS	22.82	23.89	2.91	2.93
316	47.75	43.52	9.72	10.07
316	32.07	51.60	9.74	10.16
C1010, Alonized	17.45	13.84	0.85	1.36
C1010, Alonized	20.67	16.46	0.92	1.29
C1010	Massive corrosion with expansion of coupon			

1 mil = 0.001 inch
Coupons in place 6/20/91 through 1/1/93
5500 hours flue gas and 1700 hours hot inert
(5550 hours used for rate calculation)

Table 5-5. Corrosion Rates in Adsorber Inlet and Outlet		
Coupon	Corrosion Rate, mils/yr	
	Adsorber Inlet	Adsorber Outlet
C4	0.09	0.01
C4	0.08	-0.02
C276	0.07	0.01
C276	0.09	-0.01

Table 5-5. Corrosion Rates in Adsorber Inlet and Outlet		
	Corrosion Rate, mils/yr	
Coupon	Adsorber Inlet	Adsorber Outlet
316	0.14	0.00
316	0.19	-0.02
INCO 625	0.00	0.01
INCO 625	0.04	-0.02
20CB3	0.09	0.00
20CB3	0.11	-0.00
Jessop C276	0.06	-0.00
Jessop C276	0.09	-0.00
C22	0.05	-0.01
C22	0.10	-0.01
C1010	3.69	2.11
C1010	3.78	2.08
304	0.44	0.02
304	0.48	0.01
INCO C276	0.08	-0.01
INCO C276	0.10	-0.03
446	2.09	0.10
446	1.62	-0.06
Teflon	0.06	-0.16
Teflon	0.09	-0.10
1 mil = 0.001 inch Coupons in place 6/20/91 through 1/1/93 5500 hours flue gas and 1700 hours hot inert (5550 hours used for rate calculation)		

The adsorber inlet and outlet racks showed significantly more corrosion ont he inlet than outlet. On the inlet the carbon steel corroded at 3.7 mils/yr and this was reduced to 2.1 mils/yr ont he adsorber outlet. The stainless steels corroded at 0.17 mils/yr (316 SS) and 0.46 mils/yr (304 SS) at the adsorber inlet. The specialty alloys for flue gas acid performed with corrosion rates below 0.10 mils/yr at the adsorber inlet. These metals include: C4, C276, INCO 625, 20 CB3, Jessop C276, C22 and INCO C276. These alloys should be considered equivalent in this application based on these results. All materials tested (with the exception of carbon steel) showed no measurable corrosion on the adsorber outlet.

5.2 Accelerated Corrosion Tests

Accelerated corrosion tests were also performed to supplement data collected from the corrosion coupons installed in POC vessels. These tests were conducted by Corrosion Testing Labs Inc. of Wilmington, Delaware. Corrosion coupons were placed into environments similar to, but substantially more corrosive than, the actual process. This allowed the coupons to corrode at a rapid rate and produce data for comparison of different materials. The coupons were identical to those tested in the POC regenerator.

A total of six tests were conducted at three different temperatures and two different gas conditions. These test conditions are listed in Table 5-6:

Table 5-6. Corrosion Test Conditions

Test No.	Temp (°F)	Gas Composition	Exposure Time
1	1400	50% H_2O, 20% SO_2, 20% CO, 10% H_2	186 hours
2	1600	50% H_2O, 20% SO_2, 20% CO, 10% H_2	121 hours
3	1800	50% H_2O, 20% SO_2, 20% CO, 10% H_2	160 hours
4	1400	50% H_2O, 50% H_2S	168 hours
5	1600	50% H_2O, 50% H_2S	171 hours
6	1800	50% H_2O, 50% H_2S	348 hours

Figure 5-2 is a diagram of the experimental apparatus. The corrosion coupons were placed on a glass rack (with ceramic spacers between coupons) and inserted into a ceramic tube. NOXSO sorbent from the NOXSO POC was used to fill the ceramic tube and surround the coupons. The ceramic tube was capped at each end, placed into the temperature controlled furnace, and connected to the gas feed system. The ceramic tube, sorbent, and coupons were heated to the desired temperature with nitrogen flowing through the apparatus. After heatup, the appropriate gas mixture was mixed using rotameters and water was vaporized for steam in the gas preheater. Total gas flow was 100 cc/min into the apparatus. Gases leaving the pipe pass through a scrubber for H_2S and SO_2 prior to venting. Results from the accelerated corrosion test are summarized in Table 5-7. These accelerated corrosion results show large variations between many of the duplicate samples. The corrosion rates measured are in mils/day and should be used only as a general measurement of the sample performanc eat the tested conditions. In general, the alonized coupons performed better than the unalonized metals. HR160 performed very well in comparison to the other materials.

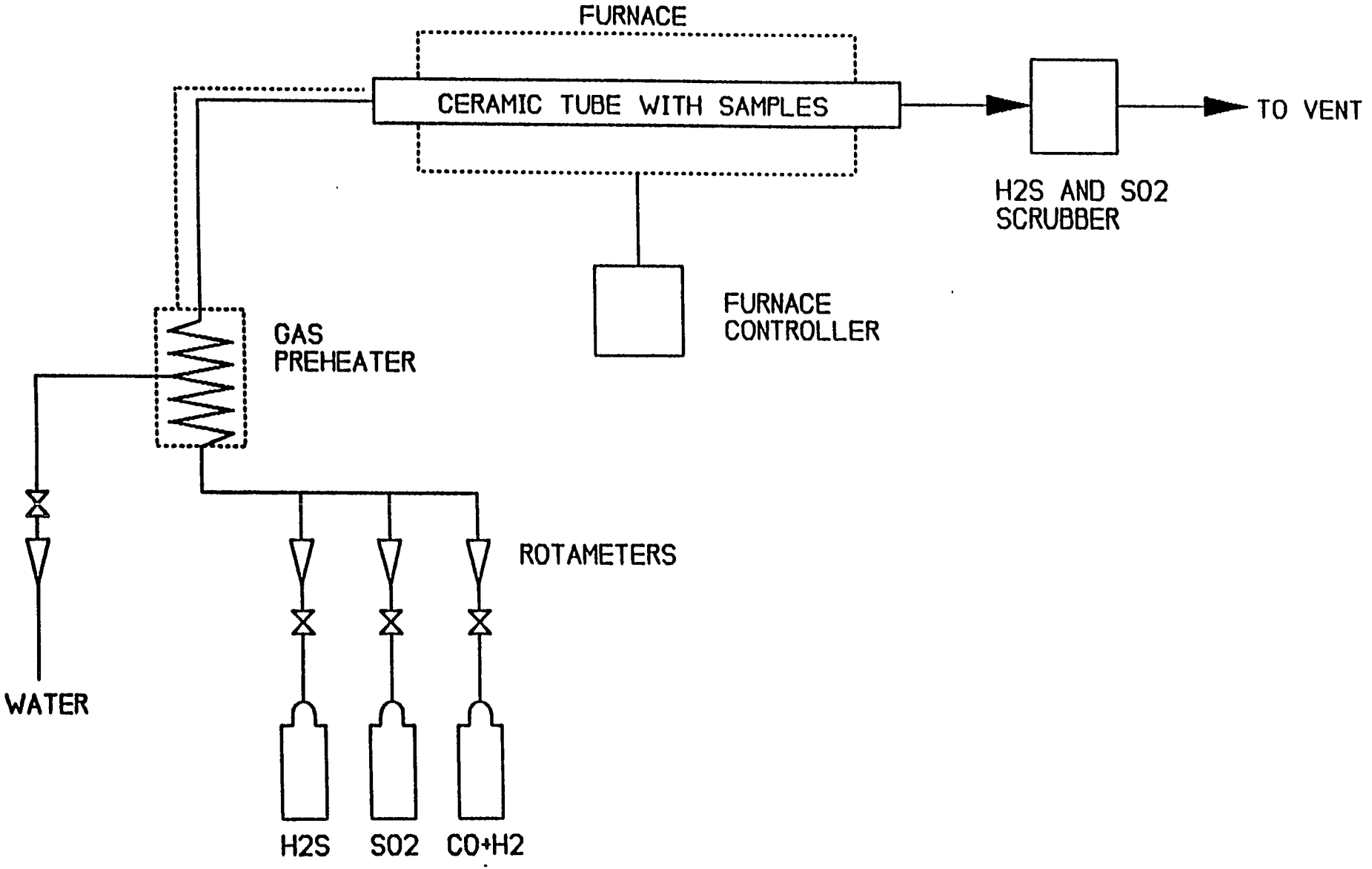

Figure 5-2
High Temperature Corrosion Test Apparatus

Table 5-7. Accelerated Test Results

Coupon	50% Steam and 50% H_2S					
	1400°F		1600°F		1800°F	
	Rate, mpd	Notes	Rate, mpd	Notes	Rate, mpd	Notes
Stainless Steels						
304 SS	1.0	I	17.0			D
304H SS	0.6	I		D		D
316 SS	1.0	I	12.0	G,I		D
316 SS	1.0	I		D	6.0	I,P
446 SS	3.0	I	11.0	G,P,I	0.3	G
446 SS	1.0	I	5.0	G	0.3	G
Carbon Steel						
1010 CS		D	969.0	G		D
1010 CS		D		D		D
Alonized						
304 SS	3.0	I	2.0	S		D
304H SS	2.0	I	0.6	S		D
1010 CS	2.0	I,P		D		D
1010 CS	3.0	P	720.0			D
316 SS	3.0	C	1.0	S	4.0	I
316 SS	2.0	C	2.0	S		D
Misc Metal						
HR 160	0.9	I	0.3	G		D
Haynes 556	0.1	I	12.0	I	3.0	I,P
Weld Overlay						
304H with HR 160	0.6	G	8.0	I		D
304H with HR 160	0.1	G	9.0	I		D
304 with 556	15.0	I	0.4	S,G		D
304H with 446	2.0	I		D		D
304 with 446	1.0	I		D		D

Notes: D - Destroyed
I - Intergranular corrosion
N - No corrosion
P - Pitting corrosion
M - Minor corrosion
C - Corrosion
G - General corrosion
S - Slight corrosion

The thermal spray on thermal sprayed coupons separated from the coupons.

Table 5-7. Accelerated Test Results (continued)

Coupon	50% Steam, 20% SO_2, 20% CO, and 10% H_2					
	1400°F		1600°F		1800°F	
	Rate, mpd	Notes	Rate, mpd	Notes	Rate, mpd	Notes
Stainless Steels						
304 SS	0.1	M	0.9	M	13.0	G,I
304H SS	0.3	M	0.8	M	1.0	M,G
316 SS	0.6	M,G	2.0	G	1.0	G
316 SS	0.6	M,G	2.0	G,P	0.8	G
446 SS	0.5	G	0.8	G	0.7	G
446 SS	1.0	G	0.9	G	0.7	G
Carbon Steel						
1010 CS	4.0	G	6.0	G		D
1010 CS	7.0	G	10.0	G		D
Alonized						
304 SS	2.0	P	2.0	P	2.0	P
304H SS	4.0	P	2.0	P	3.0	P
1010 CS	3.0	P	4.0	P		D
1010 CS	3.0	P	3.0	P		D
316 SS	3.0	P	3.0	P	3.0	C
316 SS	2.0	P	4.0	P	4.0	P
Misc Metal						
HR 160	0.9	M	0.6	M	0.6	M
Haynes 556	0.5	M,G	0.0	M	1.0	G
Weld Overlay						
304H with HR 160	0.0	M	0.2	M	0.6	M
304H with HR 160	0.0	M	0.0	M	0.2	M
304 with 556	0.9	M	0.0	M		D
304H with 446	0.0	M	0.2	M		D
304 with 446	0.2	M	0.3	M		D

Notes: D - Destroyed
M - Minor corrosion
I - Intergranular corrosion
C - Corrosion
N - No corrosion
G - General corrosion
P - Pitting corrosion
S - Slight corrosion
The thermal spray on thermal sprayed coupons separated from the coupons.

5.3 Vessel Inspections

Vessel inspections were performed on a routine basis at the NOXSO POC. Each inspection involved: 1) ultrasonic testing to determine erosion/corrosion of vessel thickness, 2) visual inspection, and 3) liquid penetrant testing of regenerator vessel welds. These inspections were conducted by Professional Service Industries, Inc. of Pittsburgh, Pennsylvania, and were performed on October 31, 1991, December 30, 1991, April 29, 1992, and February 1, 1993. Ultrasonic measurements were performed at locations outlined in Table 5-8. The results of these ultrasonic tests showed no measurable erosion or corrosion at any of the points tested. Regenerator welds were visually inspected and dye penetrant tested. The only difficulty with the regenerator welds was the flaking of the 446 thermal spray coating. No attack of the welds was observed and this flaking was caused by the differential thermal expansion of the 446 spray coat and metal vessel. The regenerator was also inspected by a W.R. Grace consultant (J.H. Van Sciver, P.E.) on March 5, 1992 and on February 1, 1993. His inspection determined the regenerator welds to be in good condition and that the 446 spray coat was cracked and disbonding at the top of the regenerator. One area in the regenerator showed pitting of the alon finish and corrosion of the base metal. This area was approximately 2" x 1/2" in size and 1/32" deep.

Table 5-8. POC Vessel and Piping Inspection Locations

Location	Inspection
Sorbent heater	Ultrasonic, 3 outside and 36 inside vessel
Regenerator	Ultrasonic, 4 outside, Internal visual inspection, Liquid penetrant testing of internal welds
Adsorber	Ultrasonic, 2 outside, Internal visual inspection
Sorbent cooler	Internal visual inspection
J-valve elbows (3)	Ultrasonic, on outside of elbow
Regenerator offgas elbow	Ultrasonic, on outside and inside of elbow

There has been only one corrosion problem during operation of the NOXSO POC Process. (This was when the incinerator outlet ductwork corroded through near the exit of the incinerator.) This occurred because the steam from the regenerator methane preheater was vented into the duct at this point. This steam/water mixture combined with the SO_2 in the incinerator offgas to form sulfuric acid at this point in the duct. The duct was repaired, the steam was rerouted to a steam trap, and the problem was eliminated.

6.0 SORBENT PROPERTIES

The NOXSO sorbent is prepared by spraying Na_2CO_3 solution on γ-alumina spheres to incipient wetness. The wet γ-alumina is dried with air and then calcined. The sorbent used in the POC tests was manufactured by the Davison Division of W.R. Grace.

The sorbent has experienced more than 5213 hours on flue gas and 1615 hours of hot inert operation in the POC tests. The properties of the fresh and the cycled sorbent after regeneration are listed in Table 6-1.

Table 6-1. Sorbent Properties

	Fresh*	After 5213 Flue Gas Hours
Sodium, wt%	5.2	5.0
Surface area, m^2/g	250.0	150.0
Compact bulk density, lbs/ft^3	40.0	42.0
Crush strength, kg	3.8	2.3-4.5
Hg Porosimeter Measurements		
Pore volume, cm^3/g	0.65	0.66
Total porosity, cm^3/cm^3	0.65	0.62
Particle density, g/cm^3	1.0	1.06
Particle Size Distribution (U.S. mesh)		
Retained on 10 mesh, wt%	0.0	0.0
Retained on 12 mesh, wt%	3.0	1.3
Retained on 14 mesh, wt%	15.0	13.6
Retained on 16 mesh, wt%	45.0	42.7
Retained on 18 mesh, wt%	30.0	35.1
Retained on 20 mesh, wt%	7.0	7.2
Mean particle diameter, um	1230.0	1210.0

* The values listed under fresh column are the specification from the sorbent manufacturer.

Only the sorbent surface area shows a significant change, from 250 down to 150 m^2/g. The major loss of sorbent surface area occurred in the beginning of the POC test. Figure 6-1 shows the change of the sorbent surface area on a daily basis. The rate of surface area loss stabilized after December 15, 1991 which corresponded to 350 flue gas hours. Since the loss of surface area reduces the sorbent's ability to remove NO_x and SO_2 from the flue gas. the loss of sorbent surface area must be considered in the design of the NOXSO Process. The design must be based not on the fresh sorbent but on the sorbent after the surface area has stabilized.

Figure 6-1

Pilot Plant Sorbent Surface Area Decay

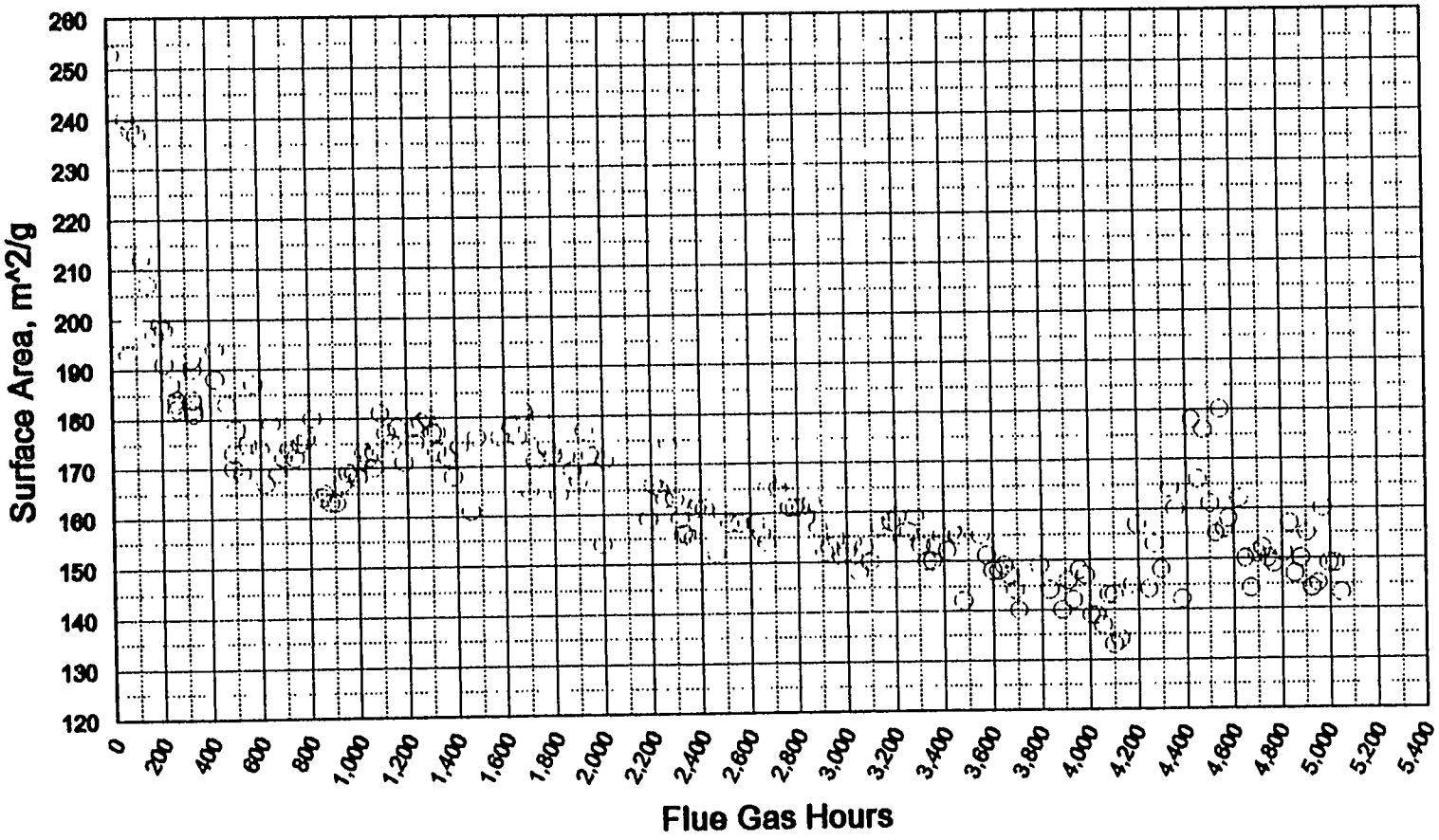

Surface area stabilizes when the rate of surface area added by sorbent makeup equals the rate of surface area decline in the system. Since the rate of sorbent makeup at the POC was relatively low, the sorbent surface area continued to decline after December 15, 1991, but at a much slower rate (See Figure 6-1). The chloride content of the sorbent was also monitored since chlorides are present in the flue gas. Figure 6-2 shows the results. High chloride content was only found in the beginning of the POC test. No sign of chloride accumulation on the sorbent was found.

Sorbent samples were taken once a day from the top bed of the sorbent cooler and tested for crush strength, surface area, pore volume, total volatiles, silica and metals content. Metals were analyzed using PIXE (Proton Induced X-Ray Emission) and ICP (Inductively Coupled Plasma). The ICP method analyses for the following elements and oxides: CaO, MgO, Fe_2O_3, TiO, ZNO, Al_2O_3, SO_4, P_2O_5, K_2O, MoO_3, Li_2O, SiO_2, Pb, Ni, Cu, Cr, Mn. Sb, Sc, and Re_2O_3. Many analytes are reported as weight percent oxide, although the analyte may exist in other chemical forms (e.g., CaO may exist as $CaCO_3$). The ICP graphs in this report; however, give the result in terms of percent elemental content. The same is true for the PIXE results, so the two data sets can be directly compared.

The data encompasses the period: December 3, 1991 through December 7, 1992. The data are summarized in Tables 6-2 and 6-3. The complete set of data is given in Appendix F.

Figure 6-2
Sorbent Chloride Content

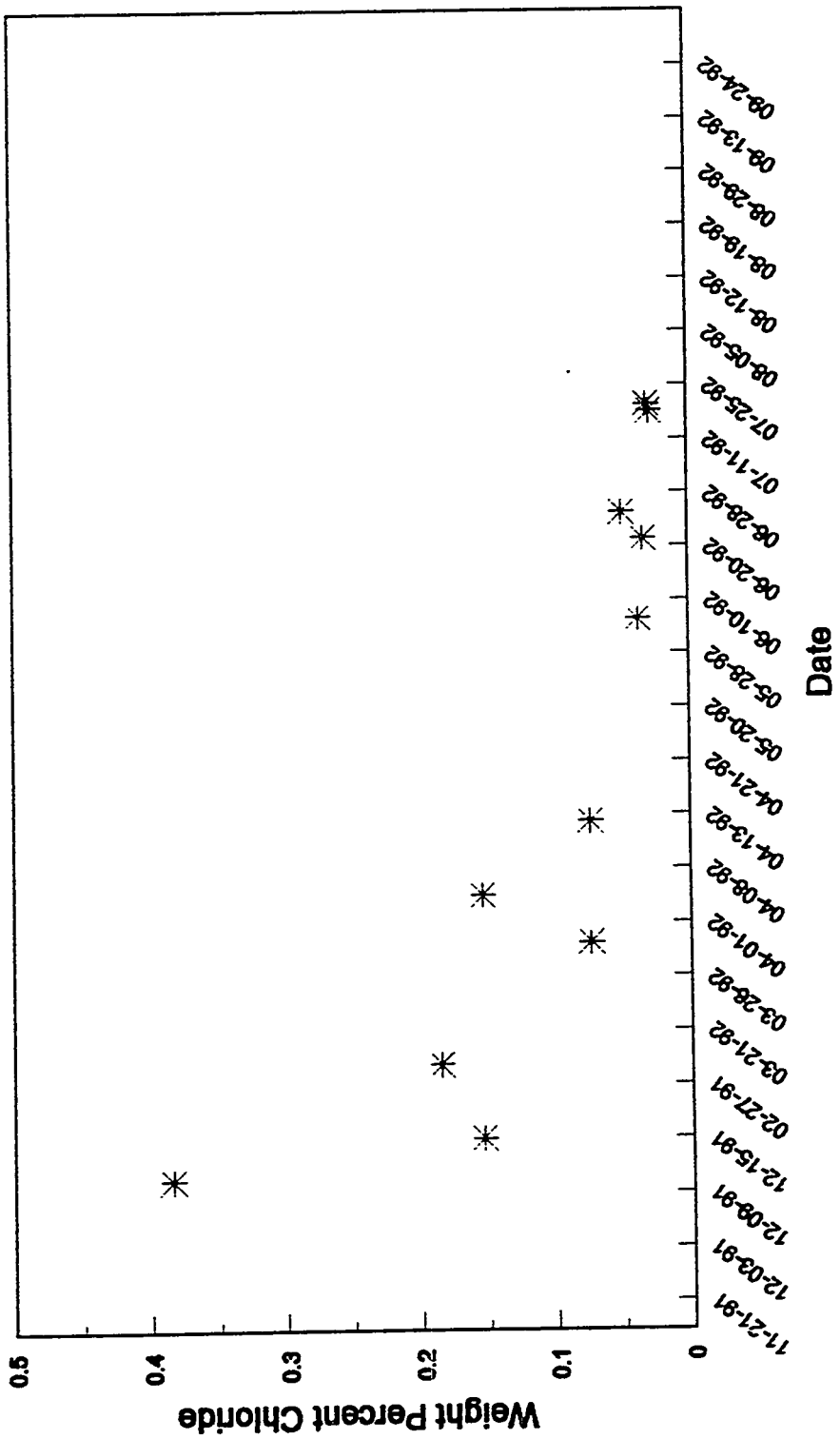

Table 6-2. Summary of ICP Data	
Element	**Results**
Calcium	Very slight increase detected 0.075 - 0.090%
Potassium	Trace amounts detected
Magnesium	Status quo, 0.01%
Iron	Increasing, 0.04 - 0.12%
Titanium	Status quo, less than 0.01%
Zinc	Oscillating between the range of 0.0006 - 0.0036%
Phosphorus	Detected between 2000 to 3000 hours (0.015 - 0.030%) and between 4200 to 4400 hours (0.030 - 0.035%). During the majority of the pilot plant run time, it was not detected.
Molybdenum	Trace
Lithium	Status quo, 0.0009%
Chromium	Status quo, 50 - 60 ppm
Copper	Detected 10 - 40 ppm
Manganese	Status quo, 25 - 28 ppm
Scandium	Detected 5 - 15 ppm
Lead	None detected by ICP throughout pilot plant run time.
Silica	Slight increase detected. ZRD was performed on a cooler sample (4904 flue gas hours), no crystalline silica was detected. Microprobe analyses will be conducted on several pilot plant samples taken at different pilot plant run times to determine if any minute quantities of crystalline silica are present and also, to determine if there is any silica present on the sorbent surface.

Table 6-3. Summary of PIXE Data	
Element	**Results**
Magnesium	Status quo, 0.2 - 0.35% detected
Silicon	Slight increase detected
Sulfur	Status quo, 0.15 - 0.35% detected
Chlorine	Gradual decrease from initial point down to 0.1 - 0.15%
Potassium	Increased from 0 - 250 ppm
Calcium	Increased from 500 - 1000 ppm
Titanium	Status quo, 5 - 30 ppm
Vanadium	Sporadic
Chromium	Slight increase 20 - 40 ppm
Iron	Increasing 0.05 - 0.15%
Manganese	Status quo, 15 - 30 ppm
Nickel	Increasing 6 - 16 ppm
Copper	Trace 1.5 - 3.5 ppm
Zinc	Increasing 0 - 10 ppm (Trace)
Gallium	Slight increase 45 - 55 ppm (Trace)
Arsenic	Increasing 1 - 18 ppm (Trace)
Selenium	Sporadic
Bromine	Decreasing 25 - 3 ppm (Trace)
Rubidium	Decreasing 1.8 - 0 ppm (Trace)
Strontium	Gradual increase 5 - 11 ppm (Trace)
Yttrium	Decreasing 2 - 0 ppm (Trace)
Zirconium	Increasing 5 - 12 ppm (Trace)
Molybdenum	Status quo, 5 ppm (Trace)
Silver	Trace
Lead	Increasing 1 - 8 ppm (Trace)
Please note that throughout the time span this package encompasses, none of the following elements were detected: Ru, Rh, Pd, Ag, Cd, In, Sn, Sb, Te, I, Cs, Ba, La, Ce, Pr, Nd, Pm, Sm, Eu, Gd, Tb, Dy, Ho, Er, Tm, Yb, Lu, Hf, Ta, W, Re, Os, Ir, Pt, Au, Hg, Bi, Th, U.	

7.0 SORBENT ATTRITION

Sorbent attrition is caused by physical and thermal stresses that come to bear on the sorbent as it is transported through the processing loop and as it resides in the fluid beds. These stresses can fracture sorbent beads and/or erode the surface of the beads. If the sorbent bead becomes small enough, it can be entrained by the gas and exit the fluid bed. Sorbent makeup is then required to maintain a constant sorbent inventory.

Sorbent is entrained by the gas when the gas velocity through the bed equals or exceeds the terminal or free-fall velocity of the sorbent particle. The terminal velocity is a function of sorbent particle diameter, particle and gas density, and gas viscosity. It can be shown that a spherical particle with a diameter of 302μm has a terminal velocity of three feet per second, which is the design gas velocity in the adsorber. The initial sorbent inventory placed in the NOXSO pilot plant had a mean particle diameter of 1230 microns. (For particle size distribution test data see Section 6.) At the design gas velocity of three feet per second, only sorbent with a diameter less than 302μm will be entrained by the gas.

7.1 Sorbent Makeup

The rate of sorbent attrition equals the rate of sorbent makeup provided the starting and ending sorbent inventories are equal. The sorbent makeup rate at the NOXSO pilot plant is summarized in Table 7-1. The sorbent inventories given in the footnote to Table 7-1 are estimated on the basis of measured reactor bed levels, fluid bed differential pressures, and estimated dense phase lift and J-valve sorbent inventories.

Table 7-1. Sorbent Makeup Rate

Operation	
Start date	7/17/92
End date	2/11/93
Flue gas, hrs	3,232
Sorbent Inventory	
Total makeup, lbs	20,307
Sorbent lost, lbs[1]	- 6,415
Increase in sorbent inventory, lbs[2]	+ 4,245
Net Sorbent Makeup, lbs	**9,647**
Sorbent Makeup Rate, lb/hr	**2.99**

(1) Operator error resulted in several sorbent discharges to the flue gas return duct. Although the weight of the discharge was not directly measured, an estimate of 6,415 pounds was made on the basis of the amount of sorbent added after each discharge to restore system inventory.

(2) Starting sorbent inventory = 27,000 lbs (estimated)
Ending sorbent inventory = 31,245 lbs (weighed)

7.2 Baghouse Collection Data

A single compartment, pulse-jet cleaning baghouse was used to collect attrited sorbent fines. Both adsorber offgas and sorbent heater offgas were passed through the baghouse before the combined gas streams were returned to the power plant ductwork. The single compartment baghouse contains approximately 330 bags. The bags are fiberglass with a Teflon B finish and have a maximum sustained operating temperature of 500°F. The frequency of pulse-jet cleaning is dictated by the pressure drop across the baghouse. The cleaning cycle begins when the pressure drop across the baghouse exceeds 7.5" H_2O.

Figure 7-1 shows a plot of cumulative hours of operation (both on flue gas and hot inert) versus the cumulative amount of fines collected in the baghouse. A least-square linear regression gives the line shown in the figure. The correlation coefficient (r-squared) equals 0.98, indicating a good fit. The slope of this line is equal to the baghouse collection rate. The baghouse collection rate is 1.59 pounds per hour. The use of baghouse collection data to quantify the rate of sorbent attrition is limited by the following:

- The material collected in the baghouse is a mixture of sorbent and flyash. The NOXSO adsorber is downstream of the power plant's electrostatic precipitator (ESP) so that the flue gas entering the adsorber contains approximately 0.5% to 5% of the total flyash leaving the boiler. Since the flyash is an order of magnitude smaller than the sorbent, the ash that passes through the precipitators passes through the fluidized bed adsorber and is collected in the baghouse. Since the sorbent is chemically similar to the flyash, it was not possible to determine by chemical analysis how much of each was collected in the baghouse. Therefore, to be conservative, all of the material collected in the baghouse was assumed to be attrited sorbent.

- The baghouse is not leak-tight. The baghouse was used previously in the HALT project and required extensive repairs prior to NOXSO operation. It was not possible to completely seal dampers in the baghouse bypass line and to completely seal the pressure relief valve in the baghouse inlet line. The sorbent attrition rate estimated from the baghouse collection data is then lower than actual by the amount of attrited sorbent that bypasses the baghouse or leaks to the atmosphere through the pressure relief valve.

7.3 Dust Sampling

Samples were taken at various locations in the process ductwork to measure particulate mass flow in the process gas streams. The particulate sampling system consisted of a nozzle, a thimble filter, a condenser, a pump and a dry test meter. Prior to particulate sampling, a velocity traverse with a pitot tube was made at each sampling location. In all locations, except

Figure 7-1
Baghouse Collection Data
7/17/92 to 12/06/92

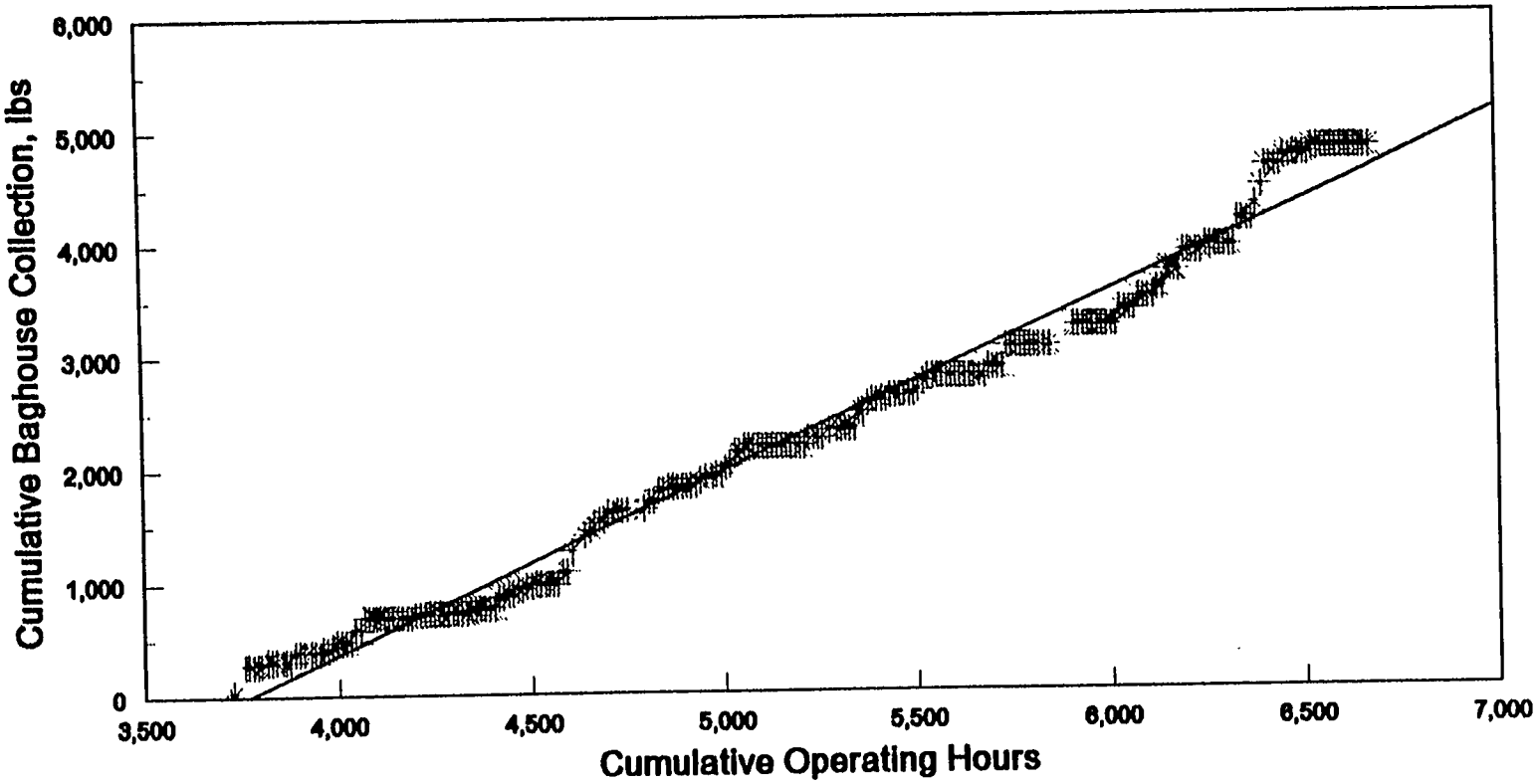

Slope= 1.59 lbs/hr

the adsorber outlet (cyclone inlet), the velocity traverse showed only small differences in gas velocities from point to point along the duct diameter.

In all cases particulate samples were taken isokinetically, i.e., the sampling velocity was controlled to equal the sampled duct velocity. Duct velocities ranged from 25 to 45 ft/sec. Since the velocity profiles across the ducts were uniform, sampling was done at one point in the center of the duct. However, several locations were not ideal for particulate sampling due to the presence of obstructions (reducers, elbows, etc.) upstream and downstream of the sampling location as shown in Table 7-2.

Table 7-2. Dust Sample Port Location and Dimension Data

Sampling Location	Duct Diameter (inches)	Obstructions (duct diameters)	
		Upstream	Downstream
Flue gas return	38	2.7	2.7
Sorbent heater offgas	20	12.4	18.8
Adsorber out/cyclone in	26	0.3	0.3
Cyclone outlet	26	1.1	14.8
Adsorber inlet	28	6.3	38.8

Only the adsorber inlet and the sorbent heater offgas would be considered good particulate sampling locations according to EPA Method 5 which requires that the sampling location be at least two duct diameters upstream and at least eight duct diameters downstream of an obstruction.

The particulate sampling results are listed in Table 7-3. The total particulate mass flowrate was obtained by multiplying the measured particulate concentration in the samples times the volumetric flowrate of gas in the ducts. The total particulate mass flowrate is the sum of the carryover (whole beads) plus attrition (what remains after whole beads are extracted).

Table 7-3. Particulate Sampling Results

Location	Carryover, lb/hr	Attrition, lb/hr	Sampling Time, hr	Duct Velocity, ft/sec
Flue gas return	0.0	0.12	12.0	38
Flue gas return	0.0	1.76	3.0	38
Sorbent heater offgas	0.0	0.91	3.0	24
Sorbent heater offgas	0.0	0.44	11.0	24
Sorbent heater offgas	0.0	1.83	2.0	31
Sorbent heater offgas	0.0	1.05	12.0	25
Sorbent heater offgas	0.0	0.91	6.0	28

Table 7-3. Particulate Sampling Results				
Location	Carryover, lb/hr	Attrition, lb/hr	Sampling Time, hr	Duct Velocity, ft/sec
Sorbent heater offgas	0.0	0.93	6.0	28
Adsorber cycle in	0.0	0.25	3.0	37
Adsorber cycle in	2.2	1.22	11.0	46
Adsorber cycle in	0.0	0.42	3.0	38
Adsorber cycle out	0.0	0.32	8.0	37
Adsorber cycle out	0.0	0.33	8.0	38
Adsorber cycle out	0.0	0.37	12.0	37
Adsorber cycle out	0.2	8.96 *	4.5	45
Adsorber inlet	0.0	2.61	5.7	33
Mac offgas	0.0	0.03	6.8	30
Mac convey	0.0	0.02	10.0	30

* Power plant switching boilers

The dust sampling results are inconclusive. Only two tests were run on the flue gas return duct (downstream of the baghouse) and the results differ greatly, 0.1 to 1.8 lb/hr. The adsorber cyclone inlet and adsorber cyclone outlet are poor sampling locations (see Table 7-2) and the sampling results vary considerably. One test at the adsorber cyclone inlet yielded 2.2 lb/hr carryover, but in the other two tests carryover was negligible and the total particulate mass flowrates were 0.25 and 0.42 lb/hr, respectively. In tests on the adsorber cyclone outlet, two tests yielded 0.33 and 0.37 lb/hr, essentially the same rate measured at the cyclone inlet which would only be possible if the cyclone collection efficiency was zero, which is unlikely. Because of this and the non-repeatability of the tests at the same locations, the data for the adsorber cyclone inlet and cyclone outlet are considered bad data.

The best particulate sampling results were obtained from the sorbent heater offgas duct, which was one of the two best sampling locations. Neglecting the highest and lowest results, there were three tests of the sorbent heater offgas in which particulate mass flowrate was measured between 0.91 and 1.05 lb/hr. Since sorbent fines are recycled to the adsorber via the cyclone, the greater part of attrited sorbent lost from the system should be entrained in the sorbent heater offgas. However, the measured particulate mass flow in the sorbent heater offgas was only 26% of the sorbent makeup rate and 66% of the baghouse collection rate. Of course, the dust samples were taken over a maximum sampling period of 12 hours; while the baghouse and sorbent makeup data are attrition rates averaged over many months.

7.4 Sorbent Attrition Summary

The sorbent attrition data are summarized in Table 7-4. As discussed above, the attrition rate based on the rate of sorbent makeup is most accurate. At this rate (3.8 pph) and with a system inventory of 25,000 pounds (actual system inventory fluctuated from 22,000 to 28,000 pounds during the tests), the entire sorbent inventory would be replaced once every 6,579 hours (9 months).

Table 7-4. Summary of Attrition Data

	Results Based On	Attrition Rate, pph
Total system	POC sorbent makeup	3.8
Total system	POC baghouse collection	1.6
Sorbent heater offgas	POC dust sampling	1.0
Total system	Previous test data*	4.3

* Measured at 0.06 MW and 0.75 MW equivalent capacity and extrapolated to pilot plant scale (5 MW).

In all previous tests of the NOXSO Process at smaller scale, the sorbent attrition rate has been 0.02 to 0.03% of fluid bed inventory per hour. The fluid bed inventory during the pilot test was as follows:

	Inventory, lbs
Adsorber	6,366*
Sorbent Heater	4,833
Sorbent Cooler	3,222
Total Fluid Bed Inventory	14,421

* Time weighted average; heater/cooler inventories did not vary.

The measured attrition rate at the pilot plant is, therefore, equivalent to 0.026% of the fluid bed inventory per hour. This is substantially the same rate measured in tests at smaller scale, which was the rate used in previously published economic evaluations of the NOXSO Process.[11]

Assume that one were to use the pilot plant data to design a NOXSO system to treat all of the flue gas from one of the 65 MW, pc-fired boilers at Ohio Edison's Toronto Power Plant. Assume further that the plant must be designed to achieve 90% removal of SO_2 and 80% removal of NO_x. A preliminary design of this plant based on the parametric test results is presented in Section 11.2.7. The pertinent design parameters from the standpoint of estimating the rate of attrition are the fluid bed inventories:

Vessel Inventory, lbs	
Adsorbers (2)	105,840
Sorbent Heater (1)	62,113
Sorbent Cooler (1)	74,536
Total Fluid Bed	242,489

The estimated rate of attrition at such a plant would be 242,489 pounds x .026%/hr or 63 pounds per hour.

8.0 FLUIDIZATION

The NOXSO Process utilizes multi-stage fluid beds to cool and heat the sorbent. A proper downcomer design is required to ensure a constant sorbent flow from one stage to another. To minimize the consumption of fan power, the sorbent residence time should be reduced as much as possible but must still be long enough to accomplish the heat transfer. The data collected in the POC plant were used to correlate the gas-sorbent heat transfer coefficient with the superficial gas velocity, and to develop a design method for sizing the downcomer.

8.1 Downcomer Design

In a multi-stage fluid bed vessel, the particles flow from stage to stage through a downcomer. A certain amount of particles are held up in the downcomer as a seal to prevent gas from bypassing the grid plate. Although the particles are moving randomly inside the fluid bed vessel, overall the particles are flowing toward the downcomer. When the particles start to pour into the downcomer, their flow pattern is considered similar to that of liquid flowing over a weir. Once the particles enter the downcomer, they flow like a moving-bed.

The continuity of mass flow requires a constant particle flowrate. Therefore, the flow of particles into the downcomer must be equal to the moving-bed flow inside the downcomer.

$$m \cdot h_c \cdot L = m \cdot A_d \qquad (8.1\text{-}1)$$

where m is the mass flux of particles, kg/m^2 sec,
h_c is the effective particle level above the downcomer, m,
L is the perimeter of the downcomer opening, m, and
A_d is the cross-sectional area of the downcomer, m^2.

The key to obtaining the required number of downcomers is to make h_cL no less than A_d so there is always enough room for particles to pour into the downcomer.

The value of A_d is determined by the pressure balance between the upper and lower stages. The cross-sectional area of downcomer should be large enough to allow the particles to reach the required flowrate but maintain a particle seal to prevent gas bypassing. The modified Ergun equation was used to estimate the required A_d.

The remaining task is to find a reliable way to estimate the value of h_c under different fluidization conditions. Test data collected from the three-stage, fluid-bed cooler at the POC plant were used to develop a correlation for h_c. The derivation of the correlation is described in the next section.

The flowrate of liquid over a rectangular sharp-edged weir can be estimated from the modified Francis formula.[9]

$$q = 0.415(L_0 - 0.2h_0)h_0^{1.5}\sqrt{2g} \quad (8.1\text{-}2)$$

where q is the volumetric flowrate, m^3/sec,
L_0 is the crest length (see Figure 8-1), m,
h_0 is the weir head (see Figure 8-1), m, and
g $= 9.8$ m/sec^2.

The product of 0.415 and (L_0 - $0.2h_0$) in the Francis formula is required to correct the changes of liquid level and the opening area as the liquid approaches the weir. In the case of over-flow, the liquid flows freely toward the downcomer. Only the change in liquid level near the downcomer requires correction. Therefore, for the flow over a downcomer the modified Francis formula is simplified as follows

$$q = 0.415L_0h_0^{1.5}\sqrt{2g} \quad (8.1\text{-}3)$$

To apply Equation 8.1-3 to particle flow, the fluid bed density at actual operating conditions has to be defined, and is given by

$$\rho = \frac{\Delta P_{bed}}{g(H - h_c)} \quad (8.1\text{-}4)$$

where ΔP_{bed} is the pressure drop across the fluid bed, N/m^2,
H is the downcomer height above the gas distributor, m,
h_c is the expanded fluid bed height above the downcomer, m, and
ρ is the particle density in the fluid bed vessel, kg/m^3.

Multiplying Equation 8.1-3 by ρ gives the mass flowrate of particles as follows.

$$F_s = 0.415Lh_c^{1.5}\sqrt{2g}\frac{\Delta P_{bed}}{g(H + h_c)} \quad (8.1\text{-}5)$$

where F_s is the particle flowrate, kg/sec, and
L is the effective perimeter of the downcomer opening, m.

The value of h_c can be determined from Equation 8.1-5 when F_s, ΔP_{bed}, H, and L are known.

The flow pattern of fluidized particles in the multi-stage fluid bed vessels was closely examined during cold flow tests conducted at the NOXSO POC plant. The examination was made by observing the flow of particles through a plexiglass manway cover. It was found that the particles between the back of the downcomer and the vessel wall were hardly moving. All the downcomers were installed about 4" from the vessel wall. The support of the gas distributor and downcomer occupied a 3" space. The hole pitch on the gas distributor is 13/16". The open area of the gas distributor between the vessel wall and the back of downcomer is not enough to provide sufficient gas flow to fluidize the particles. Assuming the particles were not fluidized

Figure 8-1
Rectangular Weir

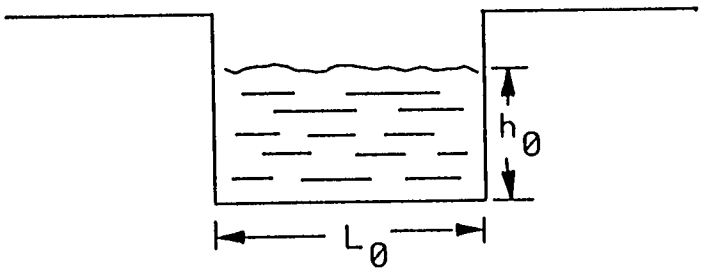

toward the back of the downcomer, the effective length for overflow will be half of the perimeter of the downcomer opening. The half perimeter assumption and POC cooler test data were then used to calculate h_c for each data point. Since the bed expansion is related to the superficial gas velocity, h_c was next correlated with the measured superficial gas velocity. The correlation (obtained from 87 data points with $r^2 = 0.8752$) is given by

$$h_c = 0.0224U_o \tag{8.1-6}$$

where U_0 is the superficial gas velocity in m/sec and h_c is in meters. The comparison between the correlation and experimental result is shown in Figure 8-2. The standard deviation, $[\sum(\text{cor-exp})^2/(n-1)]^{1/2}$, is 0.001551. Substituting Equation 8.1-6 into Equation 8.1-5 gives the particle flowrate as a function of the gas velocity

$$F_s = 0.415L(0.0244U_0)^{1.5}\sqrt{2g}\left[\frac{25.4h_w}{H + 0.0244U_0}\right] \tag{8.1-7}$$

where ΔP_{bed} is $g\rho_w h_w = 25.4gh_w$ has been used,
h_w is the height of water column, " H_2O, and
ρ_w is the water density, 1000 kg/m^3.

Equation 8.1-7 is later used to determine the minimum perimeter length of the downcomer opening.

The required downcomer cross-sectional area was calculated by assuming moving bed downflow in the downcomer.[10] In moving bed flow the movement of gas relative to the solids, not relative to the pipe walls, determines the pressure gradient in the pipe. Consider a fixed bed of solids of voidage ε_m moving downward at a constant velocity u_s (downward positive). The frictional pressure drop between any two levels in the downcomer is obtained by a slight modification of Ergun's Equation,[10] as follows:

$$\frac{\Delta p_{fr}}{l}g_c = 150\frac{(1-\varepsilon_m)^2}{\varepsilon_m^2}\frac{\mu(\Delta u)}{(\phi_s d_p)^2} + 1.75\frac{(1-\varepsilon_m)}{\varepsilon_m}\frac{\rho_g(\Delta u)^2}{\phi_s d_p} \tag{8.1-8}$$

$$\Delta u = u_g + u_s = \frac{u_0}{\varepsilon_m} + u_s$$

where d_p is the mean particle diameter, m,
Δp_{fr} is the frictional pressure drop, Newton/m^2,
Δu is the relative velocity of gas with respect to the solids, m/sec,
g_c is the unit conversion factor, 1,
l is the length of downcomer, m,
ρ_g is the gas density, kg/m^3,
ϕ_s is the particle sphericity, dimensionless
μ is the gas viscosity, kg/m sec,
u_g is the upflow velocity of gas, m/sec,

Figure 8-2
The Experimental and Correlated hc
Uo of Pilot Plant Sorbent Cooler

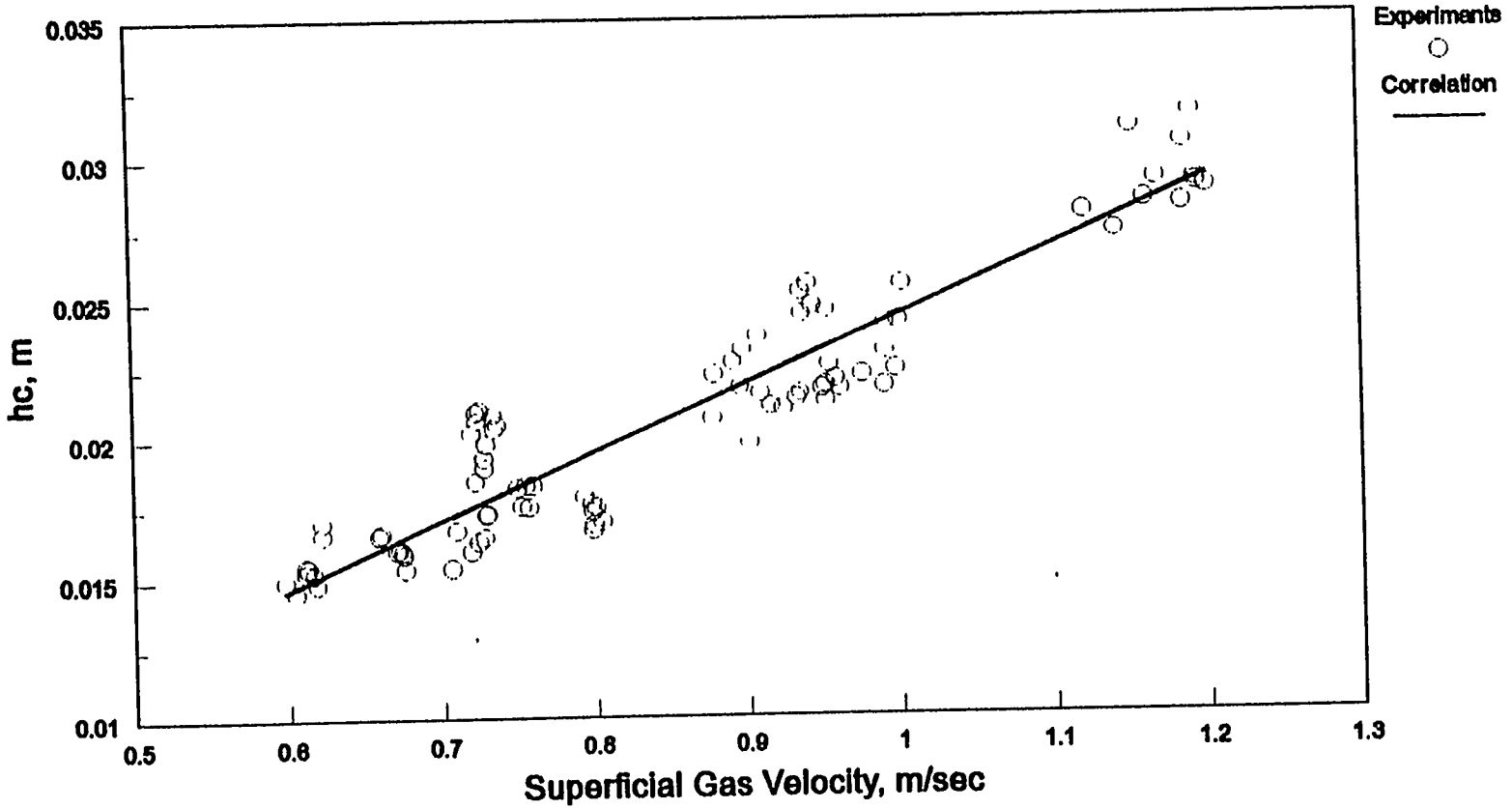

u_0 is the superficial rise velocity of gas up the downcomer, m/sec, and
u_s is the downward velocity of sorbent, m/sec.

Equation 8.1-8 should apply as long as the particles do not fluidize. The adequacy of Equation 8.1-8 was confirmed by Yoon and Kunni[10] in their experiments with a moving bed of glass beads, mean particle diameter = 130-1130μm, in 41-mm and 70-mm downcomer pipes.

However, the use of Equation 8.1-8 to determine A_d requires two more pieces of information: 1) the length of downcomer which is filled with particles and, 2) the gas velocity in the downcomer which is filled with particles. The first item provides an effective downcomer length, l, to be used in Equation 8.1-8, and the second item is required to determine the particle velocity, u_s, from the relative velocity, Δu. It is difficult to collect both pieces of information from the pilot-scale fluid beds. However, a method has been developed to obtain this information from the sorbent cooler vessel of the NOXSO POC plant. The details are described later.

The calculation of A_d is straight forward. The pressure balance requires that the frictional pressure drop in the downcomer equals the pressure drop across the fluid bed and grid plate. With given downcomer length and measured fluid bed and grid plate pressure drops, Equation 8.1-8 can be solved to obtain Δu and u_s. Then A_d is calculated as follows:

$$F_s = A_d\, u_s \rho_s (1 - \varepsilon_m) \qquad (8.1\text{-}9)$$

where ρ_s is the particle density.

The number of downcomers is determined from Equation 8.1-1. Since the perimeter of the downcomer opening is dependent on the shape of the downcomer, the required number of downcomers for a rectangular design may be different from that of a cylindrical design. In the following discussion, n stands for the number of downcomers.

For a cylindrical downcomer, let d be the diameter of downcomer, then $A_d = n\,\pi d^2/4$ and the perimeter $L = (n\pi d)^{1/2}$. Equation 8.1-1 requires $Lh_c = A_d$, which results in

$$n = \frac{A_d}{4\pi h_c^2} = \frac{A_d}{4\pi(0.0244U_0)^2} \qquad (8.1\text{-}10)$$

For a rectangular downcomer, let r be the length to width ratio and w be the width, then $A_d = nrw^2$ and the perimeter $L = 2n(1+r)W$. Equation 8.1-1 requires $Lh_c = A_d$, which gives:

$$n = \frac{r}{4(1+r)^2}\frac{A_d}{h_c^2} = \frac{r}{4(1+r)^2}\frac{A_d}{(0.0244U_0)^2} \qquad (8.1\text{-}11)$$

The test results obtained from the sorbent cooler at the NOXSO POC plant are used to determine the gas velocity and the effective downcomer length for Equation 8.1-8. Of course, the best way to determine the effective length is by observation through a transparent wall. Since the sorbent cooler is made of steel, the next reliable way is to enter the vessel and then measure the length after shutting down the plant. With known length and pressure drop, Equation 8.1-8 can be solved to obtain the relative velocity, Δu. The value of u_s is calculated from Equation 8.1-9 with the designed A_d and the measured F_s. The gas velocity can then be determined from Δu and u_s. This gas velocity will be used in the design of other vessels.

The effective downcomer length has never been measured during the NOXSO POC tests. A reasonable assumption has to be made in order to use the proposed downcomer design method. The approach is to assume a gas velocity then guess the effective downcomer length for calculating the downcomer cross-sectional area. Refine the guessed length until the calculated area agrees with the actual area. The assumptions are as follows:

1. The downcomer is about 80% filled. The total downcomer length is the distance between the gas distributor and the downcomer discharge.
2. The gas velocity in the downcomer is equal to the solid velocity but in the opposite direction.

Assumption (1) was based on observations made during cold flow tests conducted in the sorbent cooler. The gas in the downcomer flows upward against the downflowing solids when $u_g > u_s$. Conversely, when $u_g < u_s$, gas is dragged downward against the pressure gradient. Since there is no reliable way to verify the gas direction in the downcomer, an intermediate case $u_g \approx u_s$ is assumed.

The downcomer between the middle and bottom stages of the sorbent cooler in the POC plant is used as an example to illustrate the use of the method to determine the size and number of downcomers. The particle properties are listed below:

mean particle diameter, d_p	= 0.00121 m
particle density, ρ_s	= 1000 kg/m^3
particle sphericity, ϕ_s	= 0.95
void fraction in downcomer, ε_m	= 0.36

The calculation is listed in Appendix E. The results are discussed in the following paragraphs.

The calculations show that the downcomer cross-sectional area is $A_d = 0.014\ m^2$ ($21.7"^2$) and 1.3 downcomers are required. The corresponding perimeter of the downcomer opening is $L = 2n(1+r)[A_d/(nr)]^{1/2} = 0.62$ m (24.4") with r = 3. The calculated number of downcomers is higher than the actual number of downcomers. Only one downcomer is installed in each stage of the multi-stage fluid bed vessel in the POC plant. The discrepancy is caused by the shape of the cooler downcomer. The middle stage of the sorbent cooler used a tapered rectangular downcomer, of which the dimensions are shown in Figure 8-3. The narrowest opening of the downcomer is at the bottom section before discharge. Its cross-sectional area is $0.018\ m^2$ ($27.6"^2$). The perimeter of the top opening is 1.02 m (40 in). As mentioned before, only half of the perimeter of the downcomer opening is effective. The comparison between the calculation and the actual situation (21.7 versus $27.6"^2$ and 24.4 versus 20") confirms the usefulness of this method.

It should be pointed out that the downcomer in the sorbent cooler is equipped with a flapper valve to maintain particles in the downcomer during start up. The installation of a flapper valve increases the pressure drop across the downcomer to an unknown extent. It allows use of a larger downcomer area as compared with one without a flapper valve. In addition to the tapered shape of the downcomer, the flapper valve offers another explanation why the actual area is larger than the calculated area.

In order to obtain reliable design results. it is recommended to measure the effective downcomer length in the sorbent cooler of the NOXSO POC plant. Then a true gas velocity in the downcomer can be used to size downcomers for other vessels. Since the Niles Plant uses a 5-stage sorbent cooler and heater, the temperature of each stage is different. The downcomer design for each stage, therefore, should be checked by the proposed method.

8.2 Heat Transfer

The heat transfer between the gas and solid in a fluid bed is considered to be very fast. The gas and solid temperature can be assumed equal at the exit of the fluid bed. As a result, the sorbent residence time was not a concern in the design of the sorbent heater and cooler with regard to heat transfer. But from an economic point of view, the shorter the sorbent residence time in the fluid bed the better. Shorter time implies less sorbent inventory because the sorbent circulation rate is determined by the adsorber's SO_2 removal requirement. High sorbent inventory demands more fan power to fluidize the sorbent. It also increases the sorbent attrition and requires more sorbent to fill up the system. However, a minimum amount of sorbent must be maintained in the fluid bed to prevent the gas from channelling through the bed and to allow the gas and sorbent temperatures to be equal at the exit of the fluid bed.

A mathematical model which predicts the sorbent residence time and the gas and sorbent temperatures was derived from the sorbent cooler data. The assumptions used in the model are listed in the following:

1. The thermocouple in the gas phase measures the gas temperature.
2. The thermocouple in the fluid bed measures the average sorbent temperature.

Figure 8-3
Sorbent Cooler Downcomer

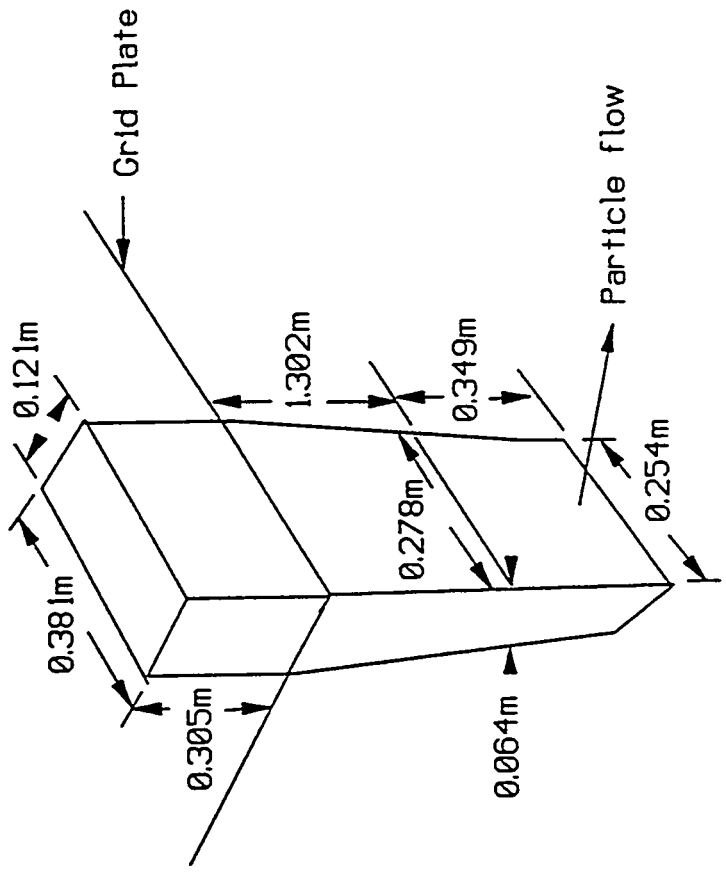

3. The gas is plug flow.
4. The sorbent is between plug and mixed flow.

The fourth assumption was based on an observation of the sorbent fluidization in a cold-flow model test which was conducted, under subcontract, by PEMM Corporation. The fluidization tests were conducted in a 48" by 8" rectangular plexiglass vessel. Colored sorbent was gradually fed into the fluid bed which was filled with uncolored sorbent. It was found that the colored sorbent beads spread laterally along the grid plate prior to dispersing into the fluid bed. The second assumption was made because the tip of the thermowell in the POC sorbent cooler is in the center of the fluid bed.

The heat transfer rate equation is given by

$$\frac{dQ}{dt} = WC_{p_s}\frac{dT_s}{dt} = h(nS_{EA})(T - T_s) = \frac{6hW}{\rho_s d_p}(T - T_s)$$

$$or \qquad \frac{dT_s}{dt} = \frac{6h}{\rho_s d_p C_{p_s}}(T - T_s) \qquad (8.2\text{-}1)$$

where C_{ps} is the sorbent heat capacity, kcal/kg °C,
d_p is the diameter of the sorbent particle, m,
h is the particle heat transfer coefficient, kcal/m^2 sec°C,
n is the number of sorbent particles,
ρ_s is the sorbent density, kg/m^3,
Q is the amount of heat transferred, kcal,
S_{EA} is the sorbent external surface area, m^2,
t is the time, sec,
T is the gas temperature, °C,
T_s is the sorbent temperature, °C, and
W is the sorbent inventory, kg.

The energy balance is given by

$$-F_g C_p(T - T_0) = F_s C_{P_s}(T_s - T_{s_0}) + UA_w(T - T_A)$$

$$T = \frac{T_0 + \frac{F_s C_{p_s}}{F_g C_p}T_{s_0} + \frac{UA_w}{F_g C_p}T_A}{1 + \frac{UA_w}{F_g C_p}} - \frac{\frac{F_s C_{p_s}}{F_g C_p}}{1 + \frac{UA_w}{F_g C_p}}T_s \qquad (8.2\text{-}2)$$

where A_w is the vessel wall surface area, m^2,
Cp is the gas heat capacity, kcal/mol °C,
F_g is the gas flowrate, kmol/sec,

F_s is the sorbent flowrate, kg/sec,
T_A is the ambient temperature, °C,
U is the wall heat transfer coefficient, kcal/m^2 sec, and
subscript 0 stands for the initial condition.

Let

$$\zeta = \frac{6h}{\rho_s d_p C_{p_s}}$$

$$\phi = \frac{F_s C_{P_s}}{F_g C_p}$$

$$\phi_w = \frac{UA_w}{F_g C_p} \qquad (8.2\text{-}3)$$

$$\Omega = \frac{T_0 + \phi T_{s_0} + \phi_w T_A}{1 + \phi_w}$$

$$\Psi = \frac{-\phi}{1 + \phi_w}$$

Substituting Equation 8.2-3 into Equations 8.2-1 and 8.2-2 yields

$$\frac{dT_s}{dt} = \zeta(T - T_s) \qquad (8.2\text{-}4)$$

and

$$T = \Omega + \Psi T_s \qquad (8.2\text{-}5)$$

substituting Equation 8.2-5 into Equation 8.2-4 and integrating the resultant equation gives

$$T_s = \frac{\Omega}{1 - \Psi} + (T_{s_0} - \frac{\Omega}{(1 - \Psi}) e^{-\zeta(1-\Psi)t} \qquad (8.2\text{-}6)$$

The time average of the sorbent temperature is given by

$$\overline{T_s} = \frac{1}{t}\int_0^t [\frac{\Omega}{1-\Psi} + (T_{s_0} - \frac{\Omega}{1-\Psi}) e^{-\zeta(1-\Psi)t}] dt$$
$$= \frac{\Omega}{1-\Psi} + \frac{(1-\Psi)T_{s_0} - \Omega}{\zeta(1-\Psi)^2} \frac{1 - e^{-\zeta(1-\Psi)t}}{t} \qquad (8.2\text{-}7)$$

The gas outlet temperature is estimated from the fluid bed energy balance along the axial direction as follows

$$-F_g C_p dt = \rho A C_{p_s} \frac{\partial T_s}{\partial t} dZ \qquad (8.2\text{-}8)$$

where A is the vessel cross-sectional area, m^2
Z is the expanded fluid bed height, m

Plugging Equations 8.2-4 and 8.2-5 into Equation 8.2-8 then integrating the resultant equation with the boundary condition $T = T_0$ at $Z = 0$ and $T = T_f$ at $Z = H$ gives

$$T_f = T_0 - \phi \frac{\Omega - (1-\Psi) T_{s_0}}{1 - \Psi} \left[1 - e^{-\zeta (1-\Psi) W / F_s} \right] \qquad (8.2\text{-}9)$$

To account for the gas velocity effect, the h was further expressed as a function of the particle Reynolds number, as follows:

$$Nu = \alpha \, Re_p^{1.3} \qquad (8.2\text{-}10)$$

where α is a constant,
k is the gas thermal conductivity, kcal/m sec°K,
Nu is $h\, d_p/k$ is the Nusselt number for gas-particle heat transfer,
Re is $d_p\, U_0\, \rho_g/\mu$, the particle Reynolds number,
μ is gas viscosity, kg/m sec, and
U_0 is superficial gas velocity, m/sec.

Equations 8.2-1 through 8.2-10 contain only two unknowns, namely, α and U. Their values were determined by trial and error as follows:

1. Assume α and U values
2. Calculate the estimated T_s and T_f according to Equations 8.2-7 and 8.2-8.
3. Calculate the standard deviation between the estimated and measured T_s and T_f according to Equation 8.2-11

$$\sigma = \sqrt{\frac{1}{n} \sum_{i=1}^{n} (X_i - X_{m_i})^2} \qquad (8.2\text{-}11)$$

where σ is the standard deviation,
n is the number of data points,
X_i is the estimated value, and
X_{mi} is the measured value.

4. Repeat Steps 1 to 3 until the lowest σ is found.

The final values for α and U obtained from thirty, 12-hour shift average data points are given below

$$N = 0.0008 Re_p^{1.3} \qquad (8.2\text{-}12)$$
$$U = 0.008$$

with the corresponding standard deviation for the top bed gas and sorbent temperature = 8.7, for the middle bed = 5.2, for the bottom bed = 3.3, and overall is 6.24. Figure 8-4 shows the comparison between the measured and estimated T_f and T_s. The quality of fit confirms the mathematical model. Figure 8-5 shows the temperature change of sorbent and gas inside the fluid bed. The required sorbent residence time is higher at the bottom bed as compared to the top bed. The time difference is due to the temperature gradient between the gas and sorbent. In the top bed, the temperature difference between the gas and sorbent is about 250°C; while in the bottom bed, the difference is only 180°C. For the optimal cooler design, the sorbent residence time should be controlled between 200 to 300 seconds.

It should be pointed out that the α value shown in Equation 8.2-12 is smaller than those listed in the literature,[10] of which $\alpha = 0.03$. The same cooler data were used to evaluate the accuracy of the literature correlation. The least error was found by setting U = 0. The standard deviation for the top bed gas and sorbent temperature is 23.6, the middle bed is 5.6, the bottom bed is 7.3, and overall is 14.8. The major error was created by the top bed. For the middle and bottom beds, the errors obtained from the literature and the current correlation are about the same. Figure 8-6 is included to show the comparison between the measured and predicted gas and sorbent temperatures using the literature correlation. According to the result obtained from the literature correlation, the sorbent requires only 80 seconds to reach the gas temperature (see Figure 8-7). For scaling the POC result to the 115 MW demonstration plant, a conservative approach should be adopted to ensure the plant has enough capacity to cool the sorbent.

The assumption that the sorbent is in mixed flow in the fluid bed was also tried to derive the gas and sorbent outlet temperatures. But the correlation result is inferior to those obtained from the previous discussion with the same data.

Figure 8-4
Comparison of Sorbent Cooler Gas
and Solid Temperatures

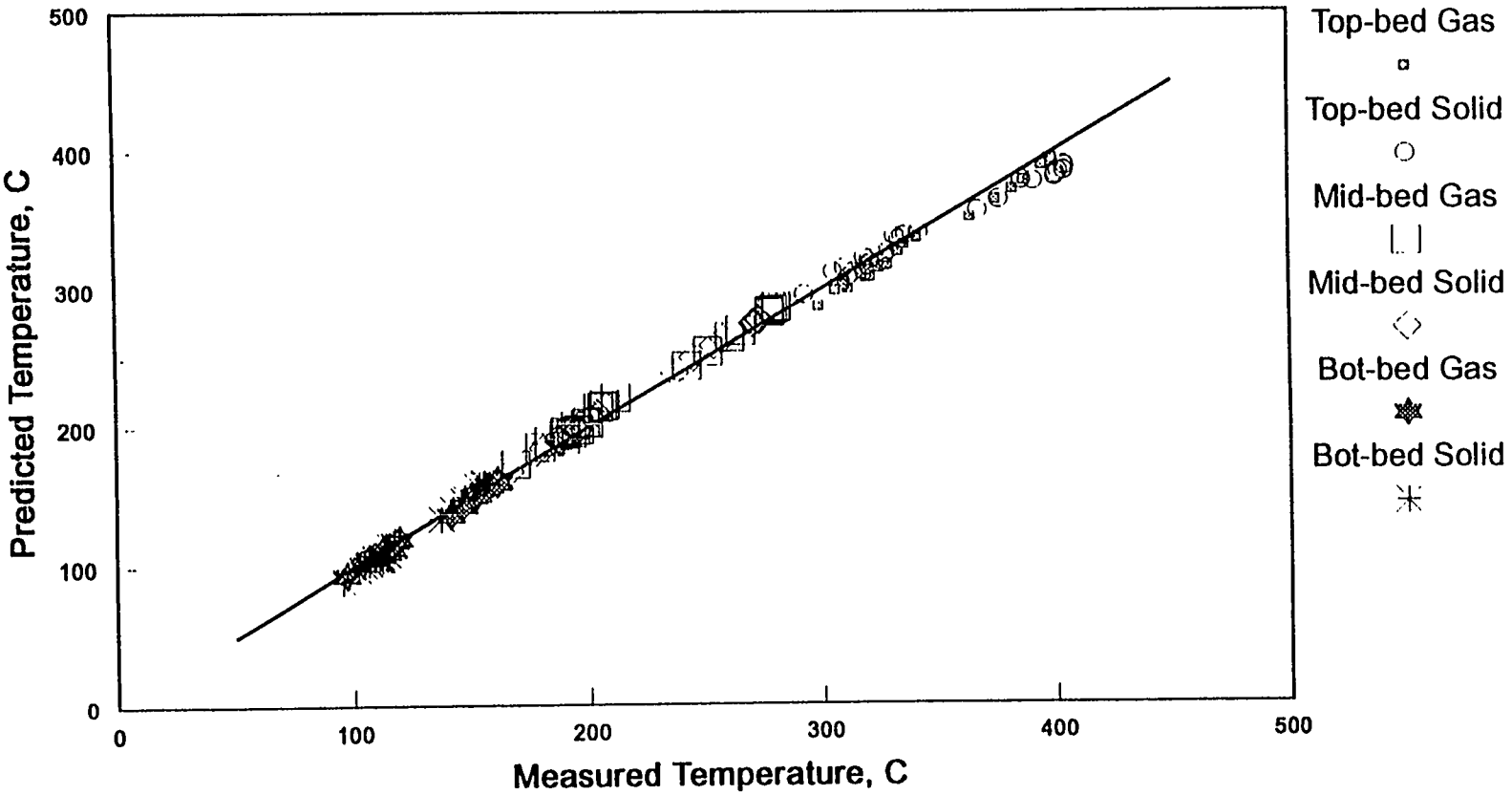

Figure 8-5
Gas and Sorbent Temperatures Inside the Sorbent Cooler at Different Sorbent Residence Times

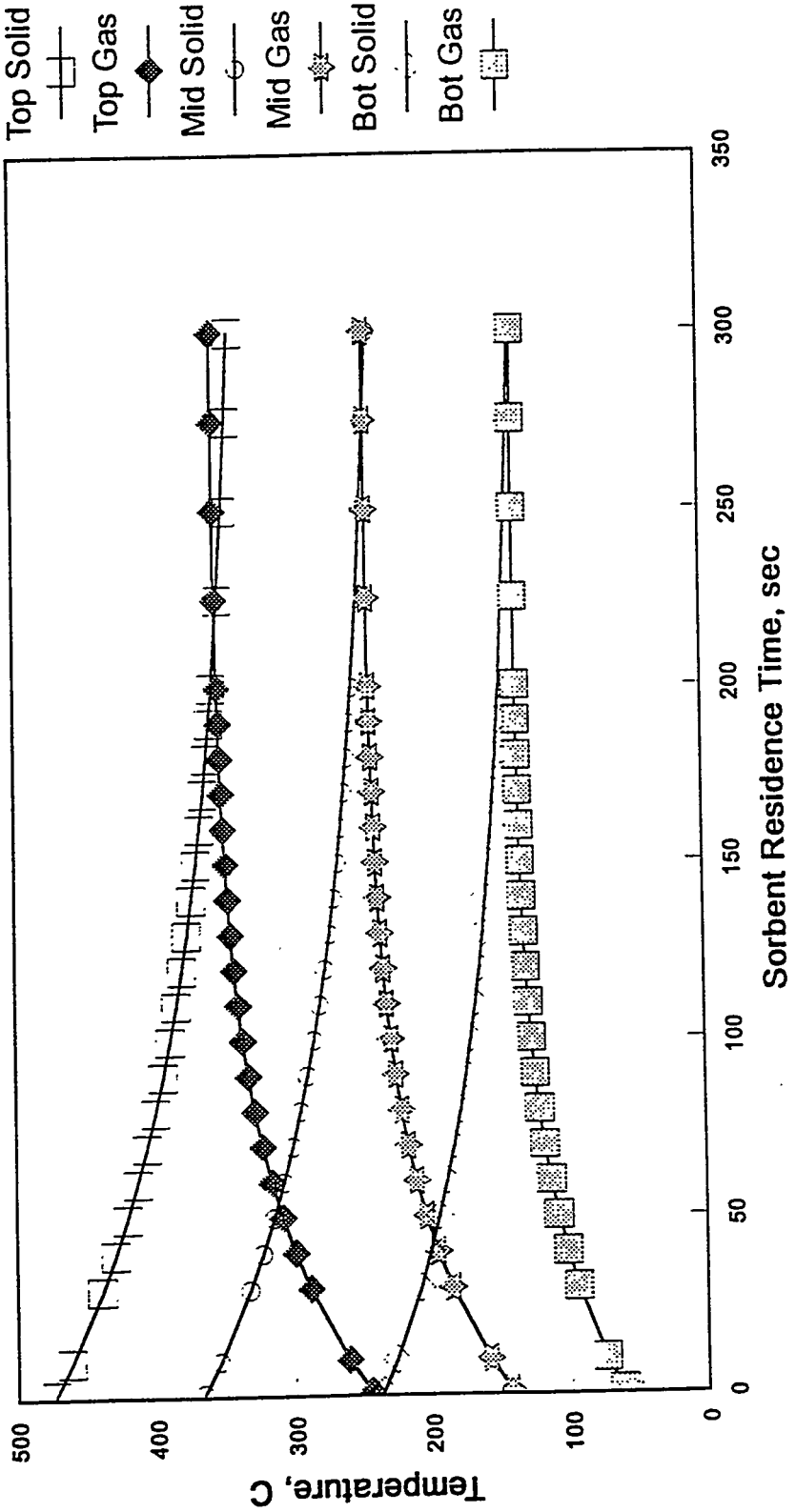

Figure 8-6

Comparison of Sorbent Cooler Gas and

Solid Temperatures (Literature Correlation)

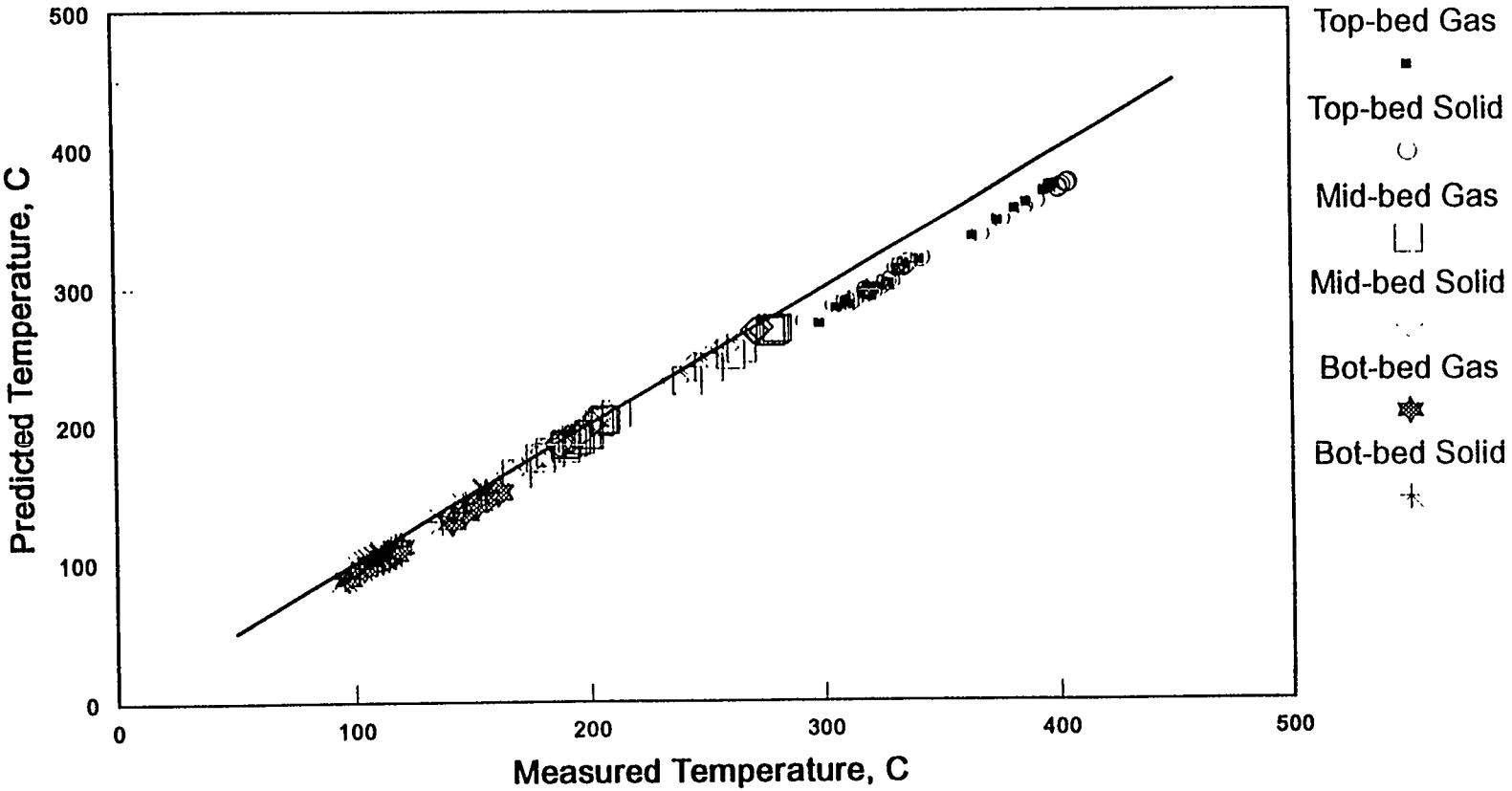

Figure 8-7. Gas and Sorbent Temperatures Inside the Sorbent Cooler at Different Sorbent Residence Time (Literature Correlation)

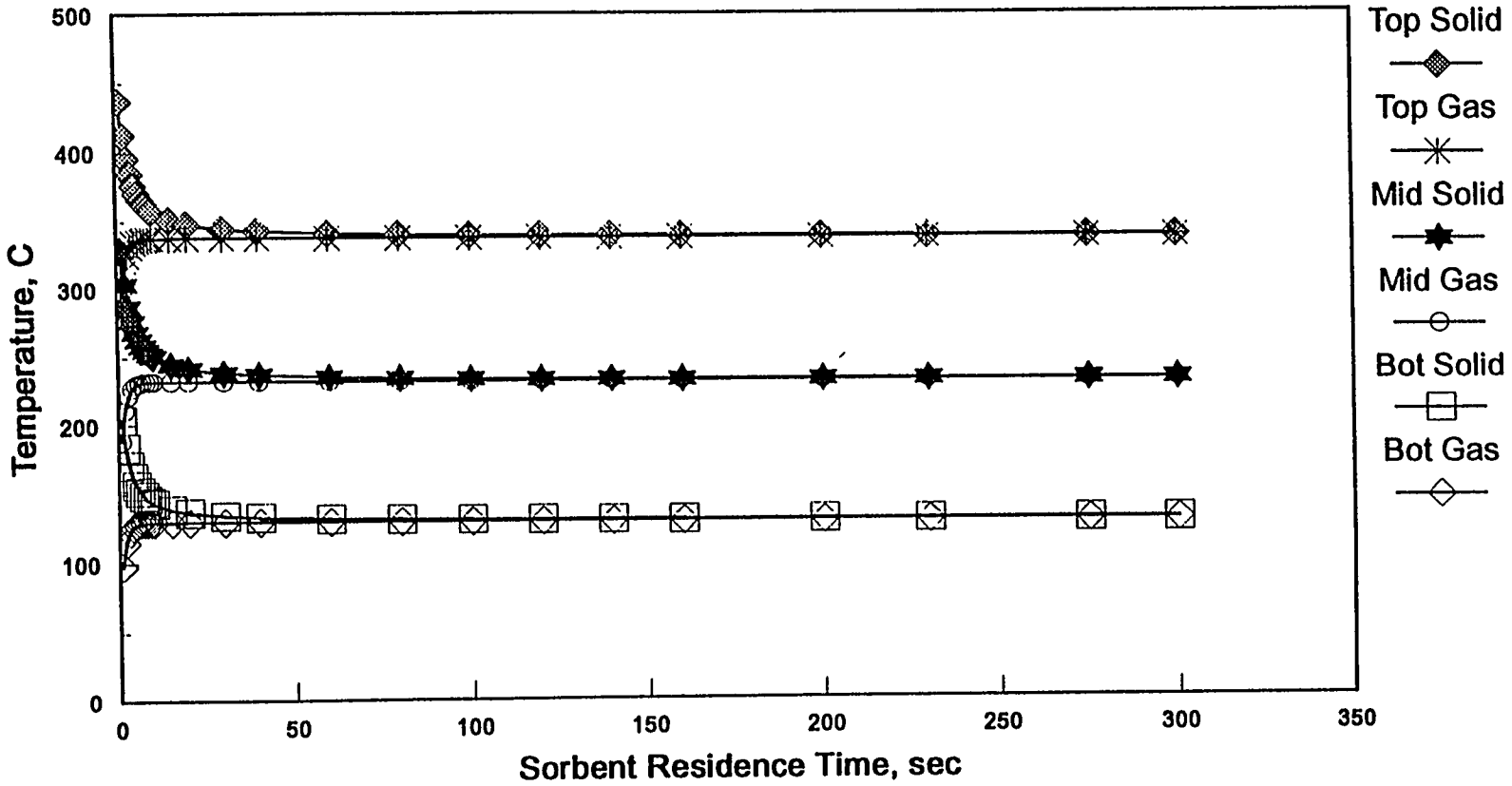

9.0 SORBENT TRANSPORT

The sorbent in the NOXSO Process is continuously circulated between the adsorber and regenerator. The sorbent transport devices used in the NOXSO POC pilot plant are one dense phase conveying system and three dilute phase J-valves. The dense phase conveying system (MAC) is provided by MAC Company. The MAC lifts the spent sorbent from the adsorber outlet to the top of the sorbent heater. The sorbent then flows into the top bed of the sorbent heater by gravity. The J-valves are used to transport the sorbent from the bottom bed of the sorbent heater to the top of regenerator, from the bottom of the regenerator to the top bed of sorbent cooler, and from the surge tank to the adsorber. The experience of using these sorbent transport devices will be discussed in the following section.

9.1 MAC Dense Phase Transport

The general arrangement of the MAC system is shown in Figure 9-1. The system consists of three vessels; surge bin, fluidizer, and disengaging vessel. The spent sorbent flows into the surge bin and fluidizer by gravity. Forty pound air was used to pressurize the fluidizer and push the sorbent to the disengaging vessel. Please note that no isolation valve was installed between the fluidier and the disengaging vessel. The sorbent moves like a plug in the vertical section.

During the POC operation, the sorbent was blown out of the disengaging vessel several times. The sorbent loss was caused by the malfunction of the high level probe installed in the disengaging vessel. The high level probe should stop the MAC transport cycle if the sorbent level in the disengaging vessel is too high. The failure of the high level probe caused the disengaging vessel to overfill. The excess sorbent was carried by the heater and MAC offgas through the offgas ducts and power plant stack and then vented to the atmosphere. In this case. the baghouse was bypassed; process offgases typically pass through the baghouse before being vented to the plant stack. Except for the malfunction of the high level probe which was later corrected, the MAC system was quite reliable.

9.2 J-Valves

The J-valves were developed by NOXSO Corporation. The valves serve two purposes: 1) to transport the sorbent from vessel to vessel, and 2) to form a seal to prevent the mixing of gases between vessels. Figure 9-2 shows the general arrangement of J-valves. It consists of a 6" stand pipe section, a 3" diameter riser section, and a gas distribution box. The stand pipe section is also equipped with aeration taps to strip gases from the sorbent as it leaves the vessel. The carrier gas enters the gas distribution box via three separate nozzles. The elbow gas prevents the sorbent from settling at the sharp turning corner and also provides the lubrication for the sorbent flow in the stand pipe. The fluidizing gas fluidizes the sorbent inside the box. The conveying gas carries the sorbent through the riser section. It was found that the sorbent flowrate can be controlled by adjusting any of these three gas flowrates. But adjusting only one gas flowrate does not provide wide enough control range for the sorbent flowrate. Since only the fluidization gas flowrate was controlled by the distributed control system to maintain vessel

Figure 9-1
MAC System

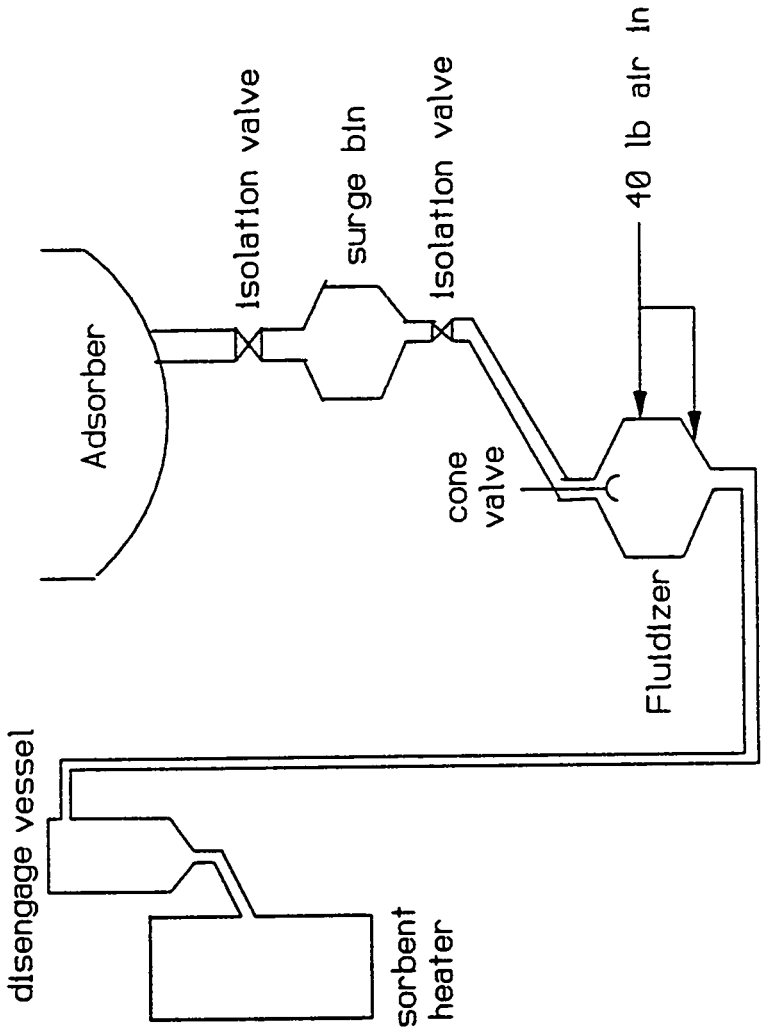

Figure 9-2
Schematic of a J-Valve

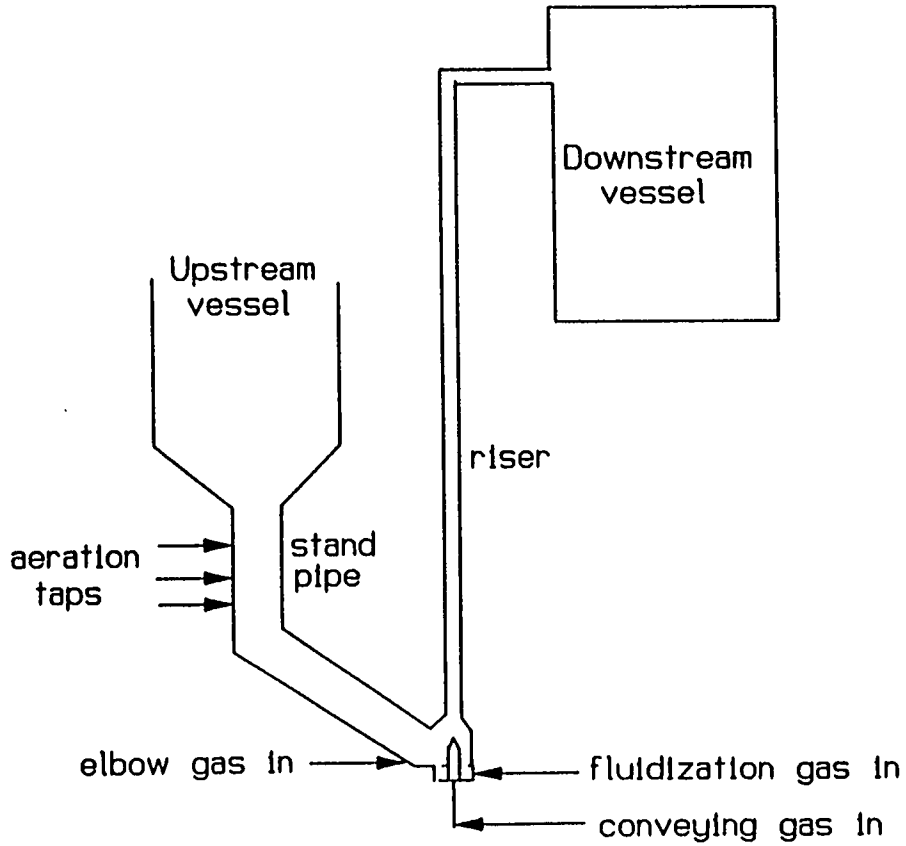

inventories, the operator must manually adjust the conveying and elbow gas flowrates in the field. However, these adjustments are only required when the sorbent flowrate is changed by the test conditions. Once the sorbent flowrate stabilizes, the J-valves can be switched to auto-control mode and controlled by the sorbent level in either the upstream or downstream vessels. Manual adjustment of these valves would not be required in a commercial application of the NOXSO Process.

10.0 PILOT PLANT OPERABILITY

10.1 Plant Shutdowns

Figures 10-1 and 10-2 show NOXSO cumulative run time versus power plant cumulative run time. The numbers shown on the figures correspond to periods of time in which the NOXSO Process was down due to repairs. The key to Figures 10-1 and 10-2 is given below.

1.	March 15, 1992	Sulfur condensed in regenerator/steam treater offgas line and plugged line at check valve. Sorbent heater top grid holes plugged with cementitious mix of sorbent and water (not whole sorbent spheres).
2.	March 22, 1992	Sulfur plug in regenerator/steam treater offgas line.
3.	April 19, 1992	The MAC high sorbent level probe in the MAC disengaging vessel failed, causing the rupture disk in the vessel to release air/sorbent to atmosphere.
4.	April 26, 1992	Sorbent heater top and middle grids plugged with sorbent/water. Sorbent heater middle and bottom grids expanded (buckled up) to interfere with the movement of the flapper valve attached to the downcomer. (The bottom edge of the flapper valve was originally 1" above the grid plate.)
5.	May 17, 1992	Regenerator pressure control valve (PV 518) stem not moving freely, which caused pressure swings in regenerator/steam treater offgas line, which produced incinerator trips.
6.	May 24, 1992	Sorbent heater middle grid plugged.
7.	May 31, 1992	Regenerator offgas valve prior to the incinerator would not turn.
8.	June 21, 1992	A hole developed in the incinerator offgas duct at the point where steam from the methane preheater is vented into the duct. The duct was replaced. The steam was re-routed to a steam trap which corrected the problem.
9.	August 9, 1992	High sorbent level probe in the MAC disengaging vessel malfunctioned. Sorbent heater middle grid plugged.
10.	August 30, 1992	Replaced motor and fan bearing in heater/cooler fan (K-103). The bearings were replaced after 4650 hours of operation.

Figure 10-1
Pilot Plant Availability
(3/1/92 to 8/16/92)

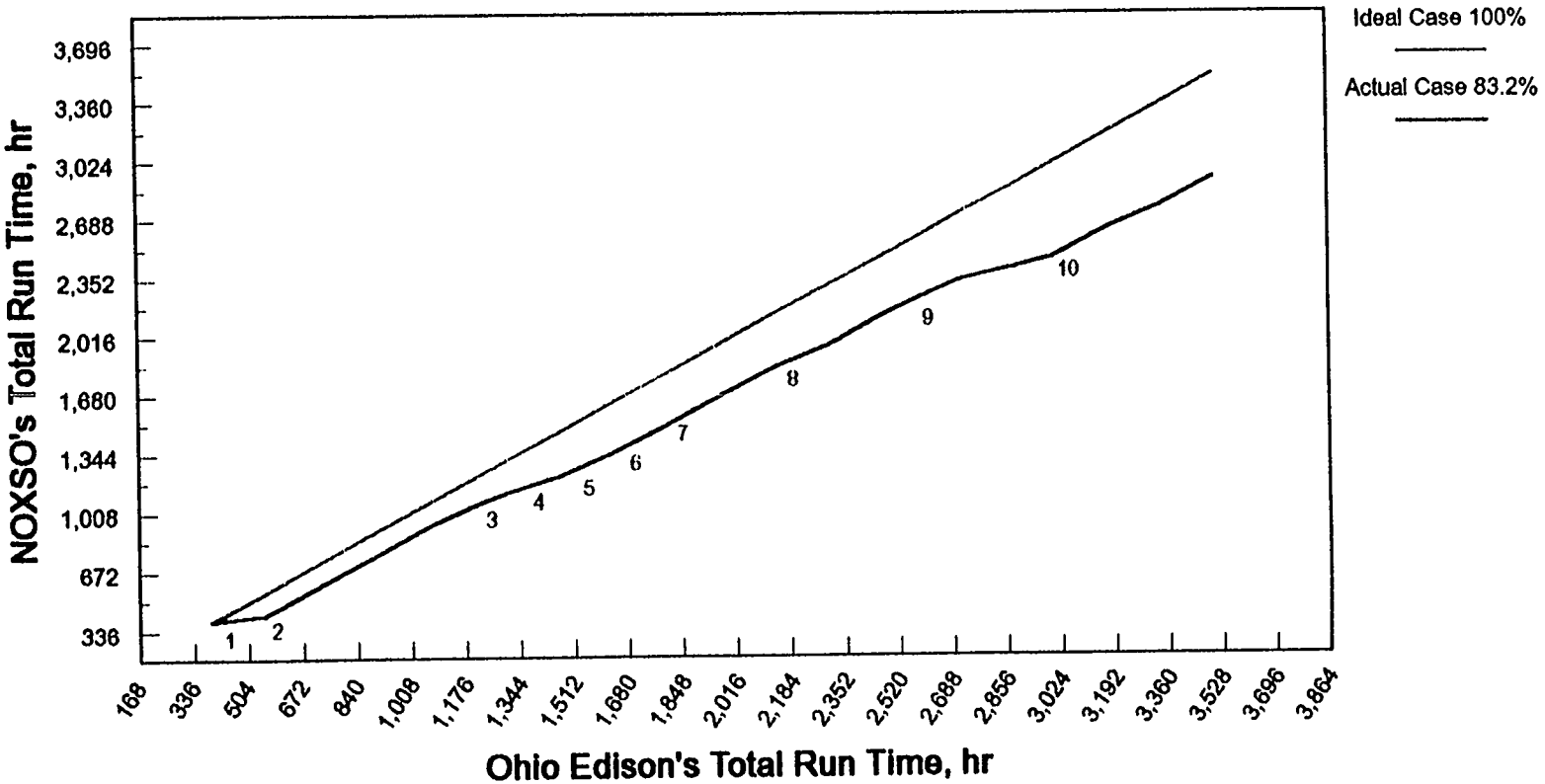

This date was taken over 24 weeks.

Figure 10-2
Pilot Plant Availability
(8/23/92 to 1/17/93)

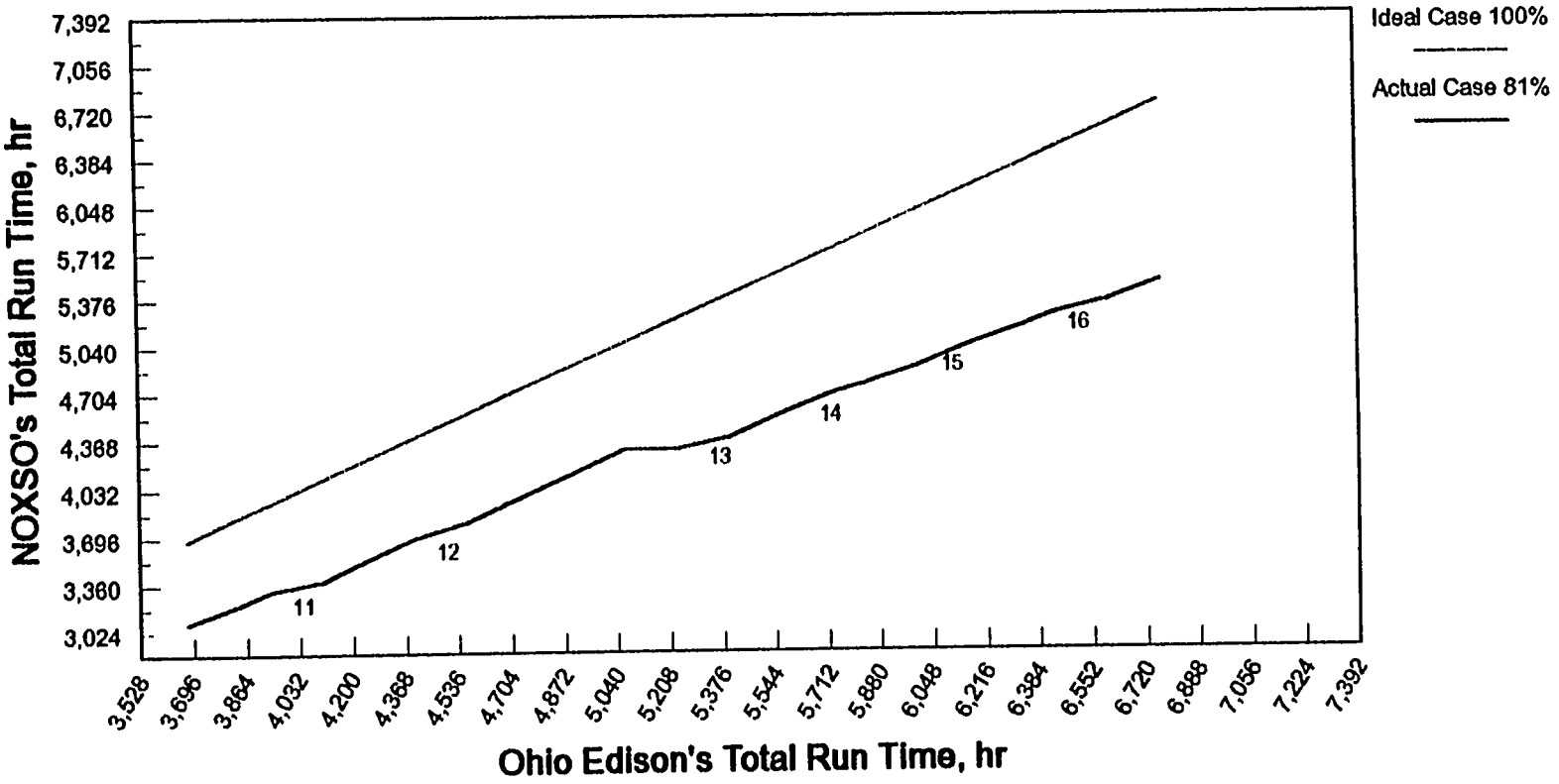

This data was taken over 23 weeks.

11. October 4, 1992 — The sorbent was over-sulfated. Flue gas was discontinued and the inventory was regenerated for several cycles until the sulfur content of regenerated sorbent returned to the normal range (i.e., 0.2-0.3 wt%).

12. November 1, 1992 — Replaced the fan bearings in the adsorber fan (K-101). The bearings were replaced after 5700 operating hours.

13. November 22, 1992 — The adsorber grid plugged with a mixture of sorbent, fly ash, and water. The flue gas flowrate was 10,000 scfm. Water was sprayed into the flue gas to reduce the temperature from 360° to 240°F. At 240°F, acid condensed and was carried with the gas through the grid holes. When acid contacts sorbent, it dissolves the binder holding the microspheres together. When the mixture dries, it forms a cementitious deposit that plugs the 1/8" grid hole.

14. December 6, 1992 — The adsorber grid plugged as in #13 above; however, in this case, the acid drain line plugged causing acid to accumulate in the elbow just below the adsorber grid. The flue gas flowrate was 7000 scfm and the flue gas temperature was controlled at 240°F by water spray.

15. January 10, 1993 — The seals on the butterfly valve between the MAC surge bin and the MAC fluidizer and on the cone valve in the MAC fluidizer were replaced after 6650 hours of operation.

16. January 17, 1993 — Over-sulfated the sorbent, ran for several cycles without flue gas.

System modifications were performed over the course of the project to make the plant easier to operate. These efforts have succeeded in reducing the number and the frequency of pilot plant outages, as shown in Figures 10-1 and 10-2. System modifications were as follows:

Regenerator/Steam Treater Offgas Line - Early in the project sulfur pluggage presented a problem. Subsequently a sulfur trap was installed at the end of the vertical section of pipe just upstream of the incinerator. Check valves in regenerator and steam treater offgas lines were removed and a single check valve was placed in the combined offgas line to the incinerator. Also operating procedures were changed so that methane was not fed to the regenerator until the temperature in the regenerator offgas line exceeded the dewpoint of sulfur vapor. These changes eliminated sulfur plugs in the regenerator/steam treater offgas line.

Sorbent Heater Grid Pluggage - Grid pluggage can be avoided by having the proper amount of transport disengaging height (TDH) between bed and grid in the 3-stage heater and cooler. The distance from grid to grid in the sorbent heater is 44"; in the sorbent cooler it is 66". No grid pluggage has occurred in the sorbent cooler. Since the spacing between grids in the sorbent heater could not easily be changed, the grid holes were countersunk (from the bottom) and the

holes in the middle grid were enlarged from 1/8" to 5/32". This reduced the frequency of plugging, but, to eliminate the problem, the spacing between grids in the heater must be increased to a minimum of 66".

Sorbent Heater Grid Impeding Flapper Valve - A pair of supports were welded to the downcomer and grid to maintain a distance of 1" between the two. A permanent solution would be to support the grid in such a way as to account for the difference in thermal expansion between the vessel, grid, and grid supports.

Adsorber Grid Pluggage - This occurred exclusively at times when the flue gas was cooled by water spray to below the acid dewpoint. NOXSO has tested a two-stage adsorber with in-bed cooling via water spray. After 350 hours of operation, no grid pluggage has been observed on either grid.

10.2 Plant Trips

The distributed control system is programmed with a number of trips and plant interlocks. Sensors continuously monitor certain process flow measurements, temperatures, pressures, etc., for safety (for complete details on the trip matrix see Section 4.0). The trips experienced at the pilot from March to December 1992 are summarized in Table 10-1. The type of trip and the frequency of the trip are given in the table.

Table 10-1. Trip Summary

March-December 1992	
Trip Type	**Number**
Incinerator trip	29
High/low dp between sorbent heater and regenerator	14
Air heater flame fail	10
Low level in bottom bed sorbent heater	6
High CH_4 in J-valves	6
High level in MAC disengaging vessel	2
Heater/cooler fan shut off	3

Incinerator Trip - This trip was caused principally by low flame signal. Most of these trips occurred prior to March, when the incinerator UV flame scanner was replaced with an IR scanner, since H_2O in the gas feed to the incinerator adsorbed some UV resulting in weak flame signals. Also early on sulfur deposits blocked the flame scanner window. The flame scanner view pipe was extended and this corrected the problem. A sulfur trap is now in the line just upstream of the incinerator.

Differential Pressure, Regenerator Sorbent Heater - This trip is principally due to unstable sorbent circulation rate which causes the upper J-valve to oscillate and dump varying amounts

of steam/nitrogen into the regenerator. An improved J-valve (i.e., better control) would reduce the number of these trips.

Air Heater Flame Fail - This trip occurred because of high temperature at either the baghouse, air heater exit, or sorbent heater offgas. All trips occurred at high sorbent circulation rate. Since heater/cooler fan capacity is limited, high sorbent circulation means high temperature at the air heater exit, high temperature at the sorbent heater outlet, and high baghouse temperature. More fan capacity would eliminate this trip.

Low Level Sorbent Heater Bottom Bed - This trip was caused by the flapper valve in the middle to bottom bed downcomer. With temperature cycling the grids deformed (buckled) and impeded the motion of the flapper valve. A properly designed grid support would reduce the number of these trips (see above).

High CH_4 in J-Valves - Anarad analyzers measure the concentration of CH4 in the upper and middle J-valves. These trips were caused by analyzer malfunctions and operator error, i.e., analyzers were sometimes not disconnected from the data highway while they were calibrated.

High Level in MAC Disengaging Vessel - This trip was caused by a malfunction of the MAC high level probe in the disengaging vessel. It has since been corrected.

Heater/Cooler Fan Shut-Off - This trip is caused by excessive current draw. At high sorbent circulation rates, fan capacity is limiting. Proper design of the fan would eliminate this trip.

10.3 Suggested Plant Modifications

Some mechanical modifications were made to the POC unit which should be incorporated into future designs. There are also items which were discovered during the operations which should be incorporated into future NOXSO Process operations. These are summarized below:

1. Regenerator pressure control valve (PV518A) and regenerator offgas valve prior to the incinerator required the addition of nitrogen bearing purges to prevent corrosion and binding of the valve mechanism. All valves used to control regenerator gases will require bearing purges.

2. Turbine flowmeters had relatively poor performance on the pilot process. Another flowmeter should be considered for future installations.

3. Additional control of steam and N_2 to the J-valves should be included in future installations. This would include flow transmitter and control valve additions to both the elbow gas and conveying gas for each J-valve. A 100 psi nitrogen source should be available at each J-valve box and plumbed so that a short burst of 100 psi nitrogen can be admitted to the J-valve box through the elbow gas line. This was found necessary to clear the J-valves of any water-sorbent composite present.

4. J-valve slide gate valves should be completely enclosed and seals purged with nitrogen. The current slide gates have a graphite packing on the end of the slide gate. This packing occasionally leaks gas and sorbent. A sealed slide gate with nitrogen purge would solve this difficulty.

5. The three J-valves never required the use of additional gas at the top elbow of the J-valves (FI-4054, FI-4050, FI-5056). Each of the elbows was provided with this, but they were never used. They can be deleted from future installations.

6. The regenerator has two differential pressure indicators which can be removed from future installations (PDT-305, PDT-307). They provided little useful information. PDT-308 is necessary to control the differential pressure between the regenerator and steam treater.

7. The regenerator also has an excessive number of temperature measurements which should be eliminated in commercial units. The thermocouples extending from the top of the unit have 32 temperature elements. There has not been any significant radial temperature gradients observed at the POC (although axial gradients are present from changes in the sorbent heater temperature). These could be replaced by three or four thermocouples in the vessel.

8. The special gas distribution slats within the regenerator and steam treater are believed to offer no advantages over a simple sparger within a vessel. Although these are currently being used at the POC the use of a sparger would simplify vessel design and reduce cost.

9. The dense phase lift (MAC) should be the sorbent circulation control point with J-valves as level control slaves.

10. All regenerator offgas lines should be steam jacketed to prevent the freezing of condensed sulfur.

11. A slide gate valve (either manual or actuated) should be installed on each J-valve downcomer. This allows the J-valve box to be isolated for maintenance and cleaning without emptying vessels of sorbent.

12. Differential pressure measurements with transmitters should be installed on each grid and fluid bed. This allows for rapid diagnosis of sorbent flow problems within multi-stage fluid beds.

13. All instrument purges should be nitrogen. The POC had some provision for switching instrument purges to steam, but these were never used. Any condensing steam from the instrument purge wets sorbent and causes the pressure tap to clog off.

14. Thermocouples should not be installed within the J-valve risers. Thermocouples in the downcomer section of the J-valves are more accurate measurements of sorbent temperature and do not interfere with sorbent flow.

15. Probes for process gas and sample gas measurements need to be installed directly into the offgas piping being sampled. Better dilution probes need to be purchased or developed for collecting samples from these streams.

16. Acid collection from cooling the flue gas by water spraying can be substantial when the flue gas is cooled to low temperatures (240°F). Alternative methods of cooling flue gas without formation of acid need to be explored and tested.

17. Nozzles for pressure taps, stripper gas, elbow gas, and steam treater steam inlets need to enter vessels and pipes approximately 1". This allows any condensation or water in the line to contact sorbent and be vaporized rather than possibly pooling at the wall of the vessel or pipe.

18. The nitrogen purge of the sorbent heater is unnecessary and has never been used during the POC operations (CV-3070, and line N-2"-56-208). It can be deleted from future installations.

11.0 PARAMETRIC TEST RESULTS

The parametric test series was designed to quantify the effects of changing operating setpoints on process performance. The operating setpoints varied were flue gas temperature inlet to adsorber, adsorber bed pressure drop, sorbent circulation rate, flue gas flowrate, regeneration temperature and regenerator sorbent inventory. The concentrations of SO_2 and NO_x in flue gas inlet to the adsorber also varied due to changes in power plant load. The operating setpoints for all tests at mini-load (35 MW) and base load (55 MW) are given in Table 11-1 and 11-2, respectively. SO_2/NO_x concentrations in inlet flue gas were also increased by spiking the flue gas with SO_2 and NO from pressurized gas cylinders. Operating setpoints for these tests are given in Table 11-3.

Table 11-1. POC Tests Conducted at Mini Load

Test No.	Flue Gas Flowrate (scfm)	Solids Flowrate (pph)	Adsorber Bed dp (" H_2O)	Regenerator Level (ft)	Regenerator CH_4 Flow (scfm)
Test 1b	6900	7000	15.4	4.8	15.0
Test 2a	5800	8000	21.3	5.1	15.0
Test 3a	5800	6000	15.8	4.1	15.0
Test 4a	5800	5900	12.9	4.4	15.0
Test 4b	5800	5900	12.9	4.4	8.9
Test 5a	6900	6900	12.9	4.4	10.5
Test 6a	5800	5900	8.5	1.5	8.9
Test 7a	8450	7900	11.4	3.7	12.9
Test 8a	8450	5900	8.5	4.4	12.9
Test 9a	8450	7900	17.2	9.5	12.9
Test 10a	5800	7900	17.2	3.7	8.9
Test 1c	8450	5900	12.9	3.0	12.9
Test 2b	6900	6900	12.5	4.4	10.5
Test 3b	5800	7900	11.4	9.5	8.9
Niles-1	10000	10000	11.8	9.5	15.0
Niles-2	6000	10000	7.1	9.5	15.0
Niles-3*	11000	7500	5.3	1.7	7.9
Niles-7	11000	7500	13.0	5.0	10.0
Niles-8	9000	7500	10.6	5.0	10.0
Niles-9	7000	7500	8.2	5.0	10.0
Niles-10	11000	7500	8.8	5.0	10.0
Niles-11	9000	7500	7.2	5.0	10.0

Table 11-1. POC Tests Conducted at Mini Load					
Test No.	Flue Gas Flowrate (scfm)	Solids Flowrate (pph)	Adsorber Bed dp (" H_2O)	Regenerator Level (ft)	Regenerator CH_4 Flow (scfm)
Niles-12	7000	7500	5.6	5.0	10.0
Niles-13	10000	10000	7.7	5.0	10.0
Niles-14	10000	6500	17.7	5.0	10.0
For all mini load tests:		Inlet flue gas temperature, °F		320	
		Heater bottom bed temperature, °F		1150	
		Treater steam flow, lbs/hr		40	

* Test designed for 0.6 wt% on sorbent after regeneration.

Table 11-2. POC Tests Conducted at Base Load				
Test No.	Flue Gas Flowrate (scfm)	Solids Flowrate (pph)	Adsorber Bed dp (" H_2O)	Flue Gas Temperature (°F)
PC-1	7000	10000	20	320
PC-2	6500	10000	14	320
PC-3	7000	10000	14	320
PC-4	7000	10000	7	320
PC-5	7000	10000	7	240
PC-6	7000	10000	20	240
PC-7	7000	10000	14	240
PC-9	7000	8000	14	240
WRG-1	5800	10000	20	320
WRG-2	5800	10000	20	240
FG-1	8000	10000	14	320
FG-2	9000	10000	14	320
FG-3	10000	10000	14	320
BB-1	10000	10000	14	320
BB-2	8000	10000	14	320
BB-3	9000	10000	14	320
BB-4	7000	10000	14	320
BB-5	10000	10000	7	320
BB-6	10000	10000	20	320

Table 11-2. POC Tests Conducted at Base Load				
Test No.	Flue Gas Flowrate (scfm)	Solids Flowrate (pph)	Adsorber Bed dp (" H_2O)	Flue Gas Temperature (°F)
BB-7	10000	10000	14	240
BB-8	9000	10000	14	240
BB-9	9000	8000	14	320
BB-10	9000	6000	14	320
Duration Test	9000	10000	14	280
All base load tests:		Heater bottom bed temperature, °F		1150
		Regenerator level, ft		5
		Regenerator CH_4 flow, scfm		10
		Treater steam flow, lbs/hr		40

Table 11-3. POC Spiking Tests						
Test No.	Flue Gas Flowrate (scfm)	Solids Flowrate (lbs/hr)	Adsorber Bed dp (" H_2O)	Flue Gas Temperature (°F)	**Inlet SO_2 Concentration (ppm)	***Inlet NO_x Concentration (ppm)
Spike-1	9000	7500	8.4	320	1800	580
Spike-2a	7000	10000	11.1	320	1800	500
Spike-2b	7000	10000	11.1	320	1800	750
Spike-2c	7000	10000	11.1	320	1800	1000
Spike-3a	7000	10000	14.0	320	2800	400
Spike-3b	7000	10000	14.0	320	2800	700
Spike-3c	7000	10000	14.0	320	2800	1000
Spike-3d	7000	10000	14.0	320	3300	400
Spike-3e	7000	10000	14.0	320	3300	1000
Spike-4a*	7000	10000	14.0	240	2800	400
Spike-4b	7000	10000	14.0	240	2800	700
Spike-4c	7000	10000	14.0	240	2800	1000

* Tests 4a-c were repeated after installation of the "bubble buster".

** 400 ppm represents nominal base load NO_x concentration.

*** 1800 ppm represents nominal unspiked SO_2 concentration.

Parametric test data reduction and analysis are presented in this section of the report. At the end of this section, an adsorption and a regeneration model are presented which can be used to predict the pilot plant data to an accuracy of ± 15%.

11.1 Material Balances

As part of the data quality assurance programs at the POC, material balances were computed over each 12-hour shift of operation. Material balances were required to close within ± 15% for the data to be considered valid. Of primary interest were the four component material balances discussed below. Closure of these four material balances from July 8, 1992 to December 15, 1992 are tabulated in Appendix D.

The mass flowrate of sulfur removed in the adsorber is determined from the flue gas flowrate and the SO_2 concentrations in Streams 1 and 2 (see Figure 11-1 for stream numbers). Alternately, the mass flowrate of sulfur adsorbed can be computed from the solids flowrate and the concentration of sulfur on the sorbent in Streams 3 and 4. The adsorber gas/solid sulfur mass balance compares the mass flowrate of sulfur adsorbed as calculated by these two methods.

During steady-state operation all sulfur removed in the adsorber is desorbed in the regenerator and sorbent heater. The total mass flowrate of sulfur desorbed is calculated from the concentrations of sulfur bearing components and the flowrate of Streams 5, 6 and 8. The adsorber/regenerator sulfur mass balance is then computed by comparing the total mass flowrate of sulfur desorbed versus the mass flowrate of sulfur adsorbed. Note, the mass flowrate of sulfur adsorbed is based on the flue gas flowrate and concentrations rather than the sorbent flowrate and concentrations.

Similar to the adsorber/regenerator balance, the NO_x balance is used to verify that all NO_x removed in the adsorber is desorbed in the sorbent heater. The rate of NO_x adsorption is calculated from Streams 1 and 2, while the rate of NO_x desorption is calculated from Stream 5. For the purpose of computing the mass balance closure, all NO_x species are treated as NO.

The purpose of the regenerator carbon balance is to ensure that the CH_4 feed to the regenerator can be accounted for in the regenerator offgas streams. Obviously, the mass flow of carbon into the regenerator is given by the CH_4 feed rate. The mass flow of carbon exiting the regenerator is calculated by the concentrations of carbon bearing species and flowrates of the two offgas Streams 6 and 8. In general, the regenerator carbon mass balance closure has varied between 80 - 90%, indicating a deficiency in the mass of carbon exiting the regenerator. Sorbent analysis has shown this deficiency results from coking or carbon deposits on the sorbent.

11.2 Parametric Results

11.2.1 Effect of Gas/Sorbent Residence Time in Adsorber

SO_2 removal efficiencies are plotted as a function of adsorber gas residence time in Figures 11-2 and 11-3. Adsorber gas residence time is the fluid bed settled bed height divided by the superficial gas velocity through the bed. The data are divided into groups with similar sorbent residence times as shown on the right hand side of the figures. Sorbent residence time is the adsorber inventory divided by the sorbent circulation rate. Since sorbent surface area

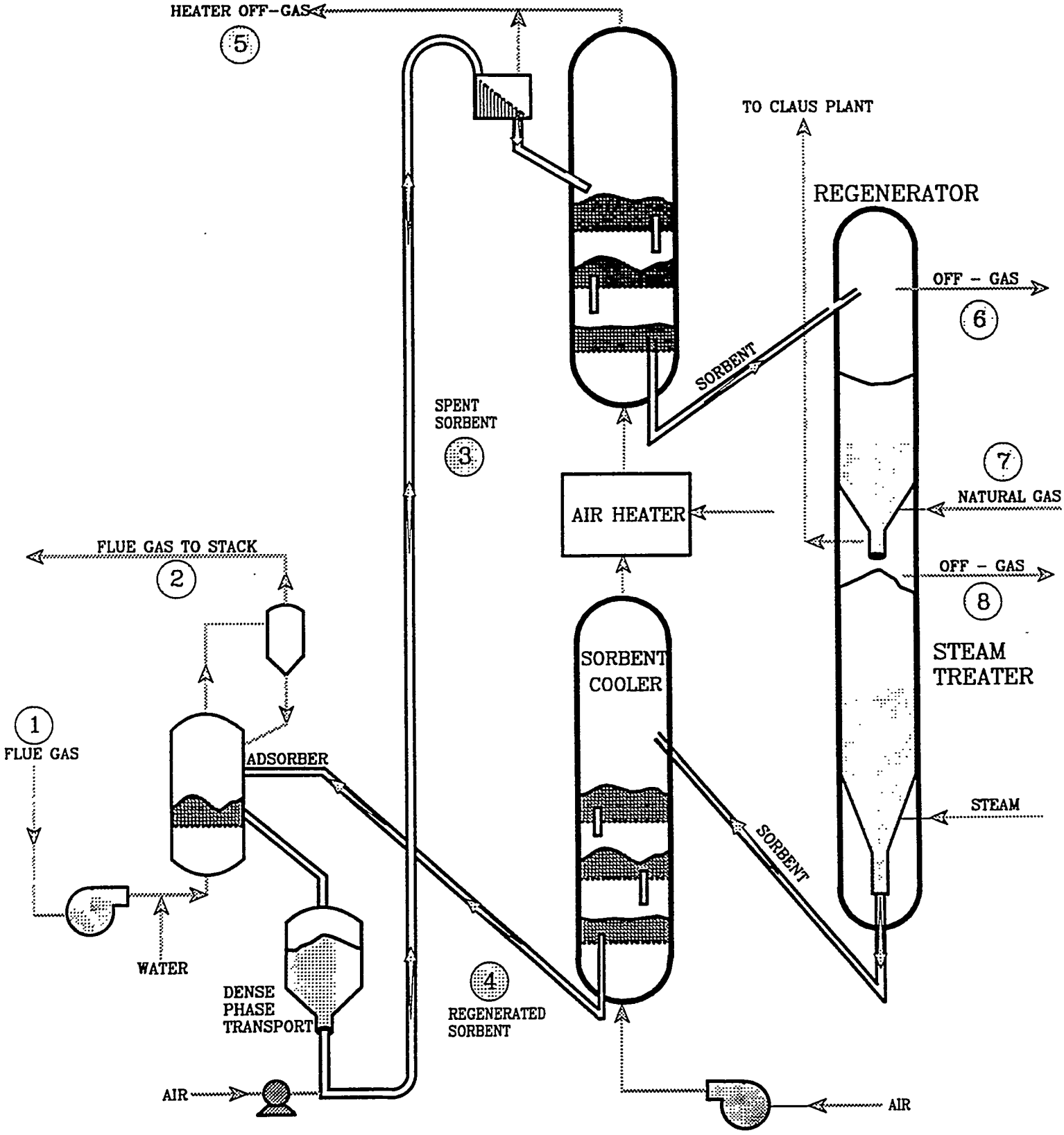

Figure 11-1
NOXSO Process Flow Diagram

Figure 11-2

SO2 Removal Versus Gas/Sorbent Residence Time

All Data From Tests at Mini and Base Load

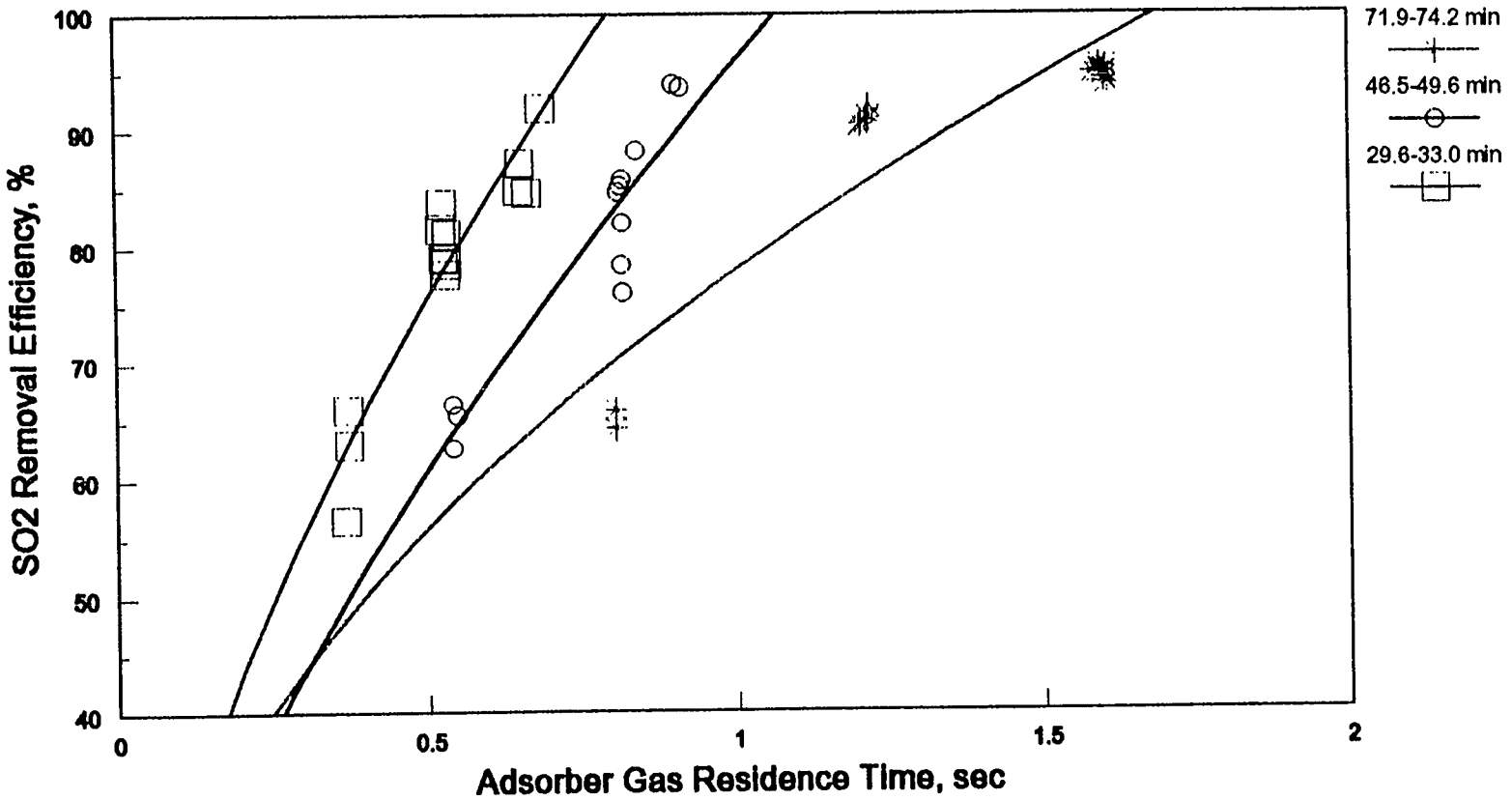

Figure 11-3
SO2 Removal Versus Gas Sorbent Residence Time
All Data From Tests at Mini and and Base Load

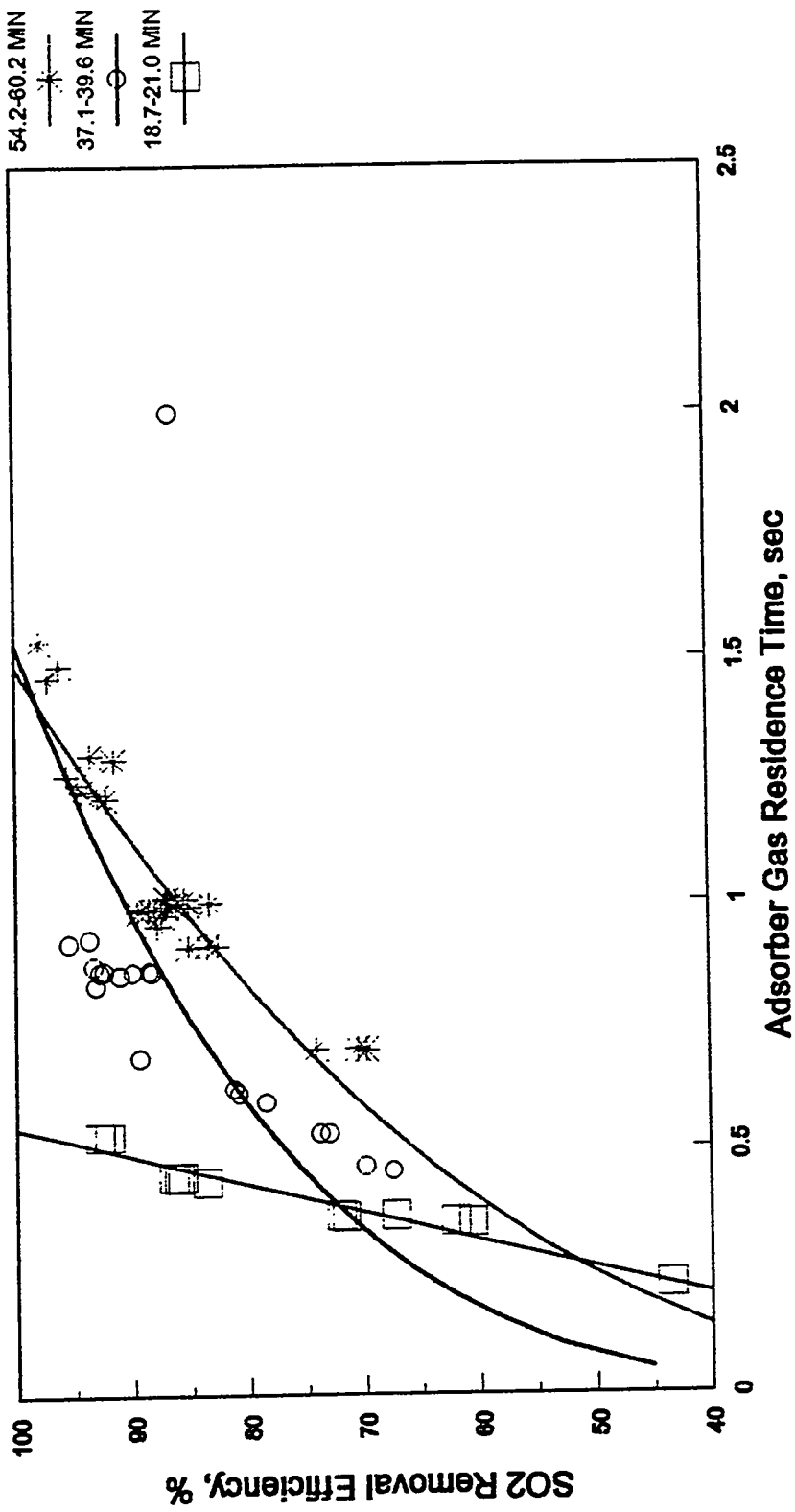

changes with time in the initial stage of the tests, the only data used is from the period of time after the initial decline in sorbent surface area (after 350 flue gas hours).

The data set consists of 104 data points of 12-hour shift averages. The range of measured operating conditions in these tests were as follows:

Adsorber bed pressure drop	=	5.3 - 21.4" H_2O
Adsorber bed temperature	=	273 - 351°F
Flue gas flowrate	=	5,853 - 11,110 scfm
Sorbent circulation rate	=	5,861 - 10,023 pph
SO_2 inlet to adsorber	=	1,332 - 2,120 ppm
NO_x inlet to adsorber	=	163 - 454 ppm
Gas residence time in adsorber	=	0.2 - 1.6 sec.
Sorbent residence time in adsorber	=	19 - 74 min.

Data from the flue gas spiking tests are not included. Spiking data is covered in Section 11-4.

A regression analysis was performed to obtain a mathematical relationship that best fits the data. The best fit is a power function. The power function curves plotted in Figures 11-2 and 11-3 show that the rate of change in removal efficiency with changing gas residence time is fast at low removal efficiency and slow at high removal efficiency. This is expected since the rate of adsorption decreases with decreasing concentration of SO_2 in the gas phase. The regression coefficients for the curves shown in Figures 11-2 and 11-3 are as follows (where $y = a\ x^b$):

Sorbent Residence Time (min.)	a	b	r^2	# of data points
71.9 - 74.2	78.0	0.48	0.82	16
54.2 - 60.2	85.9	0.39	0.87	31
46.5 - 49.6	95.9	0.65	0.89	12
37.1 - 39.6	98.2	0.43	0.93	19
29.6 - 33.0	114.8	0.60	0.89	14
18.7 - 21.0	176.6	0.93	0.95	12

Given the values of r^2 (r^2 equal to 1.0 is a perfect fit), the power function seems to give a reasonable fit to the data. The lack of a perfect fit is due to the fact that SO_2 removal efficiency also varies with SO_2 concentration in flue gas inlet to the adsorber. The concentration effect is discussed in Section 11-4.

The regression curves for each sorbent residence time interval are shown in Figure 11-4. The form of the curve at removal efficiencies less than 40%, and greater than 95%, is an extrapolation since no data were acquired in this range. It is interesting to note that, at removal

Figure 11-4
SO2 Removal Versus Gas/Sorbent
Residence Time (Data Regression)

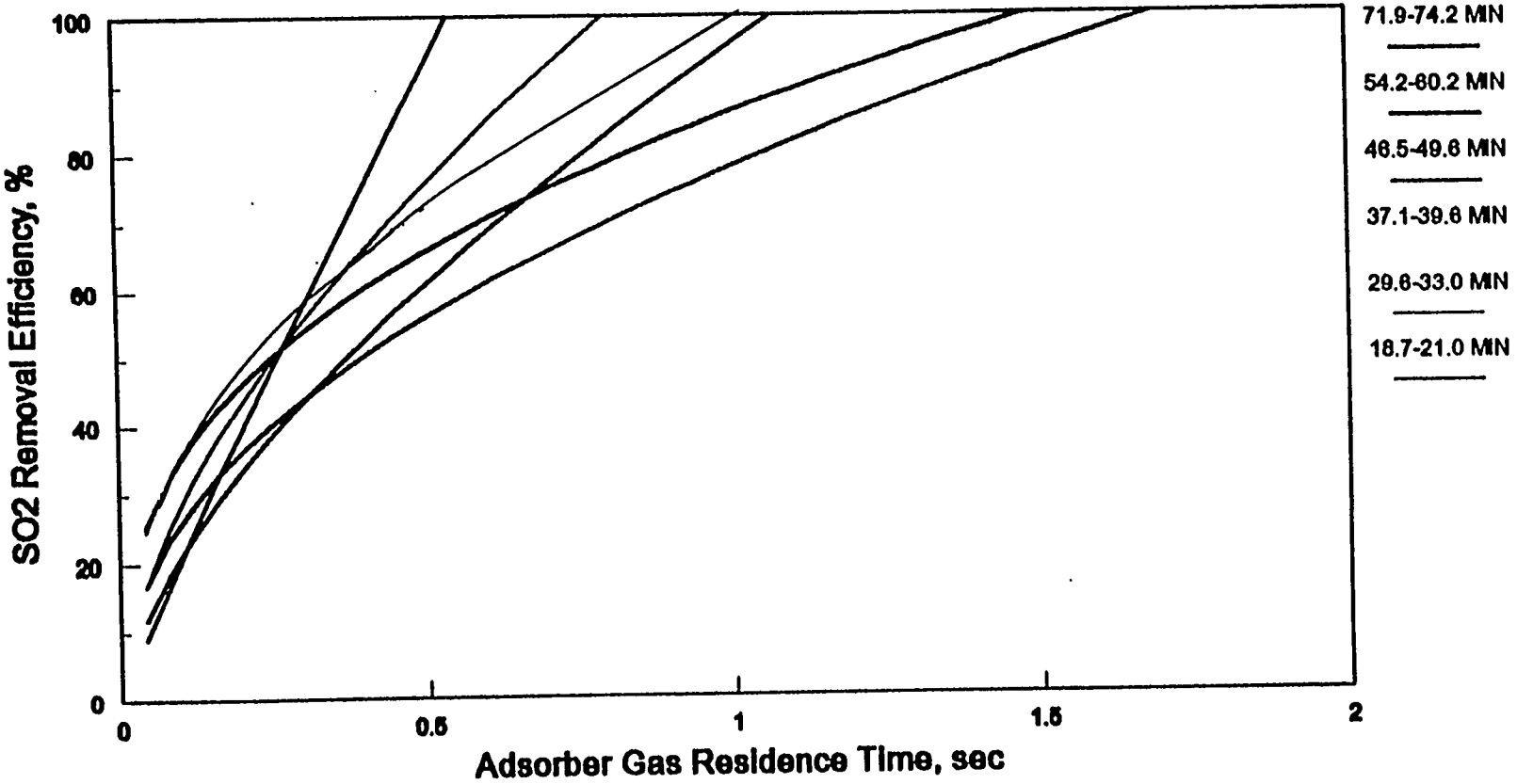

efficiencies greater than 60%, the curves follow a pattern of increasing slope with decreasing sorbent residence time. In other words, the rate of increase in removal with increasing gas residence time is greater at lower sorbent residence time.

Figure 11-5 shows sorbent residence time as a function of gas residence time for 90, 80, and 70% SO_2 removal efficiencies. Data points shown in the figure were computed using the regression coefficients listed above. Figure 11-5 can be used to get a rough estimation of the sorbent circulation rate required at a given bed height to achieve a specified removal efficiency.

The same type of data reduction was done for NO_x removal efficiency. Figures 11-6 and 11-7 show the plots of NO_x removal efficiency as a function of gas and sorbent residence time. The regression coefficients are as follows (where $y = a\ x^b$):

Sorbent Residence Time (min)	a	b	r_2	# of data points
71.9 - 74.2	75.7	0.70	0.85	8
53.2 - 60.2	83.2	0.35	0.60	34
46.5 - 49.6	92.0	0.45	0.66	9
37.1 - 39.6	92.1	0.32	0.55	17
29.6 - 33.0	106.1	0.50	0.58	14
18.7 - 21.0	119.7	0.46	0.80	9

The NO_x data do not fit the power function as well as the SO_2 data. as evidenced by the values of r^2 given above. This is because, in addition to the gas and sorbent residence time, NO_x removal efficiency is strongly affected by the concentration of NO_x in the flue gas inlet to the adsorber and by adsorber bed temperature.

11.2.2 Effect of Adsorber Bed Temperature

A series of spiking tests (see Table 11-3) were conducted in which the inlet concentrations of SO_2 and NO_x in the flue gas were increased by spiking the flue gas with SO_2 and NO_x from pressurized gas cylinders. Sorbent circulation rate, flue gas flowrate, and adsorber bed pressure drop were held constant in these tests and, as a result, gas and sorbent residence times were also constant.

Figure 11-8 shows a plot of NO_x removal efficiency as a function of NO_x inlet to the adsorber (ppm) and adsorber bed temperature. The figure shows that NO_x removal efficiency improves with decreasing temperature in the adsorber bed. At roughly 1000 ppm inlet NO_x, NO_x removal efficiency is 41% at a bed temperature of 345°F and 75% at a bed temperature of 297-312°F. The rate of decline in NO_x removal efficiency with increasing NO_x inlet to the adsorber is greater at the higher bed temperature, indicating that more active NO_x adsorption sites are present at the lower temperature.

Figure 11-5
SO2 Removal as a Function of Gas/Sorbent Residence Time (Data Regression)

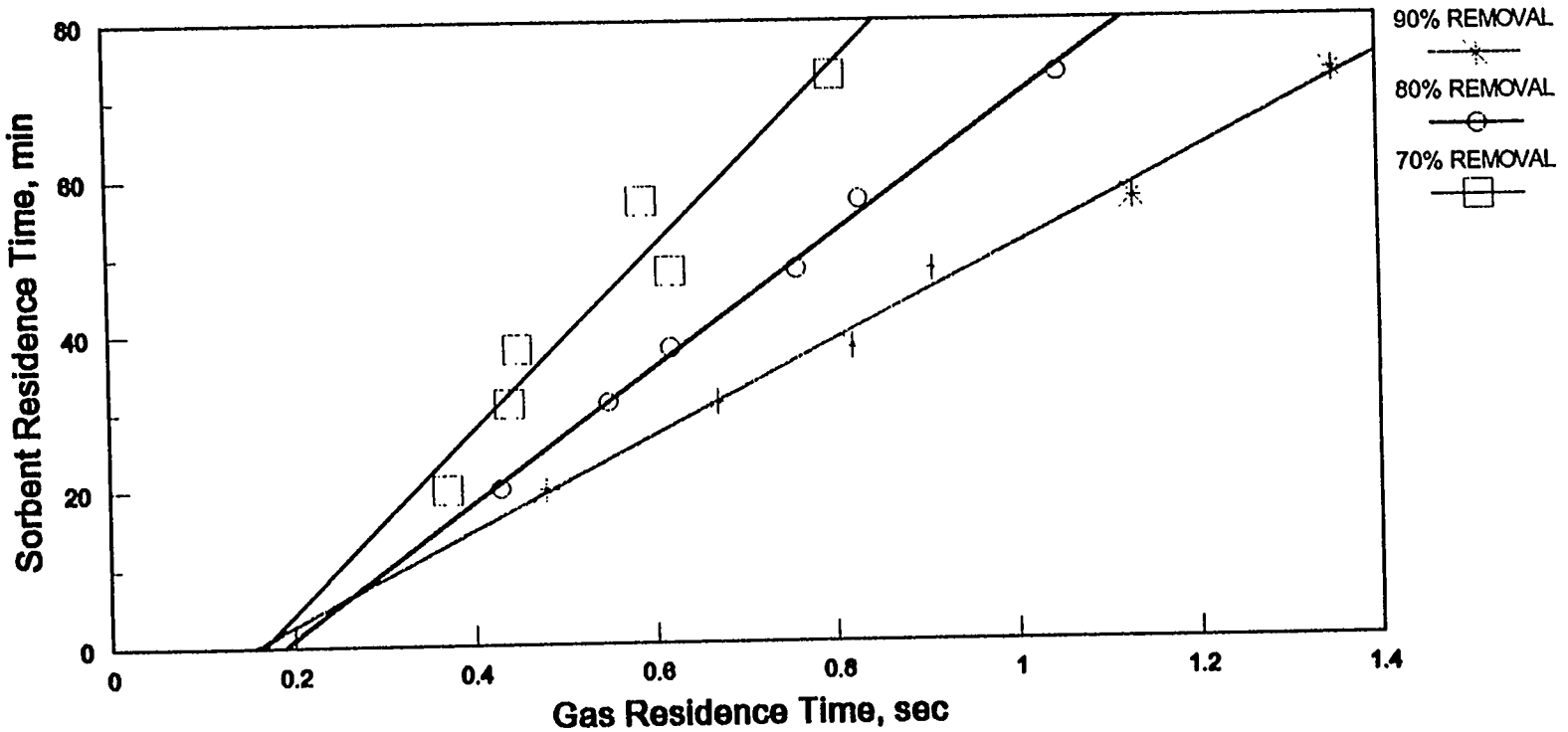

SO2 Inlet = 1300-2100 ppm

NOx Inlet = 163-454 ppm

Figure 11-6
NOx Removal Versus Gas Sorbent Residence Time
All Data From Tests at Mini and Base Load

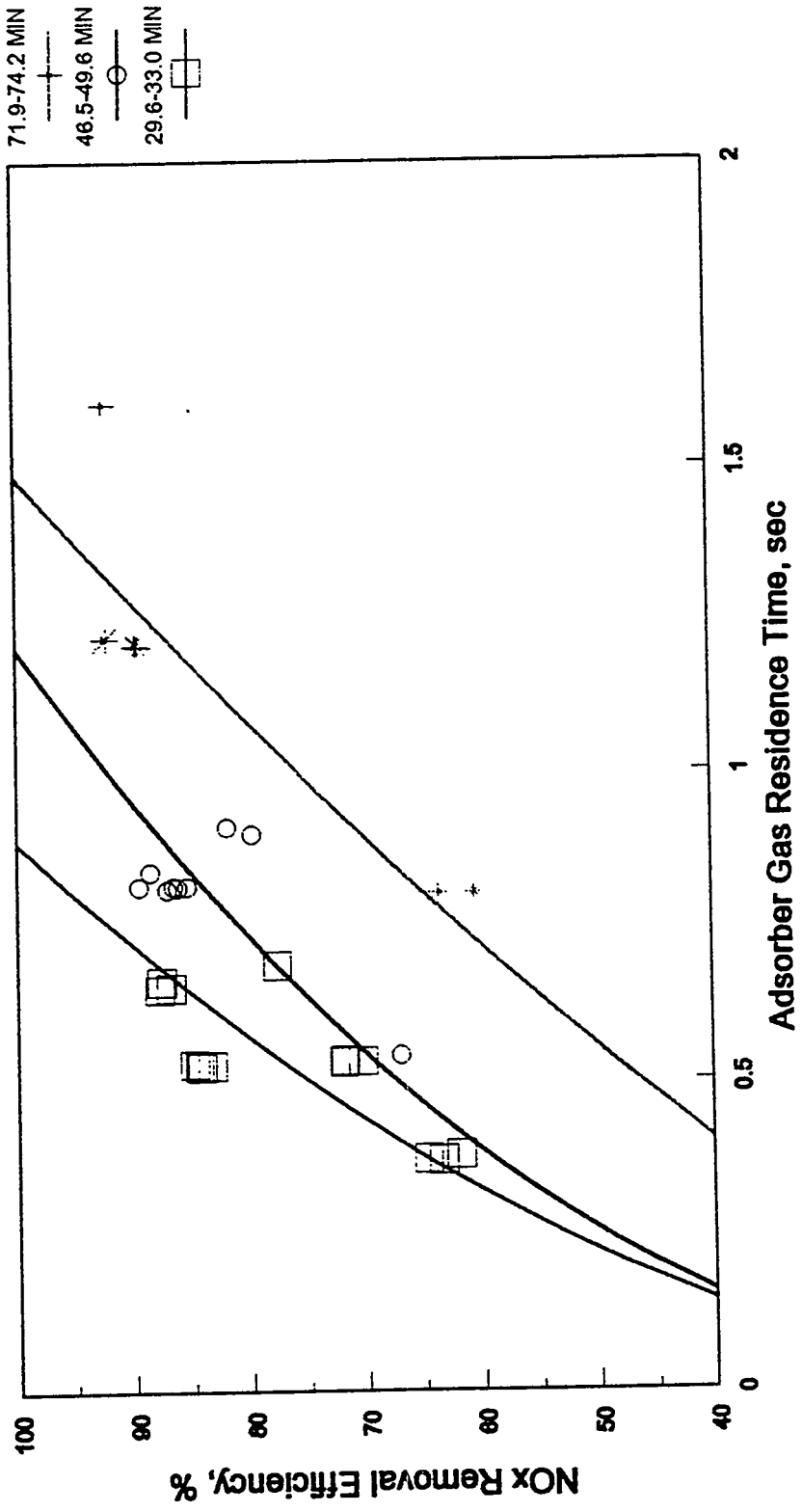

Figure 11-7

NOx Removal Versus Gas/Sorbent Residence Time

All Data From Tests at Mini and Base Load

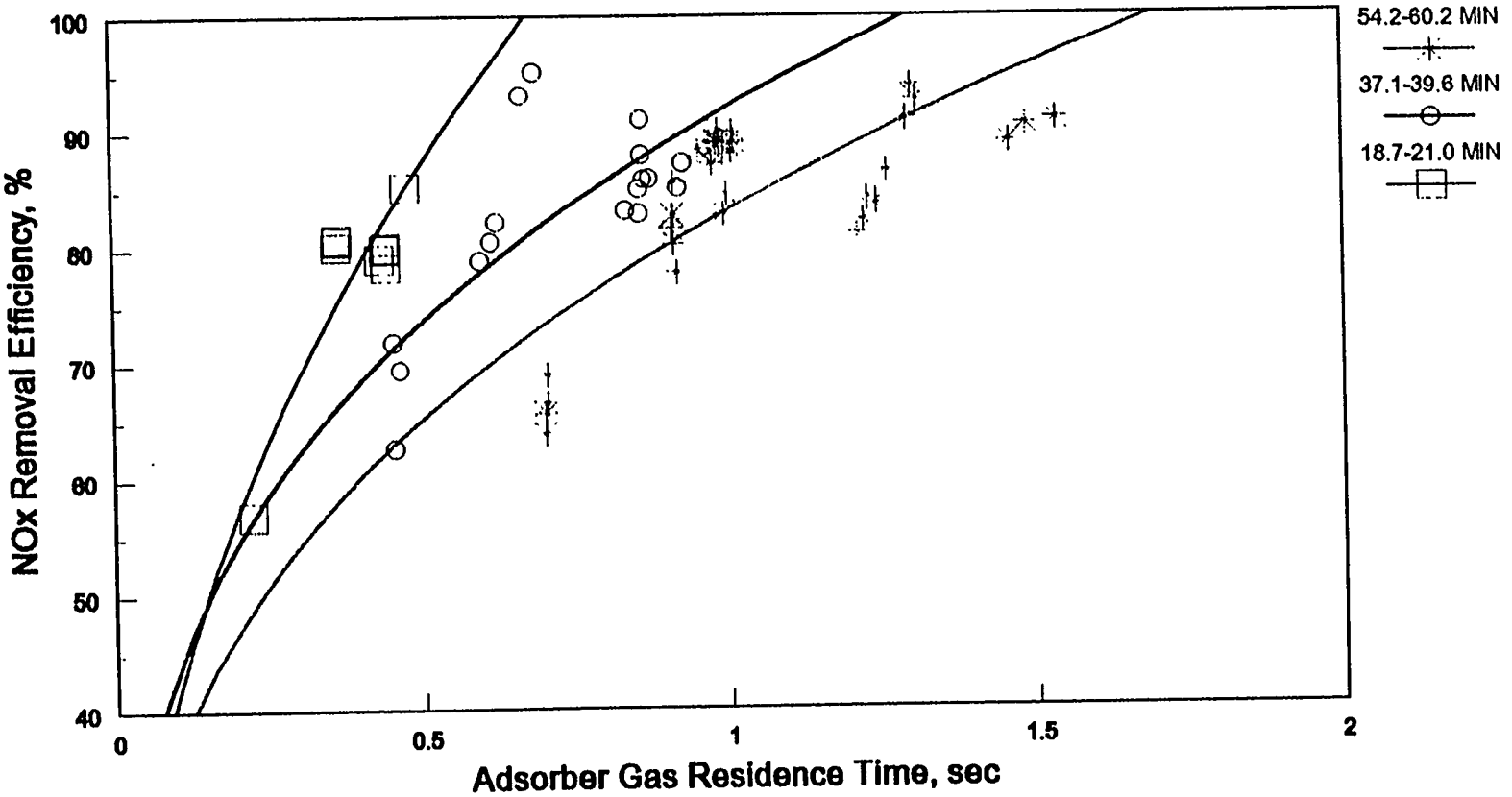

Figure 11-8
Spike Flue Gas With SO2/NOx
10000 pph, 7000 scfm, 14" H20

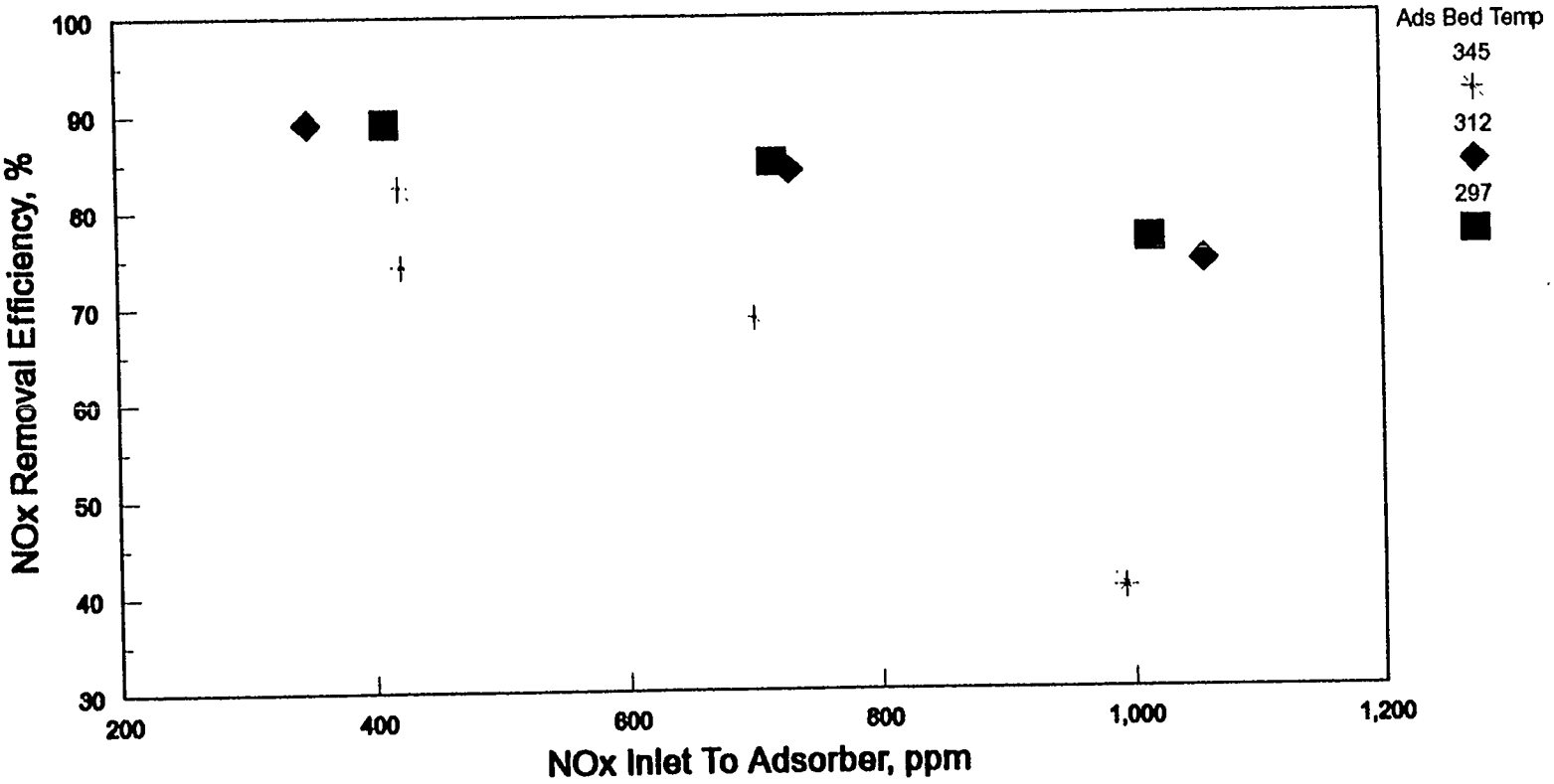

SO2 Inlet = 3132-2883 ppm

Figure 11-9 shows SO_2 removal efficiencies measured during the same set of flue gas spiking tests. The plot shows lower SO_2 removal at lower adsorber bed temperatures. However, this is due to the fact that there is competition between SO_2 and NO_x for adsorption sites and more NO_x is adsorbed at low temperature. When all the data are considered, SO_2 removal efficiency does not vary significantly with temperature (see below). A similar result was obtained in the laboratory using a fixed bed reactor (See Section 3.0). What is significant is that SO_2 removal efficiency increases with increasing concentration of NO_x in the inlet flue gas. This result substantiates one of the steps in the proposed SO_2 adsorption mechanism. As discussed earlier in Section 3.0, the existence of NO_x in the flue gas promotes SO_2 adsorption.

All the NO_x data were analyzed to determine the temperature effect on adsorption using the Freundlich isotherm. The Freundlich isotherm is:

$$\Theta_A = c\ P_A^{\frac{1}{n}} \qquad (11.2\text{-}1)$$

where:
- Θ_A is the occupied fraction of adsorption sites
- P_A is the partial pressure of adsorbate
- c,n is the constants, $n > 1$

The isotherm is based on the assumption that equilibrium is truly reached and that the adsorption (either physical adsorption or chemical adsorption) is reversible in the sense that no change in the adsorbate (in this case NO_x) occurs when cycling between adsorption and desorption. In the NOXSO Process, NO in the flue gas is adsorbed forming a complex consisting of NO, NO_2 oxygen, water, and SO_2 on the sodium-alumina surface. The sorbent is thermally regenerated with air and the products of desorption are NO and NO_2 (40:60). This does not fit the definition of a reversible reaction in the isotherm.

The NO_x isotherms are shown in Figure 11-10. The y-axis, which is the occupied fraction of adsorption sites (Θ_A in the isotherm), is approximated by the weight fraction of NO_x, expressed as NO,on the sorbent. This is because the total number of active sites is unknown. The x-axis is the measured equilibrium concentration of NO_x in the adsorber offgas which is assumed to be equal to the concentration of NO_x in the fluid bed.

A non-linear regression in the form of a power curve was used to fit the data. The results are shown in Figure 11-10 and are listed below (where $y = c\ x^{1/n}$).

Figure 11-9
Spike Flue Gas With SO2/NOx
10000 pph, 7000 scfm, 14" H20

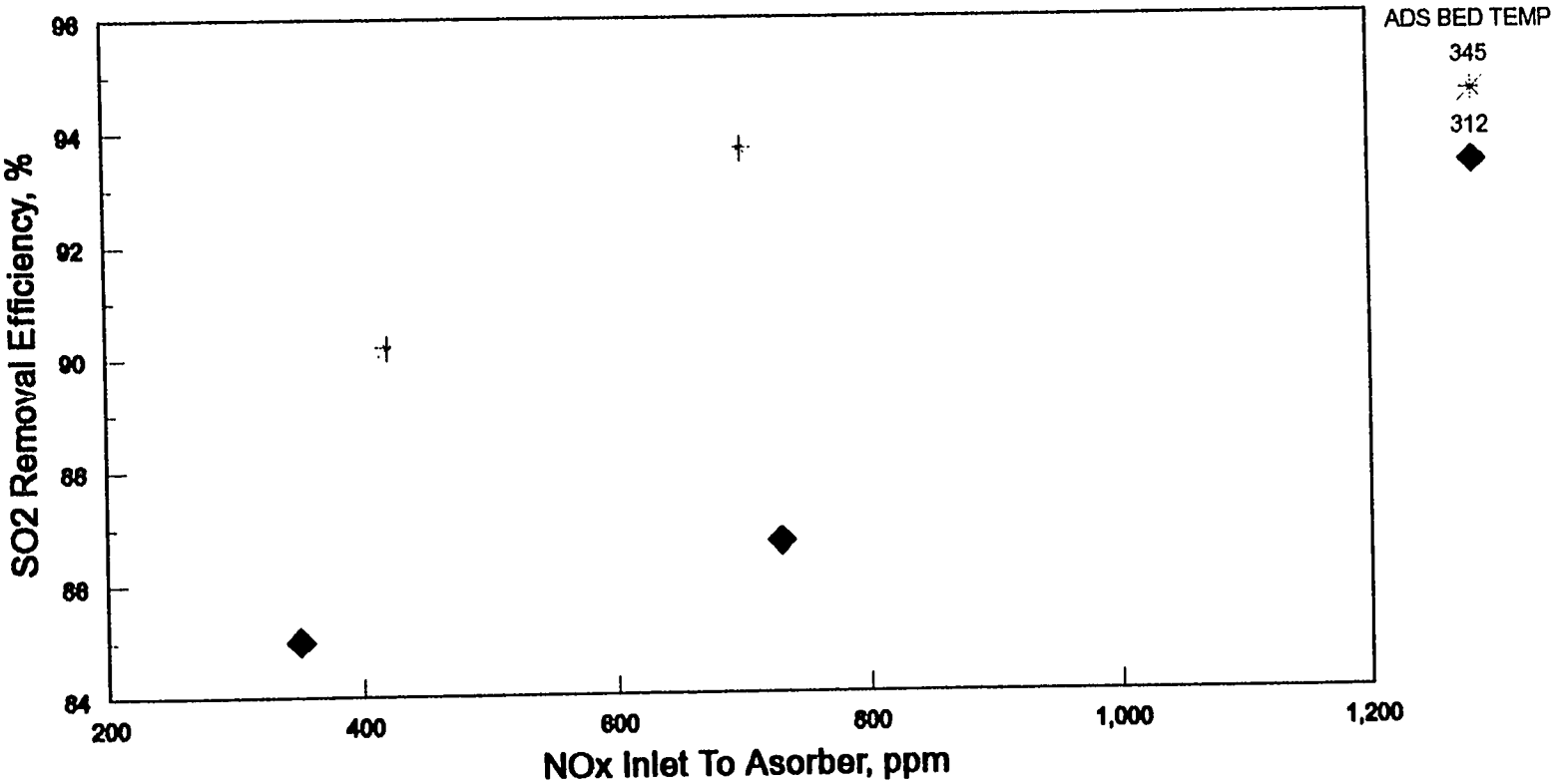

SO2 Inlet = 3132-2883 ppm

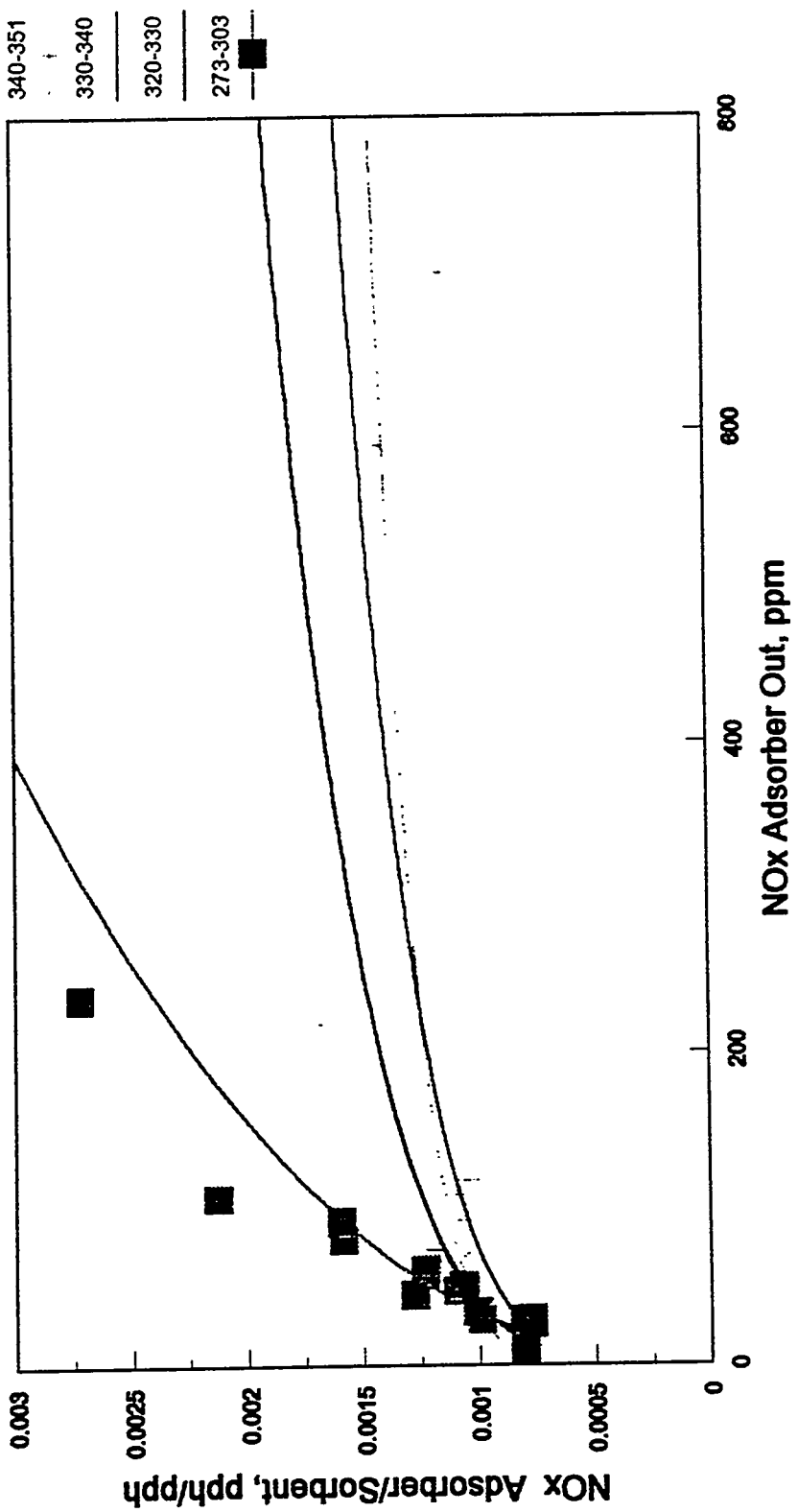

Figure 11-10
NOx Sorbent Loading at Varying
Adsorber Bed Temperatures

Temperature Range °F	r^2	c	n	# of Points
340 - 351	0.46	0.00067	9	17
330 - 340	0.63	0.00043	5	22
320 - 330	0.48	0.00046	5	45
273 - 303	0.82	0.00021	2	16

The degree of accuracy of the fit (r^2) is poor in all cases except in the temperature range of 273-303°F. This is most likely due to the fact that the NO_x adsorption process is not truly reversible. However, Figure 11-10 shows that NO_x sorbent loading was significantly higher in tests at 273-303°F than in any of the other tests.

A similar data analysis was done for SO_2 and the results are plotted in Figure 11-11. The figure shows a small improvement in SO_2 loading at the highest temperature range studied. However, the temperature effect is small compared to the temperature effect on NO_x adsorption.

11.2.3 Effect of SO_2/NO_x Concentration

Figure 11-12 is a plot of SO_2 removal efficiency versus SO_2 inlet to the adsorber at two sets of operating conditions. One test was conducted at mini-load and the other was conducted at base load, so NO_x concentrations in inlet flue gas were different. Each data set was obtained at a nearly constant gas residence time, but sorbent residence times varied by 22% in the two tests. The average operating conditions for each data set were as follows:

	Sorbent Circulation Rate (pph)	
	9949	**6877**
Flue Gas Flowrate, scfm	7257	6981
Gas Residence Time, sec	0.88	0.82
Sorbent Residence Time, min	38	49
Average NO_x inlet, ppm	404	215

The lines shown in Figure 11-12 are the best fits to the data using the method of least squares. The regression coefficients (where $7=a+bx$) are:

	a	b	r_2	# of Points
$[NO_x]_{in}$ = 350 - 421 ppm Sorbent residence time = 38 min	106.6	-0.006	0.80	6
$[NO_x]_{in}$ = 198 - 231 ppm Sorbent residence time = 49 min	116.9	-0.012	0.94	7

Figure 11-11
SO2 Sorbent Loading as a Function of
Adsorber Bed Temperature

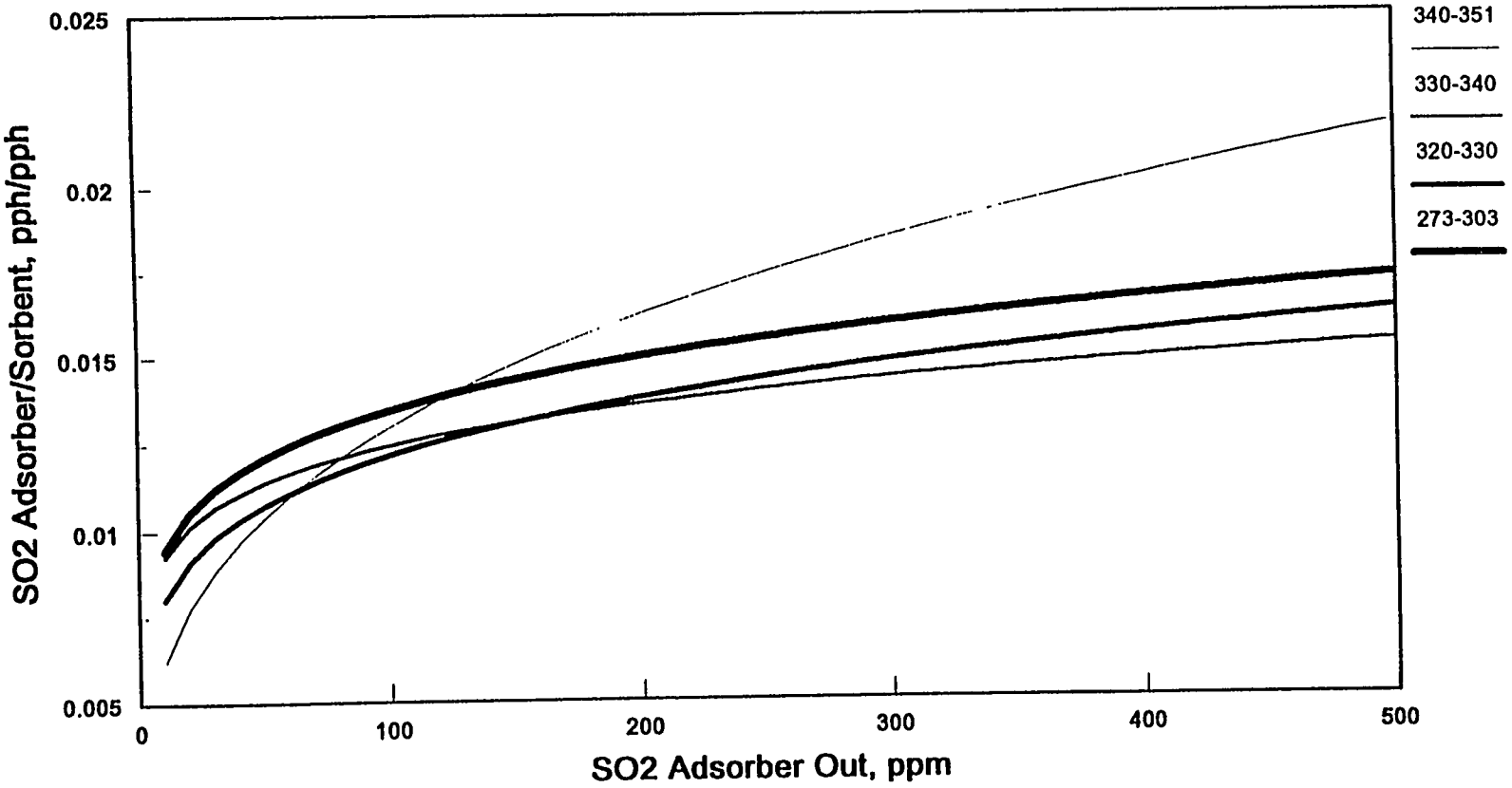

Figure 11-12
SO2 Removal as a Function of Inlet SO2
All Tests at 7000 scfm

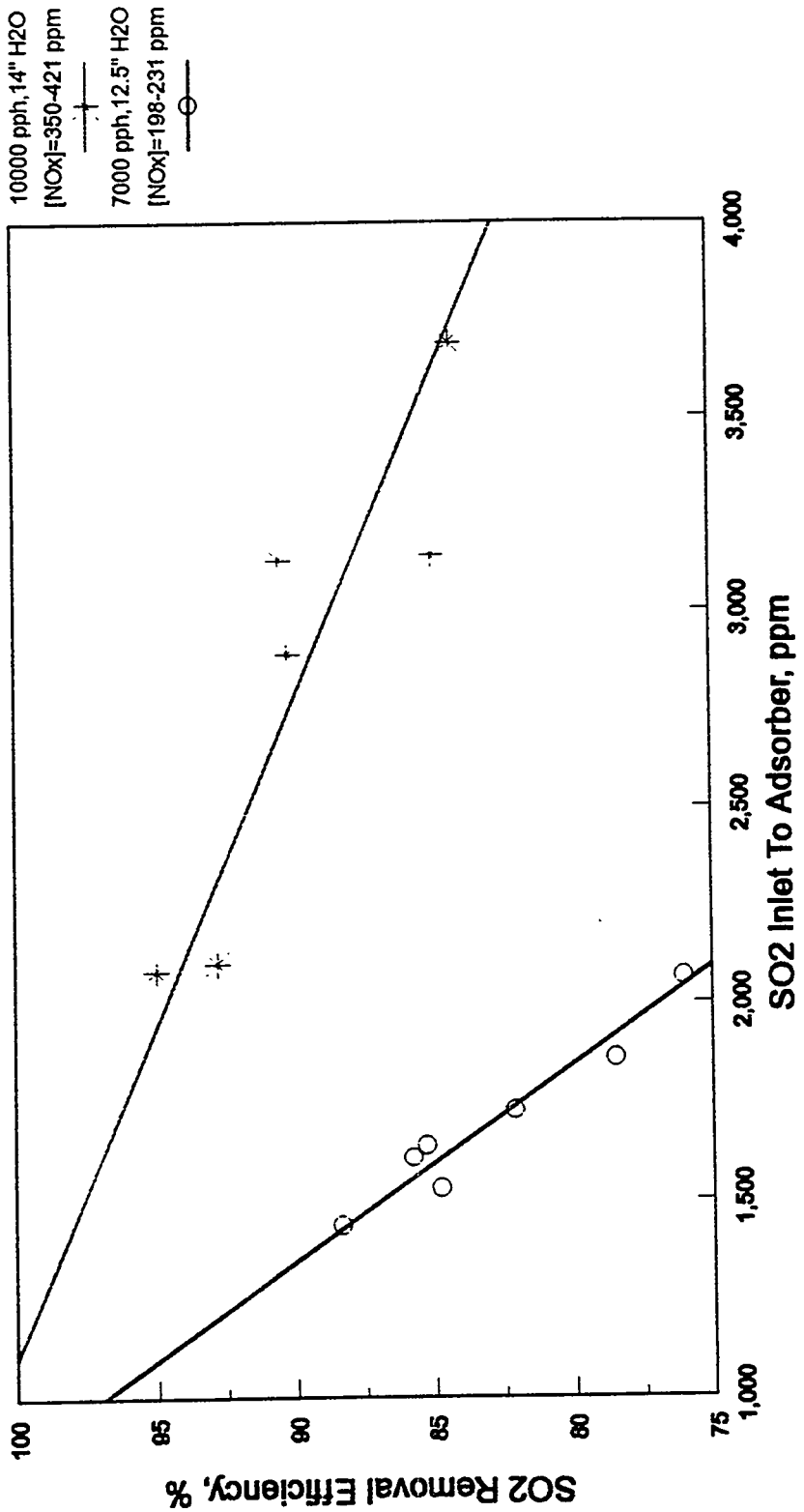

The limit as $x \rightarrow 0$ is 100%, but the y intercepts obtained by linear regression are 107 and 117. Nevertheless, the data fit the regression well, so it is concluded that SO_2 removal efficiency is a linear function of SO_2 inlet concentration assuming all the other adsorber operating variables are constant.

SO_2 removal efficiency is higher at lower sorbent residence time (i.e., as residence time decreases, active adsorption sites circulate through the adsorber at a higher rate) and at higher NO_x inlet concentration as seen in Figure 11-12. Both of these effects were discussed previously. In addition, the decay rate of SO_2 removal efficiency with SO_2 inlet concentration is different by a factor of two for the two lines in Figure 11-12, clearly showing the effect of sorbent residence time and NO_x inlet concentration, since in all other respects the test conditions were nearly identical.

The NO_x concentration effect is shown in Figure 11-13. The data cover a NO_x inlet range of 400 ppm (base load) to 1000 ppm (flue gas spiking). All data were obtained at constant gas and sorbent residence times and fairly constant SO_2 flue gas inlet concentrations ranging from 2883 to 3132 ppm. A data set was obtained at each of three adsorber bed temperatures: 345°, 312°, and 297°F.

Figure 11-13 shows that in all tests NO_x removal efficiency was higher at lower adsorber bed temperatures. This effect is clearly illustrated at 1000 ppm inlet NO_x, where NO_x removal efficiency is 41% at 345°F bed temperature, 74% at 312°F, and 77% at 297°F.

The rate of decay of removal efficiency with increasing NO_x inlet concentration is best approximated by the lines drawn in Figure 11-13. The regression coefficients are as follows (where $y=a+bx$):

Adsorber Bed Temperature	r^2	a	b	# of Points
345°F	0.91	107	-0.06	4
312°F	0.95	97	-0.02	3
297°F	0.96	98	-0.02	3

Therefore, at 10,000 pph, 7000 scfm. and 14" H_2O, the rate of decrease in NO_x removal with increasing NO_x inlet is given by the three linear equations above. The rate of decrease in NO_x removal efficiency is three times faster at 345°F bed temperature than it is at 297 or 312°F.

11.2.4 Effect of Gas-Sorbent Contacting

The effect of varying gas residence time at constant solids residence time is shown in Figure 11-14 and 11-15. The x-axis (flue gas flowrate) is proportional to gas residence time,

Figure 11-13

NOx Removal as a Function of Inlet NOx

10000 pph, 7000 scfm, 14" H20

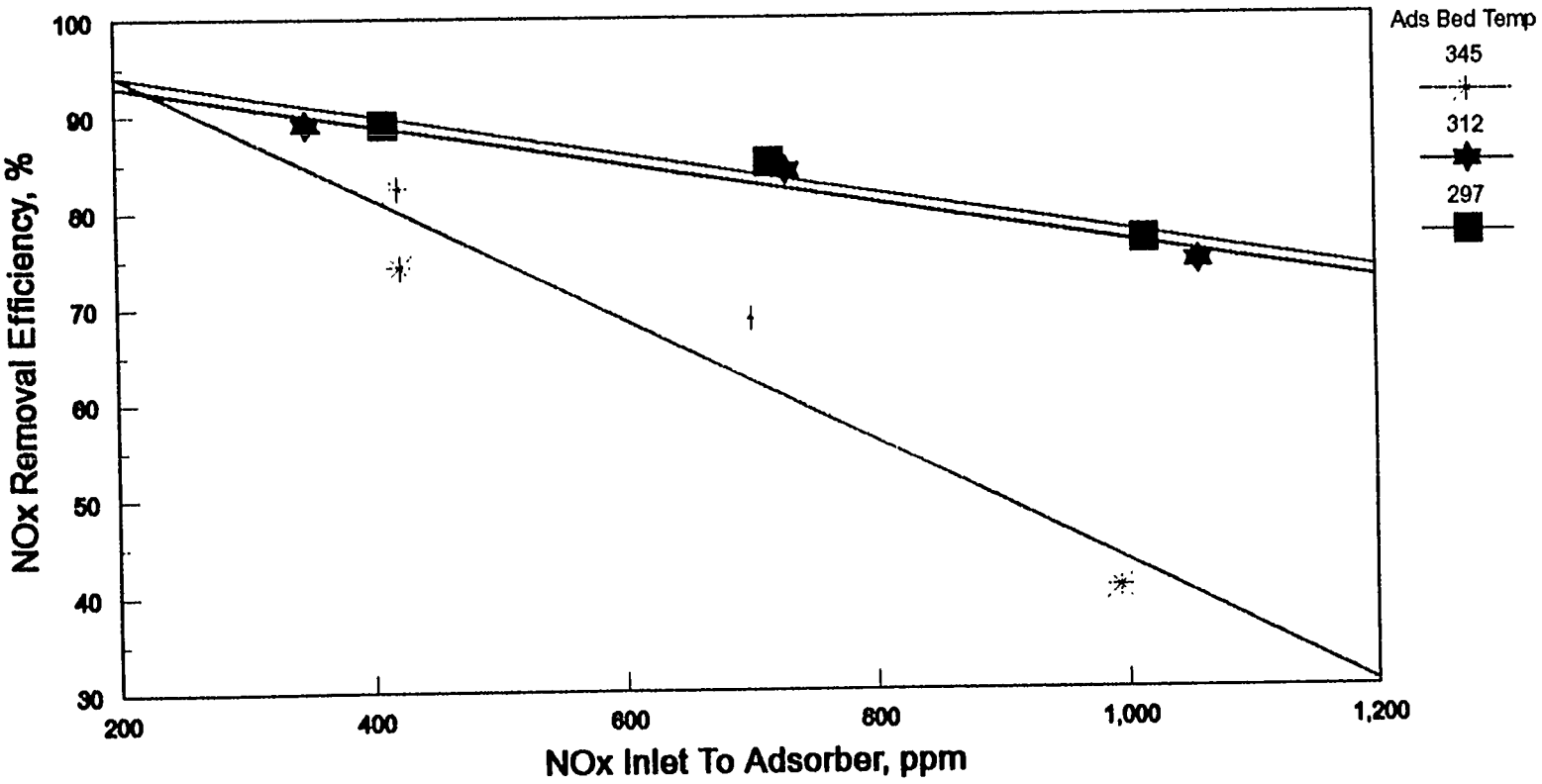

SO2 Inlet = 3132-2883 ppm

Figure 11-14
SO2 Removal Versus Flue Gas Flowrate
Effect of Bubble-Buster

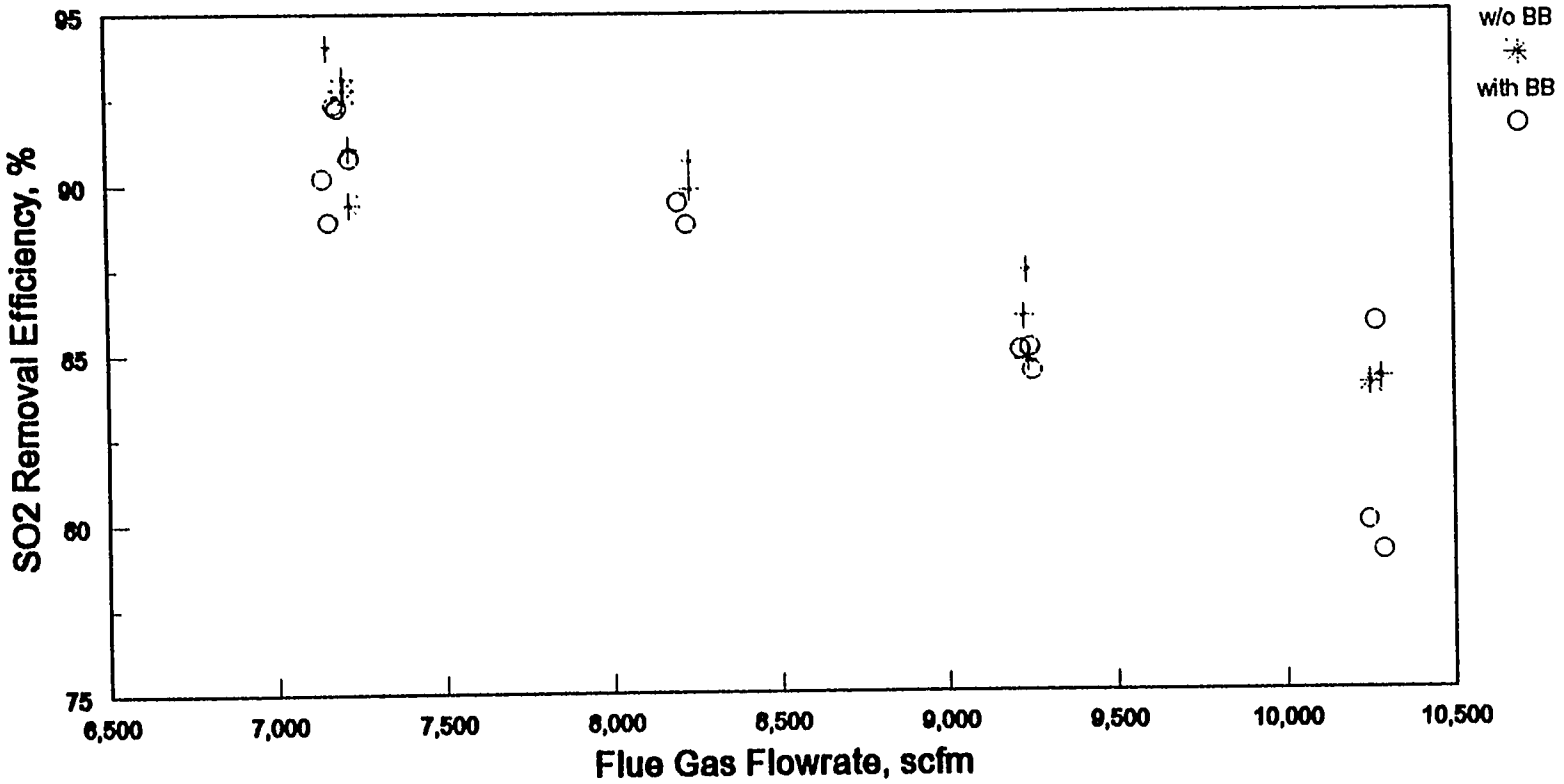

All Tests at 10000 pph, 14" H20

Figure 11-15
NOx Removal Versus Flue Gas Flowrate
Effect of Bubble-Buster

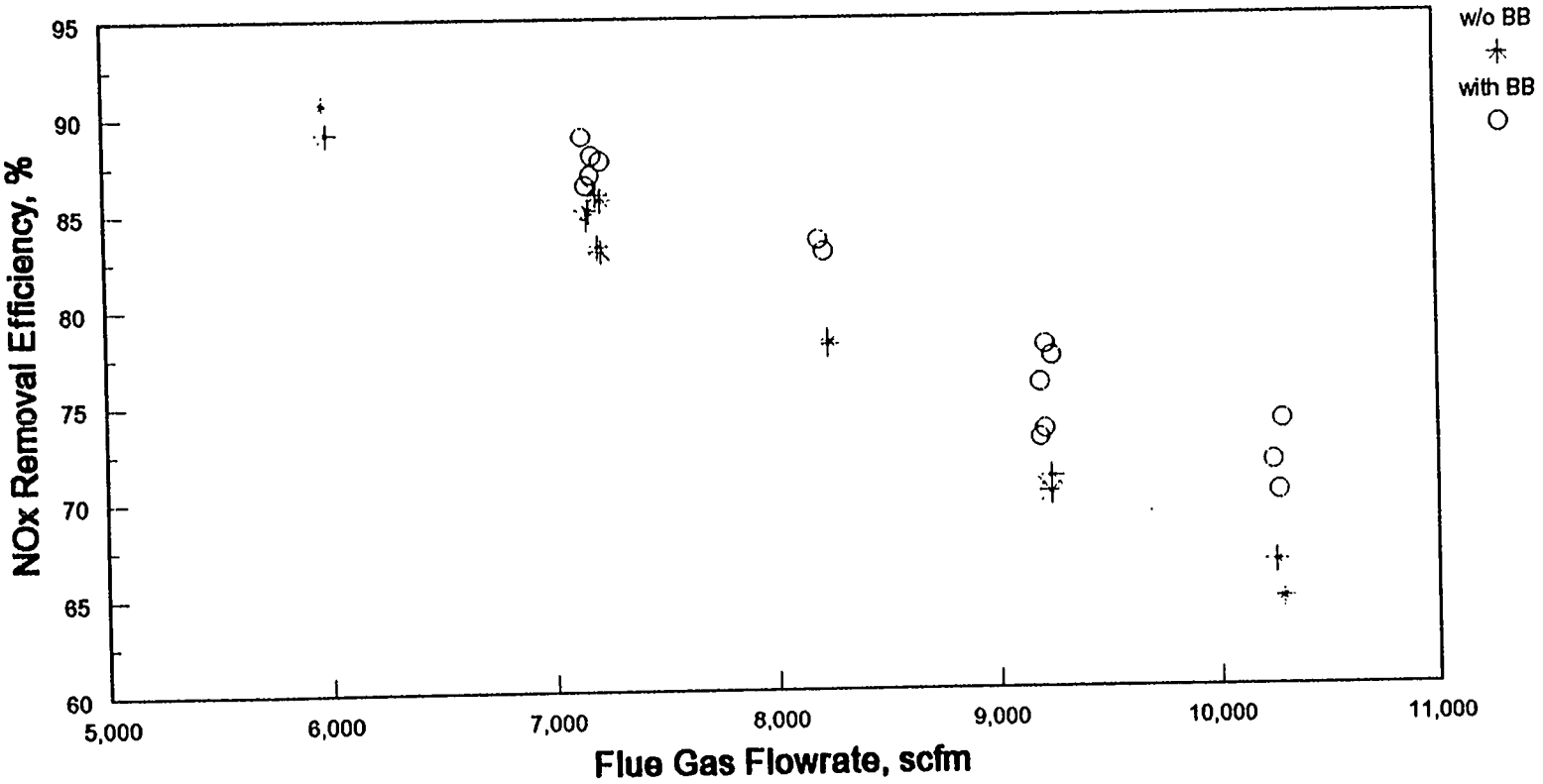

All Tests at 10000 pph, 14" H20

since adsorber bed pressure drop was held constant (13.6 to 14.1" H_2O) in all tests except those at 6000 scfm (19.8 - 20.2" H_2O). All tests were conducted at base load (i.e., SO_2 inlet averaged 1817 ppm and NO_x inlet averaged 335 ppm) and an average adsorber bed temperature of 342°F. As expected, removal efficiencies decrease as gas residence time decreases. This is because the quantity of SO_2 and NO_x entering the adsorber increases with decreasing gas residence time (at constant bed height), but the rate of active sorbent sites circulating through the adsorber (sorbent circulation rate) is held constant. The rate of decrease in removal efficiency with decreasing gas residence time can be approximated by the lines drawn in the figures. The decay rate of NO_x removal is twice that of SO_2 which substantiates the proposed reaction mechanism, i.e., two SO_2 molecules adsorb to form one active NO_x adsorption site. The linear regression coefficients are (where $y=a+bx$):

	a	b	r^2	# of Points
SO_2	114	-0.003	0.91	15
NO_x	127	-0.006	0.98	14

Tests designated SO_2 - BB and NO_x - BB represent data collected after a "bubble buster" was installed in the fluid bed adsorber. The "bubble buster" had been tested first in NOXSO's Clairton Research Center in a cold-flow, plexiglass model with a perforated grid plate identical to that used in the NOXSO pilot plant. The tests showed that bubble diameter and sorbent splash height above the fluidized bed were reduced by using the "bubble buster". The "bubble buster" consists of four rows of 1½" conduit, spaced 6" apart, and beginning 6" above the grid plate. Each row of tubes is parallel and 60° offset to the rows above and below.

The effect of the "bubble buster" on SO_2/NO_x removal efficiency is illustrated in Figures 11-14 and 11-15. Theoretically, the "bubble buster" should improve gas-sorbent mixing and thereby improve removal efficiency. The data show a slight improvement in NO_x removal efficiency but no improvement in SO_2 removal efficiency; therefore, there is no advantage to be gained by the use of this "bubble buster" and it will not be used in subsequent plants.

11.2.5 NO_x and SO_2 Adsorption Heat

The heat of NO_x and SO_2 adsorption is required to size the heat removal device that regulates the sorbent bed temperature in the large scale adsorber of the NOXSO Process. The steady-state operation data obtained from the POC adsorption studies were used to determine the NO_x and SO_2 adsorption heats. The assumptions used to derive the energy balance around the POC adsorber are as follows:

1. The air of the bottom J-valve goes directly to the top of the adsorber, and does not affect the temperature of the fluid bed. The sorbent transported by the bottom J-valve completely falls into the fluid bed.
2. The temperatures of gas and sorbent in the fluid bed are equal.

3. All the water sprayed into the flue gas is vaporized and enters the fluid bed with the flue gas.
4. The water content of the flue gas before the water spray is 8.5% by volume.
5. The effect of ambient temperature variation on the adsorber heat loss is negligible.

Applying the energy balance around the fluid bed adsorber gives

$$F_s C_{p_s}(T_s - T_b) + (F_g C_{p_g} + F_a C_{p_a} + F_w C_{p_w})(T_g - T_b) = F_g(1 - y_{H2O}) y_{SO_2} \phi_{SO_2} \Delta H_{SO_2} + F_g y_{NO_x} \phi_{NOx} \Delta H_{NO_x} + Q \qquad (11.2\text{-}2)$$

where C_{ps} is the sorbent heat capacity, kcal/kg °C,
C_{pg} is the heat capacity of the flue gas, kcal/kmol °C,
C_{pa} is the heat capacity of air, kcal/kmol °C,
C_{pw} is the heat capacity of water vapor, kcal/kmol °C,
ΔH_{SO2} is the SO_2 sorption heat, kcal/kmol,
ΔH_{NOx} is the NO_x sorption heat, kcal/kmol,
F_s is the sorbent flowrate, kg/sec,
F_g is the flue gas flowrate, kmol/sec,
F_a is the air flowrate of the water spray, kmol/sec,
F_w is the water flowrate of the water spray, kmol/sec,
ϕ_{SO2} is the SO_2 removal fraction,
ϕ_{NOx} is the NO_x removal fraction,
Q is the heat loss, kcal/sec,
T_s is the sorbent inlet temperature, °C,
T_g is the flue gas inlet temperature, °C,
T_b is the average fluid bed temperature, °C,
y_{H2O} is the adsorber inlet H_2O mole fraction,
y_{SO2} is the adsorber inlet SO_2 mole fraction, and
y_{NOx} is the adsorber inlet NO_x mole fraction.

The term $(1\text{-}y_{H2O})$ on the right hand side of Equation 11.2-2 is used to correct (y_{SO2}) which is measured on a dry basis. Only the SO_2 concentration requires the correction. Equation 11.2-2 contains three unknowns, namely ΔH_{SO2}, ΔH_{NOx} and Q. They can be easily determined by a linear regression. The data obtained from the June 25, 1992 to August 17, 1992 pilot plant operation was used to determine these unknowns. The reason to restrict the data collection period is to ensure that the ambient condition was relatively unchanged to satisfy the fifth assumption. The results obtained from 48 data points with R-squared = 0.889 are as follows:

$$\Delta H_{SO_2} = -70.154 kcal/mole$$
$$\Delta H_{NO_x} = -5.683 kcal/mole$$
$$Q = 0.590 kcal/\text{sec}$$

The comparison between the right hand side and the left hand side of Equation 11.2-2 is shown in Figure 11-16. Since the left hand side of Equation 11.2-2 contains only measurable variables, it is called the measured heat release in Figure 11-16. The right hand side is called the calculated heat release. It should be pointed out that the regression result was effected by the selection of the sorbent inlet temperature. The use of the bottom bed temperature of the cooler gives a high r-square value. The use of the temperature measured in the riser section of the bottom J-valve gives a low r-square value, 0.572. The adsorption heat reported here is the result of using the cooler bottom bed temperature, which is believed to be the most accurate, since the riser temperature is actually a measure of the dilute phase air/sorbent mixture.

The extended POC data, from June 25, 1992 to December 10, 1992, were also used to correlate Equation 11.2-2. It was found that the resultant ΔH_{NOx} ranged from 74.8 to -391 kcal/mole, ΔH_{SO2} from -89.164 to -83.36 kcal/sec, Q from 3.57 to 14.48 kcal/mol, and r-square from 0.827 to 0.753. The change of ambient temperature from June to December explains the large change of ΔH_{NOx} and heat loss. Also, there were tests conducted in September to December in which acid collected in the elbow upstream of the adsorber. Incomplete vaporization of water sprayed into the flue gas effects the calculated adsorption heat and heat loss. Therefore, it is appropriate to restrict the analysis to a period when ambient temperature does not vary considerably and all water sprayed into the flue gas is vaporized.

11.2.6 NO_2 in Adsorber Outlet

The concentration of NO_x in the adsorber offgas was continuously measured. The relative concentrations of NO/NO_2 in the adsorber offgas were measured once every two hours for a period of two months. The reason that both weren't continuously measured is that only one NO_x analyzer was employed. The NO/NO_2 data are shown in Figure 11-17.

The data are widely scattered. The data were collected over a period in which sorbent circulation rate, flue gas flowrate, adsorber bed pressure drop, and adsorber bed temperature varied, but no reliable correlation between these variables and NO/NO_2 concentration was obtained. The data set can be characterized as follows:

NO_2 (Percent of NO_x)	
Maximum	81
Minimum	11
Mean	48
Standard Deviation	14.7

The data in Figure 11-17 were all acquired at base load; i.e., roughly 400 ppm NO_x in inlet flue gas. The data in Figure 11-18 were obtained during NO_x spiking tests. These data

Figure 11-16
NOx and SO2 Adsorption Heat

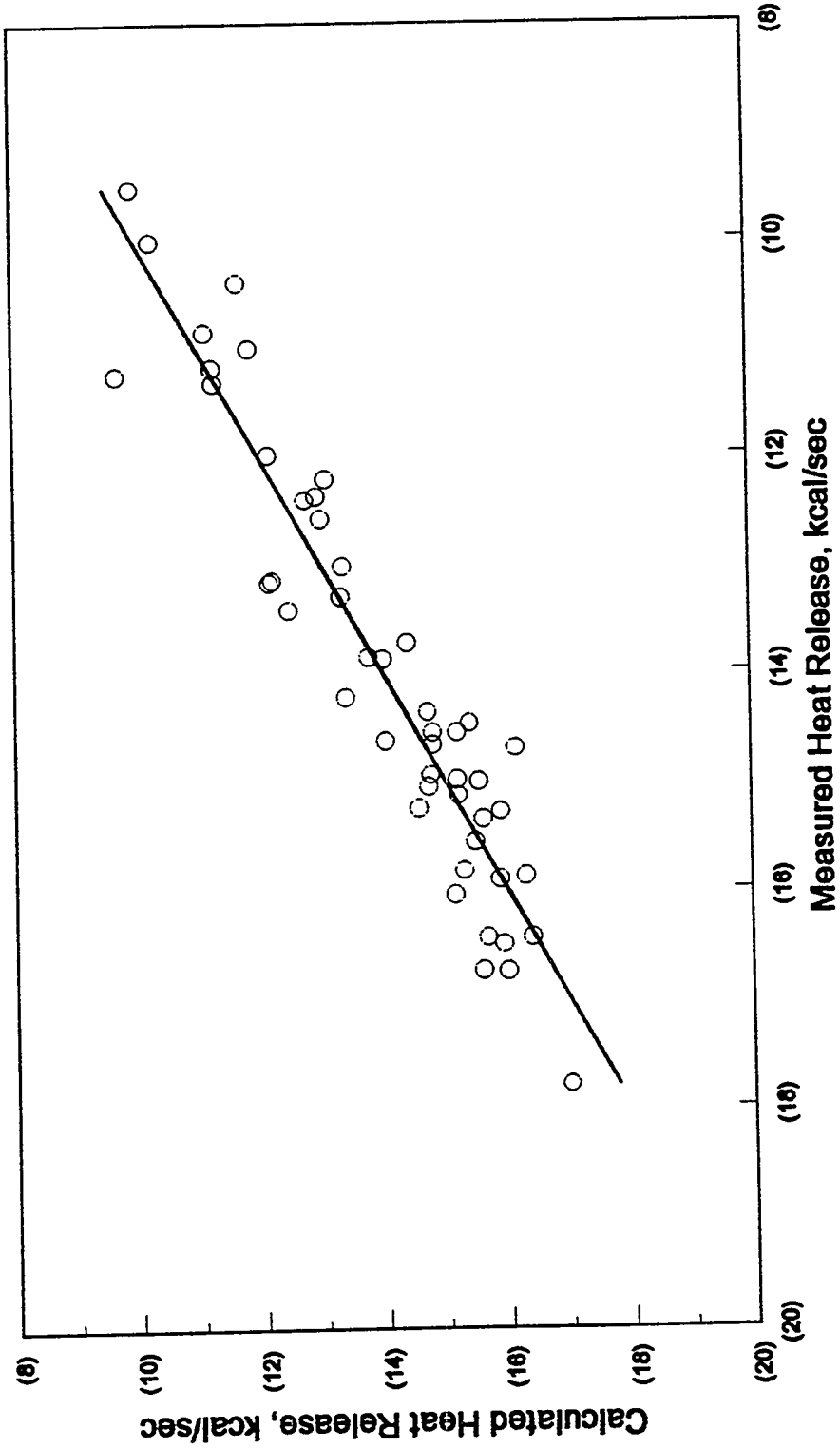

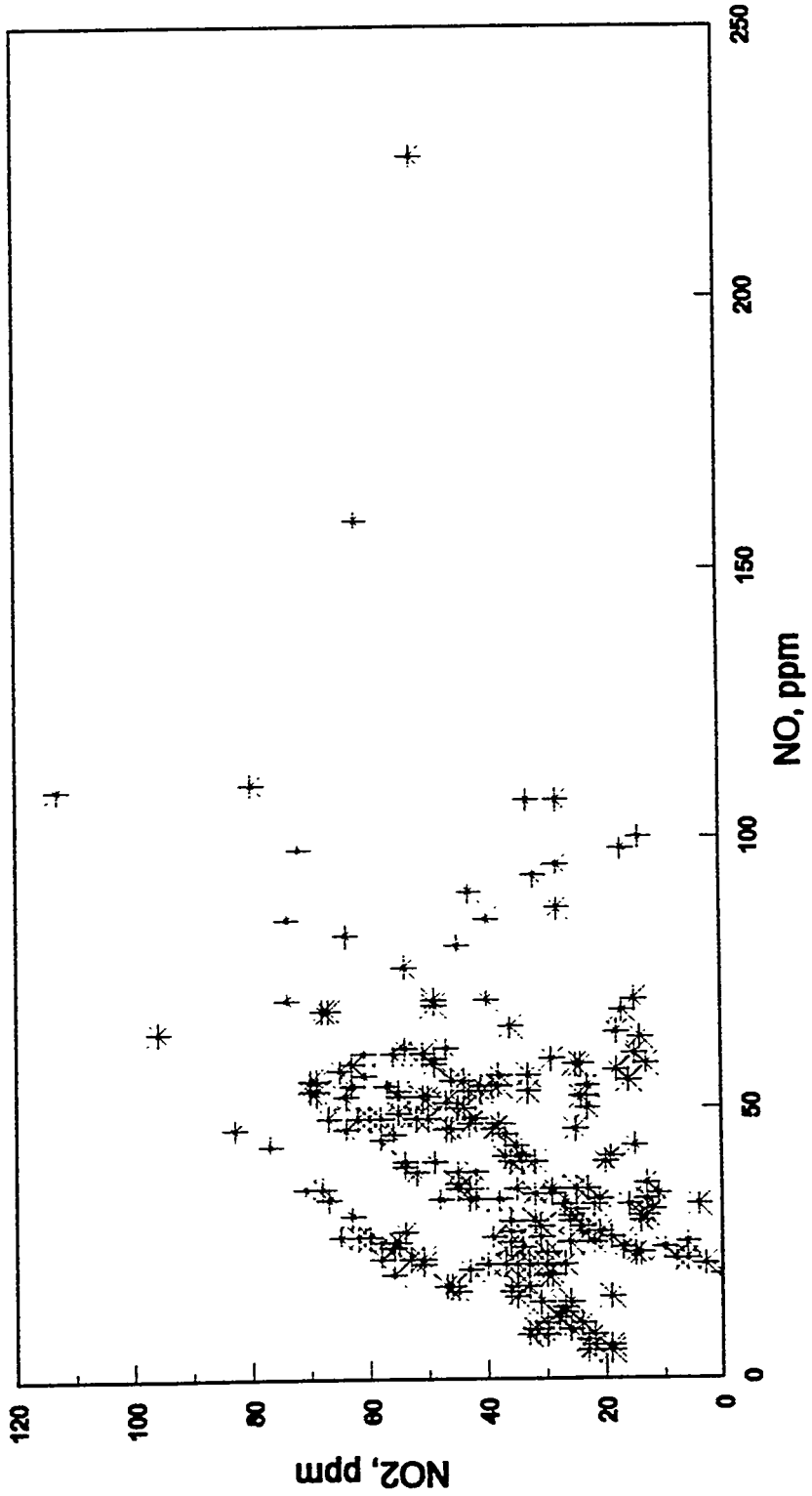

Figure 11-17
NO/NO2 in Adsorber Offgas
(11/13/92 to 1/16/93)

Figure 11-18
NO/NO2 In Adsorber Offgas
NOx Spiking Tests

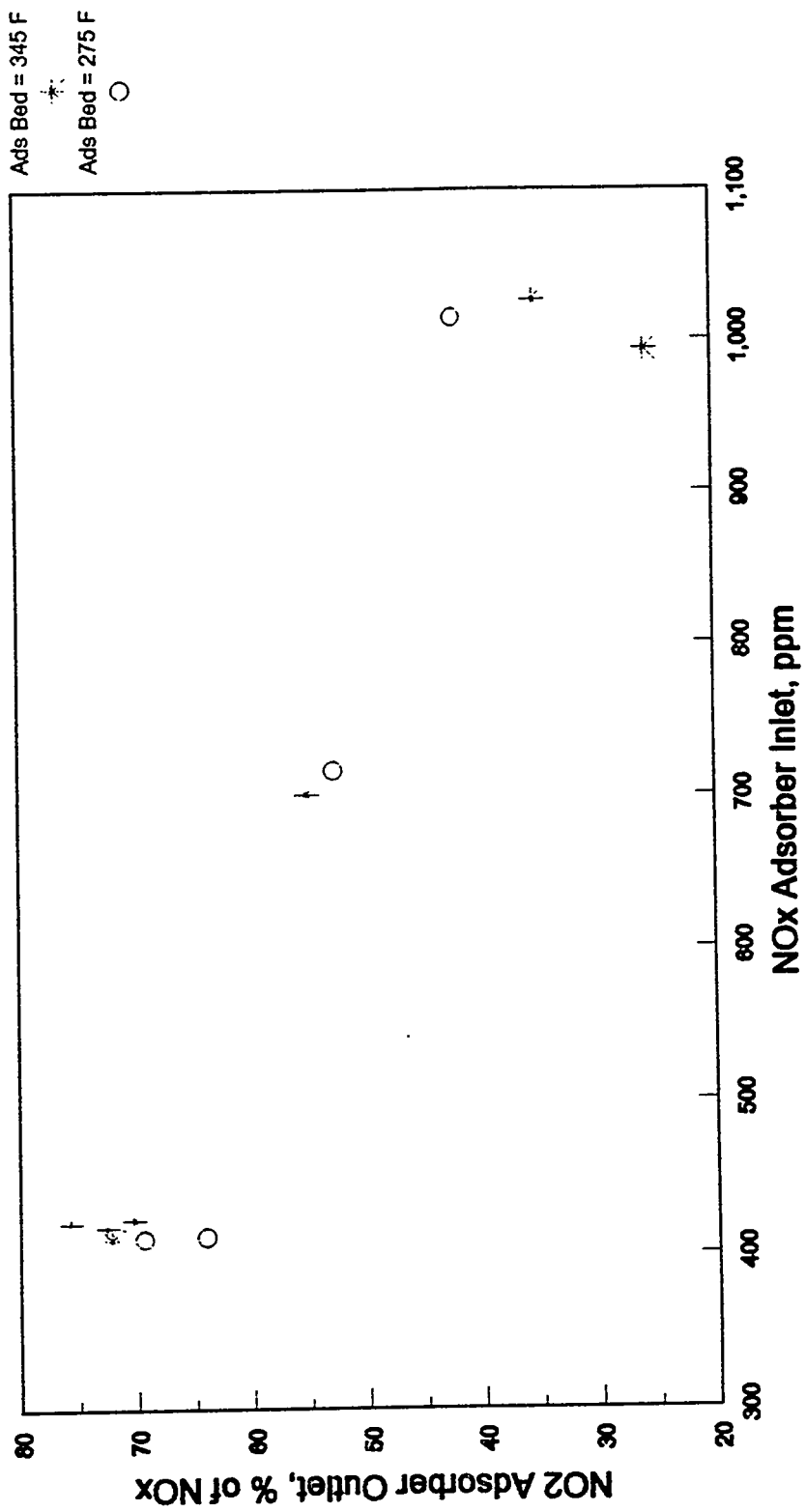

show a decrease in the NO_2 content of the adsorber offgas with increasing concentration of NO_x in flue gas inlet to the adsorber. The data at two different bed temperatures are similar, despite the fact that substantially more NO_x is adsorbed at the lower temperature. This would indicate that the decrease in NO_2 with increasing NO_x in inlet flue gas is not only due to the fact that more NO passes unreacted through the bed. However, given the variation in the data at base load, more spiking data is required before any firm conclusion can be drawn.

Federal and state law places limits on NO_x emissions from power plants. NO_2 is not separately regulated. However, NO_2 is a colored gas and may present problems with aesthetics. For this reason, NOXSO plans to test a two-stage adsorber at the pilot plant. Laboratory data indicate that NO_2 entering the second bed will adsorb and in the process produce NO via the mechanism shown in Section 3.2. NOXSO also plans tests at lower adsorber bed temperatures. The existing pilot data show that NO_x adsorption increases with decreasing bed temperature. Operating the second-stage of the adsorber at lower temperature should result in higher NO_2 removal and, hence, less NO_2 in the adsorber offgas.

11.2.7 Summary

The data analysis presented in Sections 11.2.1-11.2.5 can be used to produce a rough design of a commercial-scale adsorber. Assume that one were to design a NOXSO system to treat all of the flue gas from one of the 65 MW, pc-fired boilers at Ohio Edison's Toronto power plant. Assume further that the NOXSO Process must achieve 90% removal of SO_2 and 80% removal of NO_x. Characteristics of this model plant that are important from the standpoint of the design of the adsorber are listed in Table 11-4.

Table 11-4. Model Plant

UNIT: Toronto Unit 10 or 11, pc-fired	
SIZE: 65 MW (60 MW-base load)	
Flue Gas Flowrate	144,000 scfm (base load) 84,000 scfm (mini-load)
SO_2 Removal Efficiency	90% (net) 91% (adsorber)
NO_x Removal Efficiency	80% (net) 86% (adsorber)
SO_2 Inlet Flue Gas	2200 ppm, (3210 pph) 2418 ppm (after recycle[1]), (3528 pph)
NO_x Inlet Flue Gas	400 ppm,(273 pph) 572 ppm (after recycle[2]), (391 pph)

(1) Ten percent of the SO_2 adsorbed is recycled to the adsorber in the tail gas from the sulfur recovery plant. This was not the case in the pilot plant.

(2) All of the NO_x adsorbed is recycled to the coal combustor. The NO_x destruction efficiency in the combustor is 65%.

Figure 11-10 in Section 11.2.2 may now be used to estimate the sorbent circulation rate required to achieve 86% NO_x removal. The adsorber efficiency must be 86% to achieve an overall NO_x removal efficiency of 80%, since the concentration of NO_x in flue gas inlet to the adsorber increases with NO_x recycle. Since NO_x removal improves with decreasing adsorber bed temperature, the bed temperature selected for the model plant is 273-303°F. This is the lowest temperature tested thus far at the pilot plant. Further improvement in NO_x removal efficiency is likely at temperatures lower than those tested at the pilot plant thus far. The design equation is

$$[NO_x]_{ads}/F_s = 0.00021[NO_x]^{½}_{out} \text{ at } 273\text{-}303°F$$

where $[NO_x]_{ads}$ is NO_x adsorbed, pph,
$[NO_x]_{out}$ is NO_x in flue gas, adsorber out, ppm, and
F_s is sorbent circulation rate, pph.

Using $[NO_x]_{ads}$ = 336 and $[NO_x]_{out}$ = 80 for the model plant gives the calculated sorbent circulation rate of 178,885 pph. The pilot plant data on which the correlation is based cover a range of $[NO_x]_{out}$ from 8 to 235 ppm and $[NO_x]_{ads}$ from 5 to 27 pph.

The adsorber sorbent inventory is then determined by the SO_2 removal requirement. Section 11.2.1 showed that when all of the pilot plant data are considered, SO_2 removal efficiency approximates a power function of adsorber gas residence time when the data are grouped according to similar sorbent residence times. Figure 11-5 in Section 11.2.1 showed that sorbent residence time is directly proportional to gas residence time at constant removal efficiency. At 90% SO_2 removal, the linear relationship is:

$$t_s = 60.4(t_g)\text{-}9.4$$

where t_s is the sorbent residence time, min.
t_g is the gas residence time, sec.

Figure 11-19 shows a plot of gas versus sorbent residence time at 90% removal and at the calculated sorbent circulation rate of 178,885 pph for the model plant. The point where the lines intersect is the gas residence time required to achieve 90% SO_2 removal. This point is t_g = 0.75 sec., which is equivalent to a bed ΔP of 17" H_2O or an adsorber inventory of 105,840 pounds.

The bed temperature, adsorber inventory, and sorbent circulation rate are now known so the rest of the design is straightforward. Two adsorbers are provided to give the system turndown capability. The design superficial gas velocity is approximately 2.5 times the sorbent's minimum fluidization velocity, which gives a margin of turndown in each adsorber. All of the design information is given in Table 11-5.

Figure 11-19

Sorbent Versus Gas Residence Time

90 % Removal Versus Actual Model Plant

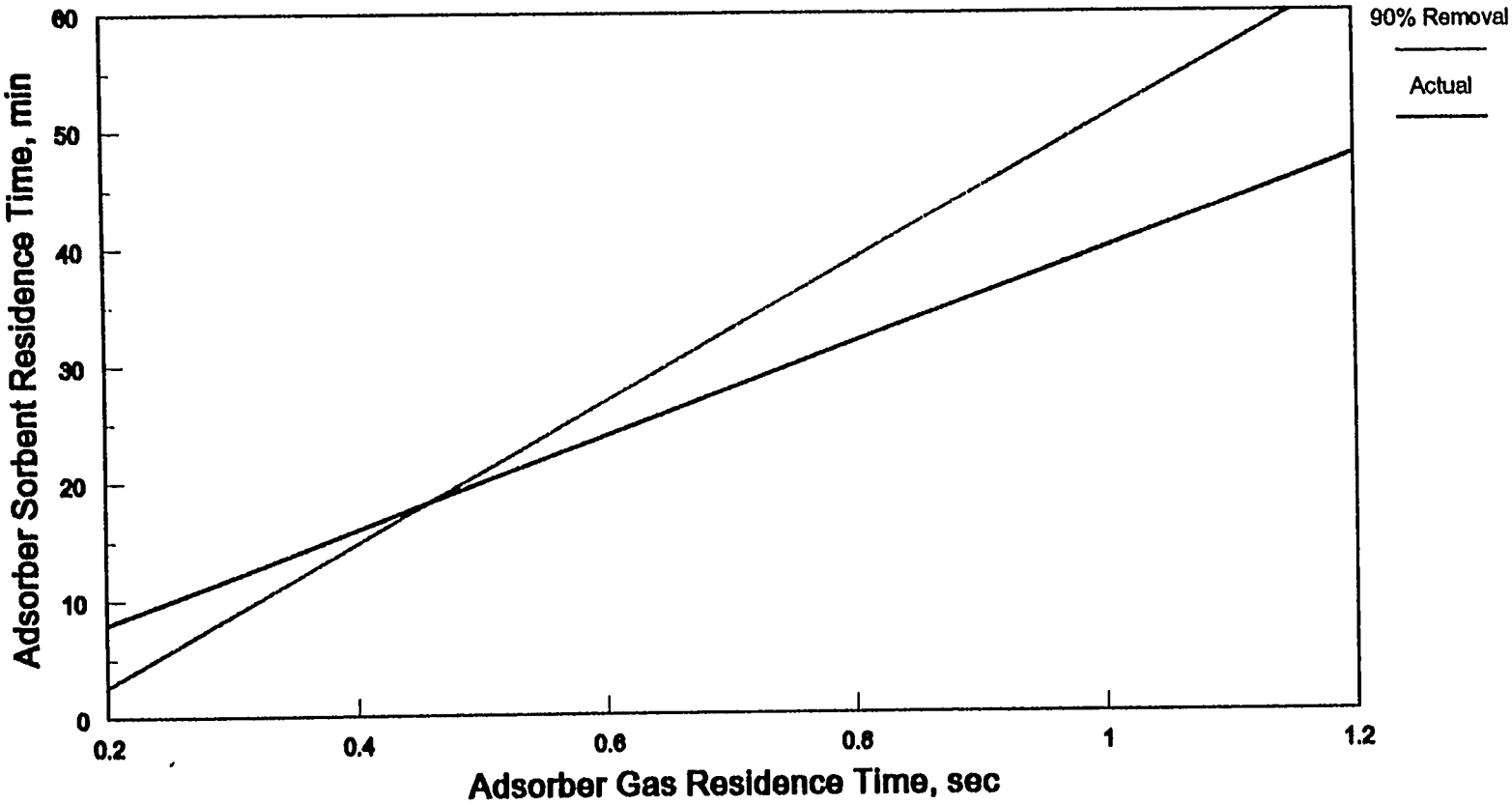

Table 11-5. Adsorber Design (65 MW)*	
Sorbent circulation rate	178,885 pph
Flue gas flowrate	144,000 scfm, 203,447 acfm
Number of adsorbers	2
Total cross sectional area	1211 ft^2
Superficial gas velocity	2.8 ft/sec (base load)
Sorbent bed temperature	275°F
Bed pressure drop	17" H_2O
Settled bed height	2.1 ft
Gas residence time	0.75 sec
Sorbent residence time	35.5 min
SO_2 removal efficiency	90%
NO_x removal efficiency	80%
SO_2 inlet	2418 ppm
NO_x inlet	572 ppm

* See Table 11-4 for model plant characteristics.

Note that this design is based solely on the empirical analysis of the pilot plant data presented in Sections 11.2.1-11.2-5. In Section 11.3 of this report a more rigorous adsorber model is presented. This model was developed using data from previous smaller-scale tests of the NOXSO Process. The model is shown to accurately predict the results generated at the pilot plant. The pilot plant results are being used to refine the model. It is this model that will be used to design future NOXSO commercial installations.

11.3 Fluid Bed Adsorber Model

A mathematical model for the fluid bed adsorber was developed from the earlier NOXSO test results. The sorbent capacity for the NO_x and SO_2 sorption were determined from the laboratory using a two inch fixed-bed reactor. The rate constants of the NO_x and SO_2 sorption used in the model were derived from the NOXSO PDU tests. These constants are global rate constants, which lump the hydrodynamics of gas-solid contact and the reaction kinetic mechanism into one variable. The PDU adsorption tests were conducted in a 40 inch square fluid bed with a bubble-cap gas distributor. The POC adsorber is 10.5 ft. in diameter and uses a perforated plate for gas distribution. The LCTU adsorber was made from a one foot diameter fluid bed using 21 J-shaped tubes as the gas distributor. It was found that the PDU adsorber model predicted the LCTU adsorption results when the change of sorbent surface area was incorporated into the model. The derivation of the PDU model and the application of the model to predict the PDU, LCTU. and the current POC adsorption results are discussed in this section.

11.3.1 Model Derivation

The data for SO_2 and NO_x removal efficiencies collected during the PDU Test were used to develop a correlation between the adsorber operating parameters and removal efficiency. Removal efficiency is defined as:

$$\textit{Removal Efficiency} = \phi \cdot 100\% = \left(1 - \frac{y_f}{y_o}\right) \cdot 100\% \qquad (11.3\text{-}1)$$

where ϕ is the removal fraction,
y_o is the mole fraction of pollutant at adsorber inlet, and
y_f is the mole fraction of pollutant at adsorber outlet.

The correlation was developed by assuming: 1) the gas to be plug flow and the solid to be mixed flow in the fluid bed adsorber, and 2) both NO_x and SO_2 sorption to be first-order reaction with respect to their own concentration[1]. The fluid bed mass balance in the vertical direction has the following form,

$$-VC_o dy_i = \rho \lambda_i n \frac{\partial X}{\partial t_a} dz \qquad (11.3\text{-}2)$$

where C_o is the molar gas concentration in the feed stream, kmole/m^3,
i is the subscript, i=1 or 2 corresponding to SO_2 or NO_x, respectively,
λ_i is the stoichiometric ratio of the i-th reactant gas to active sorbent material,
n is the sodium content on the sorbent, kmole/kg sorbent,
ρ is the sorbent density in a fluid bed reactor, kg/m^3,
t_a is the time, sec,
V is the superficial gas velocity, m/sec,
X is the conversion factor of the active sorbent material,
y_i is the mole fraction of the i-th gas species, and
z is the fluidized bed height, m.

Since the sorption is assumed to be a first-order reaction, the rate of conversion will be:

$$\frac{dX}{dt_a} = K_i P \bar{y}_i (1 - X) \qquad (11.3\text{-}3)$$

where K_i is the rate constant of the i-th gas species, atm^{-1} sec^{-1},
P is the gas pressure, atm, and
y_i is the mean mole fraction of the i-th gas species in the adsorber.

Combining Equations 11.3-2 and 11.3-3 with a mean conversion factor, X, and integrating over the entire fluid bed height with the boundary conditions,

$$at\ z=0,\ y=y_{oi} \tag{11.3-4}$$

$$at\ z=H,\ y=y_{fi} \tag{11.3-5}$$

yields

$$VC_o(y_{oi}-y_{fi}) = \lambda_i n K_i P \bar{y}_i (1-\bar{X}) \rho H \tag{11.3-6}$$

Multiplying both sides of Equation 11.7-6 by the reactor cross-sectional area, and expressing the result in terms of pollutant removal fraction gives

$$\phi_i = \frac{W}{F_g} \lambda_i n K_i P \frac{\bar{y}_i}{y_{oi}} (1-\bar{X}) \tag{11.3-7}$$

where W is the sorbent inventory in the adsorber, kg
F_g is the flue gas flowrate, kmole/sec

When sorption takes place in the adsorber, both SO_2 and NO_x compete for active sites on the sorbent. A balance on the active sorbent material in a mixed-flow reactor results in:

$$F_s(\bar{X}-X_o) = WP(K_1\bar{y}_1+K_2\bar{y}_2)(1-\bar{X}) \tag{11.3-8}$$

or

$$1-\bar{X} = \frac{1-X_o}{1+\frac{W}{F_s}P(K_1\bar{y}_1+K_2\bar{y}_2)} \tag{11.3-9}$$

where X_0 is the conversion factor of the active sorbent material at the adsorber inlet.

Combining Equation 11.3-7 with Equation 11.3-9 gives

$$\phi_i = \frac{WE_i}{F_g} K_i P \frac{\bar{y}_i}{y_{oi}} \left(\frac{1}{1 + \frac{W}{F_s} P(K_1 \bar{y}_1 + K_2 \bar{y}_2)} \right) \tag{11.3-10}$$

where the following definition of unused sorbent capacity has been used.

$$E_i = \lambda_i n (1 - X_o) \tag{11.3-11}$$

where E_i has the units of kmole i-th gas sorbed per kg sorbent.

Since both SO_2 and NO_x sorptions have the same mathematical form, Equation 11.3-10, the ratio of these sorption equations reduces to:

$$\frac{K_1 y_1}{K_2 \bar{y}_2} = \frac{\phi_1}{\phi_2} \frac{E_2}{E_1} \frac{y_{o1}}{y_{o2}} \tag{11.3-12}$$

With Equation 11.3-12, Equation 11.3-10 can then be rewritten in terms of experimentally measurable quantities such that the sorption rate constant can be determined.

For SO_2 removal,

$$K_1 P = \frac{\phi_1}{\frac{W}{F_s} \left(\frac{F_s E_1}{F_g} \frac{\bar{y}_1}{y_{o1}} - \phi_1 \bar{y}_1 \left(1 + \frac{\phi_2}{\phi_1} \frac{E_1}{E_2} \frac{y_{o2}}{y_{o1}} \right) \right)} \tag{11.3-13}$$

Similarly, for NO_x removal,

$$K_2 P = \frac{\phi_2}{\frac{W}{F_s} \left(\frac{F_s E_2}{F_g} \frac{\bar{y}_2}{y_{02}} - \phi_2 \bar{y}_2 \left(1 + \frac{\phi_1}{\phi_2} \frac{E_2}{E_1} \frac{y_{01}}{y_{02}} \right) \right)} \tag{11.3-14}$$

where y_i is taken as the logarithmic mean because of the first-order reaction and plug flow assumption.

For the gas phase, y_i can also be expressed in terms of the removal fraction as follows:

$$\bar{y}_i = \frac{-y_{oi}\phi_i}{\ln(1-\phi_i)} \qquad (11.3\text{-}15)$$

Since the alumina substrate alone also adsorbs NO_x and SO_2 from flue gas, the stoichiometric ratio of the reactant gas to the active sorbent material must include the contribution from both sodium and alumina. However, making a distinction between the sodium and alumina contribution was avoided by using data collected from a 0.017 MW-scale, fixed-bed reactor.[1] The measured stoichiometric ratios (λ) are given as follows based on the fixed-bed data:

$$For\ NO_x:\ 1/\lambda_2 = -4.789+0.075\ T_a \qquad (11.3\text{-}16)$$

$$For\ SO_2:\ 1/\lambda_1 = 0.3761+0.0052\ T_a \qquad (11.3\text{-}17)$$

where T_a is the adsorber temperature, °C.

Then the initial conversion factor of the active sorbent material, X_o, can be determined from the sorbent's sodium content,

$$X_o = \frac{1}{n}\left(\frac{S_r}{\lambda_1}+\frac{N_r}{\lambda_2}\right) \approx \frac{1}{n}\frac{S_r}{\lambda_1} \qquad (11.3\text{-}18)$$

where S_r is the sulfur content of the regenerated sorbent, kmole/kg sorbent
N_r is the nitrogen content of the regenerated sorbent, kmole/kg sorbent

The nitrogen term in Equation 11.3-18 was dropped because it was not measured during the PDU test, and measurements made during the LCTU test showed a very small nitrogen content (less than 0.2 wt%). The unused sorbent capacities for SO_2 and NO_x sorption are then approximated from Equation 11.3-11 as follows:

$$E_i = \lambda_i n\left(1-\frac{1}{n}\frac{S_r}{\lambda_1}\right) \qquad (11.3\text{-}19)$$

It should be noted that the sorbent sulfur and sodium contents were not measured in every test run conducted at the PDU and LCTU. To develop the model, a rational adjustment was made to those measurements, such as smoothing the random data and assigning values for the missing measurements. The sodium content for PDU results was first smoothed and then averaged, since the same sorbent was used through the entire test. Values of 3.5 wt% sodium and 0 wt% sulfur were used for the PDU data. The mean sulfur content of the PDU runs, 0.8 wt%, was later added into the LCTU calculation. This approach is needed because the sorbent

used in the fixed-bed, PDU, and LCTU were different. All the sodium and sulfur contents used in the calculations are listed in Appendix A1 and A2 for each data point.

The NO_x and SO_2 removal fractions obtained from the PDU test were used with Equations 11.3-13 through 11.3-19 to calculate the rate constant, K_i, for each data point. The PDU data with the calculated K_i values are listed in Appendix A1 and A2. The temperature dependence was determined by plotting the K_i values versus the reciprocal of the adsorber temperature according to Arrhenius' law, and the results are shown in Figure 11-20. A least-square method was used to obtain the best fit results which are shown below:

$$K_1 = 52.15 \exp\left(\frac{-1840.2}{T_a+273}\right) \qquad (11.3\text{-}20)$$

$$K_2 = 14.75 \exp\left(\frac{-912.14}{T_a+273}\right) \qquad (11.3\text{-}21)$$

Applying the PDU findings directly to predict the removal efficiencies for the endurance LCTU test raises concerns about the sorbent attrition rate and surface area degradation. The total sorbent surface area in the LCTU was decreased due to the high temperature steam treatment, but was increased by adding fresh make-up sorbent. The change of surface area with time must be included in the model. Since both NO_x and SO_2 removal in the NOXSO Process are a type of sorption reaction, it is reasonable to assume that the sorption rate constant is proportional to the sorbent's surface area. Hence, the long-term performance of the LCTU test can be predicted with the PDU findings by simply introducing a surface-area correction term to the sorption rate constant. Combining Equations 11.3-10 and 11.3-15, and inserting the surface area ratio gives the equations for calculating the NO_x and SO_2 removal fraction with time. The equations are:

For SO_2:

$$\ln(1-\phi_1)-\frac{W}{F_s}P\left(\frac{A}{A_o}\right)\left(K_1y_{01}+K_2y_{02}\frac{\phi_2}{\ln(1-\phi_2)}\frac{\ln(1-\phi_1)}{\phi_1}\right)\phi_1+\frac{WE_1}{F_g}pK_1\left(\frac{A}{A_o}\right)=0 \qquad (11.3\text{-}22)$$

For NO_x:

$$\ln(1-\phi_2)-\frac{W}{F_s}P\left(\frac{A}{A_o}\right)\left(K_2y_{02}+K_1y_{01}\frac{\phi_1}{\ln(1-\phi_1)}\frac{\ln(1-\phi_2)}{\phi_2}\right)\phi_2+\frac{WE_2}{F_g}pK_2\left(\frac{A}{A_o}\right)=0 \qquad (11.3\text{-}23)$$

where A is the sorbent current surface area
A_o is the fresh sorbent surface area

Figure 11-20
SO2/NOx Sorption Rate Constant
Obtained From PDU Tests

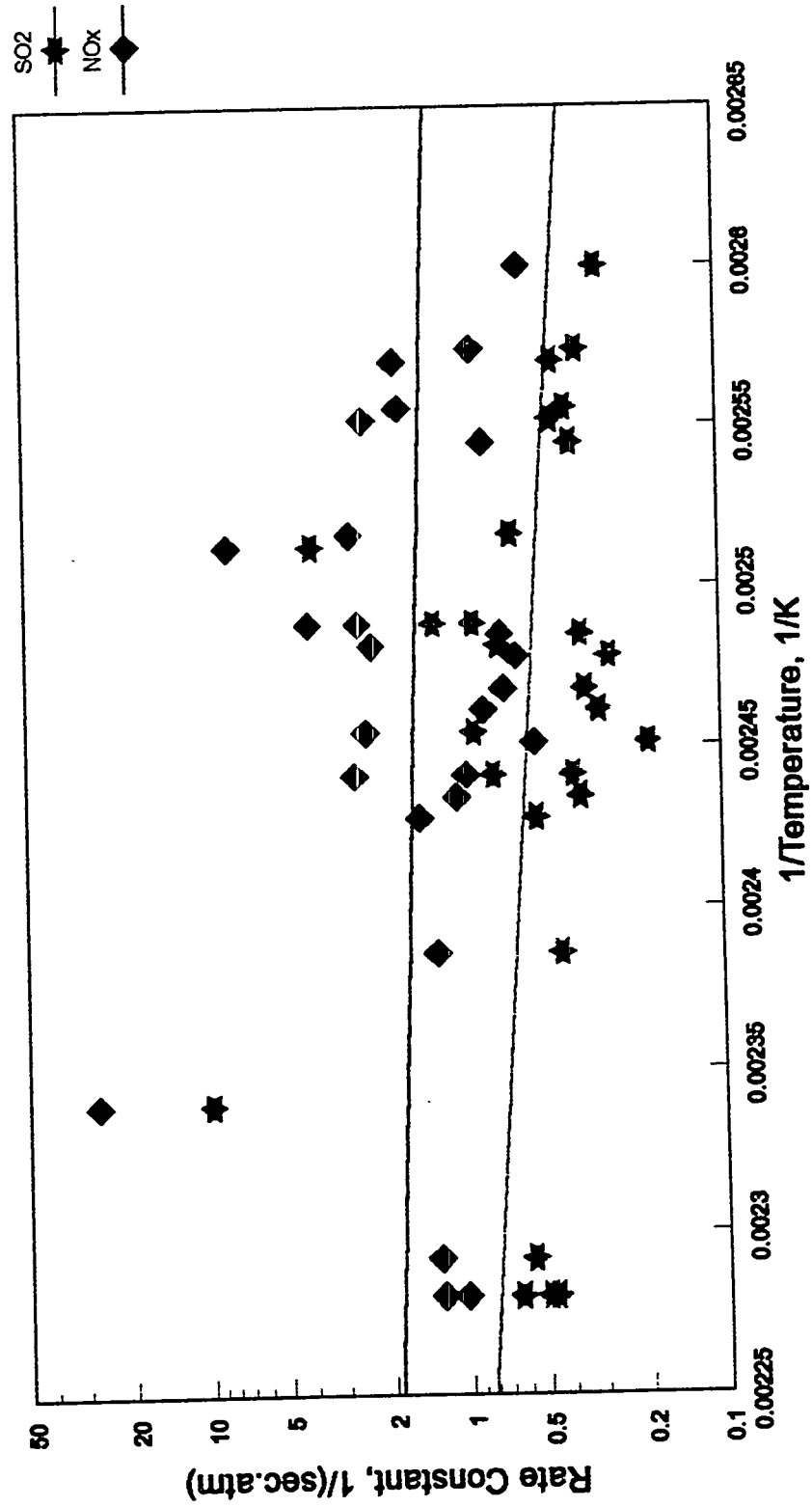

Equations 11.3-22 and 11.3-23 must be simultaneously solved to determine the removal fraction. A computer iteration scheme was developed, and the LCTU operating conditions were used to predict both SO_2 and NO_x removal efficiencies. Appendix A.1 and A.2 contain the LCTU data with the calculated removal efficiencies. Figures 11-21 and 11-22 contain both PDU and LCTU results to show the quality of fit between the model prediction and the measured NO_x and SO_2 removal efficiencies, respectively. The majority of the data points in Figures 11-21 and 11-22 fall within the $\pm$ 20% error range.

11.3.2 Comparison of POC Adsorption Results with the Model Prediction

The sorbent used in the POC tests is different from the earlier NOXSO sorbent. The POC sorbent has a higher sodium content (5.2 wt% as compared to the earlier 3.5 wt%). The sorbent also contains 6.8 wt% SiO_2 to stabilize the sorbent structure and the surface area. It was found from the laboratory that the presence of silicate reduces the sorbent activity. Approximately, one mole Si cancels about one mole Na. The NOXSO laboratory also found that the SO_2 capacity of the sorbent is proportional to the surface area of the POC sorbent. However, there is no similar finding regarding reduction of the sorbent's NO_x capacity with a drop in sorbent surface area.

The application of the PDU adsorber model to predict the POC adsorption results is straight forward. The use of the model requires information about the change of the sorbent surface area and NO_x and SO_2 capacities. The POC sorbent surface area decreased rapidly from an initial value of 250 m^2/g to 180 m^2/g within about 350 flue gas hours. After that the rate of surface area loss becomes smaller and gradually reaches 150 m^2/g. The surface area correction used in the PDU adsorber model is set to 150/250 = 0.6. The value of 0.6 was selected because the adsorption test data which are listed in Appendix A3 were collected after the sorbent surface area was stabilized. The sorbent's NO_x and SO_2 capacities are calculated as follows:

For SO_2:

$$E_1 = \left(\lambda_1 n + \frac{0.8 - S_r}{3200}\right)\frac{A}{A_0} \qquad (11.3\text{-}24)$$

For NO_x:

$$E_2 = \left(\frac{\lambda_2 + 0.8 - S_r}{3200}\right)\frac{\lambda_2}{\lambda_1} \qquad (11.3\text{-}25)$$

$$n = \frac{Na}{2300} - \frac{SiO_2}{6000}$$

where Na is sorbent sodium content, wt%
S_r is the regenerated sorbent sulfur content, wt%

Figure 11-21
Comparison of Predicted and
Measured NOx Removal Efficiency

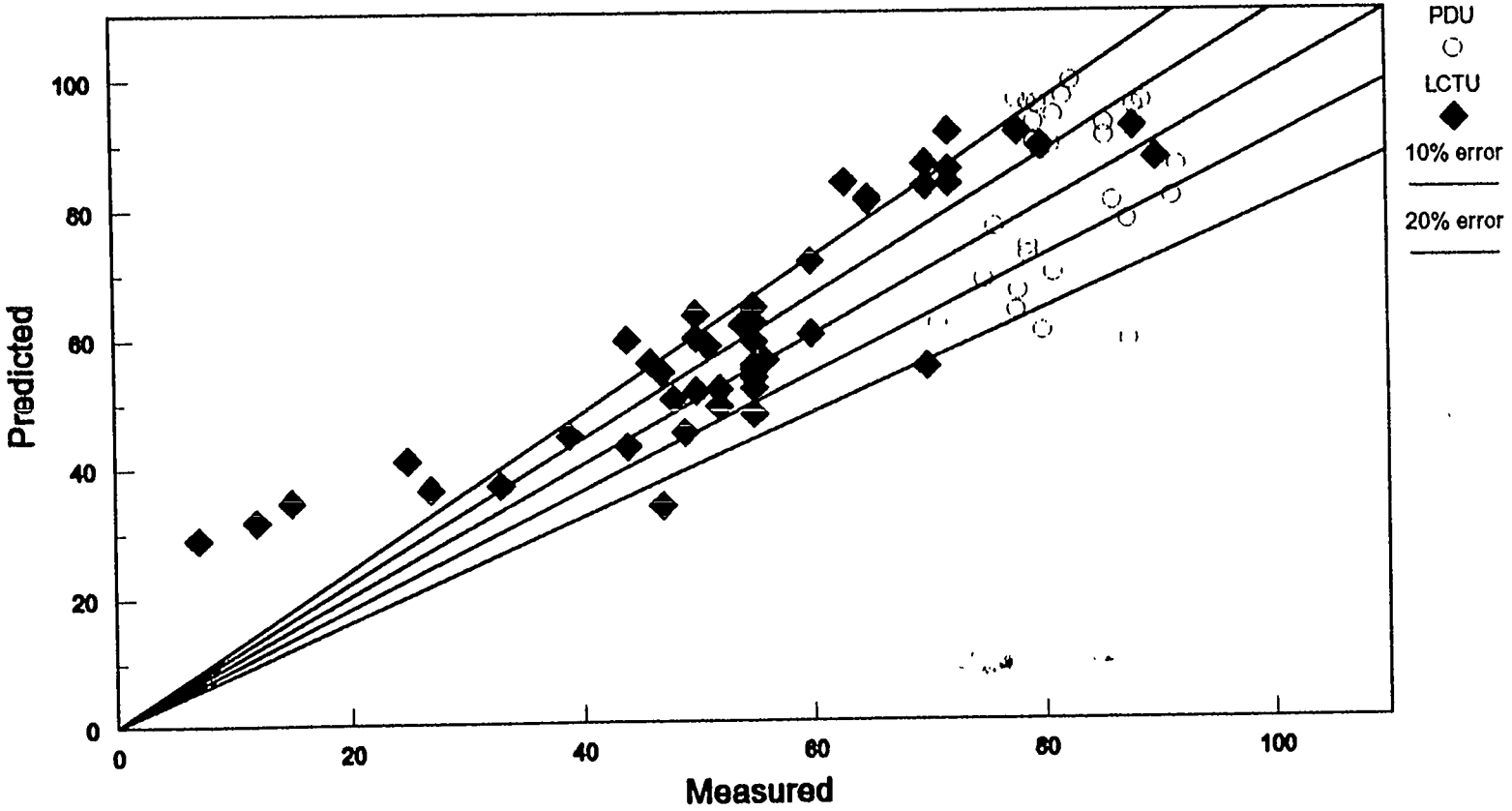

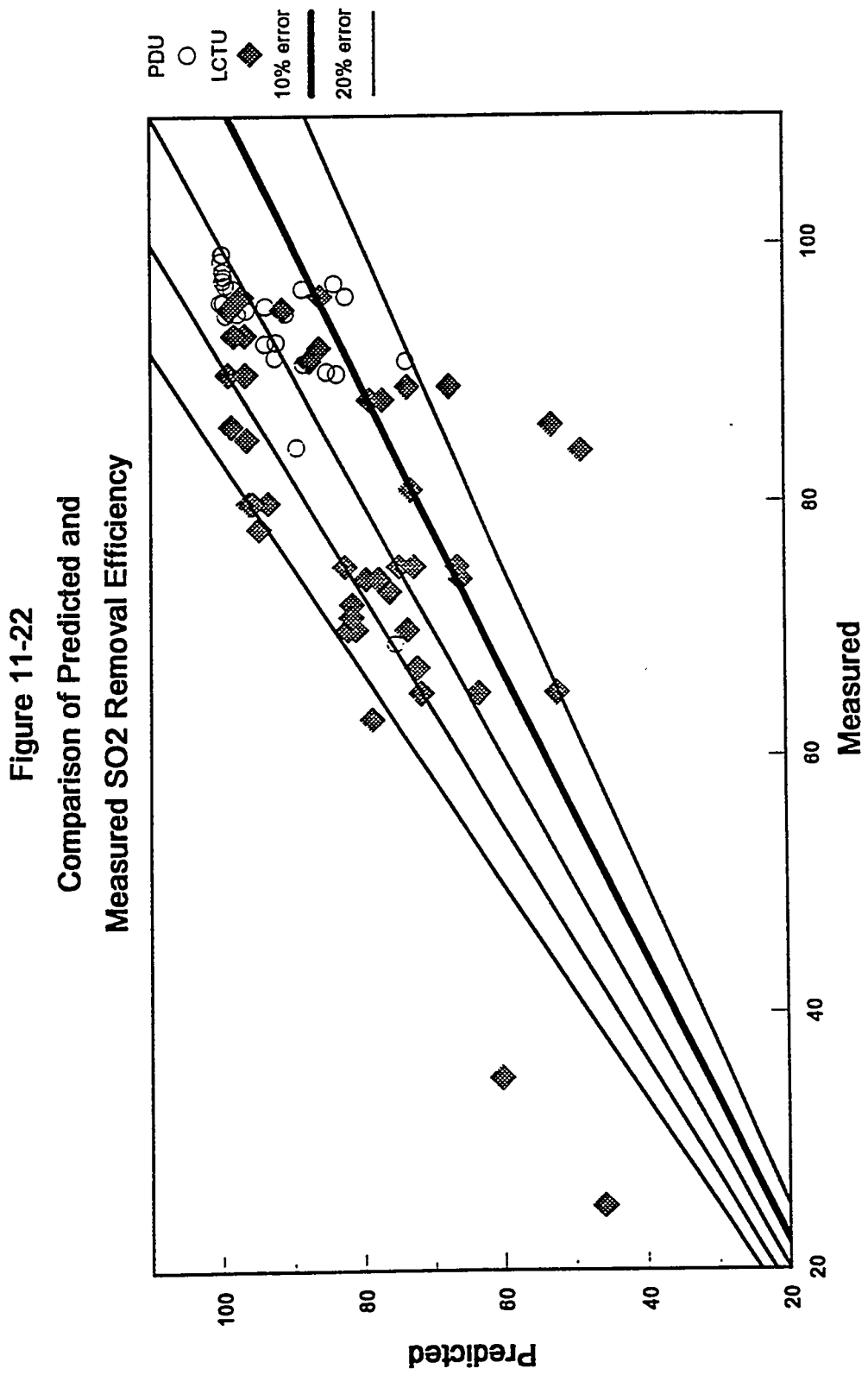

Figure 11-22
Comparison of Predicted and
Measured SO2 Removal Efficiency

SiO_2 is sorbent silicate content, wt%
A/A_0 is the correction for the change of sorbent surface area
0.8 is the averaged sulfur content of the PDU regenerated sorbent
2300, 3200, 6000 are the molecular weights of Na, S and SiO_2 times 100.

The predicted NO_x and SO_2 removal efficiencies were then calculated from Equations 11.3-22 and 11.3-23 using the sorbent capacities calculated from Equations 11.3-24 and 11.3-25. The comparison between the measured NO_x and SO_2 removal efficiencies and the NO_x and SO_2 removal efficiencies predicted by the model is shown in Figures 11-23 and 11-24, respectively. Both figures also compare the PDU and LCTU data with the SO_2 capacity corrected for the change in sorbent surface area. This correction reduces the model accuracy in predicting the LCTU SO_2 removal efficiency. The difference can be judged by comparing Figures 11-22 and 11-24.

Near the end of the POC adsorption test, a tube bundle which serves as a bubble buster was installed inside the POC adsorber to break the gas bubbles and to improve the gas solid contacting. The data designated with POCbb in Figures 11-23 and 11-24 are those obtained from the tests with the bubble buster.

11.4 Statistical Design and Analysis Results, Pilot Plant Facility

In order to develop a comprehensive understanding of key process variables in the NOXSO process, a statistical experimental design was planned. The process variables selected were:

1. Sorbent residence time in adsorber
2. Sorbent circulation rate
3. Sorbent residence time in regenerator
4. Flue gas space time (reciprocal gas flow rate)

These variables were chosen because they were expected to have a major influence on NO_x and SO_2 removal rates. Flue gas space time was selected as the metric for gas flow rate so that the interaction term between sorbent circulation rate and flue gas space time would have engineering meaning as the solid/gas contact ratio.

The experimental design was a thirty run central composite response surface design. The intent was to be able to empirically model removals as a function of the design variables, so that optimum conditions and process tradeoffs could be evaluated. The design was set up in three 10-run blocks; statistical analysis with increasing confidence could be performed as each block was completed. The experimental design is shown in Table 11-6.

Figure 11-23
Comparison of Predicted and Measured NOx Removal
(PDU, LCTU and POC Test Results)

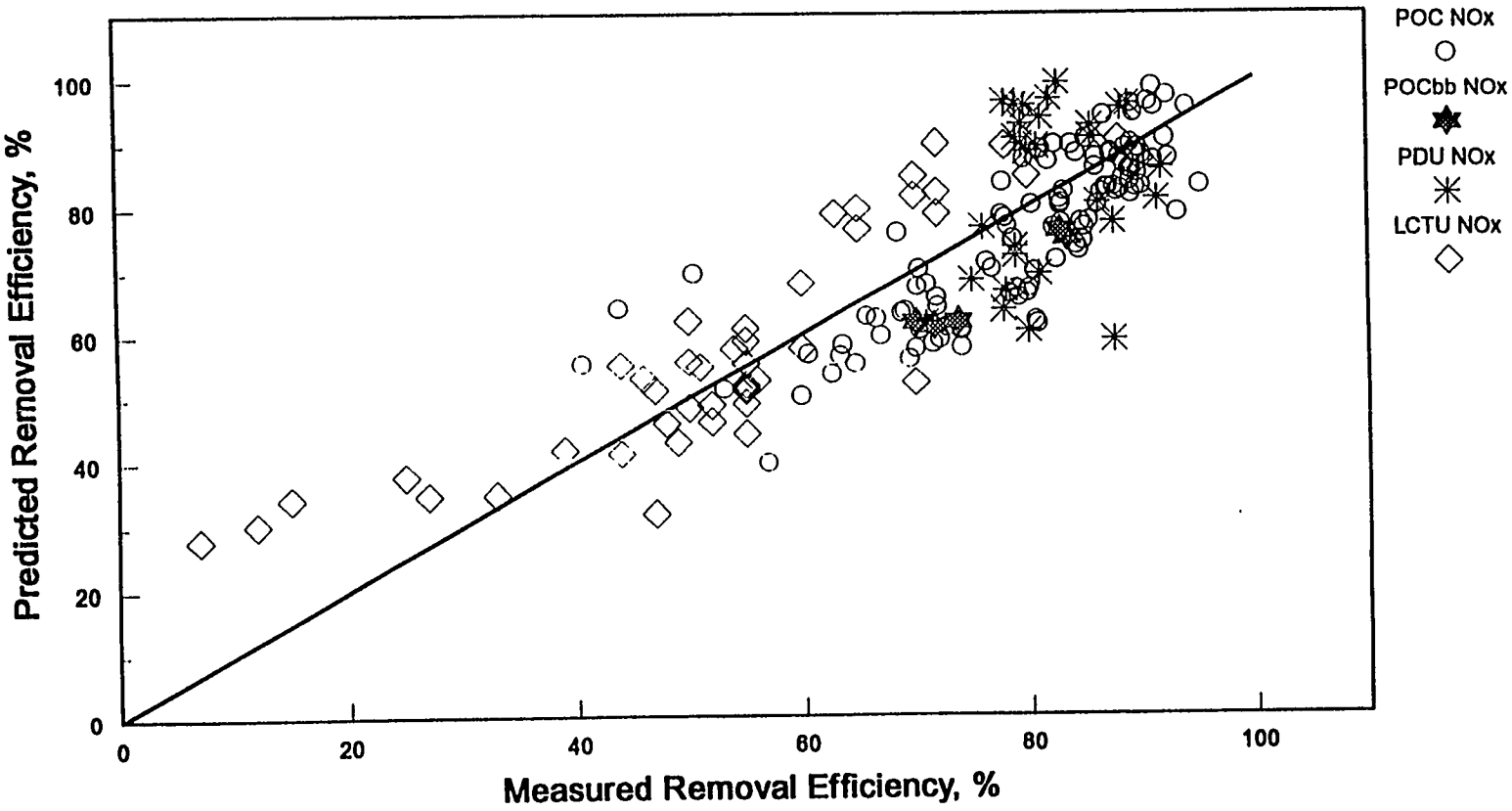

Figure 11-24

Comparison of Predicted and Measured SO2 Removal

(PDU, LCTU and POC Test Results)

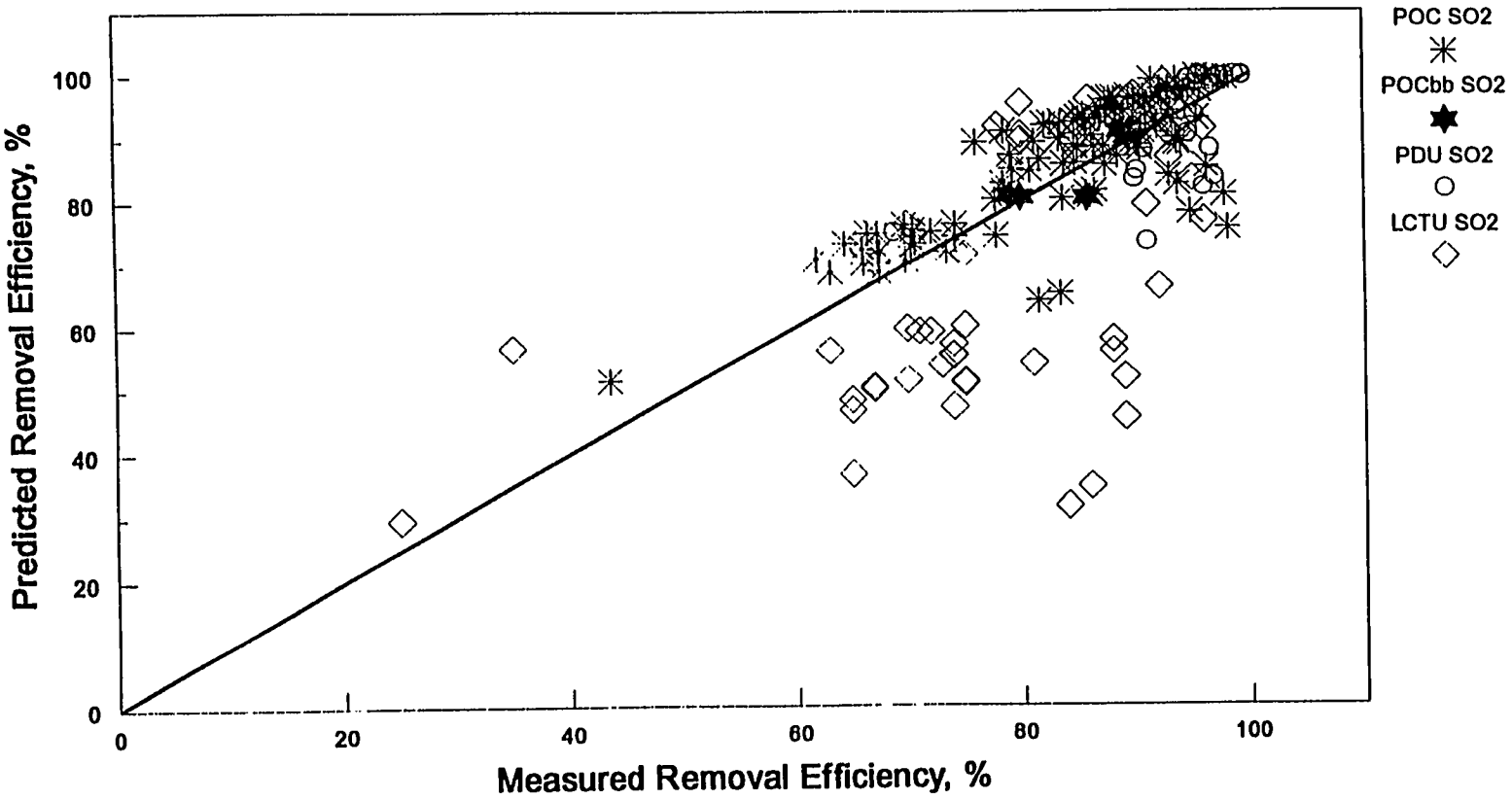

Table 11-6. NOXSO POC Experimental Design (Central Composite Response Surface)						
Run No.	Variable 1 Adsorber Residence Time (min)	Adsorber Bed-dp (in H_2O)	Flue Gas Residence Time (sec)	Variable 2 Flue Gas Flow Rate (SCFM)	Variable 3 Sorbent Circulation Rate (#/hr)	Variable 4 Regenerator Residence Time (min)
1 Block 1						
2 1	59	12.88	1.29	8450	5900	40.5
3 2	49	12.51	1.53	6900	6900	49.0
4 3	39	11.40	1.66	5800	7900	57.5
5 4	59	12.88	1.87	5800	5900	57.5
6 5	49	12.51	1.53	6900	6900	49.0
7 6	39	8.51	1.24	5800	5900	40.5
8 7	39	11.40	1.14	8450	7900	40.5
9 8	39	8.51	0.85	8450	5900	57.5
10 9	59	17.25	1.72	8450	7900	57.5
11 10	59	17.25	2.51	5800	7900	40.5
12 Block 2						
13 11	49	12.51	1.53	6900	6900	49.0
14 12	39	11.40	1.14	8450	7900	57.5
15 13	59	17.25	1.72	8450	7900	40.5
16 14	49	12.51	1.53	6900	6900	49.5
17 15	59	12.88	1.87	5800	5900	40.5
18 16	59	17.25	2.51	5800	7900	57.5
19 17	39	11.40	1.66	5800	7900	40.5
20 18	39	8.51	0.85	8450	5900	40.5
21 19	39	8.51	1.24	5800	5900	57.5
22 20	59	12.88	1.29	8450	5900	57.5
23 Block 3						
24 21	49	12.51	2.11	5000	6900	49.0
25 22	49	12.51	1.53	6900	6900	49.0
26 23	49	16.14	1.97	6900	8900	49.0
27 24	69	17.62	2.16	6900	6900	49.0
28 25	49	8.88	1.09	6900	4900	49.0
29 26	49	12.51	1.53	6900	6900	66.0
30 27	49	12.51	0.96	11000	6900	49.0
31 28	49	12.51	1.53	6900	6900	32.0
32 29	49	12.51	1.53	6900	6900	49.0
33 30	29	7.40	0.91	6900	6900	49.0

The first 10-run block was completed, and these runs were supplemented with other POC runs. A data point consisted of averaged values of process data, inlet gas concentrations and removals, where the averaging was done over a period of time from four hours up to a complete shift. Data were not used if there were instrumentation problems or process upsets. A total of 90 data values were used in the analysis discussed below.

Regression analysis was used to develop empirical prediction models for NO_x and SO_2 removals. In the final best prediction equations, adsorber bed height was substituted for adsorber residence time and adsorber bed temperature. NO_x and SO_2 inlet concentrations were included with the experimental design variables listed above. The coefficients for the prediction equations are shown in Table 11-7, along with statistical significance levels. They are written in equation form in Table 11-8. The equations effectively represent the data base; a ten-term equation in five variables explains 95% of the variability in NO_x removal, and a fifteen-term equation in seven variables explains 97% of the variability in SO_2 removal. Predicted verses measured NO_x and SO_2 removals are plotted in Figures 11-25 and 11-26.

Table 11-7. Regression Coefficients and Statistics for NO_x and SO_2 Removal Models

	NO_x Removal, %			
Term	Coefficients	Standard Error of Coefficients	T-value	Significant p-value
Constant	85.08	0.52	162.6	0.0001
~Sorbent Circulation Rate	3.18	0.34	9.4	0.0001
~Adsorber Bed Height	2.02	0.31	6.5	0.0001
~Regenerator Residence Time	-	-	-	-
~Flue Gas Space Time	8.03	0.34	23.3	0.0001
~Adsorber Bed Temperature	-1.13	0.26	-4.3	0.0001
~Inlet NO_x	-3.75	0.62	-6.1	0.0001
~Inlet So_2	-	-	-	-
~Circulation Rate*Space Time	-2.08	0.34	-6.1	0.0001
~Circulation Rate*Bed Height	-	-	-	-
~Space Time*Bed Height	-	-	-	-
~Circulation Rate*Regenerator Residence	-	-	-	-
~Circulation Rate**2	-1.81	0.32	-5.7	0.0001
~Space Time**2	-2.11	0.31	-6.8	0.0001
~Adsorber Bed Height**2	-	-	-	-
~Regenerator Residence Time**2	-	-	-	-
~Inlet NOx**2	-1.29	0.23	-5.5	0.0001
No. Cases = 90, Residence df = 80, RMS Error = 2.3, R-sq. = 0.95, R-sq-adj. = 0.95, Condition No. = 5.2				

Figure 11-25
Predicted Versus Measured NOx Removal
For Data Used to Fit Model

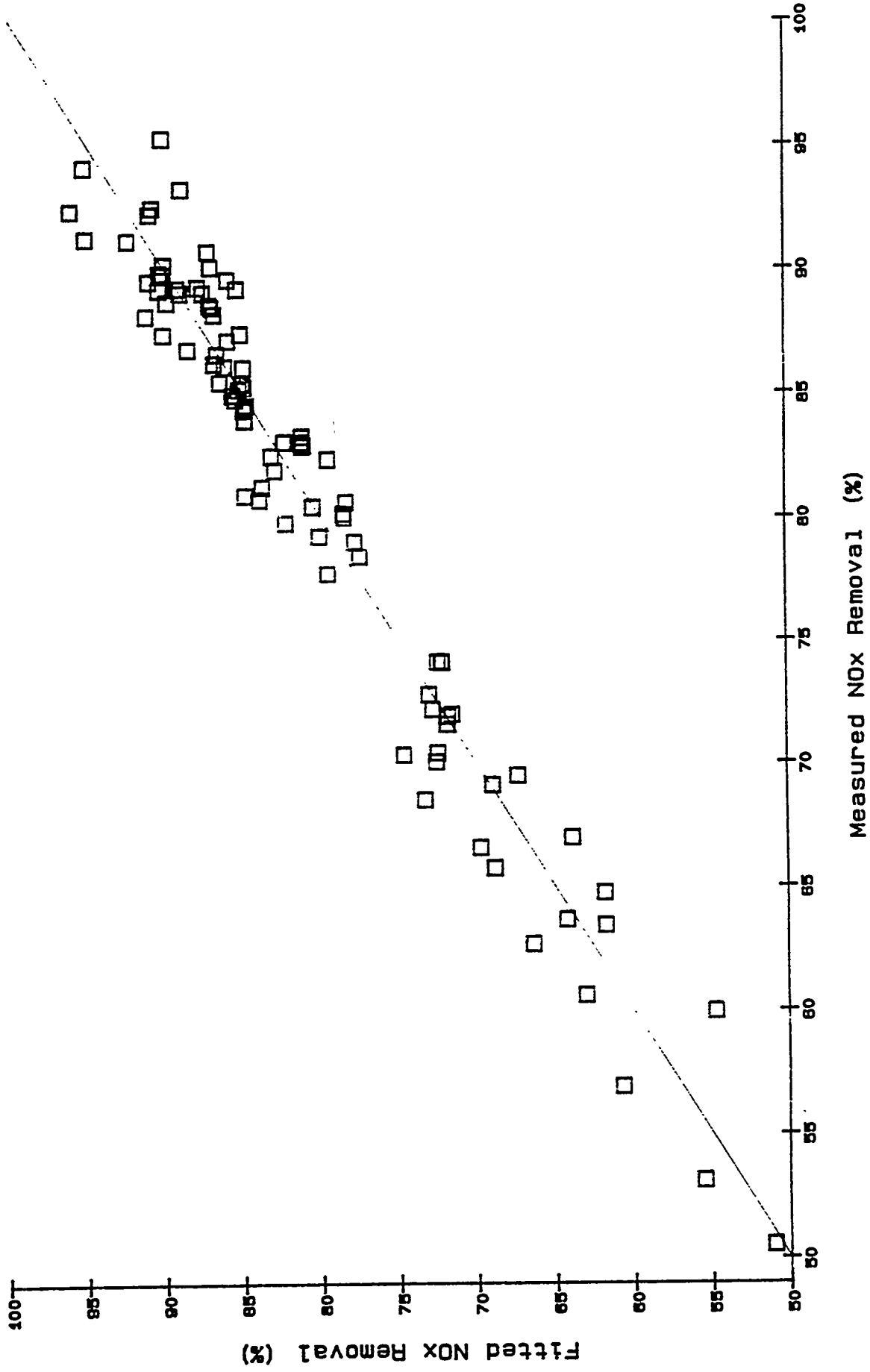

Figure 11-26
Predicted Versus Measured SO2 Removal
For Data Used to Fit Model

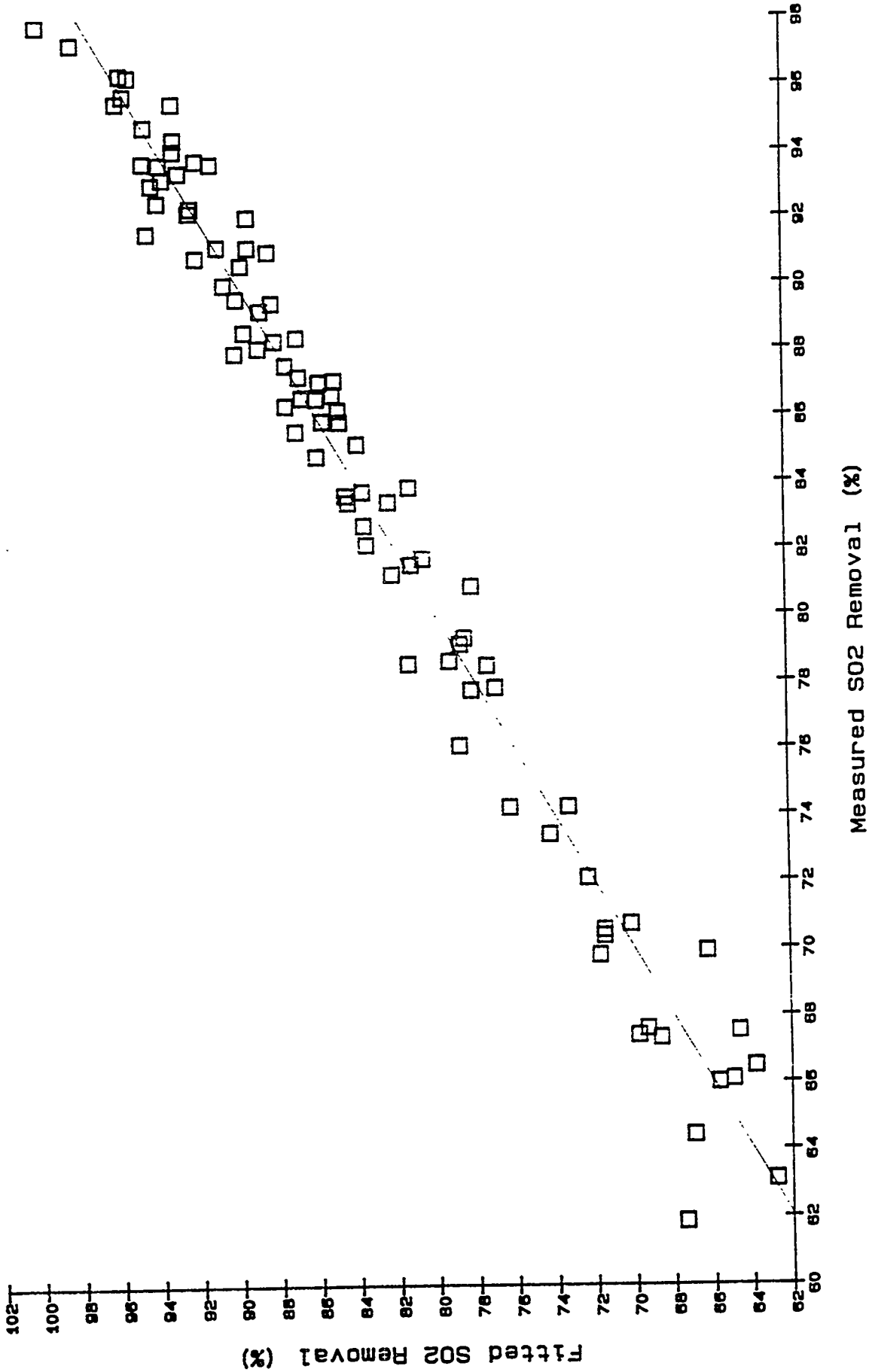

Table 11-7. Regression Coefficiencts and Statistics for NO_x and SO_2 Removal Models				
	SO_2 Removal, %			
Term	Coefficients	Standard Error of Coefficients	T-value	Significant p-value
Constant	85.20	0.38	222.6	0.0001
~Sorbent Circulation Rate	3.23	0.42	7.8	0.0001
~Adsorber Bed Height	4.87	0.27	17.8	0.0001
~Regenerator Residence Time	-0.53	0.36	-1.5	0.1433
~Flue Gas Space Time	5.46	0.29	18.8	0.0001
~Adsorber Bed Temperature	-0.52	0.22	2.3	0.0229
~Inlet NO_x	2.26	0.24	9.4	0.0001
~Inlet SO_2	-2.10	0.26	-8.2	0.0001
~Circulation Rate*Space Time	-1.89	0.27	-7.0	0.0001
~Circulation Rate*Bed Height	-1.01	0.27	-3.7	0.0004
~Space Time*Bed Height	1.04	0.28	3.7	0.0004
~Circulation Rate*Regenerator Residence	2.34	0.32	7.3	0.0001
~Circulation Rate**2	-	-	-	-
~Space Time**2	-2.17	0.27	-8.1	0.0001
~Adsorber Bed Height**2	-1.43	0.26	-5.6	0.0001
~Regenerator Residence Time**2	2.78	0.31	8.9	0.0001
~Inlet NO_x**2	-	-	-	-
No. Cases = 88, Residence df = 73, RMS Error = 1.7 R-sq = 0.97, R-sq-adj. = 0.97, Condition No. = 7.4				

~Indicates factors are transformed.
~Circulation Rate = (Circulation Rate - 7845.5)/1394
~Adsorber Bed Height = (Adsorber Bed Height - 1.67)/0/57
~Regenerator Residence Time = (Regeneration Residence Time - 47.0)/7.43
~Space Time = (Space Time - .0001366)/.00002494
~Adsorber Bed Temperature = (Adsorber Bed Temperature - 325.9)/13.0
~Inlet SO_2 = (Inlet SO_2 - 1773.0)/162.6
~Inlet NO_x = (Inlet NO_x -289.4)/121.8

The equations were used to predict removals for a subsequent series of POC runs under a variety of base load operating conditions. Results are plotted in Figures 11-27 and 11-28, and tabulated in Table 11-9. Note that the BB series are runs made with a bubble buster device installed in the adsorber to improve gas mass transfer. In order to put the BB series results on the same basis as the others (since the equations do not account for the bubble buster), the predicted NO_x removals for the BB series were increased by 3.8 percentage points, which is the average improvement due to the bubble buster. There appeared to be no bubble buster effect on SO_2 removal. The standard error for the predictions in Table 11-9 are 2.3% for NO_x removal, and 2.0% for SO_2 removal, indicating that the equations predict removals very well.

Figure 11-27. Predicted Versus Measured NOx Removal
Recent POC Runs Not Used in Model Fitting
Bubble Buster Predictions Adjusted by Adding 3.8%

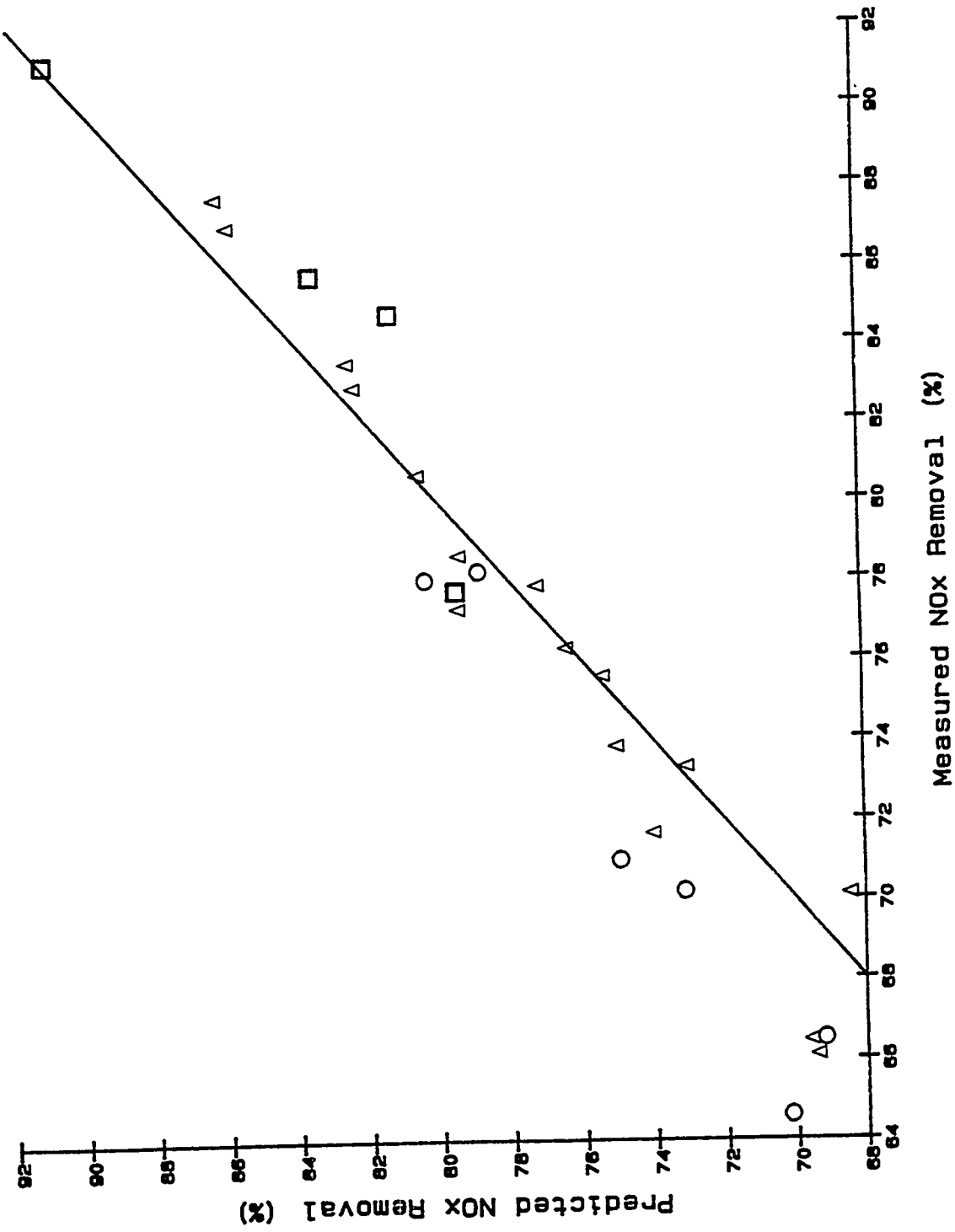

Figure 11-28
Predicted Versus Measured SO2 Removal
Recent POC Runs Not Used in Model Fitting

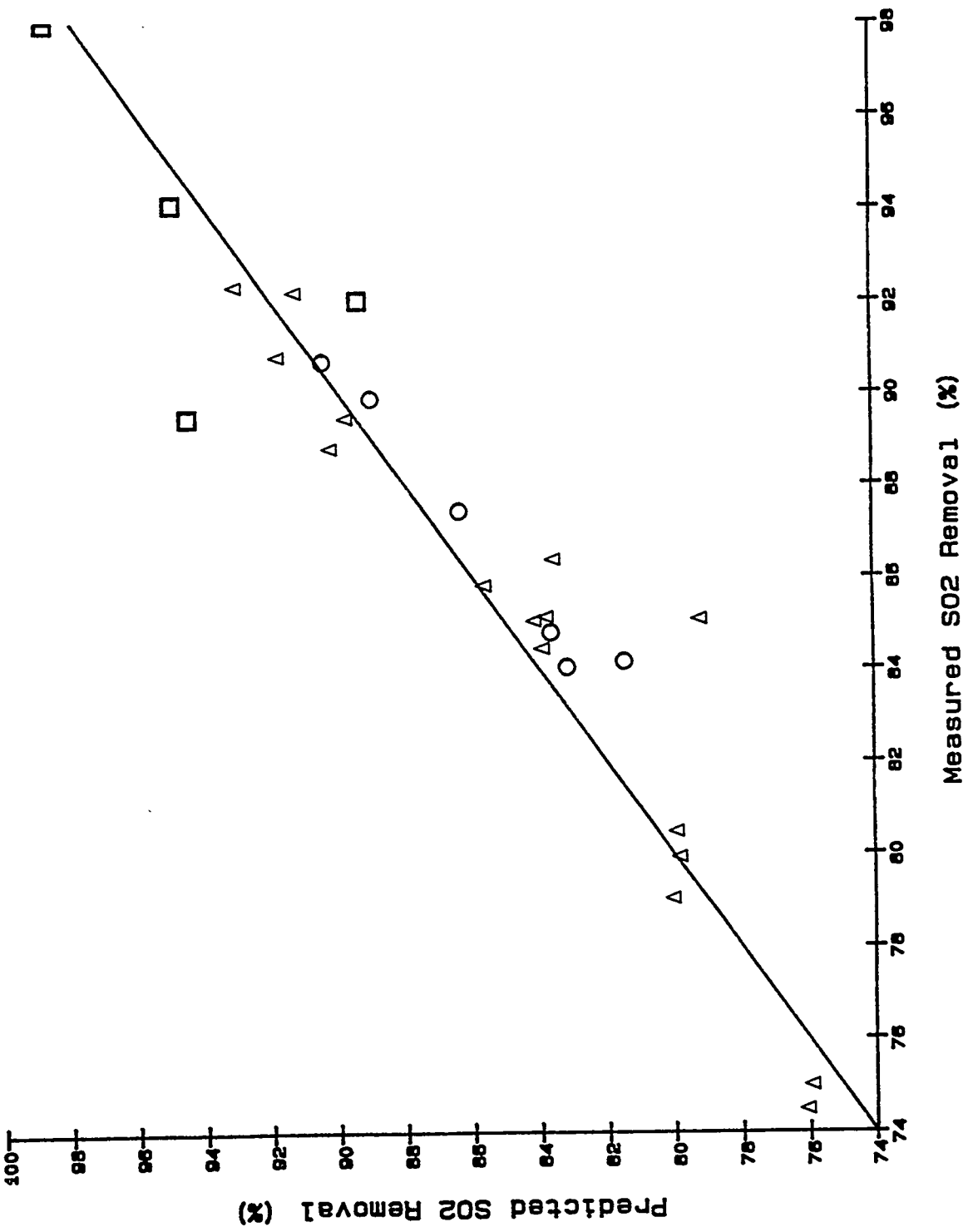

Table 11-9. Key Process Variables and Measured and Predicted NOx and SO2 Removals Recent POC Runs

Test	Shift	Sorbent Circ. Rate (lb/hr)	Bed Height (ft)	Adsorber Residence Time (min)	Bed Temp (deg F)	Flue Gas Flowrate (scfm)	Inlet SO2 (ppm)	Inlet NOx (ppm)	Regenerator Residence Time (min)	Measured NOx Conv (%)	Predicted NOx Conv (%)	Meas-Pred NOx	Measured SO2 Conv (%)	Predicted SO2 Conv (%)	Meas-Pred SO2
1 jwb	092592d	9925	1.45	30.4	341	7064	1817	413	44.8	77.7	79.5	-1.8	92.0	89.4	2.59
2 pc-3	111792n	9941	1.80	37.5	337	7220	1706	348	35.5	85.7	83.5	2.2	89.5	94.5	-5.09
3 basc	111892d	9939	1.84	38.4	356	7308	1745	410	35.5	82.2	78.8	3.4	95.0	94.4	0.55
4 base	111892d	9939	1.84	38.4	299	7308	1760	412	35.5	86.0	83.7	2.3	92.8	96.6	-3.75
5 pc-3	111892n	9932	1.82	38.1	335	7159	1784	407	35.4	84.7	81.3	3.4	94.1	95.0	-0.92
6 wrg-2	111392d2	9966	2.60	54.3	294	6101	1777	382	35.5	91.1	91.0	9.5e-02	98.0	98.8	-0.81
7 fg-1	112092n	9938	1.82	38.0	340	8237	1810	355	35.5	78.2	78.9	-0.6	90.7	90.5	0.20
8 fg-1	112192d1	9951	1.83	38.2	342	8235	1868	315	35.5	78.0	80.4	-2.4	89.9	89.0	0.85
9 fg-2	112292d	9920	1.82	38.2	350	9240	1973	317	35.6	71.0	74.9	-4.0	84.8	83.7	1.13
10 fg-2	112292n	9937	1.82	38.1	351	9236	1833	363	35.6	70.2	73.1	-2.9	87.4	86.4	1.05
11 fg-3	112392d	9927	1.83	38.3	347	10251	1793	358	35.6	66.5	69.2	-2.7	84.0	83.2	0.85
12 fg-3	112492n	9924	1.81	38.0	348	10284	1857	325	35.7	64.6	70.2	-5.6	84.2	81.5	2.70
13 bb-1*	120192n	9927	1.82	38.0	346	10271	1724	447	35.6	70.1	68.4	1.6	85.8	85.7	0.13
14 bb-1*	120292d	9973	1.78	37.1	349	10247	1988	322	35.6	71.7	74.1	-2.4	79.9	79.9	0.06
15 bb-1*	120292n	9914	1.80	37.7	346	10289	1922	295	35.6	73.8	75.1	-1.2	79.0	80.1	-1.06
16 bb-2*	120392d	9926	1.82	38.2	343	8200	1860	357	35.6	83.5	82.5	0.9	89.5	89.8	-0.38
17 bb-2*	120392n	9913	1.82	38.2	344	8226	1821	357	35.5	82.8	82.4	0.5	88.8	90.3	-1.50
18 bb-3*	120492d	9922	1.82	38.2	347	9253	1924	294	35.6		79.8		84.5	84.0	0.47
19 bb-3*	120492n	9929	1.82	38.2	348	9248	1946	301	35.6	77.3	79.5	-2.2	85.1	83.8	1.29
20 bb-3*	120592n	9960	1.83	38.2	343	2919	2052	373	35.5	77.8	77.3	0.6	85.1	84.2	0.84
21 bb-4*	120692d	9932	1.81	37.9	342	7225	1916	363	35.6	87.7	86.3	1.4	90.8	91.9	-1.09
22 bb-4*	120692n	9924	1.82	38.1	342	7181	1845	376	35.6	86.9	85.9	1.0	92.3	93.2	-0.86
23 bb-5*	120792d	9838	0.93	19.6	344	10233	1948	370	35.9	66.1	69.4	-3.4	75.0	76.0	-0.97
24 bb-5*	120792n	9928	0.91	19.1	345	10257	1943	363	35.6	66.5	69.6	-3.2	74.5	76.1	-1.64
25 bb-6*	120992n	9954	2.59	54.0	348	9747	1897	408	35.5	75.6	75.4	0.1	86.4	83.6	2.76
26 bb-6*	121092d	9914	2.56	53.6	347	10364	2025	400	35.7	73.3	73.1	0.2	85.1	79.3	5.84
27 bb-7*	121092n	9852	1.82	38.5	316	10361	2028	323	35.8	76.3	76.4	-0.2	80.5	80.0	0.50
28 bb-8*	121192d	9924	1.82	38.0	300	9508	1673	352	35.6	80.6	80.6	5.6e-0.2		89.3	
29 bb-8*	121192n	9953	1.82	38.1	300	9495	1561	379	35.5	78.6	79.4	-0.8	92.2	91.4	0.86

* 3.8% added to predicted NOx of bb tests to adjust for improved removal due to bubble buster

Table 11-8. Prediction Equations for NO_x and SO_2 Conversion	
NO_x Conversion =	
85.1 + 3.18*(Circulation Rate)' + 8.03*(Space Time)' = 2.02*(Adsorber Bed Height)	
- 1.13*(Adsorber Bed Temperature)'- 3.75*(Inlet NO_x)' - 2.08*(Circulation Rate)'*(Space Time)'	
- 1.81*(Circulation Rate)' - 2.11*(Space Time)'^{2} - 1.29*(Inlet NO_x)'^{2}	
SO_2 Conversion =	
85.3 + 3.22*(Circulation Rate)' + 5.46*(Space Time)' + 4.87*(Adsorber Bed Height)'	
- 0.52*(Adsorber Bed Temperature)' - 0.53*(Regenerator Residence Time)' + 2.26*(Inlet NO_x)' -	
- 2.11*(Inlet SO_2)' - 1.89*(Circulation Rate)'*(Space Time)'	
- 1.0*(Circulation Rate)'*(Adsorber Bed Height)' + 1.04*(Space Time)'*(Adsorber Bed Height)'	
+2.34*(Circulation Rate)'*(Regenerator Residence Time)' - 2.17*(Space Time)'$_2$	
- 1.34*(Adsorber Bed Height)'^{2} + 2.78*(Regenerator Residence Time)'^{2}	
where	
(Circulation Rate)'	= (Sorbent Ciculation Rate - 7845)/1394
(Space Time)'	= (Flue Gas Space Time - 0.0001366)/0.00002494
(Adsorber Bed Height)'	= (Adsorber Bed Height - 1.67)/0.57
(Adsorber Bed Temperature)'	= (Adsorber Bed Temperature - 326)/13
(Regenerator Residence Time)'	= (Regenerator Residence Time -47)/7.4
(Inlet NO_x)'	= (Inlet NO_x - 289)/122
(Inlet SO_2)'	= (Inlet SO_2 - 1773)/163

The equations can now be used with confidence to explore a range of operating conditions for optimum performance. Figures 11-29 and 11-30 are contour plots of predicted NO_x and SO_2 removals as functions of flue gas flow rate and sorbent circulation rate, holding bed height, bed temperature and regenerator residence time constant. Figure 11-29 is for POC base load inlet concentrations, and Figure 11-30 is for estimated Niles conditions. These equations can be used to tune operating conditions for best performance, given inlet gas flow rate and concentration.

11.5 NO_x Regeneration

The NO_x adsorbed on the spent sorbent from the adsorber can be easily regenerated by simply heating up the sorbent. The laboratory studies show that the NO_x desorption is complete around 700°F. Normally a small amount of SO_2 will also desorb on heating. The form of the desorbed NO_x and the amount of SO_2 desorbed were investigated during the POC test.

11.5.1 SO_2 Desorption

It was found in the LCTU test that about 6% of removed SO_2 in the adsorber was evolved from sorbent in the sorbent heater. But the POC test found that less than 1% of sorbed SO_2 was evolved in the three-stage sorbent heater. The difference between LCTU and POC test results was due to the following:

Figure 11-29. Predicted NOx and SO2 Removals
Bed Height = 3 ft, Bed Temp = 325 F,
Regenerator Residence Time = 30 min
Inlet NOx = 725 ppm, Inlet SO2 = 2900 ppm

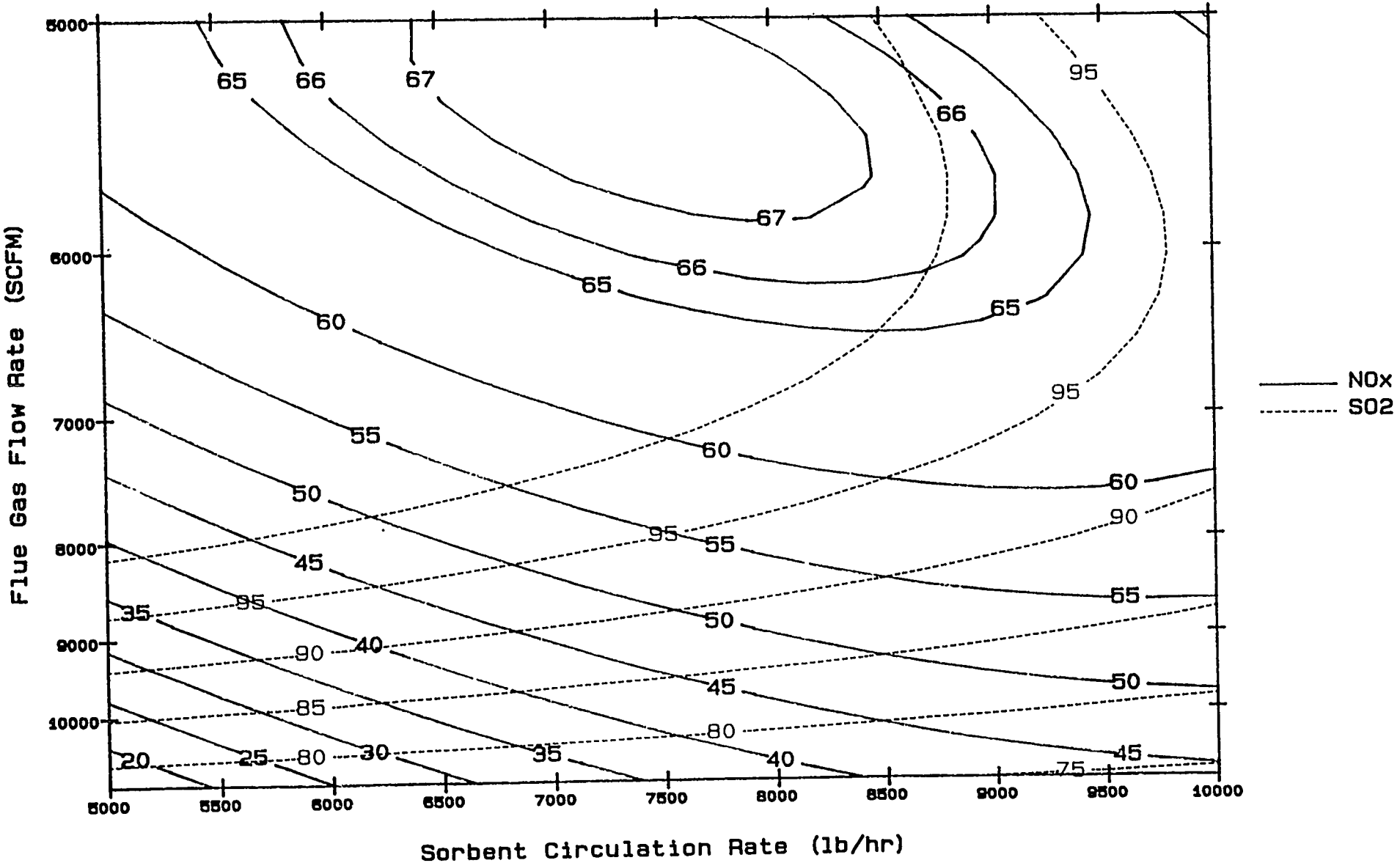

Figure 11-30. Predicted NOx and SO2 Removals
Bed Height = 3 ft, Bed Temp = 325 F,
Regenerator Residence Time = 30 min
Inlet NOx = 300 ppm, Inlet SO2 = 1800 ppm

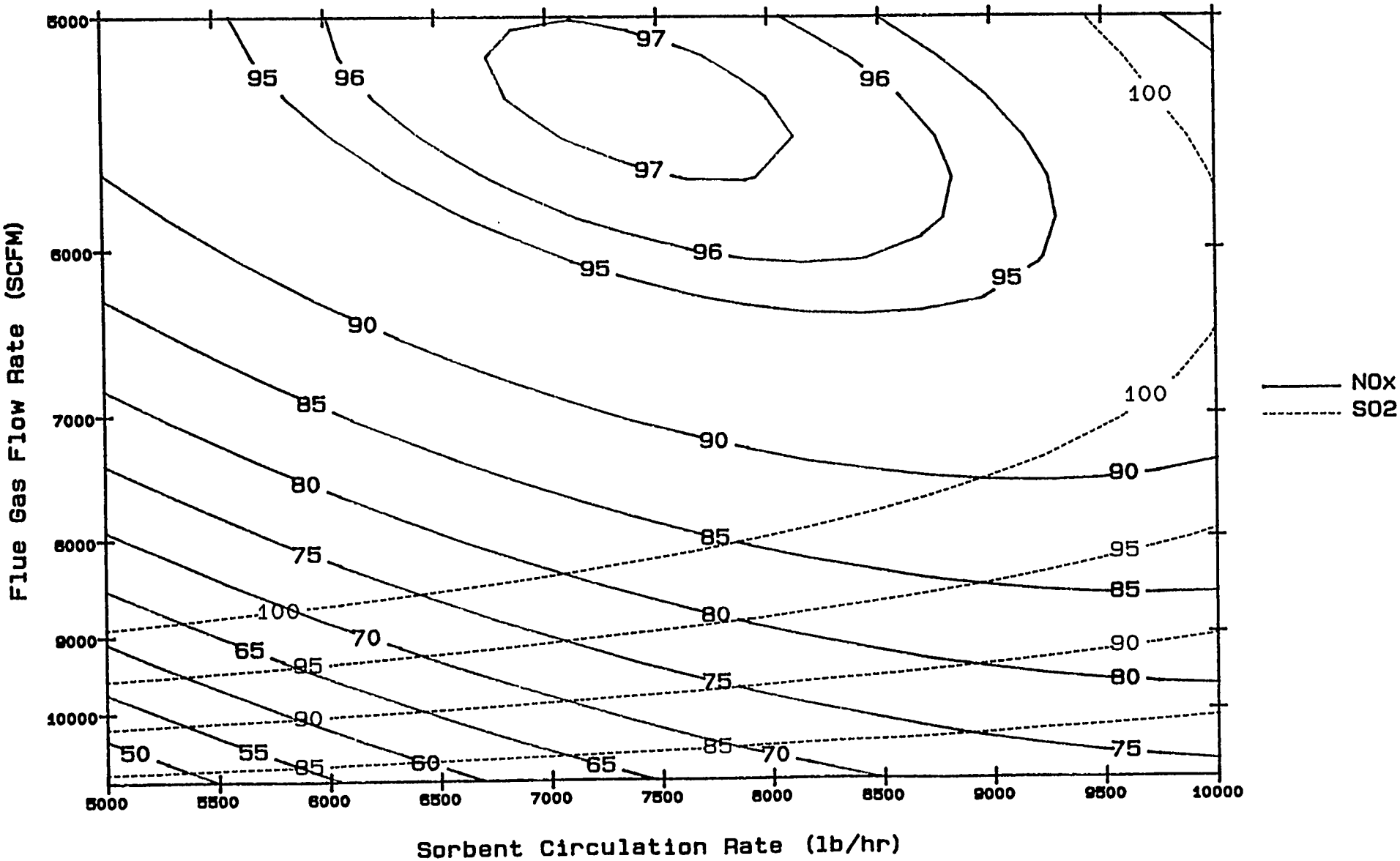

1. The sorbent sulfur loading of the POC tests is less than that of the LCTU tests: Nine tenths to 1.2 wt% sulfur in the POC tests versus 1.2 to 2.3 wt% sulfur in LCTU tests. The higher the sulfur loading, the greater the amount of SO_2 evolved on sorbent heating.

2. The temperature and the oxygen content of the POC adsorber is higher than that of the LCTU: nine versus four percent in oxygen content, and 330°F versus 270°F in temperature, respectively. Higher temperature and oxygen content produce a smaller amount of sulfite on the POC spent sorbent. The sulfate is more stable than the sulfite.

3. The oxygen content of the sorbent heater is higher in the POC than the LCTU: 19% versus less than 1% oxygen. The higher partial pressure of O_2 in the heater offgas promotes oxidation of adsorbed sulfur to the sulfate.

11.5.2 NO_x Desorption

The amount of NO_x removed in the adsorber was found to completely evolve from sorbent in the sorbent heater. The same NO_x balance result was also found during the LCTU test conducted at PETC. The LCTU test used a one-stage fluid bed sorbent heater which was inerted by nitrogen. The offgas temperature of the LCTU sorbent heater was 1200°F. The evolved NO_x remained intact, mainly in NO form. The POC sorbent heater is a three-stage fluid bed vessel, which contains about 19% oxygen. The offgas temperature is around 750°F. About two thirds of the evolved NO in POC sorbent heater becomes NO_2. The presence of NO_2 in the sorbent heater offgas may effect the efficiency of NO_x destruction when recycling the NO_x back to the coal combustor. However, the simulated NO_x recycle tests conducted in B&W's modular cyclone coal-combustor show that the NO_x destruction is independent of the form of the recycled NO_x.[8] Moreover, the B&W tests agree with the earlier PETC tunnel furnace test results.[3]

11.6 Sulfur Regeneration

The spent sorbent is regenerated in an alonized regenerator which consists of two sections as shown in Figure 11-31. The sorbent flows downward in a moving-bed, while the regenerant gases flow upward in approximately plug flow. Natural gas enters the bottom of the upper section of the regenerator and reduces the sulfate on the sorbent to SO_2, H_2S, and sulfide. The sulfide remains on the sorbent. The steam enters the bottom of the lower section and hydrolyzes sulfide to H_2S. In order to study the sulfur regeneration, the regenerator was installed with several sorbent sampling ports and thermocouples along its axial direction. During the operation, five sorbent samples were collected, once every six hours. One was obtained from the adsorber outlet, one from the regenerator outlet, and three from the regenerator. A LECO SC-132 sulfur determinator was used to analyze the sorbent samples' sulfur contents. The location of the three regenerator sampling ports is also shown in Figure 11-31. For the sake of discussion, the upper sampling port is called upReg, the middle port is called lwReg, and the lower port is called stmReg. The average temperatures of the thermocouples around the upReg

Figure 11-31
Regenerator and Sorbent Sample Ports

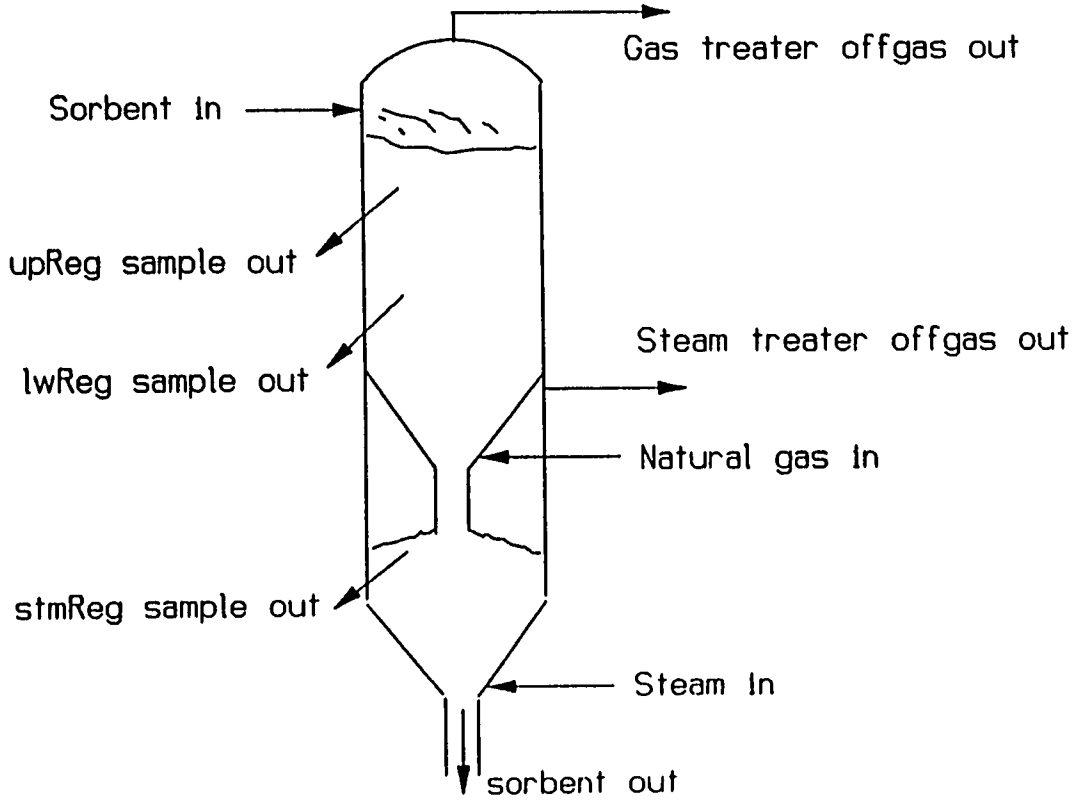

or lwReg location were taken as the sorbent temperature at those heights. The stmReg port provided the regenerated sorbent before the steam treatment. The regenerator temperature was controlled by the bottom bed temperature of the three-stage sorbent heater. Figure 11-32 shows the temperature variation in the regenerator for a test period from September 20, 1992 day shift till December 11, 1992 night shift. Each data point represents a 12 hour average. Figure 11-32 indicates that the sorbent loses its heat as it travels down the regenerator. The difference in the temperature profile in different shifts was caused by changing operating conditions to accomplish the test plan, such as changing the heater bottom bed temperature, the sorbent circulation rate, the regenerator bed height, etc. Despite the variation in the operating conditions, several periods of steady operation under similar conditions were obtained. The data obtained from those periods were used in the following discussion to estimate the regeneration heat, the offgas H_2S to SO_2 ratio, and the rate of sulfur regeneration.

Since pipeline natural gas was used in regenerating the spent sorbent for all the POC tests, one may consider the regenerator as an integral reactor with a constant gas concentration profile during a steady operation period. The sulfur molar balance gives the rate of sulfur regeneration as a function of sorbent flowrate, inventory, etc. as shown below.

$$F_s S_a dX = r_s \, dW \tag{11.5-1}$$

where F_s is the sorbent flowrate, lb/min,
r_s is the sulfur regeneration rate, (lb sulfur)/hr/(lb sorbent),
S_a is the sulfur fraction of the spent sorbent,
S is the sulfur fraction of the regenerated sorbent,
X is the conversion of sulfur regeneration, $X=1-S/S_a$, and
W is the sorbent inventory, lb.

The slope of the plot of X versus $W/(F_sS_a)$ will give the rate of sulfur regeneration. Figure 11-33 shows the plot. The data were obtained from two steady test periods of which the operation range is listed in Table 11-10.

Table 11-10. Steady Operating Data

Steady Operating Period	100592-->101892d			112092n-->121092n		
	max	min	avg	max	min	avg
Heater bottom bed temp, °F	1150.2	1141.2	1149.8	1150.2	1147.3	1149.8
upReg temperature, °F	1115.0	1088.3	1111.0	1131.7	1123.9	1127.2
lwReg temperature, °F	1110.5	1067.9	1090.6	1117.6	1108.3	1112.9
Regenerator bed height, ft	9.51	1.72	4.99	5.09	4.95	5.0
Sorbent flowrate, lb/hr	9955.4	5913.4	7715.7	9973.3	9837.7	9926.9
Natural gas flowrate, scfm	15.3	7.82	10.0	10.09	9.9	10.0
Steam flowrate, lb/hr	40.03	39.63	40.0	40.02	34.95	36.7
Spent sorbent sulfur content, wt%	1.41	0.51	0.921	1.11	0.8	0.954

Figure 11-32
Heater and Regenerator Temperature

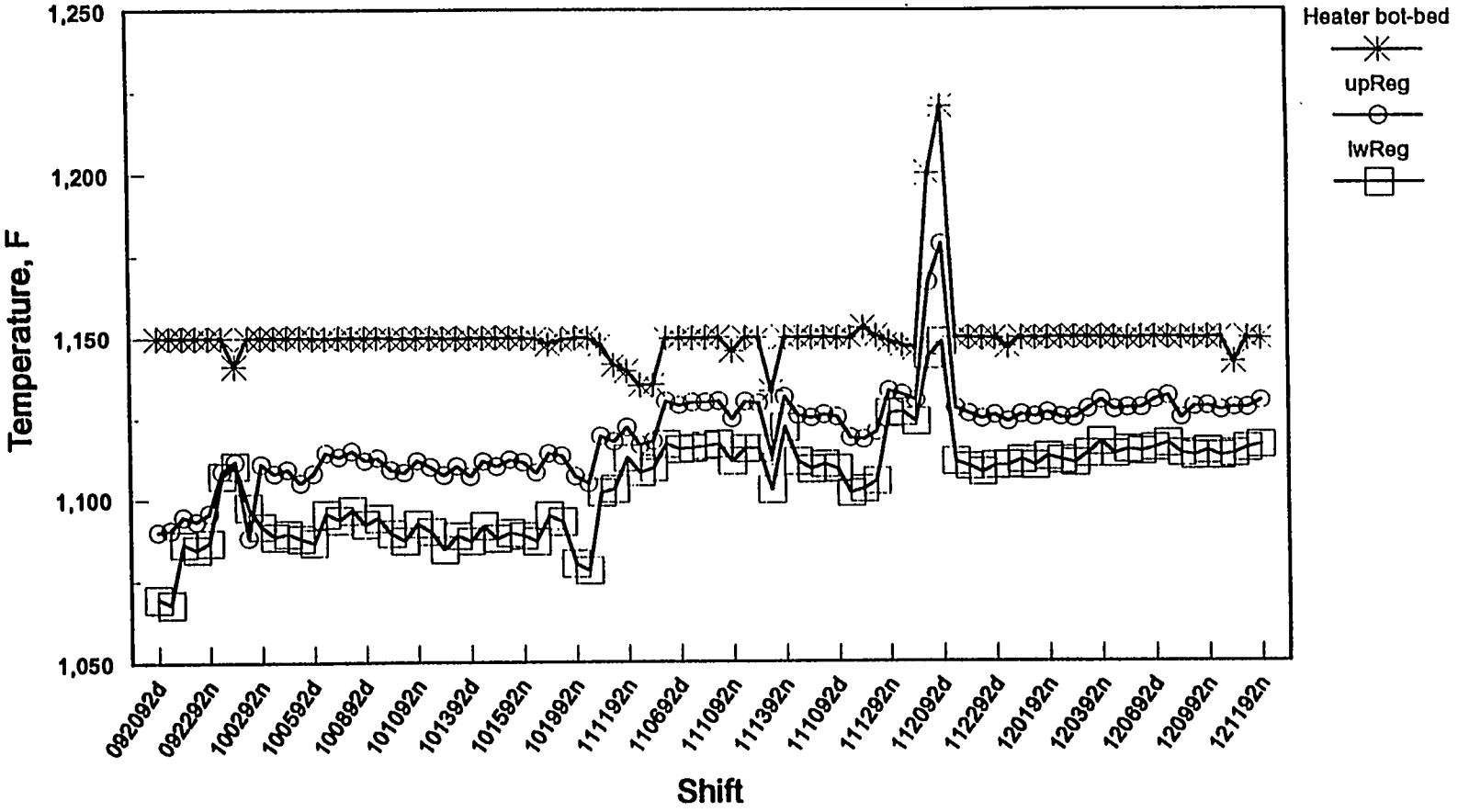

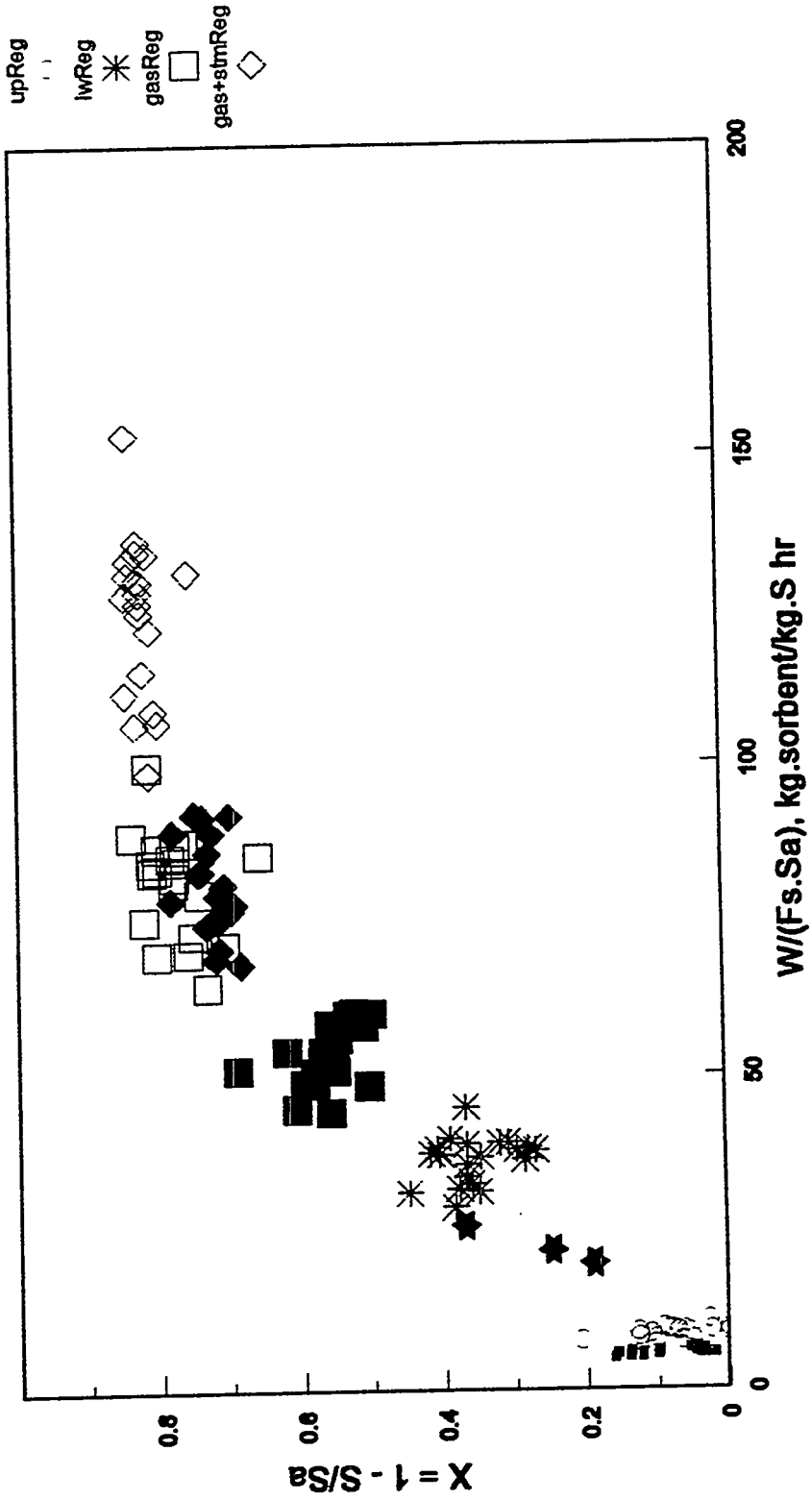

Figure 11-33 Sorbent Sulfur Regeneration
(Open Symbol: 10-05-92d-->10-18-92d)
(Solid Symbol: 11-20-92n-->12-10-92n)

The X versus $W/(F_sS_a)$ plot shown in Figure 11-33 can be approximated by two straight lines. It indicates that the regeneration consists of two main reactions, and both are first order with respect to the sorbent sulfur content. The rate of the first reaction, which occurs in the upper section of the regenerator, is about eight times higher than that of the second reaction. Since the sorbent and gas in the regenerator are in countercurrent flow, the top of the regenerator will have a high temperature and high sulfur content but low natural gas concentration, while the opposite is true at the bottom. The rate change between the first and second reaction may be caused by the temperature difference. However, the range of temperatures listed in Table 11-10 indicates that is not the case. Figure 11-34 is the X versus $W/(F_sS_a)$ plot for the data at two different bottom bed heater temperatures. The lines associated with the second reaction at different bottom bed heater temperatures have approximately the same slope. Only the data associated with the first reaction show different slopes at different temperatures. The data analysis shows that the higher heater temperature increases the rate of the first reaction but not the second. Figure 11-34 also shows that at X equal to 0.6, the sulfur regeneration shifts from the first to the second reaction for both sets of data, regardless of heater bottom bed temperature.

With Figures 11-33 and 11-34, the sulfur regeneration rate constant for the first and second reactions are determined according to the following rate equations:

$$r_{s_1} = k_1 \, e^{-\frac{E_1}{RT}} S_a \qquad (11.5\text{-}2)$$

$$r_{s_2} = k_2(1-0.6)S_a \qquad (11.5\text{-}3)$$

where E_1/R is 34554
ln k1 is 38.97
k_2 is 0.85
S_a is 0.01, the mean sulfur fraction for the steady period
T is the heater bottom bed temperature, °K

The temperature dependence of the first reaction rate constant is shown in Figure 11-35.

The contribution of the steam treater on the sulfur regeneration is shown as the difference in X between gasReg and gas+stmReg in Figure 11-33. The gasReg stands for the sorbent sample obtained from stmReg sampling port, which samples sorbent prior to steam treatment. The gas+stmReg stands for the sorbent sample obtained from the regenerator outlet, which samples sorbent after steam treatment. The slope of X versus $W/(F_sS_a)$ starts to decrease as $W/(F_sS_a)$ exceeds 50, and then drops to zero as $W/(F_sS_a)$ exceeds 100. The zero slope means no sulfur regeneration. It is concluded that the steam treater is useful in sulfur regeneration when $W/(F_sS_a)$ is less than 100. In other words, the steam treater will become unnecessary if the sulfur regeneration in the natural gas treater can push X beyond 0.8.

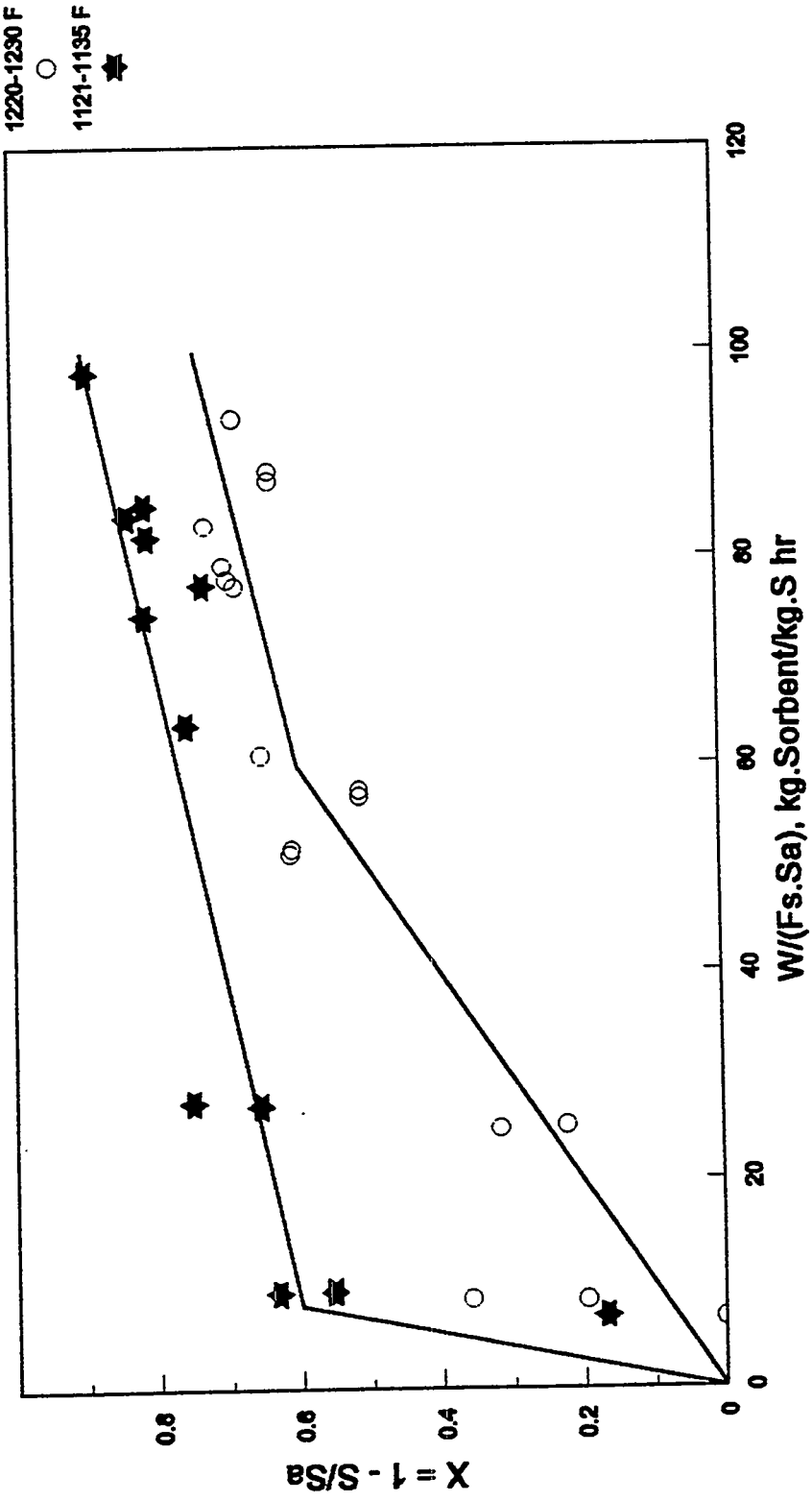

Figure 11-34
Effect of Heater Bottom-Bed
Temperature on Sulfur Regeneration

Figure 11-35
Temperature Effect of the First
Regeneration Rate Constant

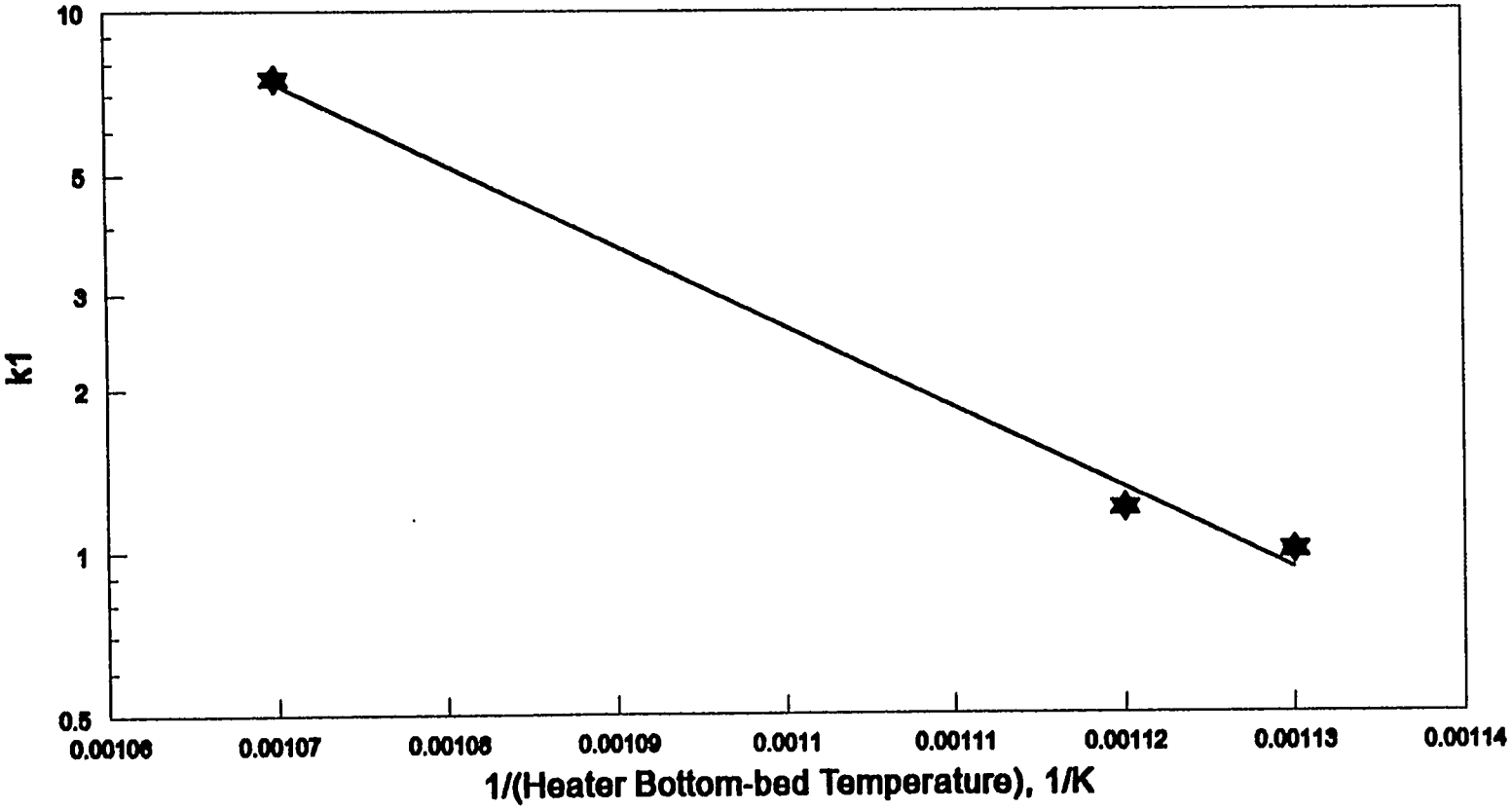

The regeneration offgas concentration profile obtained through a two inch fixed-bed reactor always shows a SO_2 peak ahead of H_2S. The H_2S concentration does not take off until the SO_2 concentration diminishes. The sequence of SO_2 and H_2S appearance in the offgas explains the two main reactions observed in the POC regeneration studies. It would be appropriate to assume that the sulfur regenerated by the first reaction becomes SO_2 and those from the second reaction becomes H_2S. The offgas H_2S/SO_2 ratio could be estimated from the ratio of sulfur regenerated by the two reactions. Figure 11-34 indicates that the change from the first to the second reaction occurs at X = 0.6. The final X is about 0.9 and 0.8 for the heater bottom bed temperature at 1250 and 1150°F, respectively. The H_2S/SO_2 ratio could be roughly estimated as follows:

$$\text{at } 1150^\circ F \quad \frac{H_2S}{SO_2} = \frac{0.8 - 0.6}{0.6} = 0.333$$

$$\text{at } 1250^\circ F \quad \frac{H_2S}{SO_2} = \frac{0.9 - 0.6}{0.6} = 0.5 \qquad (11.5\text{-}4)$$

The estimated H_2S/SO_2 ratio is compatible with the POC measured H_2S/SO_2 ratio, which is presented in the next section.

The offgases from the upper and lower regenerator sections are continuously monitored by a Milton Roy Prospec 2000 mass spectrometer. Because of the presence of water and sulfur in the sampling lines, the data quality is relatively poor as compared to the adsorption. To ensure good data quality, the analysis only uses the measurements in which the sulfur balance around the entire plant closed to within ± 15%. Those data are shown in Figure 11-36, of which the H_2S/SO_2 ratio was plotted against the spent sorbent sulfur content. The relationship between the sorbent sulfur content and the H_2S/SO_2 ratio is obvious when the sulfur content is less than 0.8 wt%. Once exceeding 0.8 wt%, the H_2S/SO_2 ratio seems to be independent of the sulfur content. The mean H_2S/SO_2 ratio is around 0.4 which is fairly close to the estimated values.

The reaction heat of sulfur regeneration is estimated by applying the energy balance around lwReg and upReg of the regenerator. Since the upReg and lwReg are located in the middle of the regenerator, one can assume that the gas and solid temperatures are equal. As shown in Table 11-10, the natural gas flowrate is very small as compared to the sorbent flowrate; the enthalpy change of the gas phase is, therefore, neglected in the calculation. Neglecting the heat loss, the energy balance gives

$$\Delta T = \frac{\Delta H}{C_{P_s}} \Delta S \qquad (11.5\text{-}5)$$

where ΔH is the reaction heat, BTU/lb sulfur,
C_{Ps} is the sorbent heat capacity, 0.254 BTU/lb °F,
ΔT is the temperature difference between upReg and lwReg, °F,
ΔS is the difference in the reduced sulfur fraction from upReg to lwReg.

Figure 11-36
Regenerator Offgas H2S/SO2 Ratio

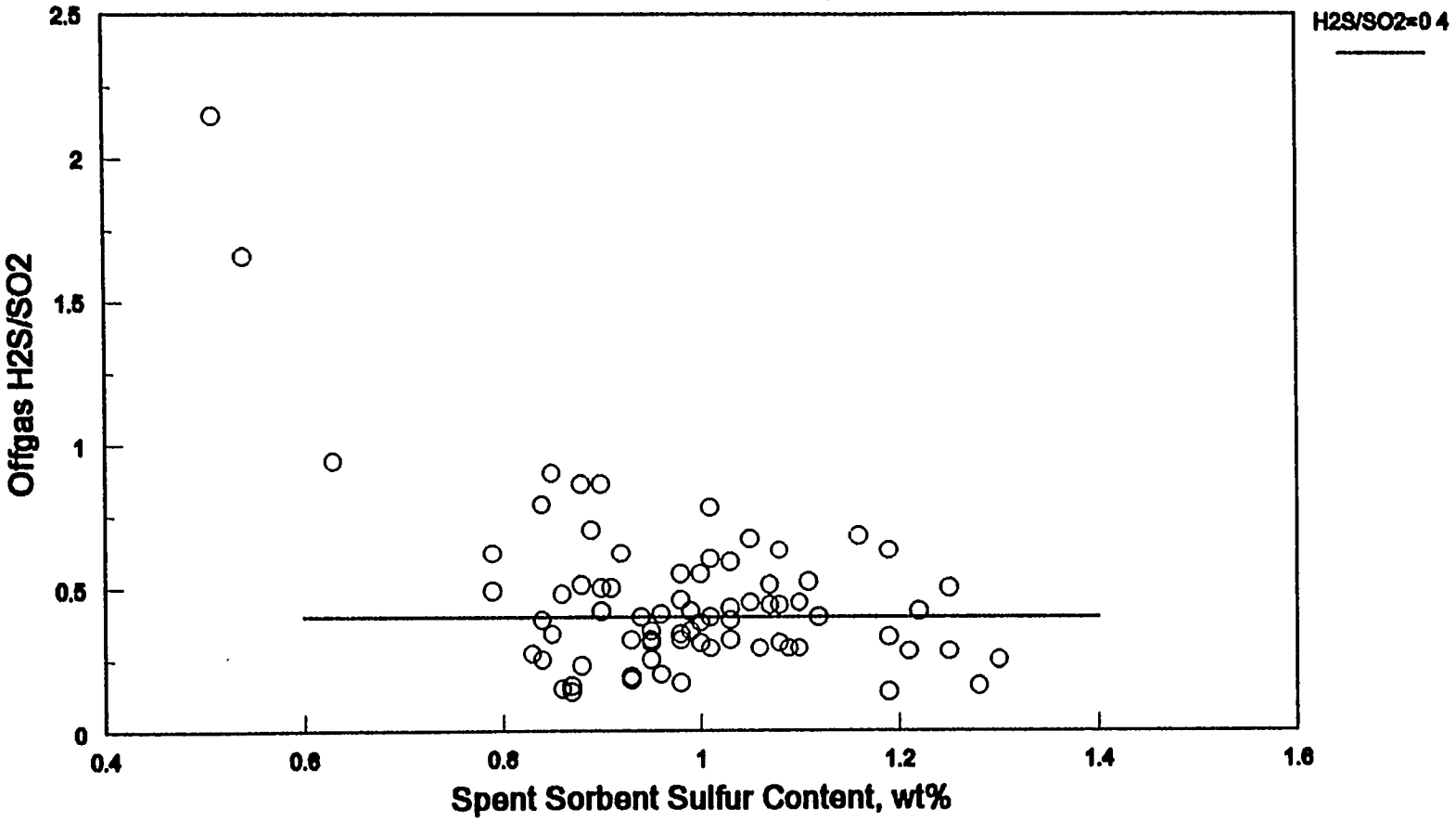

The ΔH is then determined from the slope of ΔT versus ΔS plots. Before making the ΔT versus ΔS plots, the POC data were grouped according to the heater bottom bed temperature and sorbent flowrate. Since the rate of regeneration is temperature dependent, grouping the data by temperature will reduce the reaction rate effect. The delineation of the sorbent flowrate is also required to reduce the residence time effect. Residence time is proportional to sorbent flowrate because the reactor volume between upReg and lwReg is constant. Figure 11-37 contains the ΔT versus ΔS plot, which shows two cluster of data. One has a small change in sulfur content (0--0.4), the other is large (0.0--0.9). Since the sulfur regeneration consists of two main reactions, and one is about eight times faster than the other; it is likely that the first cluster of data is the result of the slow reaction, while the second cluster is from the fast reaction. The estimated regeneration heats obtained from these two data clusters are given by

$$\Delta H_1 = \frac{32.5}{0.9/100} * 0.254 = 917.2 \ \textit{Btu/lb sulfur} \qquad (11.5\text{-}6)$$

$$\Delta H_2 = \frac{32}{0.4/100} * 0.254 = 2032 \ \textit{Btu/lb sulfur}$$

11.7 65 MW Model Plant

A 65 MW coal-fired power plant is used as an example to illustrate the use of POC test results in sizing the adsorber and regenerator for a NOXSO flue gas treatment plant. The pertinent design information is listed below:

Flue gas flowrate = 144,000 scfm
SO_2 concentration = 2200 ppm
NO_x concentration = 400 ppm
Required SO_2 removal efficiency = 90%
Required NO_x removal efficiency = 80%

Since the NOXSO flue gas treatment plant contains NO_x and SO_2 recycle loops, the adsorber inlet NO_x and SO_2 concentrations will be higher than those provided by the power plant. The adsorbed NO_x is recycled through the NOXSO sorbent heater to the power plant's coal combustor to destroy the NO_x. About 65% recycled NO_x will be destroyed in the coal combustor[8]. The tail gas from the NOXSO sulfur plant will be incinerated to form SO_2 and recycled to the adsorber. Tail gas recycle has little effect on the adsorber design, but reduces the capital cost of the Clause plant since only 90% conversion of SO_2 to sulfur is required with flue gas recycle. Applying the material balance around the NOXSO system and the power plant, gives the actual duty of the adsorber as follows:

Flue gas flowrate = 144,000 scfm
SO_2 concentration = 2418 ppm
NO_x concentration = 572 ppm
Required SO_2 removal efficiency = 91%
Required NO_x removal efficiency = 86%
Adsorber fluid-bed temperature = 275 °F

Figure 11-37
Regeneration Reaction Heat
(Heater Bottom-bed Temperature = 1150 F)

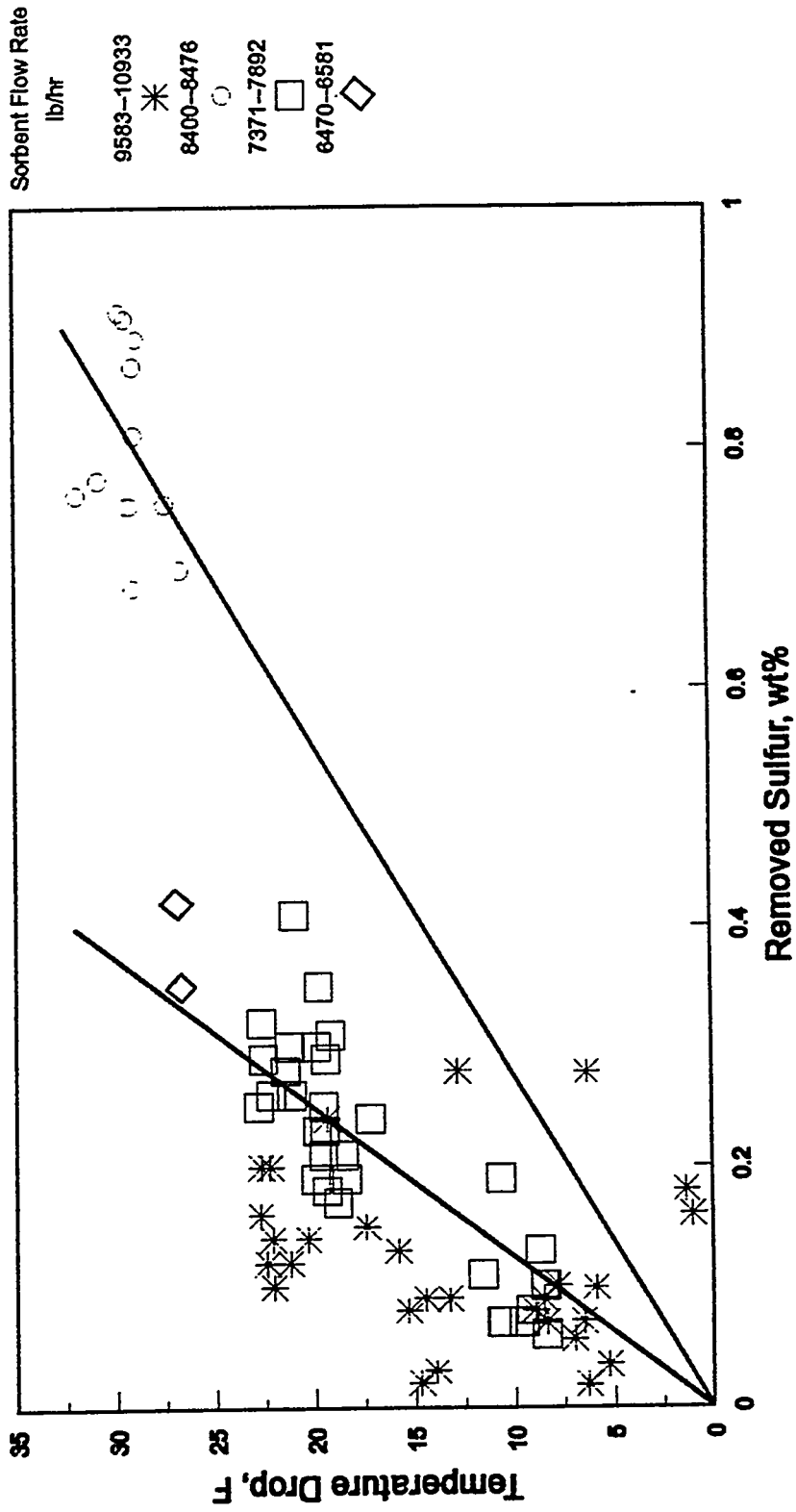

The volume of tail gas is negligible compared to that of the flue gas. Only the increase of the adsorber inlet SO_2 concentration is considered in the design. NO_x removal efficiency increases with decreasing adsorber temperature. The 275°F fluid-bed temperature is the lowest temperature tested at the pilot plant thus far.

The stabilized NOXSO POC sorbent is used in sizing the adsorber. The results are shown in Figure 11-38. The design information was generated by the adsorber model developed in Section 11.3. The stabilized sorbent has 150 m^2/g surface area, 5.2 wt% Na, 6.8 wt% SiO_2, and 0.25 wt% sulfur. Figure 11-38 shows that the required NO_x and SO_2 removal efficiencies can be achieved by increasing the adsorber's sorbent inventory and the sorbent flowrate. The sorbent inventory is expressed in terms of the pressure drop across the adsorber fluid-bed in Figure 11-38. The increase in sorbent inventory results in a higher pressure drop across the fluid-bed adsorber. The higher the pressure drop, the more power is consumed by the flue gas fan. The increase in sorbent flowrate increases the heat duty of the sorbent heater and cooler. It requires a bigger cooler fan and a larger air heater, which implies more electricity and natural gas consumption. The criteria of process capital and operating cost has to be used to determine the best combination of adsorber inventory and sorbent flowrate for a given removal efficiency.

For the case of the 65 MW model plant, the required sorbent flowrate will be between 200,000 and 250,000 lbs/hr with adsorber fluid-bed pressure drop between 24" and 18" H_2O. respectively. The spent sorbent sulfur content will be between 0.99 to 0.84 wt%. Because of the high sorbent flowrate, the sorbent gains only 0.74 to 0.59 wt% sulfur in passing through the adsorber. A remedy is recommended to increase the sorbent reactivity by reducing the SiO_2 and increasing the Na content of the sorbent. As pointed out in Section 11.3.2, the presence of silicate reduces the sorbent activity but it stabilizes the sorbent structure and the surface area. A compromise solution would be to reduce the silicate content by half and increase the Na content to 6 wt%. A comparison result using POC and low silicate sorbent is shown in Figure 11-39. With 100,000 lb/hr sorbent flowrate, the low silicate sorbent can achieve the required NO_x and SO_2 removal efficiency with 16" H_2O pressure drop, while the POC sorbent can achieve only 61% SO_2 and 58% NO_x. The advantage of using the low silicate sorbent is obvious.

Since the sulfur content of the sorbent affects both the adsorber and the regenerator sizes. there is an optimum sorbent sulfur content which minimizes the sizes of the adsorber and regenerator. The POC test results discussed in Section 11.3 were used in sizing the regenerator and the adsorber with different sulfur content of the regenerated sorbent. The results are shown in Figure 11-40. Both the POC and the low silicate sorbent are used in the calculation to achieve the NO_x and SO_2 removal requirement of the 65 MW model plant. The optimum sulfur content of the regenerated sorbent is around 0.8 wt%. The detailed results are listed in Table 11-11.

If the power consumption of the flue gas fan is the major concern in the NOXSO system design, the designer can lower the pressure drop across the adsorber fluid-bed by either reducing the sulfur content of the regenerated sorbent or increasing the sorbent flowrate. Both methods

Figure 11-38. NOx and SO2 Removal Efficiencies of the 65 MW Model Plant with Different Sorbent Flowrates (100,000 -- 250,000 lbs/hr)

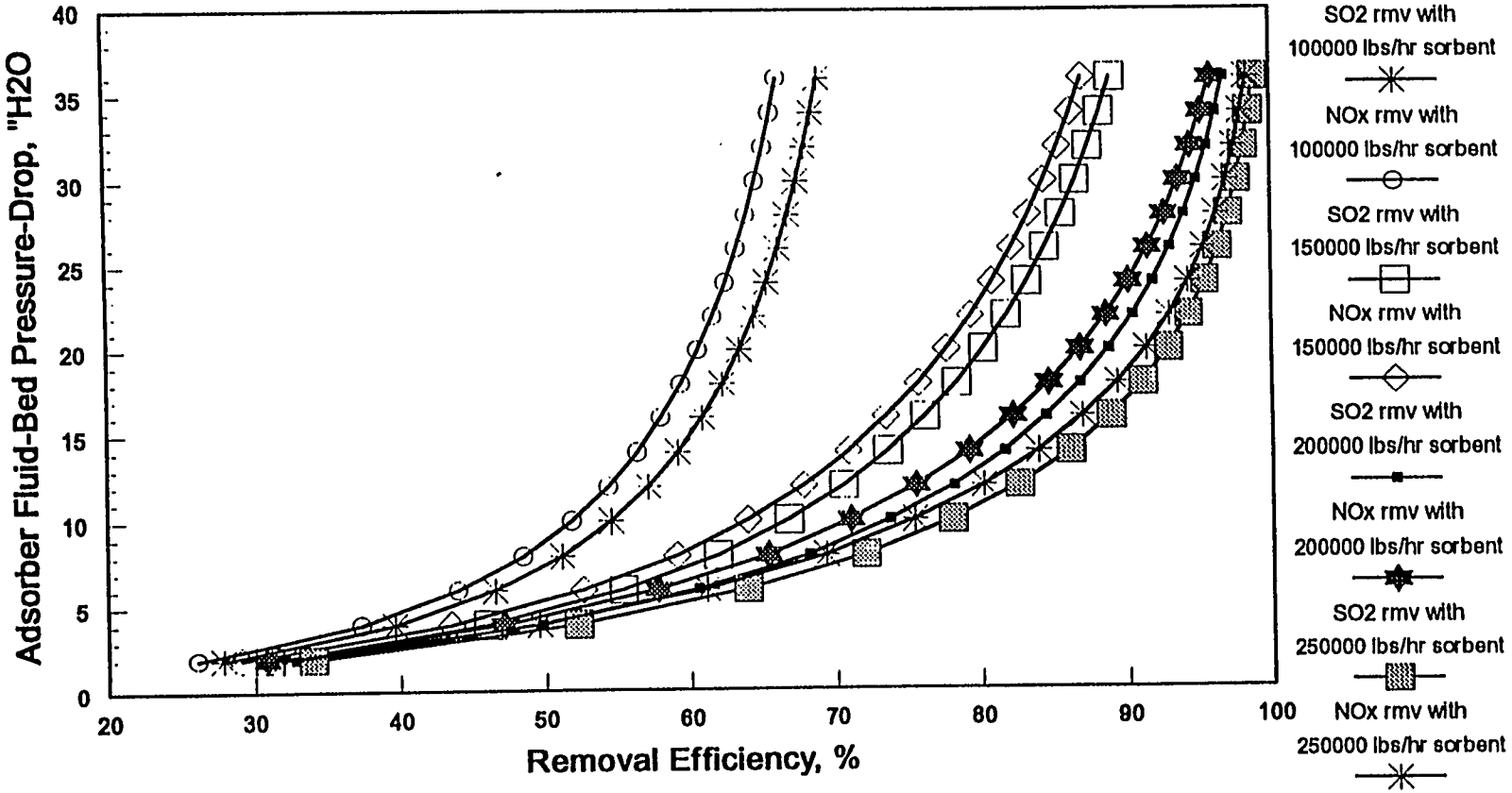

Figure 11-39. NOx and SO2 Removal Efficiencies of the 65 MW Model Plant Using Different Sorbent Na and SiO2 Loading (100,000 lbs/hr Sorbent)

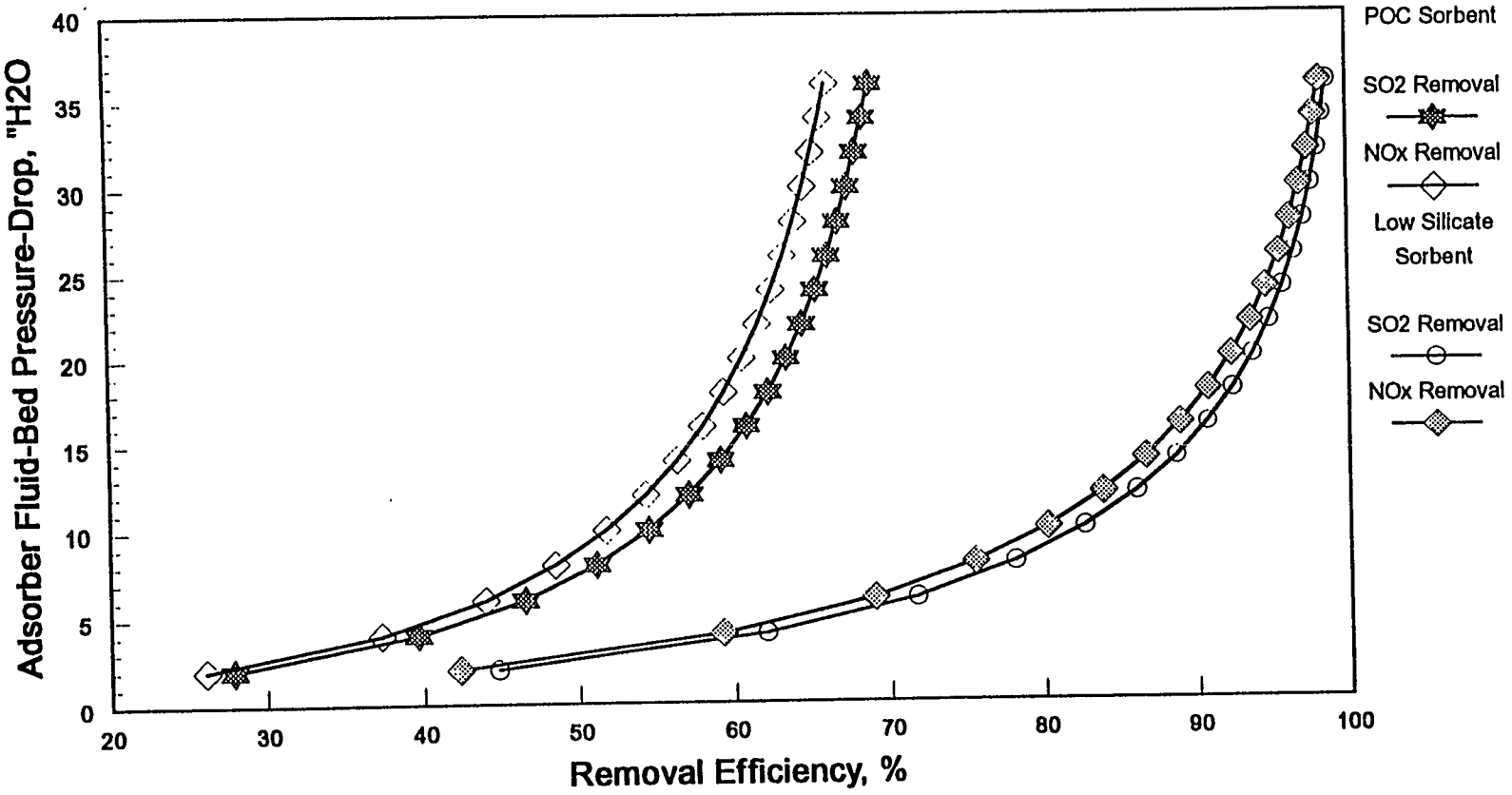

Figure 11-40 Optimum Residual Sulfur Content of Regenerated Sorbent for Reaching 90% SO2 Removal Efficiency in the 65 MW Model Plant

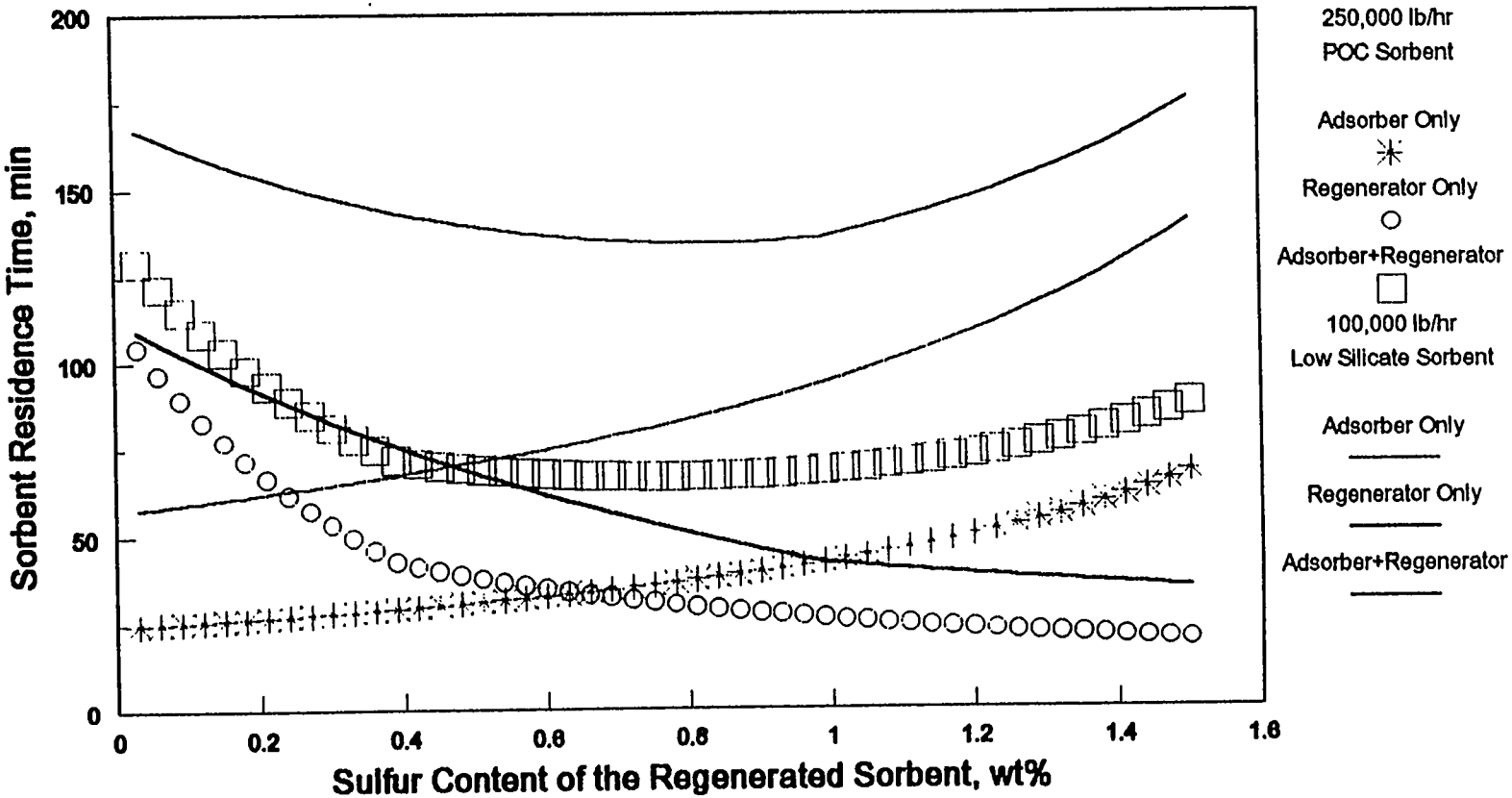

were applied to the 65 MW model plant, and the results are summarized in Table 11-12. Note that as the sulfur content of the regenerated sorbent decreases, the amount of pressure drop that can be reduced by lowering the sulfur becomes smaller. As a result, to further lower the pressure drop requires an increase of the sorbent flowrate. Reducing the sulfur content of the regenerated sorbent also results in a longer regeneration time.

Table 11-11. Optimum Regenerated Sorbent Sulfur Content for 65 MW Coal-Fired Model Plant

Sorbent	Stabilized POC	Low Silicate
Sorbent flowrate, lbs/hr	250,000	100,000
Adsorber NO_x removal efficiency, %	89.48	89.70
Adsorber SO_2 removal efficiency, %	91.21	91.41
Adsorber sorbent residence time, min	36.03	84.08
Regenerator sorbent residence time, min	30.98	50.36
Adsorber+regenerator time, min	67.0	134.44
Adsorber temperature, °F	275	275
Regenerator temperature, °F	1130	1130
Spent sorbent sulfur content, wt%	1.34	2.29
Regenerated sorbent sulfur content, wt%	0.75	0.81
Adsorber fluid-bed pressure drop, " H_2O	23.83	22.24

Table 11-12. The Effect of Sorbent Flowrate and Sulfur Content on the Adsorber Fluid-Bed Pressure Drop for the 65 MW Model Plant

	Stabilized POC Sorbent		Low Silicate Sorbent			
Sorbent flowrate, lbs/hr	250,000	250,000	100,000	100,000	100,000	110,000
Regenerator sorbent sulfur, wt%	0.75	0.24	0.81	0.24	0.03	0.24
Adsorber fluid-bed ΔP, " H_2O	23.83	18.04	22.24	16.70	15.29	14.00
Regenerator sorbent time, min	30.98	61.8	50.36	88.14	109.25	86.02

12.0 DURATION TEST RESULTS

A one week duration test was performed at the POC after completing the parametric test program. The primary objective of the duration test was to demonstrate 80% NO_x and 90% SO_2 removal efficiencies for an extended period of operation. A second goal of the duration test was to collect reliable data on utility requirements to solidify current estimates of full scale operating costs. It should be noted that the duration test was initially scheduled for three months in order to demonstrate process operability. This was determined unnecessary, however, as the reliability of the NOXSO process was established during the six months of parametric testing when the on-stream time averaged 76% (April-December 1992). Furthermore, this high rate of on-stream time was accomplished when process operating conditions were frequently changed to conform with the parametric test plan.

The process set-points used during the duration test are listed in Table 12-1 and were selected to yield roughly 80% NO_x and 90% SO_2 conversions while processing as much flue gas as possible. Stable adsorber performance depends largely on the plant's ability to operate at the set-points for solids flowrate and adsorber bed pressure drop. Plots of these two process variables versus time throughout the duration test are provided in Figures 12-1 and 12-2. Control of both variables was fairly good although problems occurred near the end of the test because of difficulties in operating the heater/cooler fan.

Table 12-1. POC Duration Test - Set Points

Flue gas flowrate, scfm	9000
Flue gas temperature, °F	280
Adsorber bed dp, "H_2O	14
Solids flowrate, lbs/hr	10000
Heater bottom bed temperature, °F	1150
Regenerator level, ft	5
Regenerator CH_4 flow, scfm	10
Treater steam flow, lbs/hr	35

Throughout the duration test process material balances and performance calculations were done following each 12-hour shift, using the procedure outlined in Section 4.3 - Data Acquisition and Reduction. Duration test results are summarized in Tables 12-2, 12-3, and 12-4. Over the entire duration test the average removal efficiencies were 78% NO_x and 89% SO_2. The NO_x and SO_2 removal efficiencies obtained during each shift are plotted in Figures 12-3 and 12-4.

Figure 12-1
POC Duration Test

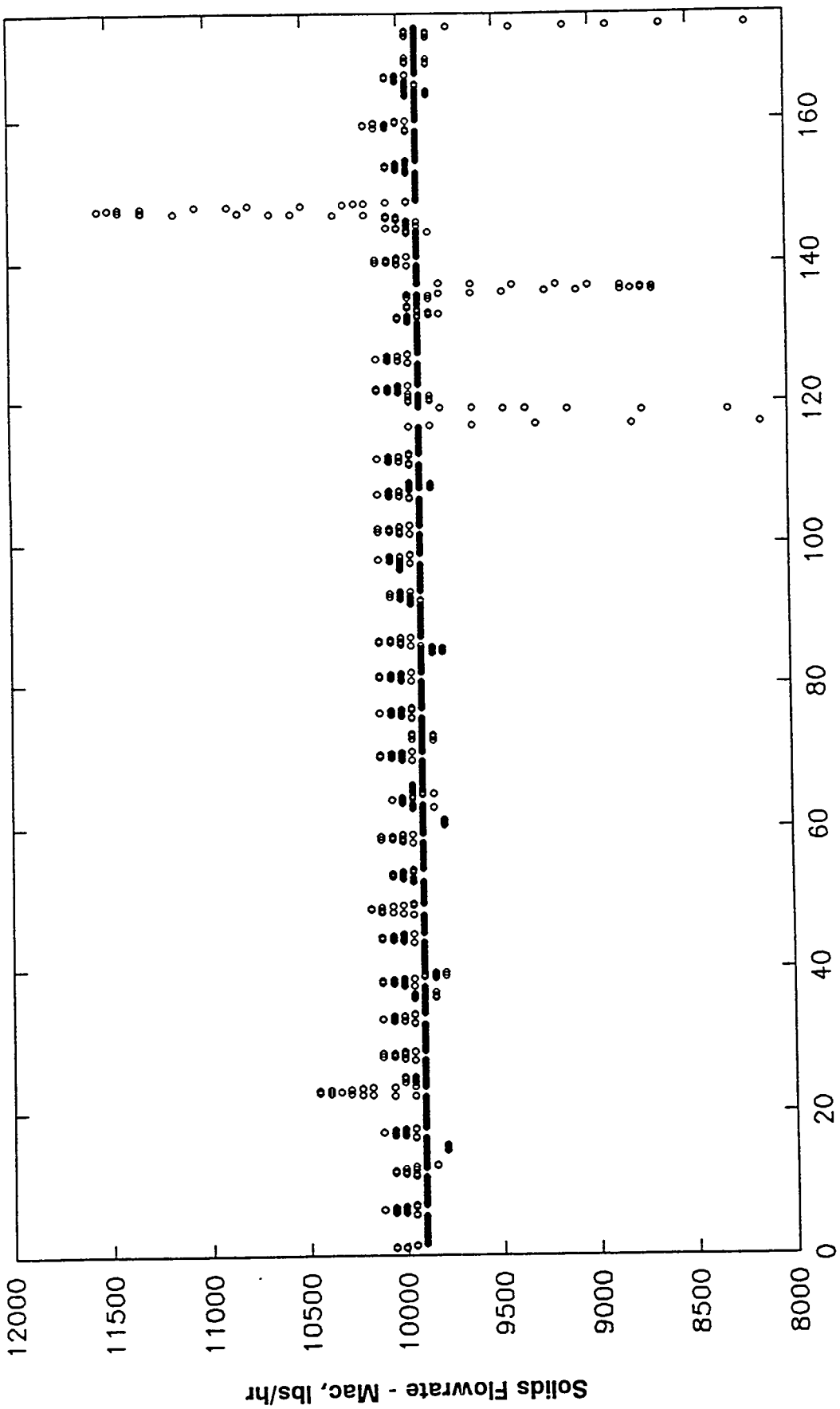

Figure 12-2
POC Duration Test

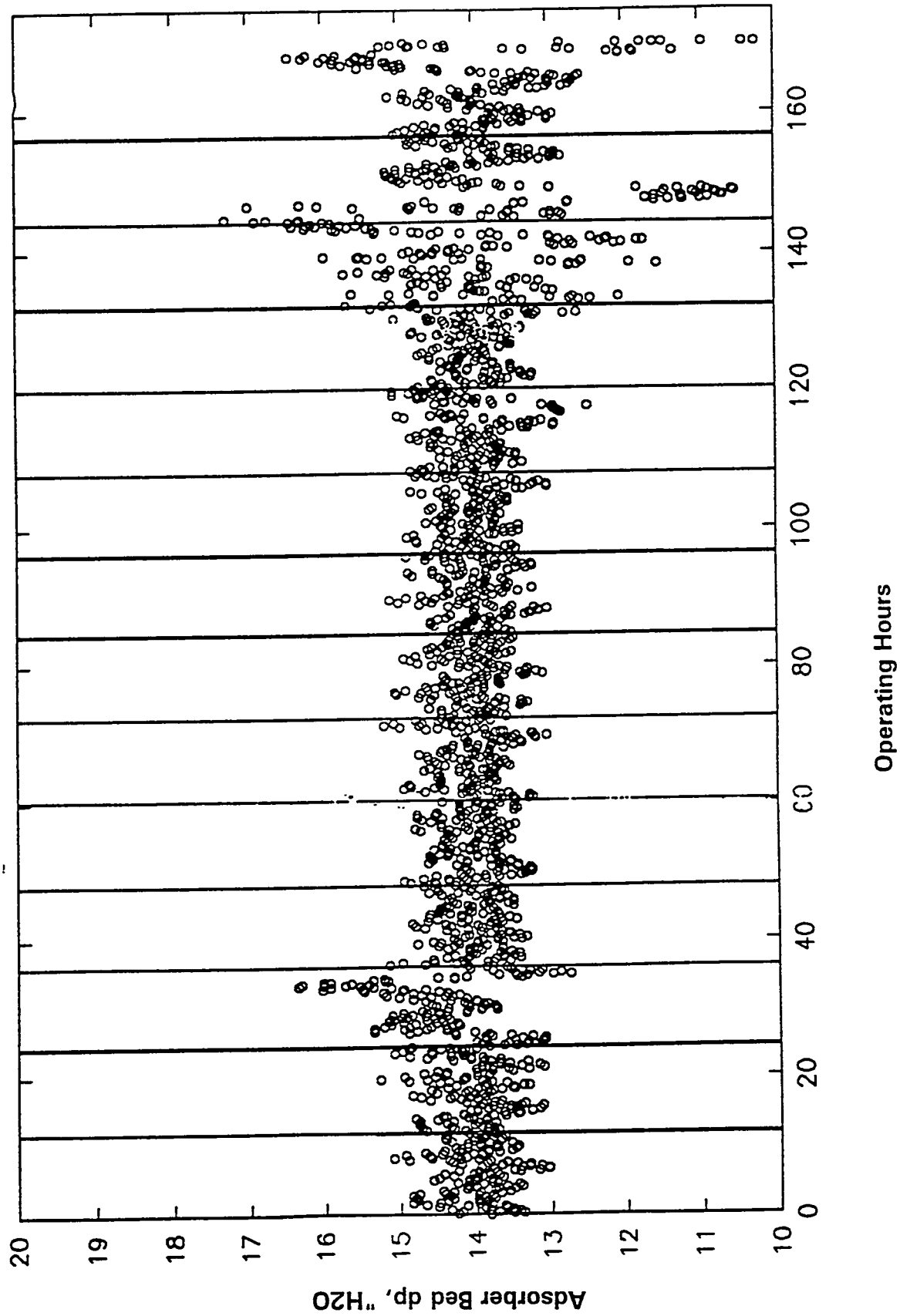

Table 12-2. POC Duration Test

Shift	Regen (wt% S)	Ads (wt% S)	Solids Flow (lbs/hr)	Bed dp ("H2O)	Bed Ht (ft)	Resd Time (min)	Bed Temp (F)	Flue Gas Flow (scfm)	Linear Vel (ft/s)	Adsorber Space Vel (/hr)	Circ (Solids/ SO2)	Inv (Solids/ SO2)	Ads SO2 In (ppm)	Ads NOx In (ppm)	Ads SO2 Conv (%)	Ads NOx Conv (%)
121792d	0.19	0.75	9938.82	13.95	1.81	37.94	328.24	9326.94	2.66	5281.44	63.82	40.35	1644.93	297.68	90.04	79.46
121792n	0.20	0.84	9915.71	13.99	1.82	38.13	328.28	9346.16	2.67	5277 97	63.59	40.42	1643.71	310.10	90 94	79 14
121892d	0.22	0.78	9934.74	14.49	1.88	39 42	328.58	9327.88	2.66	5087.18	61.52	40.42	1705.60	332.90	90 67	79.48
121892n	0.23	0.84	9931.86	14.01	1.82	38.13	330.94	9348.55	2.68	5289.55	62.73	39.86	1668.41	369.52	90.34	78.09
121992d	0.20	0.77	9935.68	14.02	1.82	38.14	334.20	9339.91	2.68	5299.23	63.42	40.31	1652.59	348.42	90.14	76.28
121992n	0.19	0.89	9927.69	14.02	1.82	38.17	332.15	9344.68	2.68	5289.26	62.59	39.82	1672.74	348.71	90.03	76.78
122092d	0.20	0.76	9922.45	14.01	1.82	38.16	330.65	9339.29	2.67	5282.76	61.20	38.93	1710.26	326.72	88.79	79.51
122092n	0.21	0.81	9927.89	13.98	1.82	38.06	329.98	9353.89	2.68	5297.92	62.27	39.50	1679.20	326.15	90 29	79.65
122192d	0.17	0.79	9947.83	14.01	1.82	38.06	328.61	9345.13	2.67	5271.05	59.83	37 96	1752.95	301 90	89 08	
122192n	0.20	0.80	9913.07	13.98	1.82	38.12	329.15	9341.49	2.67	5282.90	59.89	38.05	1745.73	428 88	88 05	
122292d	0.23	0.84	9936.92	13.99	1.82	38.05	337.58	9269.23	2.67	5291.70	59.49	37.73	1775.48	461 44	87.65	74.68
122292n	0.26	0.91	9819.18	14.08	1.83	38.76	336 87	9258 57	2 67	5249.68	54.62	35 28	1912.84	449 98		
122392d	0.22	0.98	9936.16	14.10	1.83	38.35	339.68	9270.68	2.69	5271.07	54.80	35.03	1926.68	461.13	85.94	76 46
122392n	0.25	0.85	9930.00	13.96	1.82	38.00	335.44	9270.18	2 67	5296 42	56.56	35.82	1865.79	458.37	86.41	78.36
averages	0.21	0.83	9922.71	14.04	1 83	38 25	332.17	9320.18	2 67	5269.15	60.45	38.53	1739.74	372.99	89 11	77.99

Table 12-3. POC Duration Test

Shift	Level (ft)	Resd Time (min)	CH4 Feed (scfm)	Space Vel (/hr)	Inlet C/S	Offgas Flow (scfm)	H2O (%)	CH4 (%)	CO2 (%)	H2S (%)	SO2 (%)	CS2 (%)	COS (%)	Total H2S/SO2	CH4 Conv (%)
	Upper Regenerator														
121792d	5.00	35.55	10.09	4.11	0.70	53.98	54.51	2.65	10.87	2.26	15.07	0.18	0.09	0.20	82.74
121792n	5.00	35.63	10.10	4.12	0.63	55.95	54.99	2.80	10.48	2.16	15.00	0.16	0.07	0.20	81.24
121892d	4.99	35.54	10.02	4.09	0.67	56.35									
121892n	5.00	35.57	10.17	4.15	0.63	67.45									
121992d	4.99	35.54	10.09	4.12	0.68	55.20	50.32	2.95	11.40	2.00	15.81	0.21	0.07	0.17	80.65
121992n	5.00	35.59	10.12	4.12	0.59	57.60									
122092d	5.00	35.61	10.02	4.08	0.69	58.89	57.75	2.77	11.47	1.94	17.05	0.15	0.08	0.16	79.25
122092n	5.00	35.59	10.16	4.14	0.66	60.30	58.85	2.72	11.24	2.16	16.07	0.16	0.09	0.19	78.90
122192d	5.00	35.52	10.17	4.15	0.67	57.57	58.17	3.11	11.12	2.05	17.18	0.17	0.07	0.18	77.22
122192n	5.00	35.64	10.03	4.09	0.66	57.09	61.65	3.34	11.66	2.06	17.74	0.15	0.08	0.19	74.02
122292d	5.01	35.58	10.15	4.13	0.63	56.99	60.98	3.53	11.33	1.87	18.61	0.16	0.07	0.17	73.98
122292n	4.99	35.96	10.09	4.12	0.58	56.91	59.96	3.91	10.97	1.55	20.03	0.15	0.07	0.14	72.27
122392d	5.00	35.56	10.06	4.10	0.53	63.65	57.13	2.93	9.21	1.35	16.47	0.10	0.04	0.12	78.87
122392n	5.00	35.58	10.11	4.12	0.62	64.52	62.77	3.06	9.84	1.49	17.26	0.09	0.05	0.13	75.23
averages	5.00	35.60	10.10	4.12	0.64	58.75	57.92	3.07	10.87	1.90	16.94	0.15	0.07	0.17	77.67

Table 12-4. POC Duration Test

Shift	Resd Time (min)	Steam Feed (lbs/hr)	Offgas Flow (scfm)	Treater H2O (%)	Treater H2S (%)	Treater SO2 (%)	Treater CO2 (%)	Treater CH4 (%)	Treater CS2 (%)	Treater Temp (F)	Regen Max Temp (F)	Mass Balance Closures NOx	Mass Balance Closures Carbon	Mass Balance Closures S Solids	Mass Balance Closures S Regen
121792d	19.35	35.00	8.85	37.55	4.99	0.68	1.59	4.04	0.00	1119.82	1137.43	98.18	76.54	80.82	73.84
121792n	19.40	35.00	8.79							1117.03	1133.49	98.19	77.97	91.31	74.93
121892d	19.36	35.01	8.97							1117.27	1135.40	90.46		77.46	
121892n	19.37	34.99	8.83							1116.60	1134.93	92.21		86.48	
121992d	19.36	35.01	8.75							1117.95	1137.16	92.90	83.29	81.71	77.00
121992n	19.37	34.98	8.42	36.54	4.34	0.69	1.54	4.16	0.00	1115.47	1136.92	94.02		99.38	
122092d	19.38	35.00	9.19							1117.63	1137.62	94.93	89.87	78.63	85.74
122092n	19.37	35.01	9.23	50.68	6.51	0.98	2.27	6.08	0.00	1118.04	1135.94	93.96	89.41	84.40	84.97
122192d	19.34	35.01	9.34	55.06	6.10	1.08	1.84	6.34	0.01	1114.87	1137.03		87.02	84.82	83.12
122192n	19.40	35.01	9.61	68.35	7.56	1.55	2.59	8.01	0.01	1115.02	1135.81		94.33	83.21	87.29
122292d	19.36	35.00	8.93	66.44	8.17	1.42	3.02	7.87	0.00	1113.49	1135.83	95.95	91.76	84.52	89.38
122292n	19.59	34.99	9.24							1110.57	1133.59		91.67	85.11	89.06
122392d	19.36	34.97	8.70	34.96	4.22	0.77	1.35	3.67	0.00	1112.22	1135.43	92.58	79.80	99.21	78.44
122392n	19.37	35.01	9.02							1111.21	1132.56	92.70	89.62	80.23	88.28
averages	19.38	35.00	8.99	49.94	5.98	1.02	2.03	5.74	0.00	1115.51	1135.65	94.19	86.48	85.52	82.91

Figure 12-3
POC Duration Test

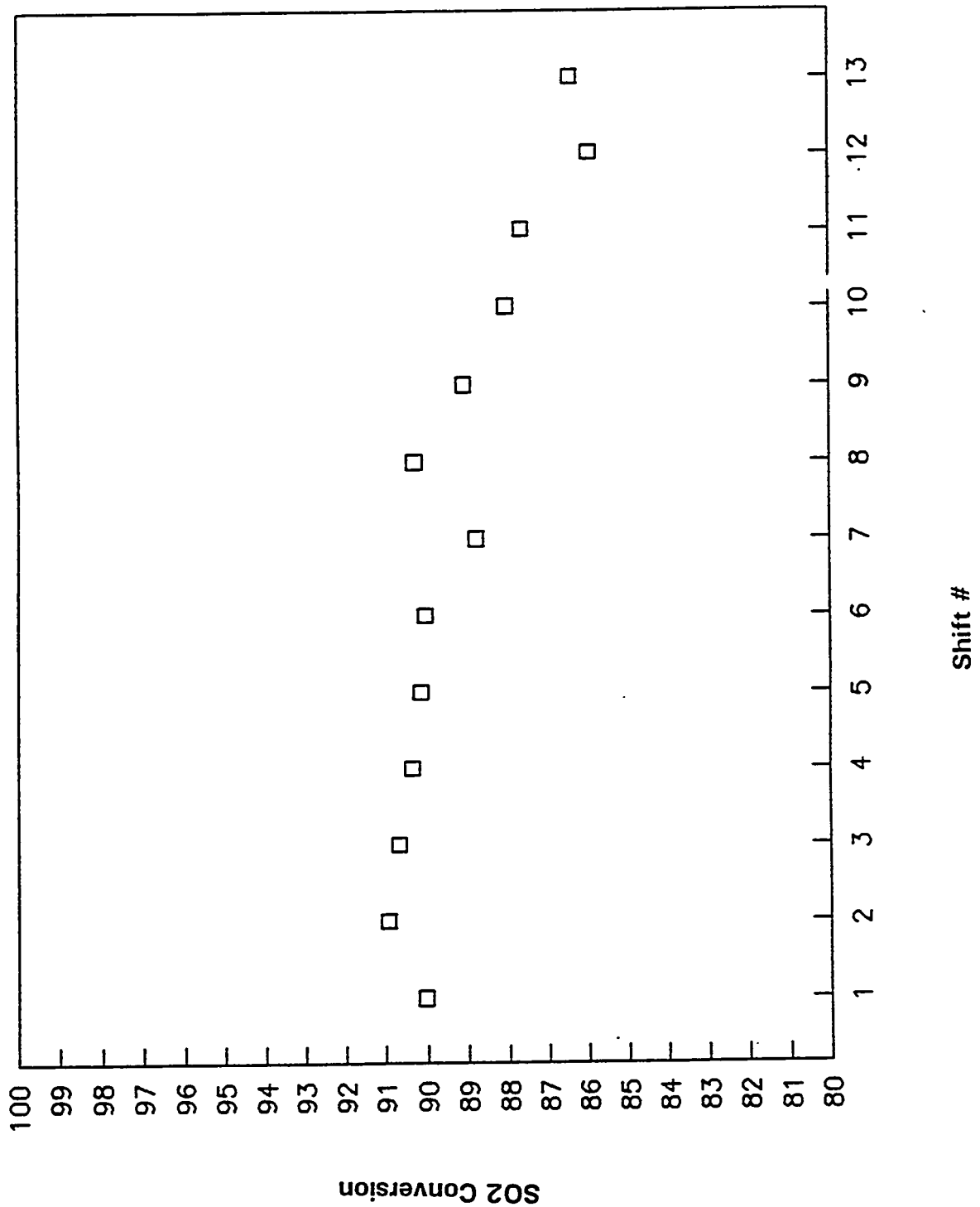

Figure 12-4
POC Duration Test

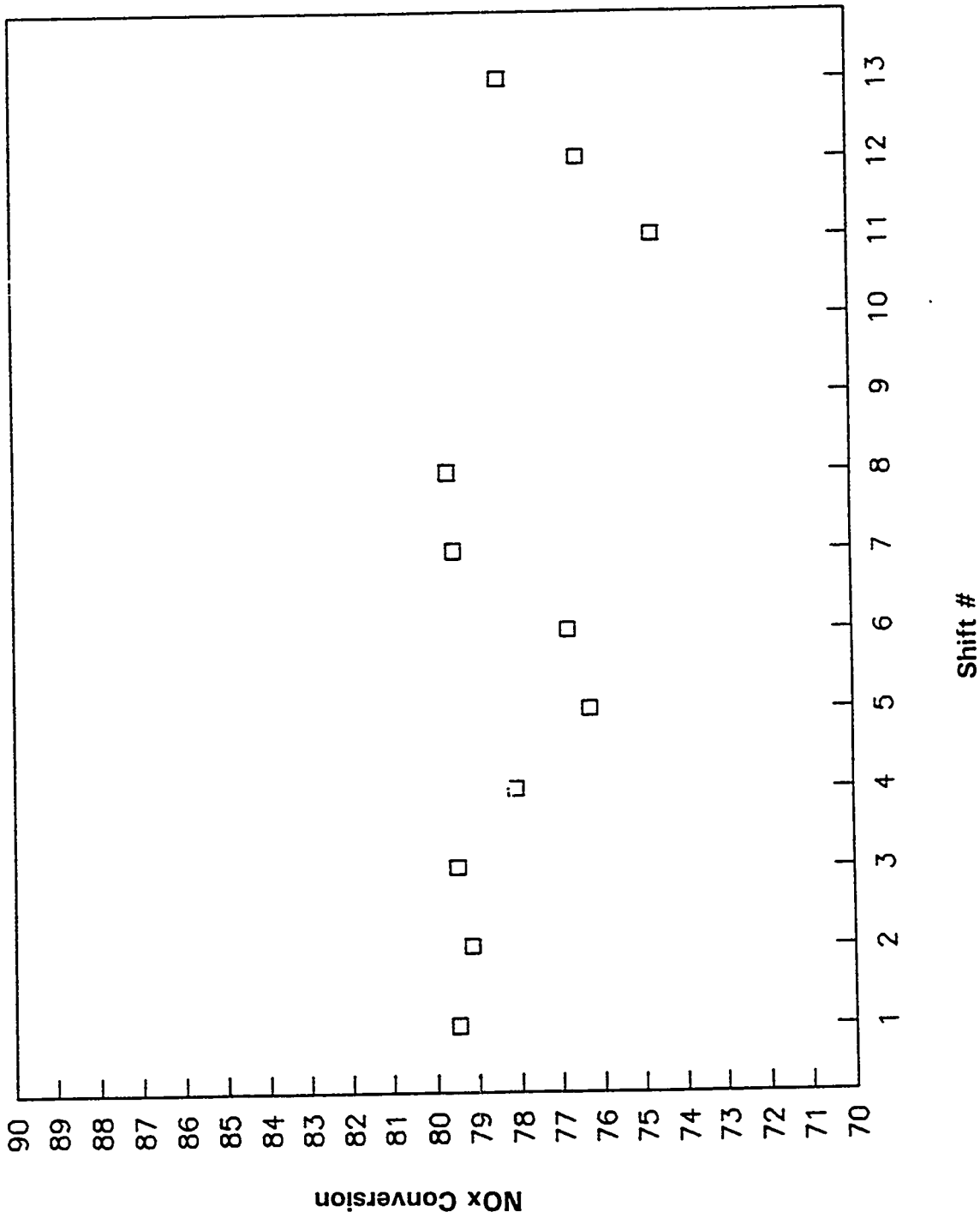

Variations in the removal efficiencies are caused in part by changing NO_x and SO_2 feed concentrations. Variations in the inlet NO_x and SO_2 concentrations versus time are shown in Figures 12-5 and 12-6. The decrease in SO_2 conversion towards the end of testing most likely resulted from the increase in flue gas SO_2 concentration. Unfortunately, the NO_x measurements during the first half of the test are suspect because the NO_x analyzer was calibrated using only NO_2 and because of a faulty sample pressure regulator. Both problems were corrected after 100 operating hours and resulted in an increase of roughly 100 ppm in the measured inlet NO_x concentration.

Utility requirements over the course of the duration test are listed in Table 12-5. Actual (measured) consumption figures are shown along with design values. The design figures were obtained from the NOXSO commercial design model using as input the pilot plant operating conditions during the duration test. The actual power consumption shown in Table 12-5 is about 25% higher than design for the following reasons:

- The adsorber and cooling fan at the pilot plant are high speed (3600 rpm) fans with discharge-side dampers and therefore are not as energy efficient as the moderate speed (1200 rpm) fans with suction-side dampers to be used in the commercial design.

- The air compressors at the pilot plant were inherited from the HALT project and are oversized. For example, the compressors generate 125 psig air, but the maximum pressure required at the pilot plant is 45 psig for the dense phase lift.

Table 12-5. POC Duration Test - Utility Consumption

	Actual	Design
2300 V power, kW	160	103
480 V power, kW	238	215
Spray water, gal/min	1.6	0.6
Natural gas, scfm	63	53
Steam, scfm	129	50

The parasitic power consumption at the pilot plant is 7.96% (actual) or 6.36% (design). Approximately 70 kW of this power consumption is auxiliary power used for the heating/cooling of the control and analyzer building, heating the gas sample lines, and powering gas analytical equipment: analyzers, pumps, fans, etc. This auxiliary power requirement scales directly from pilot to commercial scale. If one neglects auxiliary power consumption at the pilot plant, parasitic power requirements drop to 6.56% (actual) or 4.96% (design).

Figure 12-5
POC Duration Test

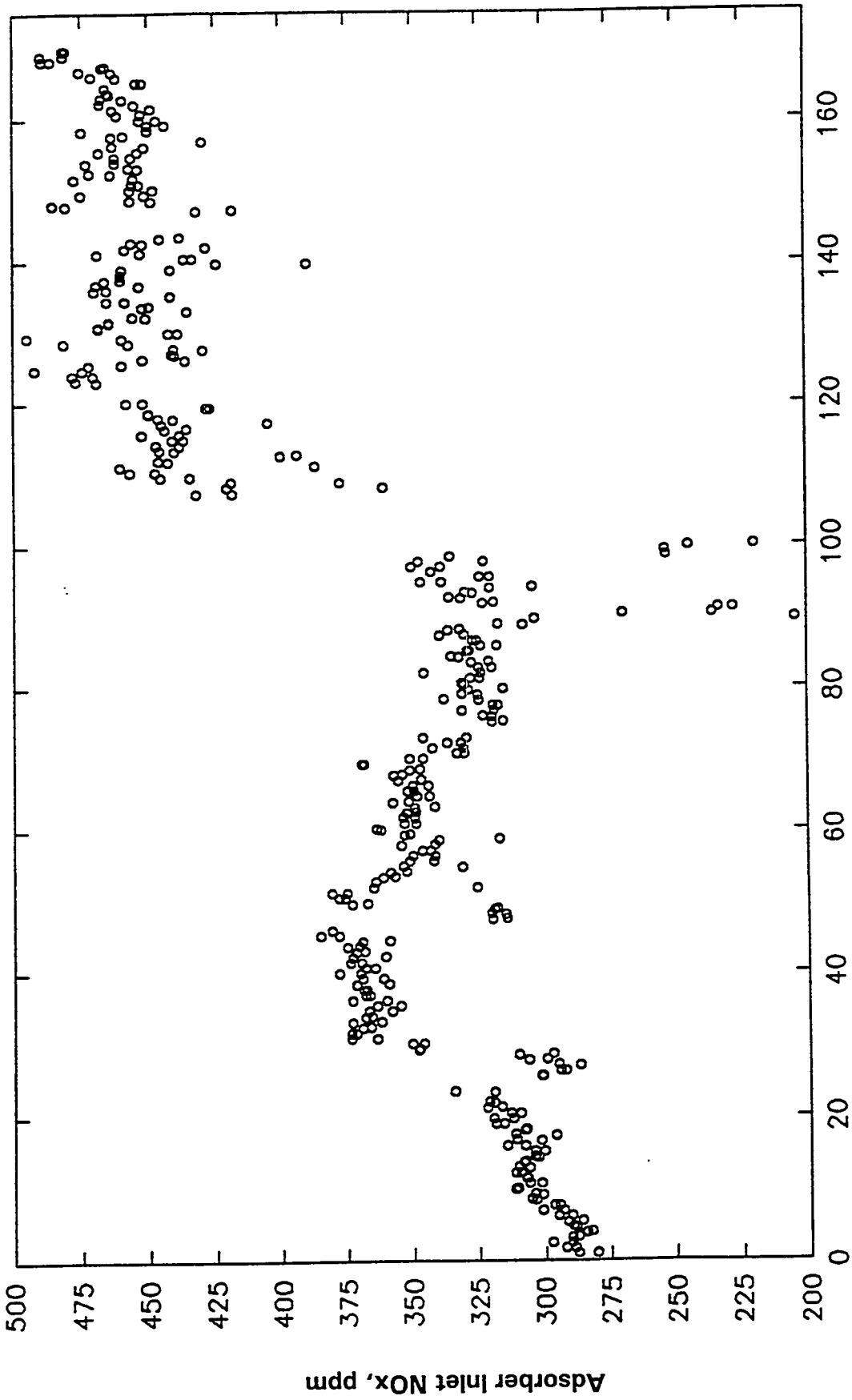

Figure 12-6
POC Duration Test

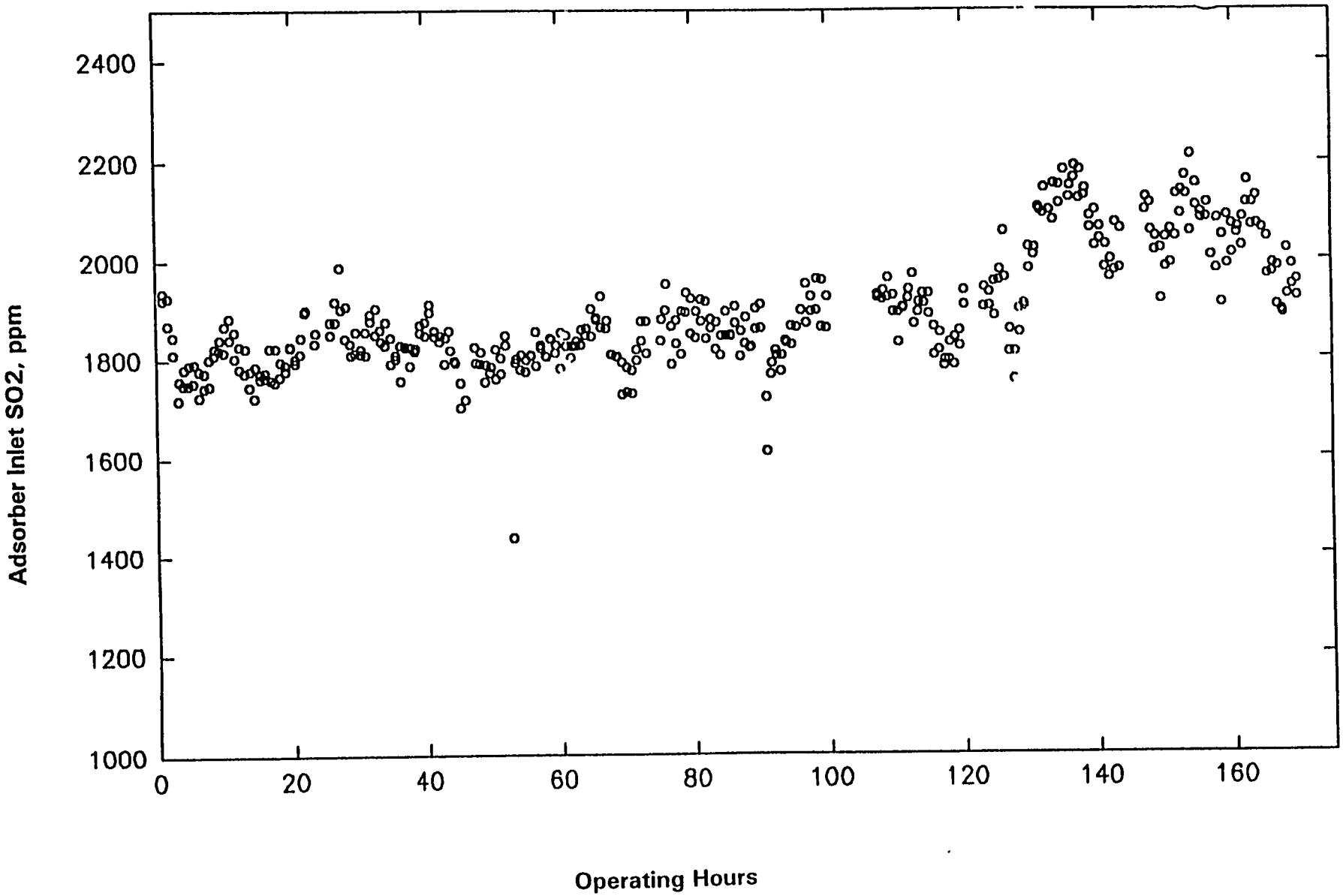

The actual spray water consumption in Table 12-5 is more than twice the design value. This is because a portion of the water sprayed into the duct was not vaporized and had to be drained from the elbow upstream of the adsorber. Improved nozzle design and orientation would eliminate this problem. Also, NOXSO plans to test in-bed water spray cooling which has several potential advantages over the in-duct water spray used in the duration test.

The actual natural gas consumption in Table 12-5 is 19% higher than design. This is because the design number was calculated without considering heat loss, since there was no way to accurately measure heat loss at the pilot plant. The duration test was conducted in December, a month in which ambient temperatures were in the 0-20°F range. The difference between actual and design natural gas consumption was only 5 scfm in July when ambient temperature was in the 70-90°F range.

Actual steam consumption was significantly higher than design because roughly 50% of the steam consumed in the pilot plant was vented to the atmosphere. This was necessary because the steam from the Toronto power plant was of a poorer quality than that anticipated in the design. Since the steam flow required by the pilot plant is low, steam was vented to keep steam lines hot and avoid condensation.

13.0 SUMMARY AND CONCLUSION

The project team designed, constructed, and tested a 5 MW NOXSO pilot plant. The *pilot plant ran better than* expected for a first-of-a-kind installation. The pilot plant availability factor over the last seven months of operation averaged 80%. This is a testimony to the soundness of the design and the simplicity of the process.

Over 5500 hours of tests were conducted. The sorbent batch's physical and chemical characteristics were monitored as the sorbent was exposed to over 1480 cycles of adsorption and regeneration. The analytical results show no significant increase in the amount of trace metals, chlorides, etc. on the sorbent with sorbent cycling. The sorbent does show a decline in surface area similar to that observed in previous tests. The decline is rapid (240 to 180 m_2/g) in the first 400 hours of operation, after which the rate of decline is much slower. Since surface area never fully stabilized during the pilot test, it may be necessary in future plants to makeup fresh sorbent to the system to maintain stable surface area.

The sorbent attrition rate at the pilot plant was lower (3.8 pph) than projected (4.3 pph). The projected rate was based on previous tests of the sorbent attrition in smaller-scale fluid beds. This projected rate did not include an estimate of attrition due to sorbent transport, since the sorbent transport system was tested for the first time at the pilot plant. The sorbent used at the pilot plant was a new sorbent designed to have greater attrition resistance. It can be concluded from the results that the POC sorbent does attrit less than previous sorbents and that the attrition caused by the sorbent transport system is negligible.

The pilot test showed that 90% SO_2 removal and 70-90% NO_x removal can be achieved. SO_2/NO_x removal efficiency increased with increasing gas residence time and decreasing sorbent residence time in the adsorber. A significant improvement in NO_x removal efficiency was obtained by lowering the temperature of the adsorber bed. The sorbent's capacity at the pilot plant was somewhat less than that measured in previous tests. The drop in capacity occurred because the sorbent used in the pilot tests was made with an additive that reduces the rate of surface area decay. This additive also has the effect of reducing the sorbent's activity. so that more sodium was impregnated on the POC sorbent (5.2 wt%) than had been used in previous tests of sorbent with no additive (3.5 wt%). As stated in the report, the sorbent's equivalent capacity based on its performance in the pilot test is 2.6 wt% sodium. The results suggest that the sorbent's capacity could be improved by optimizing the relative amounts of sodium and additive.

Sorbent regeneration was successfully accomplished with pipeline natural gas and steam at 1150°F sorbent heater bottom bed temperature. The design temperature was 1225°F. Lower temperature is preferred from the standpoint of natural gas consumption, sorbent performance, and vessel construction, although at lower temperature the reaction rates are slower and more sorbent residence time is required (i.e., larger reactors). The ratio of H_2S/SO_2 in the regenerator

offgas was on average 0.4, although H_2S/SO_2 ratios as high as 2.0 were measured in tests where sorbent sulfur loading was low: 0.5 wt% on spent sorbent. Since the stoichiometric ratio of the Claus reaction is $H_2S/SO_2 = 2.0$, the regenerator offgas must be pretreated to adjust the H_2S/SO_2 ratio prior to the Claus reactor.

The pilot plant data are sufficient to design the commercial-scale demonstration plant. The goal of the POC program was to obtain the engineering data required to produce a cost effective design of a commercial NOXSO system at an acceptable level of technical risk. A secondary goal for the test was to optimize performance while maintaining the high level of system reliability demanded by the utility industry. The project accomplished both of these goals.

NOXSO engineers plan to test two process modifications at the pilot plant that have the potential to significantly improve pollutant removal efficiencies. These are a second sorbent bed in the adsorber and in-bed water spray to cool the sorbent beds directly. Preliminary results of tests on these process modifications are very promising. The work is being funded by the Ohio Coal Development Office. A report will be issued in September 1993.

14.0 REFERENCES

1. Haslbeck, J.L., Wang, C.J., Neal, L.G., Tseng, H.P. and Tucker, J.D., "Evaluation of the NOXSO Combined NO_x/SO_2 Flue Gas Treatment Process", NOXSO Corporation Contract Report submitted to U.S. DOE Report No. DOE/FE/60148-T5, November 1984.

2. Haslbeck, J.L., Neal, L.G., Wang, C.J. and Perng, C.P., "Evaluation of the NOXSO Combined NO_x/SO_2 Flue Gas Treatment Process", NOXSO Corporation Contract Report submitted to U.S. DOE Report No. DOE/PC/73225-T2, April 1985.

3. Yeh, J.T., Drummond, C.J., Haslbeck, J.L. and Neal, L.G., "The NOXSO Process: Simultaneous Removal of SO_2 and NO_x from Flue Gas", Presented at the 1987 Spring National Meeting of the AIChE, Houston, Texas, March 29 - April 2, 1987.

4. Haslbeck, J.L., Ma, W.T. and Neal, L.G., "A Pilot-Scale Test of the NOXSO Flue Gas Treatment Process". NOXSO Corporation Contract Report submitted to U.S. DOE Contract No. DE-FC22-85PC81503, June 1988.

5. Yeh, J.T., Ma, W.T., Pennline, H.W., Haslbeck, J.L. and Gromicko, F.N., "Integrated Testing of the NOXSO Process: Simultaneous Removal of SO_2 and NO_x from Flue Gas", Presented at the AIChE Spring National Meeting, Orlando, Florida, March 1990.

6. Ma, W.T., Haslbeck, J.L. and Neal, L.G., "Life-Cycle Test of the NOXSO Process", NOXSO Corporation Contract Report submitted to U.S. DOE Contract No. DE-FC22-85PC81503, May 1990.

7. Haslbeck, J.L. and Neal, L.G., "The NOXSO Process Development: An Update". The Ninth EPA/EPRI Symposium on Flue Gas Desulfurization, Cincinnati, Ohio, June 1985.

8. Zhou, Qian, Haslbeck, J.L. and Neal, L.G., "An Experimental Study of NO_x Recycle in the NOXSO Flue Gas Cleanup Process", NOXSO Corporation Contract Report submitted to U.S. DOE Contract No. DE-AC22-91PC91337, March 1993.

9. Perry, H.P. and Chitton, C.H., "Chemical Engineers' Handbook", 5th ed., New York: McGraw-Hill, 1973, p.5-17.

10. Levenspiel, O., "Chemical Reaction Engineering", 2nd Edition, p. 383, John Wiley & Sons, Inc., New York, 1972.

11. KVB, Inc., "Evaluuation of Dry Sodium Sorbent Utilization in Combustion Gas SO_x/NO_x Reduction", EPRI Final Report, May 1990.

12. Personal communication, Skip Jones, IT Corporation, April 14, 1993.

APPENDICES

The data collected from the 5 MW POC pilot plant are listed in Table A1 through D. These Tables also contain the predicted SO_2/NO_x removal efficiencies calculated by the correlation for each data entry. The following information is included to further clarify the Tables.

Appendix A - Adsorption Test Data

Table A1 Adsorption test data from 0.75 MW Process Develop Unit (PDU).

Table A2 Adsorption test data from 0.06 MW Life Cycle Test Unit (LCTU).

Table A3 Adsorption test data from 5 MW Proof-Of-Concept pilot plant (POC). The predicted NO_x and SO_2 efficiencies are calculated based on the following information:

Sorbent bulk density = 641 kg/cm^3
Sorbent sodium content = 5.2 wt%
Stabilized sorbent surface area = 150 m^2/g
Fresh sorbent surface area = 250 m^2/g
Adsorber cross-sectional area = 8.044 m^2
Missing data = -1

Following values are assigned to the missing data in the PDU-adsorber model calculation.

Regenerated sorbent sulfur content = 0.2 wt%
Fluid-bed inventory = 2865.341 kg
(equivalent to 14" H_2O fluid-bed pressure drop)

Appendix B - POC Sulfur Regeneration Test Data

Table B1 Solid phase data of regeneration.

Table B2 Gas phase data of regeneration, of which the material balance closures around the entire plant are within $\pm$ 15%. The following information will be helpful in interpreting the data:

Regenerator cross-sectional area = 1.167 m^2.
Missing data = -1

The CH_4 and steam treaters' offgas flowrates listed in Tables B1 and B2 include the flowrate of N_2 used in the regenerator instrumentation purge and that of steam used in the J-valves. As a result, the offgas flowrates are significantly higher than those of the feed gases.

The data listed in Table B1 was obtained independently from the gas monitoring system, but those listed in Table B2 were not. Because of the sulfur condensation in the offgas sampling line, which results in a false reading in the mass spectrometer, the *number of data listed in* Table B2 is much less than those in Table B1.

Appendix C - Sorbent Cooler Test Data

The following information was used in calculating the values for the derived variables.

Sorbent cooler cross-sectional area = 2.34302 m^2
Vessel wall area for heat loss calculation, A_w = 9.1 m^2
(equivalent to 66" height, distance between two grid plates)
Downcomer overflow width, W = 0.1207 m
Downcomer overflow length, L = 0.381 m
Downcomer overflow height above the grid, H = 0.3366 m
Mean particle diameter = 0.00121 m
Sorbent particle density = 1000 kg/m^3
Sorbent heat capacity, kcal/(kg °C):

$$Cps = [22.08 + 0.008971 * T - 522500/T^2]/102$$

where T = arithmetic mean of sorbent temperature, °K

Air heat capacity, kcal/(kg °C):

$$Cp = [6.8717 + 0.000844 * T - 39417/T^2]/28.84$$

where T = logarithmic mean of air temperature, °K

Air thermal conductivity, kcal/(m °K sec):

$$kapa = [2.0772 + 0.01465 * T]/10^6$$

where T = logarithmic mean of air temperature, °K

Air viscosity, kg/(m sec):

$$mu = [0.0177485 + 0.0000334 * T]/1000$$

where T = logarithmic mean of air temperature, °K

Fs = sorbent flowrate
Fg = air flowrate
Estimated sorbent and air temperatures are the results of using $Nu = 0.0008\ Re_p^{1.3}$.

Appendix D - Material Balance Closures for NO_x, Sulfur and Carbon

The closure = 100% means the material balance was closed.

Appendix E - Example of Sizing the Downcomer in a Multi-Stage Fluid-Bed Vessel